University of Strathclyde
Department of Electronic and Electrical Engineering

# Software Sensor Designs for Urban Wastewater Systems

By

**Farid Benazzi**

A thesis presented in fulfilment of the requirements for the degree of Doctor of Philosophy

# Copyright

# Dedications

*To Sam, Camilla & the rest of my Family...*

# Acknowledgements

I would like to first express my gratitude to Dr. Reza Katebi who introduced me to the challenge of modern wastewater treatment monitoring, for his advices and reading of the thesis.

I also would like to express my most sincere gratitude to Dr Ulf Jeppsson, for the support, valuable comments and enthusiasm he has always shown for my work. Six weeks spent at the Department of Industrial Electrical Engineering and Automation, Lund University, Sweden, were both really interesting and fruitful. This department is a great place to work and I want to thank its entire staff for contributing in an excellent working and friendly environment. I would especially like to express my sincere gratitude to Dr Krist Gernaey for his valuable comments and the interest he has always shown for my work, Dr Joaquim Comas for discussions and comments and for the good time we spent in the city of Lund and Prof Gustaf Olsson for thoughtful advices.

For the supply of the integrated urban wastewater system I am grateful to Erick Lindblom, Danish Technical University, Copenhagen. I am also grateful towards Nizar Rajabaly for his assistance during his placement at the Industrial Control Centre. For her reading of the thesis, articles, reports, etc. and the time we spent working in the Industrial Control Centre, I am most grateful to Dr. Marie O'Brien.

Prof Jean-Philippe Steyer is also gratefully acknowledged, for his interest and involvement toward my work. I am also most grateful to Dr (to be) Camilla Magnussen for her great support during these three and half years. I would have never reach the point I am today without her.

I have the privilege of being part of a large, interdisciplinary research group, WWT&SYSENG, working within the field of wastewater treatment. I would like to take this opportunity to thank all my friends and colleagues within the WWT&SYSENG network, especially Dr Vrecko Darko, Erick Linblom, Botond Raduly, Dominika Pradzynska, Irina Cosma, Joanna Boguniewicz and Gladys Tapia.

I wish to thank my lab mates from the Industrial Control Centre including Dr Pawel Majewick, Dr Leonardo Giovaninie, Dr Jonas Balrue, Dr Alberto Sanchez, Dr Matthew Wade and Dr (to be) Luisella Balbis.

I am also grateful to my friends from Glasgow, in particular Dr Christophe Lafon, Panos Louridas, Dr Stefan Martin, Dr Walter Lubeigh, Dr Phillipe Brachet, Jérome

Joly, Mehdi Soufi, David Gutierrez and Benoit Guilhabert, which all contributed to make these last three years memorable and unforgettable.

Last but not least I thank my parents and the other members of my immediate family for the love, support and trust that they have always shown towards me.

The financial support provided through the European Community's Human Potential Programme under contract HPRN-CT-2001-00200 (WWT&SYSENG) is gratefully acknowledged.

*Glasgow, July 2006*
*Farid Benazzi*

# Abstract

The objective of this thesis is the design of software sensors for an urban wastewater system. The dynamic behaviour of urban wastewater systems are typically described by highly non-linear deterministic models. These non-linearities are mainly caused by important variations in the influent flow rate. In addition, there is a clear lack of instrumentation and automation systems. Therefore, this thesis contains a thorough discussion of software sensors, with applications to urban wastewater treatment systems and a special emphasis on the wastewater treatment plant.

Since the original activated sludge process model utilised in this work is not observable, three reduced order models, based on the activated sludge model no.1, are proposed. A linear piece-wise observability analysis based on the Kalman rank theory is investigated on each of the reduced models, prior to non-linear observability analyses based on the Lie derivative. Furthermore, a procedure to remove the unobservable modes and to design software sensors in the presence of disturbances is proposed.

The main objective of the work on state observers and parameter estimators design is to achieve on-line estimation of non-measurable concentrations and parameters based on extended Kalman filters. Initially, on-line monitoring of abnormal substrate concentrations is proposed. The designed state observer can detect substrate shock loads with a reasonable response time. Then, as on-line measurements of the biomasses concentrations are not available in real wastewater treatment plants, on-line monitoring of the heterotrophic biomass and autotrophic biomass concentrations is proposed. Finally, a joint state and parameter estimation application is presented, where the reduced model is augmented with an additional state variable. The main objective aims at demonstrating the parametric estimation difficulties when designing software sensors on such complex augmented non-linear model.

The work on robust non-linear filtering is motivated by the fact that the extended Kalman filters presented significant drawbacks. Applications based on $H_\infty$ filtering, in which the model describing the activated sludge process is corrupted by significant process noise is presented. A comparative study between both types of software sensors is performed. The final contribution of this work is toward software sensing applications on an integrated urban wastewater system. A software sensor is implemented on the treatment plant and the sewer network effect on the estimated concentrations is demonstrated through simulation studies.

# Table of Contents

# Part I

# General Introduction to the Integrated Urban Wastewater System

# Chapter I

## Introduction

Water is the most important and precious natural resource in the world, since without it there would be no life on Earth. Between 70 and 75 percent of the Earth's surface is water-covered but only 0.3% of it is available for human necessities. A person can survive several days without food, but on the contrary, the absence of water in an organism can have fatal consequences within days. Therefore, the presence of a safe and reliable source of water has always been a precondition for the establishment of a stable community.

All societies, from the time of early civilisations, had to face problems related to the provision of safe drinking water, flood protection, drainage and sanitation (Chocat *et al.*, 2001). Depending on the geographical location of inhabitants, water related difficulties remain unsolved and others are currently arising. For instance, insufficient drinking water in Africa is leading to a migration of their inhabitants to Europe. It is not surprising that water sources have been the cause of numerous conflicts over centuries. Even in areas of abundance of water, crises in water supplies have emerged due to the effects of human, industries and agricultural wastes upon the environment (Tebbutt, 2002). For instance, untreated industrial wastewater can have drastic consequences on the aquatic life of the receiving water, which may lead to negative impacts on the fishing industry.

Prior to modern society, water was purified naturally with the hydrologic cycle. However, the growing demands of water resources necessitated the introduction and operation of municipal drainage systems. The main objectives were (1) to maintain public hygiene in

order to avoid disease causing bacteria and viruses (e.g. Typhoid, Cholera, Dysentery, Polio, and Hepatitis), which were of a real threat to human health and (2), to prevent flooding. In certain countries, downstream use involving human contact is still a real threat, as some of the bacteria or diseases remain in the water (Tebbutt, 2002). The introduction of wastewater treatment plant facilities was initially proposed to enhance the natural cycle and improve the water quality in order to avoid environmental damages. However, it is an individual approach that is not often sufficient to prevent the menace of the polluted water. Therefore, today's challenge is to move from this individual consideration to an integrated management of the urban wastewater system. Consequently, the consideration of an Integrated Urban Wastewater System (IUWS), as presented in Figure (1.1), is an essential step in reducing the pollution level of the receiving body (also called receiving water).

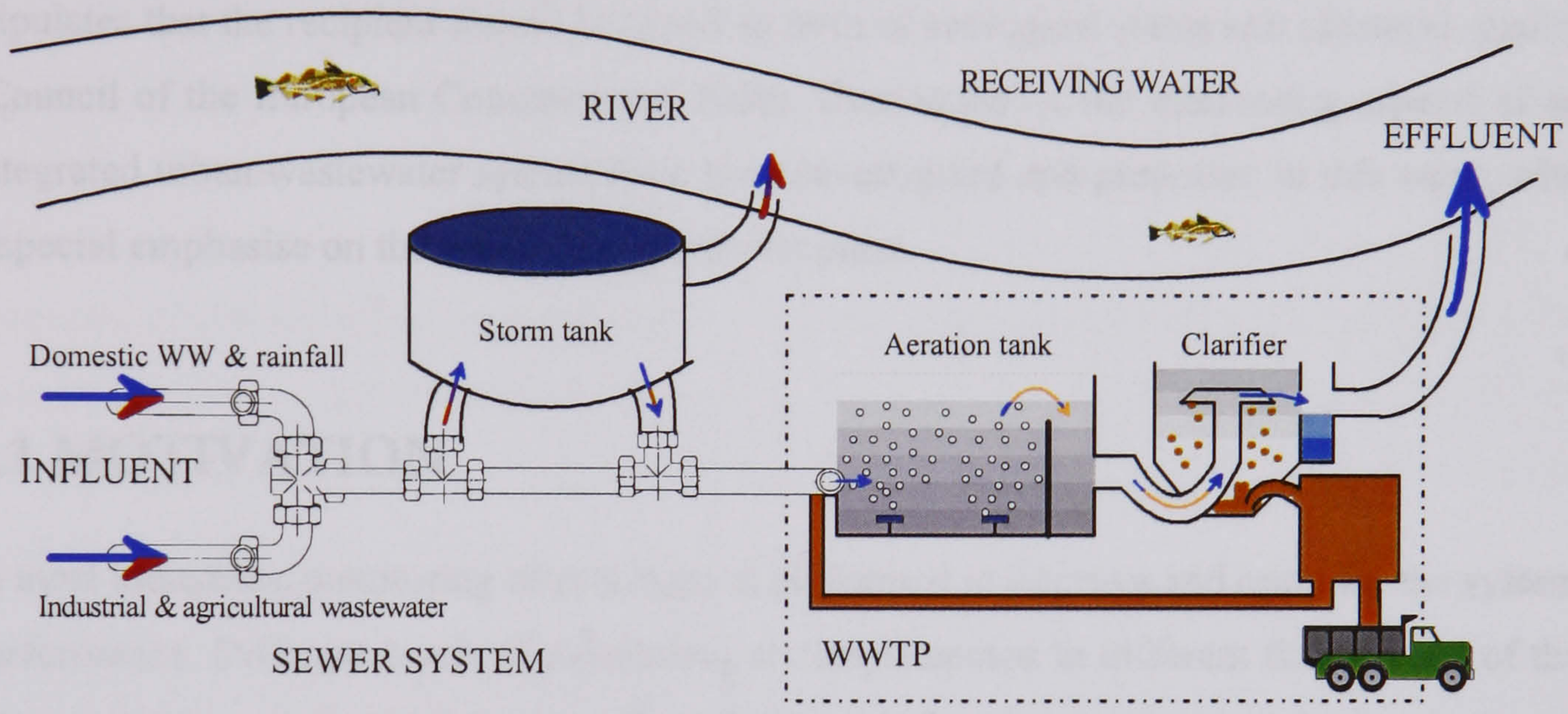


**Figure 1.1** A simplified integrated urban wastewater system including the sewer network, a storm tank utilised for combined sewer overflows, the wastewater treatment plant and the recipient (also called receiving water/body), which in this case assumed to be a river. Note that certain parts of the global water system such as the raw water source, water purification plant, rural streams, groundwater, agricultural runoff and seas will not be considered in this thesis for the reasons of simplification.

The main difficulty with an integrated approach is the high complexity involved in the prediction of the system's behaviour. Appropriate numerical tools, which involve mathematical modelling, remain probably the best solution to describe the dynamic

behaviour of such complex systems. In addition, they are also important in the design of monitoring and control strategies, and in assessing their effectiveness. The modelling stage is probably the most critical phase in the solution of estimation and control problems (Jeppsson, 1996), due to high nonlinearities together with important uncertainties and disturbances. Furthermore, any advanced (or simple) monitoring strategies are based on models that must carefully describe the dynamics of the systems. Within the bioprocess industry, even if the basic principles are known (Lijklema *et al.*, 1993), the complete systems behaviours are not clearly understood and are still undergoing intensive research.

Even if integrated urban wastewater systems remain complex, it is probably a suitable solution to enhance the quality of the receiving water in order to comply with the recently adopted Water Framework Directive (WFD) of the European Union (EU). This directive stipulates that the recipient should be 'good' in term of ecological status and chemical quality (Council of the European Communities, 2000). Consequently, the monitoring aspects of an integrated urban wastewater system have been investigated and presented in this work, with a special emphasise on the wastewater treatment plant.

## 1.1 MOTIVATION

In most industries, monitoring of processes is performed to improve and optimise the system performance. Different levels of monitoring are implemented in different fields. State of the art monitoring technologies are often developed for the nuclear, petrochemical and pharmaceutical industries. Wastewater treatment industries cannot be considered as pioneers in the monitoring field and are still far from being the most diligent and systematic users of such technologies. However, the enforcement of governmental regulations or those of other authorities has forced industries to consider more than few keys influent qualities in order to improve the quality of discharged wastewater (Rosen, 2001).

Water has become one of the sectors with the most widespread coverage in EU environmental regulation. This has been motivated by European inhabitants, who believe that wastewater issues should be prioritised by governmental institutions. Therefore, water directives characterise the different stages of environmental policy regulation with an emphasis on public health protection, environmental protection, “end of pipe” solutions, and preventative and integrated management approaches. The recently adopted WFD of the EU, initiated a new area in EU environmental policy, setting common approaches and goals for

the management of water in 27 countries that should conform in the long-term with community law.

Ecosystem-based objectives and planning processes at the level of the river basin are institutionalised by the WFD, which set a fundamental objective of 'good' overall river quality. However, the challenges in reaching this goal within the time-scale are immense. For instance, a significant progress has been made regarding point source pollution while there has been less achievement with the abatement of dispersed pollution. In fact, scientific questions have emerged concerning the precise qualitative and quantitative understanding of how dispersed pollution deteriorates the ultimate receiving water (Johnson *et al.*, 2001).

Significant changes are also undergoing regarding the industry aspects of the urban cycle (water-wastewater-river-basin). In many countries, localised and fragmented organisations are often selected in the industry to work in a unified operational framework. In some cases, creations of the necessary corporate infrastructures for holistic control of water and wastewater resources are merged between public bodies and companies. Therefore, these practices, which are often slow moving, require new organisational working methods to be established. Thus, integrated computer system operations on a regional river basin scale are a pre-requisite for an industry, which is traditionally passive, and often rely on manual control systems (Johnson *et al.*, 2001).

Regional management of the water and wastewater resources on river basin level can be seen as a large-scale geographically distributed control system problem. The level of difficulty is technologically comparable to the management of a nation's high voltage transmission network, or any other of the high-tech utility networks that support urbanisation. Comparing these well-supported networks with regional wastewater treatment and river basin water quality control, a clear insufficient investment in control infrastructure or basic research has emerged. If regional river basin and energy efficient wastewater treatment process is to be a success, a clear understanding of the system dynamics and an efficient development of systems engineering is required (Johnson *et al.*, 2001).

Thus, a European Network named 'WWT & SYSENG', which is in collaboration between seven institutions of the EU (University of Strathclyde, Lund University, Technical University of Denmark, Imperial College, Universitat Autonoma de Barcelona, University of Pavia, Technical University of Crete), has been created in 2001. The WWT&SYSENG

project, which is an abbreviation for 'Getting Systems Engineering into Regional Wastewater Treatment Strategies', was initiated and financed by the European Commission in order to develop tools and concepts required to investigate some of the following questions:

- How can the regionally integrated sewer systems, wastewater treatment plants and the receiving water system be modelled and simulated?
- What is the importance of diffuse pollution sources, and to what extent are they controllable?
- What large-scale control systems are needed to achieve the EU regulatory requirements? How would these large-scale control systems be implemented?
- What is the impact of Internet technologies on the operation of the control system?
- How should individual wastewater treatment plants and sewer systems be run inside this large-scale control system framework?

Not all key aspects of the above mentioned targets are covered in this thesis. It is the objective of all 'young researchers' of the WWT&SYSENG network, as a group, to tackle these problems.

An IUWS approach alone would not be sufficient in contribution to the fulfilment of the WFD. Other established practices related to Instrumentation Control and Automation (ICA) need to be incorporated within the entire system. However, within the last three decades, the use of ICA in WWTP for instance, is still considered as minimal. The main reasons for this lack of process control is summarised as follow (Beck, 1986; Olsson, 1994; Vanrolleghem, 1994):

- A lack of a clear understanding of the treatment processes
- Inadequate and insufficient instrumentation
- Plant constraints (e.g. insufficient possibilities to act on the processes)
- Economic motivation (ICA does not directly lead to increased profit)
- Lack of education/training of the operators and engineers
- Insufficient communication between operators, designers, equipment suppliers, researchers and government regulatory agents.

Even when ICA is considered within certain WWTPs and/or the entire urban wastewater treatment system, other problems arise due to the complexity of the processes. A particular issue is related to the monitoring and control strategies that are designed for processes. A schematic representation of a typical computerised control chain is represented in Figure (1.2).

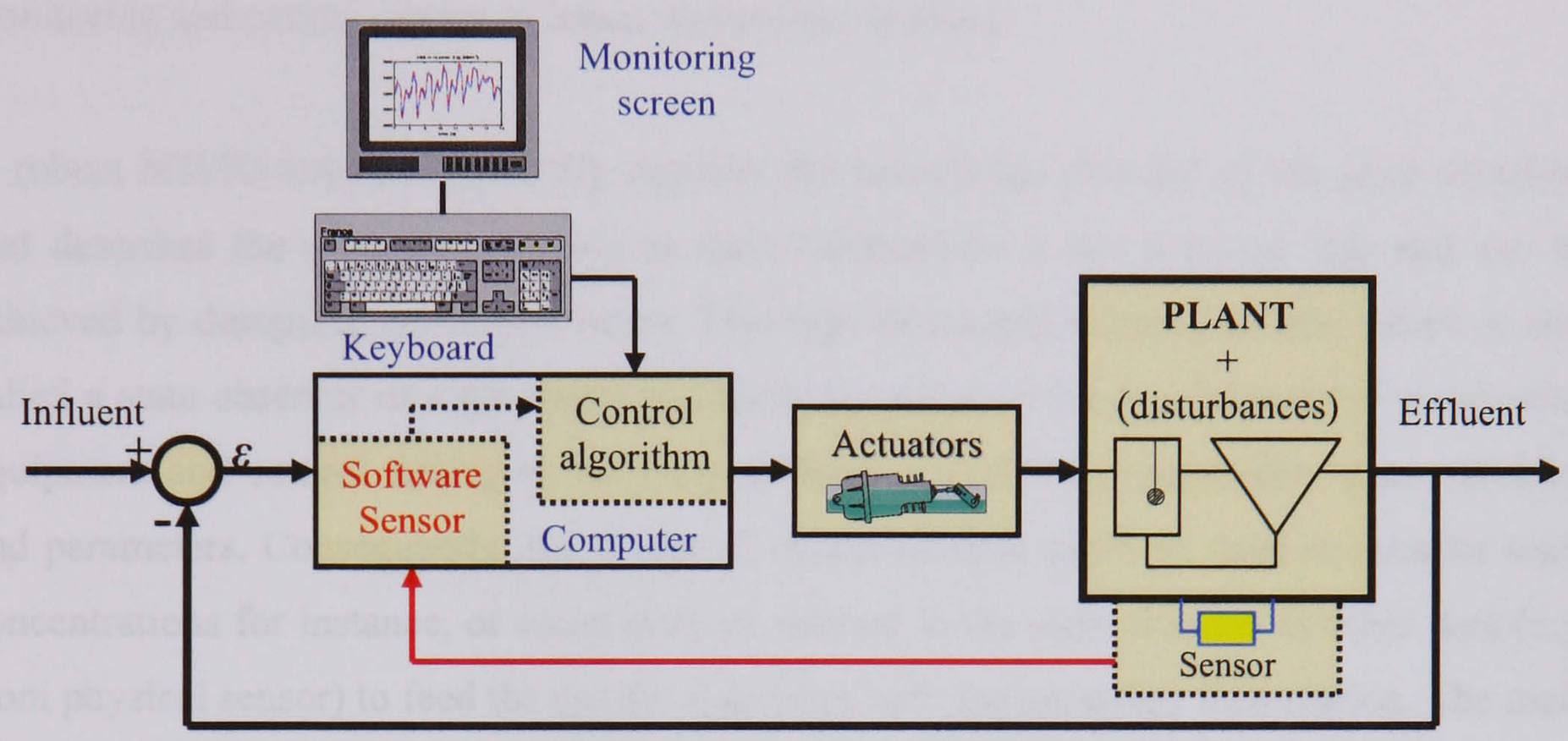


**Figure 1.2** A typical computerised control chain for WWTPs. The physical sensors feed the software sensor, which contribute in governing the quality of the control algorithm.

For instance, some of the obstacles that must be overcome when monitoring urban wastewater systems can be described as follow:

- High non-linearties and complexities in the models
- Stochastic properties of the models
- Large disturbances in the influent flow
- Sensors failures, time delays and measurement noise
- Multiple time scale (very slow and fast dynamics)
- Coupling of the state variables describing the processes
- Lack of flexible actuators

Furthermore, some of the available models that describe the plant behaviour are not observable and identifiable. For instance, the model considered as state of the art for the modeling of Activated Sludge Processes (ASP, e.g. the ASM1), which has been developed

by the International Water Association (IWA, Henze *et al.*, 2000), is not observable. In addition, the most common control strategies implemented in WWTPs, which are developed with simple Proportional Integral Derivative (PID) controllers, are commonly based on Single-Input Single-Output (SISO) design. Consequently, it is extremely difficult to guarantee the robustness of the proposed control strategies. Hence, the use of Multiple-Input Multiple-Output (MIMO) design is a pre-requisite for improving the above-mentioned monitoring and control aspect of urban wastewater systems.

A robust MIMO structure generally requires the knowledge of most of the state variables that describes the processes. Access to such information is not a trivial task and can be achieved by designing software sensors. This type of computer-based sensor, which is also called a state observer or a parameter estimator is crucial in the development of monitoring equipment and control strategies, as it can estimate on-line non-measurable state variables and parameters. Consequently, the produced estimated data could be used to monitor toxic concentrations for instance, or could even be utilised in the same manner as other data (e.g. from physical sensor) to feed the control algorithm with the necessary information. The main drawback when designing such estimators relies on the accuracy of the estimates, which is clearly dependent on the quality of the available measurements and mathematical models that describe the ASP behaviour. The design of state observer and software sensors, which is a key issue in the monitoring of urban wastewater systems, has been investigated, with a special emphasis on the WWTP, and will be presented in this work.

## 1.2 OBJECTIVES

Increasingly, scientific arguments are presented stating the importance of considering the IUWS as one system rather than regarding it as different sub-systems if cost-effective quality of the receiving water is to be achieved (Lijklema *et al.*, 1993; Rauch *et al.*, 1998; Schilling *et al.*, 1997; Meirlan, 2002). Furthermore, an IUWS approach could also be utilised for the design of control strategies, which could be a promising approach to achieve the water quality standards (Rauch and Harremoës, 1999). As a result of this, and since it is impossible or extremely expensive to directly monitor all discharges into the receiving water (Combined Sewer Overflows (CSOs), WWTP effluents, storm water outfalls), an integrated approach has been selected to investigate the monitoring aspects of urban wastewater systems, with a special focus on the wastewater treatment plant.

More precisely, the specific purpose of this work is related to the development of monitoring equipment that will allow an accurate or approximate estimation of concentrations that cannot be measured in real urban wastewater systems. The main technique that is used to achieve such goals is the design of advanced and robust non-linear filtering and estimation techniques. This type of approach has been investigated to overcome the lack of instrumentation. Gaining access to such data could provide a better understanding of urban wastewater systems behaviour. As a result of this work, robust control strategies could eventually be considered and an adjustment of the plant's operational strategy could also be performed to improve the plant effluent quality, or to reduce the pollutant impact of the receiving water and offer cost reductions of operation of the IUWS.

## 1.3 OUTLINE OF THE THESIS

In order to make the content more comprehensible, and also to make it easier for the reader to locate areas related to his/her special interests, this thesis is organised in three different parts.

- Part I (Chapters I, II and III): General introduction to problems related to wastewater treatment, followed by a descriptions of the elements composing the IUWS, as well as definitions and derivations of the theories behind software sensors;
- Part II (Chapters IV, V and VI): Main contributions of the thesis, related to linear piece-wise and non-linear observability, the development of observable reduced-order models and the design of state observer and software sensors based-Extended Kalman Filter (EKF) and Extended H-infinity Filter (EHF) on various WWTPs and an IUWS;
- Part III (Chapters VII): Conclusions and future works.

The seven Chapters are organised in the following way:

**Chapter II:** *The integrated urban wastewater system*

In Chapter II, a brief introduction to the main elements that form the IUWS is provided. This includes the sewer system, wastewater treatment plant and receiving water. A review of state-of-art in monitoring and sensing for all sub-processes and the IUWS itself is also provided. Then, the Chapter includes a discussion of the mathematical models that have been

selected for describing the sewer, WWTP and river, as well as the interactions issues within all sub-systems. Simulations studies are proposed to illustrate the CSOs flow effects on the river. A summary of the aforementioned topics ends this Chapter.

**Chapter III:** *Non-linear state and parameter estimation*

Chapter III provides the theoretical background used throughout the thesis, selected to perform joint state and parameter estimation. A brief historical review of the most common linear and non-linear filtering techniques is initially proposed. Then, the selected linear and non-linear observability theories are presented. Subsequently, the algorithms for the linear and extended Kalman and $H_\infty$ filters are introduced, prior to a brief discussion on parameter identifiability. Finally, two examples based on an ASP model are proposed for on-line monitoring of the concentrations and some model parameter estimations based on the extended Kalman and $H_\infty$ filters. The proposed results aim at illustrating the multiple-parametric estimation problems, the drawbacks of the EKF with a stochastic model, as well as the measurement noise effect on the parametric estimation. This Chapter ends with a brief summary of the Chapter content and its results.

**Chapter IV:** *Non-linear Observability of WWTP models*

In Chapter IV, three reduced-order models based on the original ASM1, which is first introduced, are proposed. Initially, the simplifying assumptions in producing these reduced models are described, as well as their dynamics behaviour compared with the original ASM1 model. Following this, piece-wise linear observability analyses are performed on each of the reduced models. Subsequently, non-linear observability analyses are performed, based on Lie-derivatives, and the results are compared with the piece-wise approach, yielding interesting results. Finally, a general procedure for model reduction and software sensor implementation is proposed. This Chapter ends with a conclusion of this study and its simulations results.

**Chapter V:** *Non-linear filtering based-extended Kalman filters*

Chapter V presents three case studies with a focus on the WWTP. These applications aim at providing estimates of concentrations and parameters that cannot be measured on-line in real WWTPs. The initial case study emphasises the general procedure proposed in Chapter IV. A

state observer with unknown input concentrations, also called disturbances, is implemented. The method that is selected is based on an augmented model were the unknown inputs are modelled with 1st order and 2nd order transfer functions, fast Fourier transform and spectral analyses. Furthermore, particulate nitrogen estimation is achieved based on fractions of the slowly biodegradable substrate ($X_S$). The subsequent case study proposes a new approach for on-line monitoring and detection of abnormal readily biodegradable substrate ($S_S$) and slowly biodegradable substrate ($X_S$) concentrations, for example due to influent substrate shock load. Considering that off-line measurements of $S_S$ and $X_S$ concentrations are not available in real WWTPs, the $S_S|X_S$ state observer provided significant results as it can detect these abnormal substrate concentrations with a fast response time. The final application, separated into two cases, first illustrates a state estimation application were the heterotrophic and autotrophic biomasses concentrations are estimated on-line, using fraction of the TSS concentration. This case study also yielded interesting results as on-line monitoring of $X_{B,H}$ and $X_{B,A}$ concentrations is not available on WWTPs, since no specific on-line sensors exist for these concentrations. Finally, the last case illustrates a joint state and parameter estimation algorithm, where the heterotrophic yield is estimated on-line by a software sensor based-EKF. It demonstrates the parametric estimation difficulties when applied to a complex non-linear reduced model, as well as the need for a robust non-linear filtering technique. The Chapter concludes with a conclusion of the main results.

**Chapter VI:** *Robust non-linear filtering based-extended $H_\infty$ filters*

In Chapter VI, a robust non-linear filtering technique, based on extended $H_\infty$ filter, is investigated. The first application concentrates on illustrating the observers' robustness properties with a stochastic ASM1 model (e.g. corrupted by unknown process noise source statistics). The convergence and tracking performances of the state observer are also investigated when disturbances are considered and results are compared with the standard extended Kalman filter. It is demonstrated that robust estimation can be achieved with stochastic models when an extended $H_\infty$ filtering technique is considered. In the second application, the robustness properties of the EHF are investigated, and compared with the EKF, when joint state and parameter estimation is considered. Furthermore, the software sensor performances are investigated when sudden variations in a selected stoichiometric parameter occur. The final application concentrates on state observers based-EKF and EHF when applied to the integrated urban wastewater system. The main objective, which is to illustrate the impact of the sewer system on the WWTP estimated concentrations, is

demonstrated through simulation results. Finally, the Chapter ends with a conclusion of these comparative studies and its simulations results.

**Chapter VII:** *Conclusions and future works*

In Chapter VII, general conclusions and direction for further work concerning the proposed results are discussed.

## 1.4 CONTRIBUTIONS

The major contributions are in the areas of (in order of appearance in the thesis):

**Development of reduced-order ASM1 models**

In Chapter IV, three reduced-order models are developed based on the original activated sludge model no.1. The simplifying assumptions are clearly stated and their dynamics are compared with the original ASM1 model. These reduced models present the advantages of being accurate enough for the proposed monitoring applications. Furthermore, their performances are compared with well established IWA/COST benchmark simulation model no.1.

**Linear piece-wise and non-linear observability analyses comparison**

In Chapter IV, a linear piece-wise approach is investigated for the proposed reduced models. This approach is compared with a non-linear observability analysis method, based on the Lie derivatives. This comparison revealed that the linear piece-wise approach can be applied, to a certain extent, to non-linear systems.

**General procedure for model reduction and software sensor implementation**

A general procedure for model reduction and software sensor design has been proposed. It is based on a six steps procedure, which provides methods for model reduction, observability analyses, modelling disturbances and finally, joint state and parameter estimation algorithm implementation.

**State observer and software sensors for bioprocesses**

In Chapter V, various state observers and software sensors are applied on the WWTP. This work contributes in the development of monitoring equipment that are currently not

available in the market. The main applications are proposed to overcome the lack of monitoring equipment. Firstly, a new SS|XS state observer, which can detect abnormal substrate concentrations within the WWTP, is proposed. Secondly, a novel approach for heterotrophic and autotrophic biomass concentrations monitoring based on total suspended solid measurements is investigated. Finally, joint sate and parameter estimation are demonstrated, where the heterotrophic yield is estimated online.

**Robust non-linear filtering for bioprocesses**

In Chapter VI, robust nonlinear filters based on extended $H_\infty$ filtering theory are developed. This approach is particularly useful with stochastic biological systems, as the noise source statistics are unknown. A comparative study between the EKF and EHF is performed to demonstrate: (1) the failure of the EKF when the mathematical model describing the plant behaviour is stochastic, and (2) the tracking and robustness performances of the EHF with similar stochastic properties.

## 1.5 Publications

Several parts of the work presented in this thesis have previously been presented at international / national conferences and workshops. A list of the references is given below. Several parts of the work might also lead to international journal publications in the coming future. However, these have been excluded from the following list.

**2003**

Benazzi, F., Katebi, R. and Wilkie, J. (2003). Application of Extended Kalman Filter to Activated Sludge Process. *2nd WWT&SYSENG Workshop, EU Research Training Network, HPRN-CT-2001-00200*, September 17-20 2003, Copenhagen, Denmark.

**2004**

Benazzi, F. and Katebi, R. (2004). Software Sensor Based-Extended Kalman Filter Applied to Activated sludge Process. *3rd WWT&SYSENG Workshop, EU Research Training Network, HPRN-CT-2001-00200*, September 5-11 2004, Pavia, Italy.

**2005**

Benazzi, F. and Katebi, R. (2005). Nonlinear Observability of Activated Sludge Process Models. *In Proc. 16th IFAC World Congress*, July 4 – 8 2005, Prague, Czech Republic.

Benazzi, F, Linblom, E. and Katebi, R. (2005a). Software sensor application to WWT processes and future perspectives when applied to integrated urban wastewater systems. *In Proc. 4th World Wide Workshop for Young Environmental scientists*, 10-13 May 2005, Paris, France.

Benazzi, F., Gernaey, K.V., Jeppsson, U. and Katebi, R. (2005b). On-line Estimation and Detection of Abnormal Substrate Concentrations in WWTPs using a Software Sensor: A Benchmark Study. *In Proc. 2nd IWA Conference on Instrumentation, Control and Automation (9th ICA series)*, 29 May - 2 June 2005, Busan, Korea.

Benazzi, F., Gernaey, K.V. and Katebi, R. (2005c). Joint state and parameter estimation based extended Kalman filter of activated sludge processes. 4th *WWT&SYSENG Workshop, EU Research Training Network, HPRN-CT-2001-00200*, August 20-25 2005, Crete, Greece.

Benazzi, F., Jeppsson, U. and Katebi, R. (2005d). On an Application of Extended Kalman Filtering to Activated Sludge Processes: A benchmark study. *In Proc. 10th International Conference on Urban drainage*, August 21 – 26 2005, Copenhagen, Denmark.

Benazzi, F., Gernaey, K.V. and Katebi, R. (2005e). Joint state and parameter estimation based extended Kalman filter of activated sludge processes: A benchmark study. *In Proc. 17th European Symposium and Exhibition*, October 20-22 2005, Marseille, France.

**2006**

Benazzi, F. and Katebi, R. (2006). Extended Kalman filter versus extended $H_\infty$ filter - An application to activated sludge processes. *In Proc. 6th UKACC Control Conf*, 30 August - 1 September 2006, Glasgow, UK.

Benazzi, F., Steyer J.P. and Katebi, R. (2006). On an application of extended $H_\infty$ filtering to activated sludge processes: a benchmark study. *In Proc. 4eme colloque STIC et Environement*, April 5-7 2006, Narbonne, France.

## Reports

Benazzi, F. and O'Brien, M. and Wilkie, J. (2003). "Control Technology Report" (J. Wilkie ed). *Technical report, EU Research Training Network, HPRN-CT-2001-00200*, February 2003, Glasgow, UK.

Benazzi, F., Botond, R., Boguniewicz, J., Chindris, B., Comas, J., Gernaey, K.V., Lazar, C., Lindblom, E., O'Brien, M. and Tapia, G. (2005). "System Process Modelling Report" (Lindblom, E., Raduly, B. and Mikkelsen, P.S. eds). *Technical report, EU Research Training Network, HPRN-CT-2001-00200*, March 2005, Copenhagen, Denmark.

Benazzi, F., Boguniewicz, J., Chindris, B., Comas, J., Gernaey, K., Lazar, C., Lindblom, E., O'Brien, M., Raduly, B. and Tapia, G. (2005). "Case study Report". (Capodaglio I.A.G ed), *Technical report, EU Research Training Network, HPRN-CT-2001-00200*, January 2005, Pavia, Italy.

Benazzi, F., Boguniewicz, J., Chindris, B., Comas, J., Gernaey, K., Lazar, C., Lindblom, E., O'Brien, M., Raduly, B. and Tapia G. (2005). "Simulation study Report". (Papageourgiou, M. ed), *Technical report, EU Research Training Network, HPRN-CT-2001-00200*, Decembre, Crete, Greece.

# Chapter II

# The Integrated Urban Wastewater System

In this Chapter, the simplified integrated urban wastewater system displayed in Figure (1.1), which is composed of a sewer system, WWTP, and receiving waters as its main element, is presented. Firstly, a short introduction of the physical elements that compose the IUWS is provided, in addition to the common monitoring equipment and actuators available within each sub-process. Secondly, the modelling aspect of the IUWS is presented with a simplified mathematical description of the sewer network and river. The ASM models are also introduced with a special emphasis on the IWA/COST Simulation Benchmark No.1 (BSM1), which is the principal WWTP configuration utilised throughout this thesis. Finally, a simulation study is performed to provide an insight into the IUWS model where some impacts of combined sewer overflows are illustrated.

## 2.1) INTRODUCTION

Many of the urban wastewater systems that can be found in practice are operated with little or no control (Schütze *et al.*, 2004). This can be explained by the fact that on-line monitoring equipment within the area are very poor. Very few advanced case studies can be found in literature (Schilling, 1989; Meirlaen *et al.*, 2001; Meirlaen and Vanrolleghem, 2002; Schütze *et al.*, 2003; Schütze *et al.*, 2004). An explicit state of the art review of Real Time Control (RTC) of urban wastewater systems is proposed by Schütze *et al.*, (2004). The author and co-workers discussed the importance in the development of sensors, which also include software sensors, in achieving successful control strategies on IUWS. Nevertheless, prior to

any design or implementation of software sensors, a clear understanding of the system is necessary. Consequently, the following description of the IUWS is provided for a better understanding of the selected urban wastewater system.

## 2.2) PHYCAL DESCRIPTION OF THE INTEGRATED SYSTEM

As mentioned previously in Chapter I, the global water system is linked with other parts such as drinking water production, groundwater, rural streams, agricultural runoff and seas. However, the focus of this work lies in state observer and software sensor design and its implementation upon an urban wastewater system. Therefore, only the corresponding subsystems are discussed.

### The sewer system

According to Smith and Scott (2002), waterborne sewage systems existed in India around 4500 Before Christ (BC) and near Baghdad about 2500 years BC. Modern urban sewerage and drainage concepts date back some 200 years (Harremoës, 2002). Today's sewer system technologies, which are used to transport both rainwater and wastewater from the urban area until the WWTP or receiving waters, mainly consists of interconnecting pipes. These pipes, which constitute the main elements of the sewer systems, are either combined, separated or partially separated systems. These types of sewer systems still form the majority of modern sewer systems all over the world (Brombach *et al.*, 2005). A schematic overview of combined and separate sewer systems is displayed in Figure (2.1). A brief description of each type of sewer pipes is provided, as follows:

- The combined sewer system: It has a unique pipe where stormwater, domestic wastewater and industrial effluents are transported and mixed together. The main advantage of the combined sewer system is only cost related, as only one pipe is needed. However, this technology presents disadvantages by reducing the efficiency of the treatment plant during periods of heavy rains. When the flow to the treatment plant increases, whilst the pollutants are diluted, the flow in the sewer system becomes higher than the hydraulic capacity of the pipes or the WWTP. Consequently, combined sewers are generally supplied with combined CSOs that divert excess wastewater flow down a stormwater sewer and thence into the nearest

receiving water (Smith and Scott, 2002). However, CSOs structures do not avoid critical pollution at discharge points.

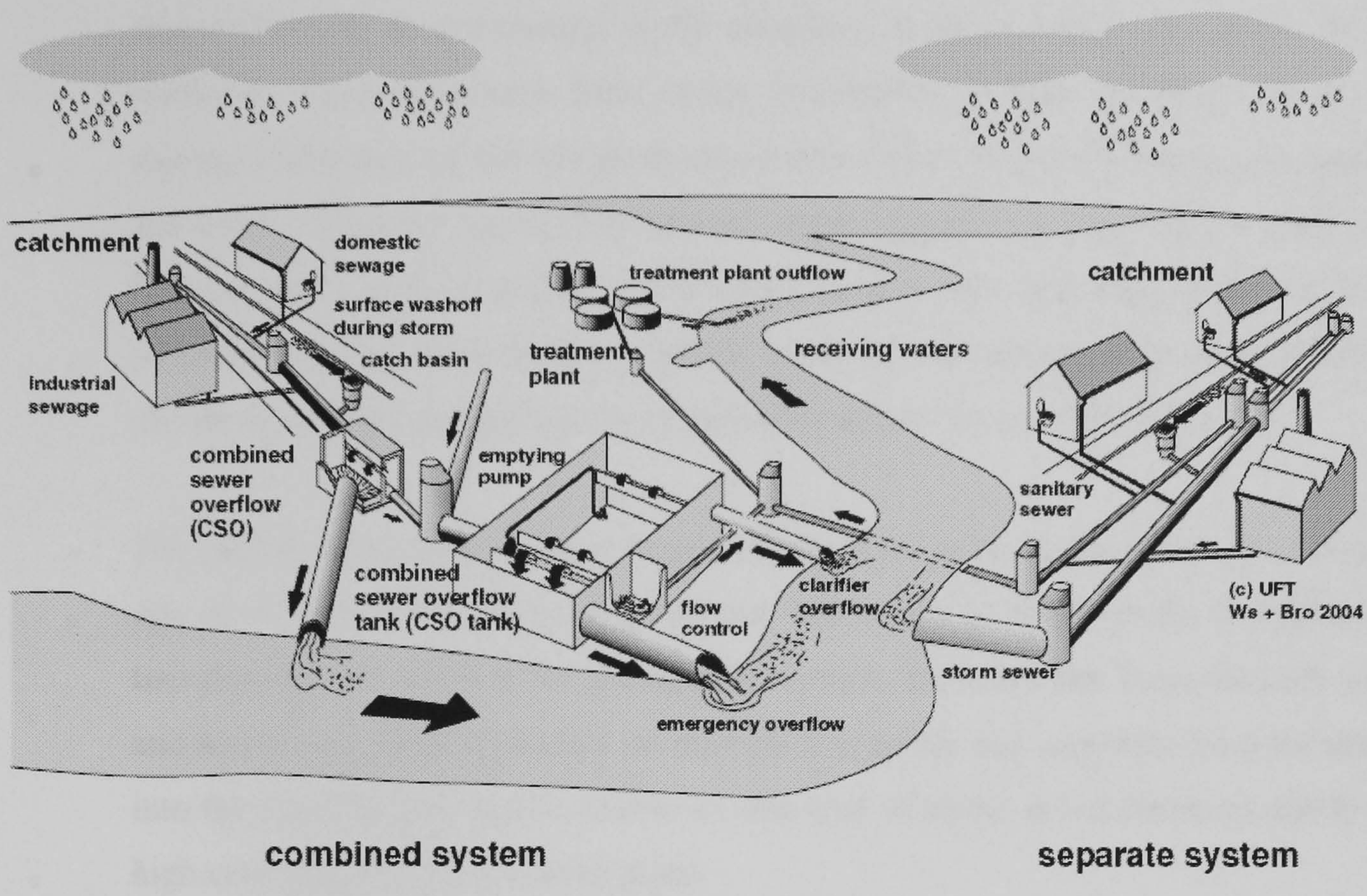


**Figure 2.1** Combined and separate sewer systems including CSO structures and the WWTP (from Brombach *et al.*, 2005)

Some of the common solutions that can be used in reducing the number of CSOs are related to ICA implementation, stormwater infiltration and building (or increasing if basins are already available) storm tanks. However, such approaches requires a clear understanding of the current wastewater treatment facilities in order to avoid drastic expenses without systematically reducing the pollution peaks at the discharged points. Furthermore, throughout western societies, sustainable urban drainage methods are becoming a driving force (Chocat *et al.*, 2001). This consists of incorporating permeable surfaces, ponds, swales and other infiltration devices, for a maximum infiltration of the wastewater into the soil and for the recharging of the ground water (Smith and Scott, 2002). These types of drainage techniques, introduced in the late 1980s (Chocat *et al.*, 2001) are more and more used in urban areas such as in France, for instance, with the advantage of not requiring any downstream drainage network (Barraud, 2002).

- The separate sewer system: Also called the rigidly separate system, this is composed of two different pipes, one conveying the stormwater, the other transporting the domestic wastewater and industrial effluents towards the treatment facility. As a result, the stormwater is discharged directly into the receiving water and should not cause pollution, in comparison to the combined systems (Smith and Scott, 2002). However, separate systems have major drawbacks, as they are likely to be (1) expensive (because of the two pipes required to avoid mixing processes), (2) sudden and strong hydraulic impact to rivers can occur, (3) there are risks of misconnection between pipes and (4) higher heavy metal load to the receiving water can arise (Meirlaen, 2002). Nevertheless, separate systems will overcome the peak pollution discharge problem during high rainy periods that can occur from CSOs.

- The partially separated sewer system: This is a system in which each street has two sets of sewer, one for stormwater and one foul sewer. In other words, it consists of two separate networks, as for the separate system, but rainwater from the back yard and house back roofs is drained off into the foul sewer and rainwater from the roads into the surface water sewer. However, this type of sewer is not common due to its high cost requiring two network pipes.

Nowadays, the most common sewer systems are of the combined despite the fact that they are regarded as causing high pollution and hygienic risks. However, there is a strong worldwide trend (at least in industrialised nation) toward separated systems regardless of the high construction and maintenance costs. In the United States, for instance, the Water Act of 1972 (WEF, 1997) recommends separate systems. On the other hand, Brombach *et al.*, (2005) concluded that the cost-benefit ratio of a separate sewer system is unfavourable when compared with that of the combined system. Therefore, an alternative approach in reducing CSOs impacts upon the receiving water remains the implementation of monitoring tools (e.g. software sensors). Such techniques are undoubtedly dependent on sensors, which are generally expensive and sometimes not reliable, and still remain a challenging solution in the wastewater industry. Sensor technologies could offer particular advantages for early warning systems, process control and on-line monitoring of the sewer system (Alcock, 2002), which could contribute in reducing peak pollutions discharges into the receiving water. Indeed, perfect reliability of the results within the sewer facilities is not ensured because of the measurement state conditions (Piatyszek, 2002). Therefore, access to on-line concentrations of the pollutants, rather than obtaining data only during a particular event, could be more

beneficial in ensuring that results accurately represent the state conditions. Furthermore, such approach could lead in a long-term basis in the investigation and implementation of robust control strategies.

## Monitoring

Sensors are mainly used for three different purposes: (1) for monitoring (operator support), (2) in automatic control systems and (3) as tools for plant auditing/ optimisation /modelling of consultant (Vanrolleghem and Lee, 2003). They can provide an added value in monitoring pollution in wastewater (Alcock, 2004; Dominguez and Alcock, 2002) and are crucial for the control of urban wastewater systems. They can govern the accuracy and reliability of the proposed controlled processes. Access to data from instrumentation is also essential for the design of control strategies. In addition, it could be useful in practice to obtain accurate data for a number of reasons that include:

- Inspection by governmental enforcement agencies of compliance with source measurement requirement
- As a legal evidence of compliance
- Health and property protection for both workers and public at large

On-line monitoring of pollutant concentrations in the sewer system remains a challenging area. Nowadays, it is mainly performed via sample analysis within laboratories (Bertrand-Krajewski, 2004). Piatyszek (2002) stated that measurement devices are widespread within the sewer system. On the other hand, the growing demand for sensing technologies is still of significant interest and there is still a strong need in the conception of applications. Few attempts have been made to overcome this lack of instrumentation. Hansen and Carstensen (1997), successfully performed an on-line monitoring investigation of the sewer system of Copenhagen during four years. A total of nine monitoring stations were used, where measurements of water levels, flows, rainfalls, pumping activity and gates positions were collected. In addition, an ultrasonic and pressure transducer and two different type of ultrasonic transmitter were utilised. However, it was concluded that RTC systems are vulnerable to failures in the on-line monitoring system. Gudjonsson *et al.*, (2002), measured continuously (upstream and downstream) during two months the Dissolved Oxygen (DO) in an intercepting sewer. However they failed to predicted short-term variations due to the insufficient knowledge of the variability of the wastewater composition.

## State of the art sensing

State of art sensing for sewer systems has found very few successful applications, of which those few are mainly achieved through laboratories or pilot systems. Bertrand-Krajewski (2004), performed a Total Suspended Solid (TSS) concentration estimation in a sewer from turbidity measurements. This study compared this approach with a sample concentration measurement technique and obtained satisfactory results. The research concluded by suggesting that turbidity measurements could replace traditional samples. Stumwöhrer *et al.*, (2003), investigated the applicability of Ultraviolet (UV)-absorption measurements at CSOs, under different storm water conditions. This work demonstrated that the applicability of this type of spectrometer for the control of storm water is questionable. Horoshenkov *et al.*, (2003), determined the sewer roughness and sediment properties using acoustic techniques. Results from pilot scale model experiments demonstrated that the proposed acoustic method is very sensitive to the variation in the boundary conditions of an air-filled pipe.

## Actuators

Some of the aforementioned applications would have been impossible without the use of actuators. Indeed, the development of sensors for the purpose of control strategy design involves the integration of actuators in the control chain. Actuators (also called regulators) play an important role in urban wastewater treatment because they can operate or activate the final control element. The most common actuators (electrical, pneumatic or hydraulic) employed are: flow regulators (control valves, position regulators) weirs, gate, dumper, motor, heater and blowers. For a detailed review about actuators, the reader can refer to Marinaki *et al.*, (2003), or Metcalf and Eddy (2003).

# The wastewater treatment plant

The wastewater collected in the sewer system is directly transported to the treatment plant. The WWTP is at the heart of the process dealing with domestic, industrial and agricultural waste. A suitable introduction in the field of municipal wastewater treatment is found in Metcalf and Eddy (2003), Henze *et al.*, (1995), or Andrews (1992). A schematic overview of a typical municipal WWTP configuration is proposed in Figure (2.2). The main objective of domestic wastewater treatment, which is 99% water, is the removal of the 1% pollutants as economically as possible (Smith, 2002). More precisely, WWTPs are about reducing

nitrogen, phosphorous, organic matter and suspended solids. In most countries and cities, the wastewater is treated in biological treatments plants rather than receiving physical treatment (like sedimentation or filtration) or chemical treatment (like precipitation or flocculation), as detailed by Metcalf and Eddy (2003).

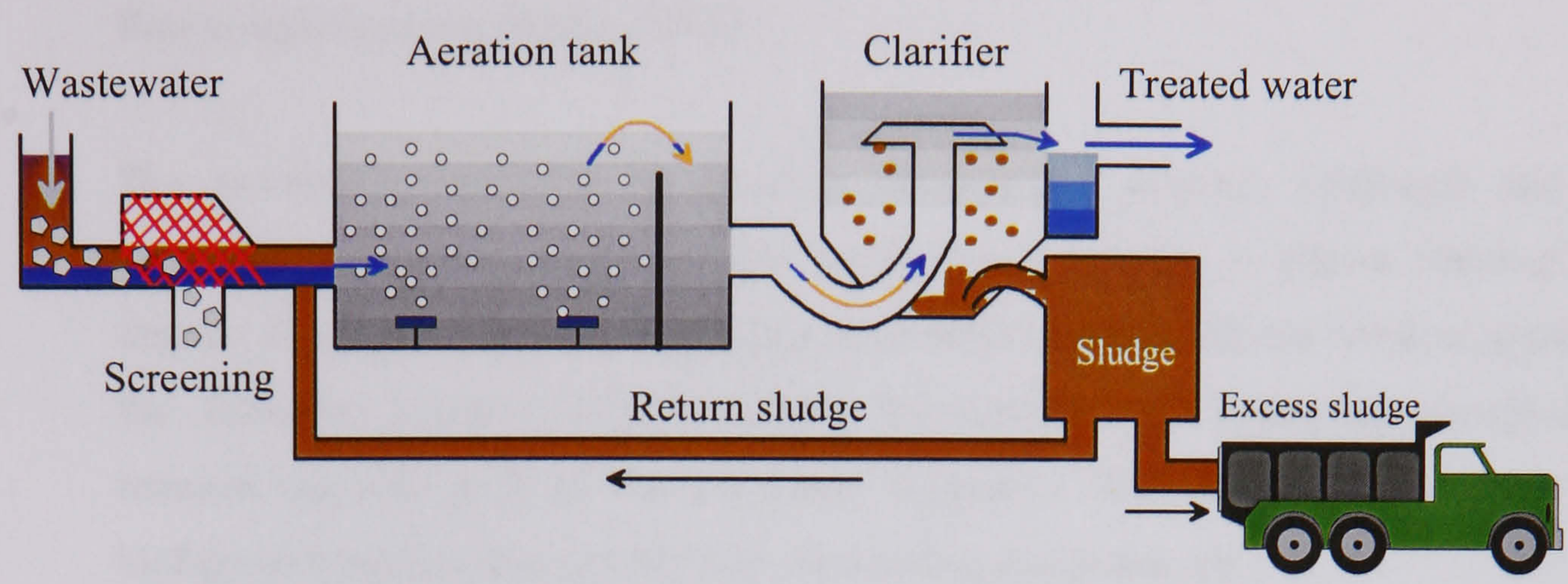


**Figure 2.2** Schematic outline of the main detachment in a municipal wastewater treatment plant.

Furthermore, different plant layout can be designed depending upon effluent quality specifications from local authorities. However, one of the common system configurations consists of unit processes like activated sludge systems, anaerobic systems, biofilters in combination with one or more physical or chemical treatment processes. A brief review of the most common technologies and processes that can be found within the WWTP follows. This description emphasises on the activated sludge process, as the software sensors presented in this work are mainly implemented on this specific unit process.

- *The preliminary treatment:* Also called mechanical treatment, this allows removal and reduction of various types of suspended solids, generally aimed at protecting equipment in later treatment. These mainly consist of the removal of large solids (tyres, Christmas trees, etc.), grit chambers (to separate sand and gravel from the wastewater), rags and grit by screens (for separating materials into sizes), comminutors (for cutting up the solids caught on the screen) and grit channel (for extracting grit from wastewater).

- *The primary treatment:* Also called primary sedimentation, it is the first major treatment process that immediately follows grit removal. It consists of releasing settled wastewater for biological treatment and removes organic solids as sludge.

The design is often based on the surface loading rate, where radial flow sedimentation tanks or horizontal flow sedimentation tanks are normally used. To ensure 50 to 70% removal of suspended solids and about 30% removal of Biological Oxygen Demand (BOD), which is a measure of the amount of biodegradable organic substances in water, from domestic water, a rate of 30 to 45$m^3$ $m^{-2}d^{-1}$ at maximum flow is a prerequisite (Smith, 2002).

- *The secondary treatment:* It typically follows the primary treatment and is commonly composed of an aerobic biological treatment. It allows removal of organic solids (not removed in primary treatment) together with the 90% or more of the dissolved organics (Smith, 2002). Nitrification and biological phosphorus removal are also parts of the secondary treatment. The most common types of biological treatment that can be employed during this phase are:
  - *Aerobic processes:* Based on aeration of the wastewater, this treatment process results in oxidation of the carbonaceous and nutrient material (substrate) by chemical reactions initiated when the biomass utilises these components for biological growth. The carbonaceous material is oxidised to carbon dioxide ($CO_2$) and the nutrients to more benign forms of the compound (Henze, 1997).
  - *Anaerobic processes:* This treatment process occurs in the absence of free oxygen or nitrate. The microorganisms breakdown the complex organic material by hydrolysis to smaller molecules. Acid-forming bacteria break these protein, fat and carbohydrate molecules into long-chained amino acid and fatty acids, amongst other. The products of this process are formic acid, acetic acid, methanol and ethanol, which are further broken down into $CO_2$ and methane ($CH_4$). To successfully perform the degradation stages, this process requires a number of different types of bacteria, which are sensitive to factors such as pH, temperature, toxicity or even oxygen (Henze, 1997).
  - *Anoxic processes:* This treatment process occurs in the absence of free oxygen but in the presence of nitrate, which provides a source of oxygen for denitrifying bacteria.

The principle of activated sludge plant is that of a mass flow of wastewater kept in continuous motion through the plant by gravity, mixing, aeration and pumping. Such approaches lead to a treatment that is performed in an effective and controllable

manner. However, it is essential to maintain the biology in the secondary phase long enough for biomass growth through contact with the substrate and the subsequent associated reactions. The length of time that the biomass remains in the secondary treatment is known as the sludge age. A balance between the sludge age and the hydraulic retention time (HRT) is necessary so that the process kinetics can take place. The Return Activated Sludge (RAS) feedback loop recycles sludge from the secondary clarifier to the aeration tank in order to maintain the sludge concentration. Excess sludge, which is wasted from the secondary clarifier, is treated separately with sludge collect from the primary clarifier. Sometimes, to supplement the nitrate concentration in the anoxic zone, an internal nitrate recycle may also be used. Typically, the anoxic zone (denitrification) is situated prior to the aeration (nitrification) tank. The internal recycle is a loop between the end of the aeration tank and the inlet to the anoxic zone. Various wastewater treatments also involve the addition of chemicals to allow removal of the phosphorus. The chemical treatment process consists of mixing a chemical (typically an iron or aluminium salts) that binds phosphate molecule and forms floc that can be removed by sedimentation. It also contribute to pH adjustment; disinfection by chlorine or ozone; precipitation of heavy metals, often as hydroxides; precipitation of phosphate; conditioning of sludge; water softening, etc. (Smith, 2002).

- *The tertiary treatment:* Also known as effluent polishing or advanced treatment, it is implemented in few plants to further improve the wastewater quality discharged from the WWTP. This last treatment is often considered in the plant design when the treated wastewater has to be immediately reused for industrial or semi-industrial purposes (i.e. farming). Otherwise, this solution can also be adopted if the receiving water has a relatively small flow and consequently low dilution. Basically, it consists of removing the fine suspended matter that remains in the effluent (i.e. after aerobic biological treatment) with a consequent reduction in BOD. Tertiary processes also include aquatic based natural treatment systems, maturation ponds, microstrainers, rapid gravity filters, slow and filter. Wastewater disinfection is also sometimes considered as tertiary treatment (Smith, 2002).

Most of the monitoring and control strategies are centred in the secondary treatment, which is where most of the biological treatment occurs. Therefore, sensing technologies within this

treatment is of the main interest as the quality of the estimation provided by software sensors is directly dependent on the available instrumentation.

## Monitoring

At present, and at most treatment plants, there is an infrequent monitoring of wastewater quality. When compared with other process industries, the automation of wastewater systems is not as developed as it should be. This is mainly caused by the hostile environment in which sensors must to be located (Bourgeois *et al.*, 2001). Furthermore, widespread acceptance of sensors is complicated as many of the original WWTP are not designed to further be updates with ICA.

A widespread perception is that sensors represent the weakest link for implementing on-line process control of WWTPs (Harremoës *et al.*, 1993; Vanrolleghem and Lee, 2003). On the other hand, during the last decade, the performance and reliability of many on-line sensors (e.g. nutrient sensors, respirometers) has improved remarkably and can be used directly in many different control strategies (Jeppsson *et al.*, 2002), or for on-line monitoring. Hence, the use of new monitoring equipment should be regarded as a valuable alternative to increasing reactor volumes for outdated treatment plants that require considerable investment in upgrading (Vanrolleghem and Lee, 2003). Ingildsen (2002), Bourgeois *et al.*, (2001) and Vanrolleghem and Lee (2003), provided detailed state of the art reviews of on-line monitoring equipment for wastewater treatment processes. The latter of these classified sensors in two basic types, summarised as follow:

i) Simple, reliable and low maintenance

ii) Advanced, high maintenance and mainly used in auditing, model calibration and optimisation.

The most common sensors, in addition to the most advanced, are described in Table (2.1), reproduced (with permission from the lead author) from Vanrolleghem and Lee (2003). The major contribution of the work proposed in this thesis is in application upon activated sludge processes. Therefore, a more detailed description of sensor characteristics follows. For further information about sensors in anaerobic digestion, nutrient removal and sedimentation, the reader is referred to Bourgeois *et al.*, (2001), Vanrolleghem and Lee (2003).

| Physical measurements | | | Physico-chemical measurements | | | (Bio-) chemical measurements | | |
|---|---|---|---|---|---|---|---|---|
| Variable | Process | Range | Variable | Process | Range | Variable | Process | Range |
| Temperature | G | ∀ | pH | G | ∀ | Respirometry | 2, 3 | ∀ |
| Pressure | G | ∀ | Conductivity | G | ∀ | Toxicity | 2, 3 | ∀ |
| Liquid level | G | ∀ | Oxygen concentration | 2, 3 | ∀ | $BOD_{st}$ | 2, 3 | ∀ |
| Flow rates | G | ∀ | Fluorescence | 2, 3 | ∃ | COD | 1, 2, 3 | O |
| Suspended solids | G | ∃ | Redox | 1, 3 | ∀ | TOC | 1, 2, 3 | ∀ |
| Sludge blanket | 4 | ∃ | $NH_4^+$ (ISE) | 3 | ∀ | $NH_4^+$ | 3 | ∀ |
| Sludge volume | 4 | ∃ | $NO_3^-$ (ISE) | 3 | ∃ | $NO_3^-$ | 3 | ∀ |
| Settling velocity | 4 | O | Digester gas | 1 | ∃ | Micro-scale NOx | 3 | ∀ |
| Sludge morphology | G | O | ($CH_4$, $H_2S$, $H_2$) $CO_2$ | 1, 2, 3 | ∀ | $PO_4^{3-}$ | 3 | ∃ |
| Calorimetry | 1, 2, 3 | O | | | | Bicarbonate alkalinity | 1, 3 | ∃ |
| UV absorption | G | ∃ | | | | VFA | 1, 3 | O |

Process: Unit process in wastewater treatment plants where the sensor can be implemented 1: Anaerobic Digestion; 2: Activated Sludge; 3: Nutrient Removal; 4: Sedimentation; G: All processes. Applicability Range: ∀: State of the Technology; ∃: Application in certain cases; O: Requires development work

**Table 2.1** State of art on-line monitoring equipment for WWT processes (from Vanrolleghem and Lee, 2003)

## Sensors characteristics for activated sludge

The DO sensor is probably the most widespread instrument within WWTPs. It is considered reliable and accurate but care is pre-requisite for proper location installation and for fouling prevention (Watts *et al.*, 1990; Harremoës *et al.*, 1993). In activated sludge processes and the associated aeration cost, oxygen plays a key role that account for up to 40% of the running costs (Healey, 1989). This sensor is actively implemented for both the control strategies design, as proposed by Holmberg *et al.* (1989), Demuynck *et al.* (1994) and for monitoring of the central process of any activated sludge system (Vanrolleghem and Lee, 2003). Respirometry, which is an interpretation of the respiration rate of activated sludge, is frequently used in the description of wastewater and activated sludge kinetics. It is defined as the amount of oxygen per unit of volume and time that is consumed by the microorganisms in the activated sludge. Respirometers can be classified with two criteria: (1) the phase where oxygen is measured, and (2) the flow regime of both the gas and liquid phase, which is either flowing or static (Spanjers *et al.*, 1998). For details concerning respirometry, the reader can refer to Spanjers *et al.*, (1998a), Spanjers *et al.*, (1998b), Copp and Spanjers, (1999).

The most widely used parameter of the biodegradable component of wastewater, which is measured off-line, is the standard 5-days Biological Oxygen demand ($BOD_5$). It is defined as a measure of the DO used by microorganisms for the biochemical oxidation of organic

matter in five days from the time when the test sample is seeded with a microbial system (Bourgeois *et al.*, 2001; Metcalf and Eddy, 2003). Further details about BOD can be found in Brookman, (1997), An *et al.*, (1998) and Qian and Tan, (1998). The Chemical Oxygen Demand (COD) is one of the most intensively monitored variables in WWTPs. It is defined as a means of measuring the organic strength of domestic and industrial wastewater (Bourgeois *et al.*, 2001). It is often implemented as batch systems and flow-through continuous COD monitors. Further details on these automated laboratory procedures can be found in Ademoroti, (1986), Korenaga *et al.*, (1990) and Meredith, (1990).

The Total Organic Carbon (TOC) measurement has become more common since its appearance in the seventies (Bourgeois *et al.*, 2001). It is usually utilised for the conversion of organic carbon to carbon dioxide and measuring this product in the evolving gas phase, generally with an infrared off-gas analyser (Vanrolleghem and Lee, 2003). An interesting comparison between TOC, BOD and COD tests, in obtaining information about the kinetic processes in a rotating biological contactor system, is performed by Wilson (1997). UV-absorbance measurements were introduced in the early fifties to assess the quality of an effluent (Dobbs *et al.*, 1972). It consists of an interaction of light with a sample and can be classified in two categories (Bourgeois *et al.*, 2001):

1) Light absorption measurements (Ultraviolet/Visible (UV/VIS) spectrophotometry, Infra Red (IR) spectrometry.
2) Fluorescence (spectrofluorometry).

The most common technology is based on optical methods, despite the significant progress fibre optic technology has made in the last decade. Bourgeois *et al.*, (2001) and Vanrolleghem and Lee (2003), provided a detailed review of these technologies.

## State of the art sensing

State-of-art sensing is moving toward new tools such as infrared optical sensors for water quality monitoring, which are a promising concept with regards to continuous assessment of pollution levels in the liquid and gas phase (Mizaikoff, 2003). Moreover, microelectrode array sensors for water quality monitoring have been developed and applications including dissolved oxygen in activated sludge and preliminary measurements of trace arsenic are available (Gobet *et al.*, 2003). New chalcogenide glass chemical sensors for Sulphide ($S^{2-}$)

and dissolved hydrogen sulphide (H2S) monitoring are proposed by Miloshova *et al.* (2003), to allow reliable process control of the natural potential of hydrogen (pH) of wastewaters. Furthermore, a submersible UV/VIS spectrometer for in-situ real time measurement has been developed to simultaneously measure the COD, filtered COD, TSS and nitrate with just a single instrument (Langergraber *et al.*, 2003a). Russell *et al.* (2003), demonstrated through laboratory analysis that non-contact measurement of wastewater suspended solids and organic load based on measurements of light scatter and fluorescence is a viable method.

To monitor the activated sludge activity on which the performance of the treatment plants depends, an integrated sensor has been developed. This last one is shown to successfully monitor and provide in-depth insight into nitrification, denitrification and carbon source degradation processes occurring in Biological Nutrient Removal (BNR) plants (Sin *et al.*, 2003). Even if respirometry is considered reliable, it is not employed as a standard tool for monitoring due to the long experimental time that is required. Therefore, Langergraber *et al.* (2003b) proposed a rapid automated detection to measure on-line the nitrification kinetics and nitrification inhibition. Alex *et al.* (2003a) successfully studied the advantages and practical applicability of a wireless communication tool. The author and co-workers proposed on-line measurement data of wastewater systems via Wireless Application Protocol (WAP) mobile phones for the use in remote facilities where no staff are available. Information concerning progress in sensor technology for activated sludge systems is given by Rieger *et al.* (2003) and Alex *et al.* (2003b). Challenges and solutions required for multivariate online monitoring of modern WWT operation are discussed in details in Rosen *et al.* (2003).

## Actuators

For a description of actuator technology that is commonly used in WWTPs, the reader can refer to Section (2.2, e.g. motors, pump, flow etc.) and/or to Marinaki *et al.* (2003) and Metcalf and Eddy (2003). Indeed, actuators are similar for sewer systems and WWTPs.

# The receiving water

The receiving water considered within this thesis is a river, as this is the most common discharge point for effluent from the WWTP and since the CSOs typically spill into rivers,

stream or brooks. Wastewater discharged impacts on the receiving water are generally grouped into chemical, bio-chemical, physical, hydraulic, hydrologic, hygienic and aesthetic impacts (Rauch *et al.*, 1998). Urban rivers are commonly associated with other functions such as fishing, drinking water production, transport, recreation, irrigation and habitat for aquatic fauna. Combination of the quality and quantity of the water in the river is a key point for achieving "good" quality, in terms of ecological status and chemical quality, of the receiving waters. In other words, the effluent quality and quantity from the WWTP will govern the existence or extinction of the aforementioned functions.

The sewer and the WWTP are not the only inputs to the system that can govern the water quality of the receiving water. Processes taking place in the receiving water (i.e. bacteria) should also be considered as they play an important role in the conversion processes. The water quality of the receiving water can be judged on the basis of several parameters that are usually classified as (Meirlaen, 2002):

- Physical: Temperature, conductivity and turbidity.
- Chemical: DO, BOD or COD, pH, alkalinity, hardness, nutrients (nitrogen and phosphorous), toxic compounds and organic volatile compounds.
- Biological/ecological: Biocenosis of bacteria, coliform bacteria, plants and animals, and variety and complexity of the food chain.

It should be emphasised that these parameters all interact between each other and are crucial for providing information on the quality of the receiving water.

## Monitoring

Over the past decade, the advance in monitoring of water quality in the receiving waters has been growing steadily (Butterworth *et al.*, 2002), as a consequence of the general progresses made in the field of environmental monitoring. Gunatilaka and Dreher (2003), and Butterworth *et al.*, (2002) review these developments related to robust chemical and biological sensors. The progresses in micro-electronics in the past two decades contributed to the advancement of sensor technology for real-time monitoring, data collection and data transmission (Gunatilaka and Dreher, 2003). However, sensors are still the weakest part of the monitoring and control chain (Lynggaard-Jensen *et al.*, 1996).

The physical-chemical parameters that are typically continuously measured are: pH, temperature, molecular dioxygen ($O_2$) concentration, turbidity and conductivity. The most commonly measured concentration is the DO, depletion of which can be caused mainly by the degradation of soluble organic matter and chemical oxidation of reduced pollutants. Low DO concentrations can drastically affect the aquatic life of the receiving body (e.g. river). Therefore it is important to maintain its concentrations within thresholds to allow a self-purification power of the receiving water. Detection and monitoring of micropollutants such as pesticides and industrial pollutants occurred only with the sophistication of the chemical technology. It should be emphasised that the on-line sensors developed for the receiving body differ slightly from the ones commonly used in WWTPs. Indeed, to satisfy the environmental regulators for natural water investigations, lower detection limits are required.

## State of the art sensing technologies

A consistent review of novel on-line sensors such as screen-printed biosensors, lateral flow devices, protein microarray technology etc., which are quite promising and differ from conventional sensors, are reviewed in Butterworth *et al.*, (2002). The development of sensitive and specialised biosensors has been possible since power tools from biochemistry, molecular biology and genetics are available (Janata *et al.*, 1998; Nielsen *et al.*, 2000; Wilderer *et al.*, 2002). Mietzel *et al.*, (2003), proposed a quick way to predict bacteria contamination by observing different on-line parameters such as flow, conductivity or spectral absorption coefficient. The author and co-workers concluded that exceeding the bathing water standard for bacteria can be predicted by evaluating the spectral absorption coefficient with an acceptable accuracy (e.g. only after several days). Such results are promising as the main parameter to monitor the quality of bathing waters (e.g. urban river) is known as the fecal coliform bacteria, which so far, cannot be rapidly monitored (e.g. twice a year).

Marini and Weilguni (2003), proposed an hydrological information system based on an on-line monitoring telemetry network. The preliminary results of their system (implemented in the Brantas, river basin, East Java, Indonesia) illustrated the possibility of continuous measurements of indicative parameters (e.g. water temperature, conductivity, pH, DO, turbidity and nutrients) for early warning, control and polluter identification. Operational problems and experiences of collecting data over a period of one year are presented in Pressl *et al.*, (2004). The author and co-workers implemented in-line sensors in the Danube River to

measure long time behaviour as well as spot-events (e.g. CSOs). However, they concluded that the proposed sensors required supervision by a controlling concept, as the automatic calibration of their analyser was non-existent.

### Actuators

There are very few actuators implemented in the receiving water. For instance, design of control strategies with respect to the river are quasi non-existent. However, moveable weirs and gates are some of the only actuators available in river control. In addition, it is also suggested by Schutze *et al.*, (2003) that no important developments will occur in the field of actuators as exiting ones could be utilised in a more creative way and objective drive. As the focus of in-river conditions is becoming of main interest, developments of applications including actuators in the river (e.g. aeration, flow regulation) might become a solution in the next future.

The aforementioned review of monitoring equipment motivates the need to further improve the instrumentation toward IUWSs. This progress can be achieved by designing new approaches based on mathematical models that can describe the urban wastewater system. Indeed, modelling plays a key role in the development of monitoring equipment as it can contribute in providing technical solutions at a minimum price.

## 2.3) MODELLING OF THE IUWS SYSTEM

As for many industrial processes, models have always played an important role in the process design. Jepsson (1996), defined mathematical models as follow:

'*Mathematical models are an excellent method of conceptualising knowledge about a process and to convey it to other people. Models are also useful for formulating hypotheses and for incorporating new ideas that can later be verified (or discard) in reality*'.

The challenges in mathematical modelling lie in the aspect of describing complex systems using sets of differential equations. This task could be straightforward in an ideal world but unfortunately; our world is different in reality. A good and consistent introduction to

mathematical modelling can be found in Jeppsson (1996). The reader is also referred to Murthy *et al.*, (1990), for further information on fundamental mathematical modelling.

Integrated modelling of an urban wastewater system can be seen as an approach of modelling the interconnection between all sub-systems (e.g. the sewer system, the WWTP and the receiving water). Therefore, the following description is intended at describing the models utilised in representing the integrated system as well as providing simulation studies of the full-scale model. A schematic overview of the integrated model under study in this thesis is displayed in Figure (2.3). The sewer model, proposed by Linblom, is detailed in Linblom *et al.*, (2005a), while the river model, based on the River Water Quality Model No.1 (RWQM1, Reichert *et al.*, 2001a), is partially illustrated in Linblom *et al.*, (2005b). Note that the IUWS is still under development and validation by the last author. The WWTP considered is the IWA/COST Benchmark Simulation Model No. 1 (BSM1, Copp, 2002).

## Influent modelling

The provision of influent data as sewer input is a prerequisite for modelling the urban systems dynamics. The influent model structure of the sewer system considered in this thesis is that presented, and provided by Gernaey *et al.*, (2006).

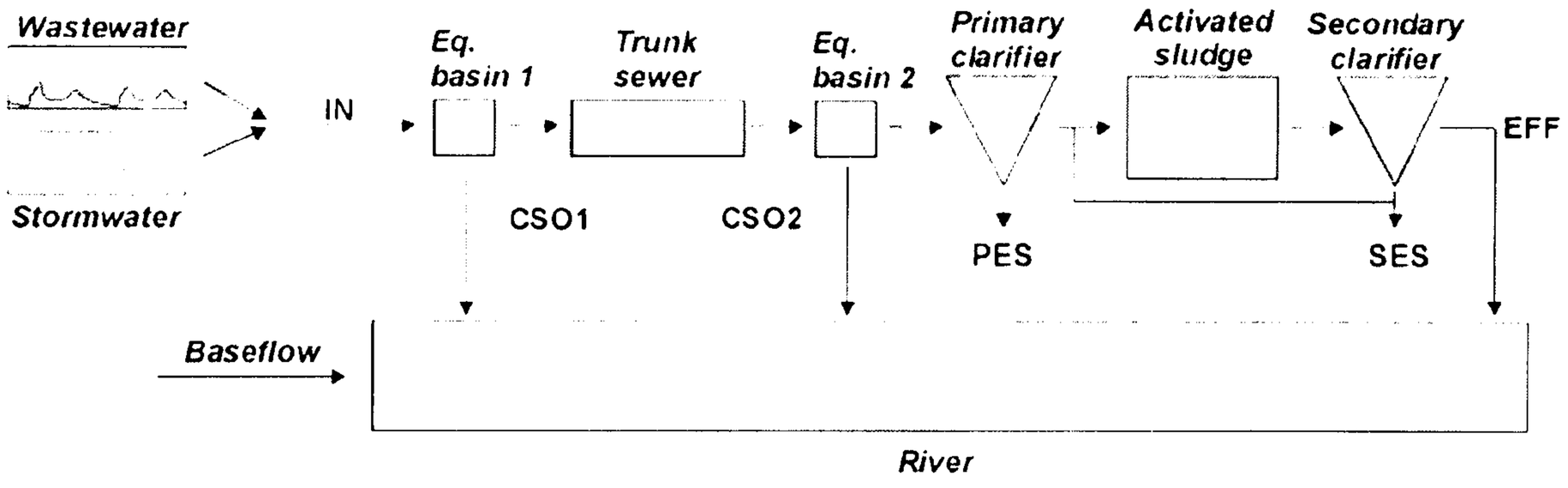


**Figure 2.3** The integrated urban wastewater system model. EFF – Effluent. PES – Primary Excess Sludge. SES – Secondary Excess Sludge.

It is based on phenomenological models (not mechanistic as they do not contain the detailed process knowledge of specific processes), which reproduce typical phenomena observed in the influent of full-scale WWTPs, with a minimum number of parameters (Gernaey *et al.*, 2006). More precisely, it consists of 360 days of influent data that includes diurnal, weekend,

seasonal (e.g. temperature) and holiday effects, as well as rainfall. Further details on the modelling aspect of the influent wastewater data are available in Gernaey *et al.*, (2005).

## The trunk sewer

The influent data enters the sewer through equalisation basins. The water motion in a sewer network is generally modelled utilising an application of the unsteady open channel flow model, based on the Saint Venant equations. This approach allows an accurate description of the hydraulic effects, to an extent that 'if the simulation does not fit the data very well, then the information about the system may be faulty, rather than the model itself' (Harremoës and Rauch, 1999). In order to make the St. Venant equations applicable for surcharged flows, Preissmann (1961), introduced the concept of hypothetical open slot at the top of the pipe. However, flow routing models have been developed since the solution of the St Venant equations (or their approximation) is computationally demanding. This underlying concept, which consists of cascaded reservoir in series with the water being routed downstream, is considered here. This approach has been initially selected because it allows rapid simulations. On the other hand, effects such as pressurised flow and backwater cannot be (directly) simulated.

The modelling approach that is commonly used to describe the sewer processes involves the use of the SOBEK and Mouse models. These packages include the studies of CSOs, sanitary sewer overflow, design of new site developments, RTC schemes development, analysis, etc. (Zacharof *et al.*, 2003). However, these models are not considered in this thesis mainly because they do not include a WWTP. The selected model for biological transformations in the trunk sewer, which is based on the same terminology as the ASM1 model, was developed by Vollertsen and Hvitved-Jacobsen (2000).

### Hydraulics and dimensions

The trunk sewer, detailed in Figure (2.4), is a conduit that transports wastewater from the first equalisation basin to the second equalisation basin, located just ahead of the WWTP. The length (L=2000 meter) of the pipe is modelled as a series of sixteen completely mixed reactors (n=16) with variable volumes. The pipe, geometrically a sequence of identical cylinder stretches, is characterised by a maximum flow rate obtained when the pipe is

completely full due to gravity, an inner pipe diameter and a total length (Linblom *et al.*, 2005a).

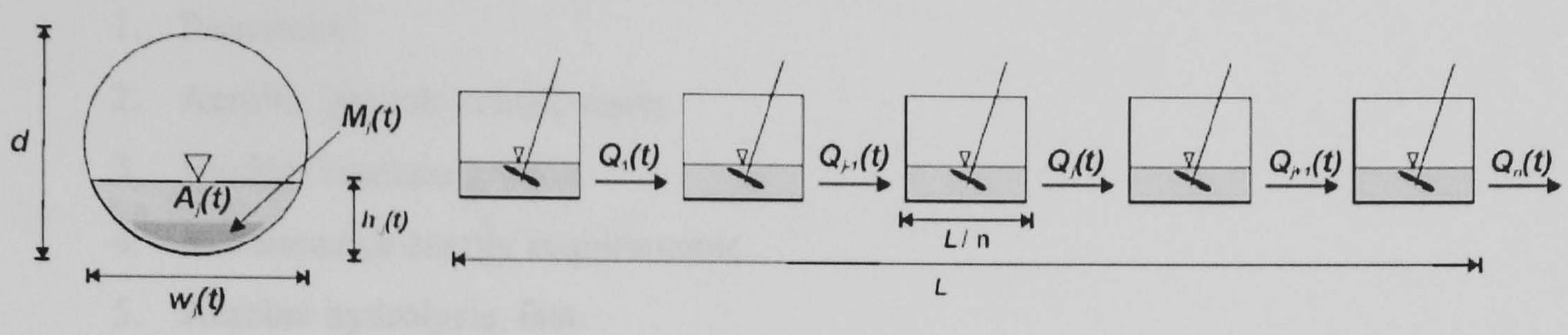


**Figure 2.4** The concept of the trunk sewer model. It is composed of a series of 16 completely mixed reactors (n=16) with a the length of pipe being L=2000 meters

The hydraulic capacity of the trunk sewer is assumed to be twice the hydraulic capacity of the WWTP, 5000 $m^3/h$, corresponding to a diameter of d=1 m and a slope of 3 mm/m. No sedimentation is assumed to take place in the trunk sewer pipe. The hydraulic mass balance for each stretch is given by:

$$\frac{\mathrm{d}A_j(t)}{\mathrm{d}t} = \frac{1}{L/n}\left(Q_{j\text{-}1}(t) - Q_j(t)\right) \tag{2.1}$$

where $A_j(t)$ is the water filled cross-sectional area of segment stretch $j$ ($m^2$) and $Q_{j\text{-}1}(t)$ and $Q_j(t)$ are the influent and effluent flow rates of stretch $j$, respectively. The outflow depends on the fill factor ($h(t)/d$) and is calculated according to an empirical equation derived by Bretting (1941):

$$\frac{Q_j(t)}{Q_{\text{full}}} = 0.46 \cdot 0.5\cos\left(\pi\frac{h_j(t)}{\mathrm{d}}\right) + 0.04 \cdot \cos\left(2\pi\frac{h_j(t)}{\mathrm{d}}\right) \tag{2.2}$$

where $h_j(t)$ is the water level height and $Q_{\text{full}}$ is the flow rate when the pipe is completely full due to gravity. The biological and chemical processes in the trunk sewer are modelled with fourteen state variables, which are described in Table B.1 of Appendix B, and can be divided into COD and nitrogen components, and finally a state describing the sewer stretch volume. In much, the process model follows Hvitved-Jacobsen *et al.* (1998).

## Process reactions and model parameters

Eight processes are considered to describe the biological reactions as described:

1. Reaeration
2. Aerobic growth in bulk water
3. Biofilm biomass growth
4. Maintenance energy requirements.
5. Aerobic hydrolysis, fast.
6. Aerobic hydrolysis, slow.
7. Hydrolysis of entrapped organic nitrogen
8. Ammonification

Processes one to six are based on the process model derived in Vollertsen and Hvitved-Jacobsen (2000). The kinetic and stoichiometric parameters are also adopted from this paper. The implementation of the fourth process is not identical to the one in its original paper. The formulation here requires that the readily biodegradable substrate ($S_S$) is always present and that the heterotrophic active biomass in the water phase ($X_{BW}$) does not support maintenance energy (endogenous respiration). To fulfil nitrogen balances, the sixth and seventh processes are implemented similarly to the ASM1 model. However, anoxic processes are not considered since an absence of autotrophs is assumed. Furthermore, the re-aeration process requires an abundance of hydraulic and geometrical parameters to be calculated which lead to a large number of outputs (Linblom *et al.*, 2005a).

## Equalisation basins

At the beginning and end of the trunk sewer, overflow structures allow water to be discharged directly to the recipient if the flow rate exceeds the hydraulic capacity of the system. The two-equalisation basins are modelled as completely mixed 1000 $m^3$ variable volume reactors with an outflow that is proportional to the actual volume:

$$Q(t) = \frac{Q_{max}}{V_{max}} V(t) \tag{2.3}$$

where $Q(t)$ is the equalisation basin effluent, $Q_{max}$ denotes the capacity of the downstream unit (in this case the trunk sewer or WWTP) and $V_{max}$ the volume capacity of the equalisation

basin. When the basin is full, the maximum flow rate is passed on to the downstream pipe while the remainder is discharged as a combined sewer overflow:

$$\begin{aligned} Q_{\text{overflow}}(t) &= Q_{\text{in}}(t) - Q(t) \quad \text{if } V(t) = V_{\max} \text{ and } Q_{\text{in}}(t) > Q(t) \\ Q_{\text{overflow}}(t) &= 0 \end{aligned} \tag{2.4}$$

else, the hydraulic mass balance for the equalisation becomes:

$$\frac{dV}{dt} = Q_{\text{in}}(t) - Q(t) - Q_{\text{overflow}}(t) \tag{2.5}$$

The equalisation basin model does not describe settling, and no distinctions are made between dissolved and suspended components. The biological model for the equalisation basin is the same as for the trunk sewer with one exception: reaeration is not modelled. The inputs to the equalisation model block mimic the ones to the sewer trunk (Linblom *et al.*, 2005a).

## Modelling of the activated sludge process

Wastewater treatment processes are generally described by complex nonlinear systems that include biological, physicochemical and biochemical processes. The model considered state of the art for modelling biological nitrogen removal processes is the ASM1 model of the International Water Association (IWA, Henze *et al.*, 2000). This model, which describes carbon removal and nitrification-denitrification processes, is used intensively since it was first been introduced in the 1980s. It is a complex non-linear model due to multiple time scale dynamics, large perturbation in flow and load, together with uncertainties concerning the composition of the incoming wastewater (Alex *et al.*, 1999). The state variables description is displayed in Table B.2 of Appendix B. The eight processes that are considered in the description of the biological reactions of the ASM1 model are listed in Chapter IV, Section (4.1).

In 1995, the Activated Sludge Model No.2 (ASM2), which is more complex than the ASM1 model, was introduced to describe nitrogen removal and biological phosphorous removal. At this time, the role of denitrification in relation to biological phosphorous removal was still unclear and was not described by the model. However, in 1994, the development in research

was fast enough to expand the ASM2 model to the Activated Sludge Model No.2d (ASM2d) where Phosphorous-Accumulating Organism (PAOs) were included for improved modelling of the processes (Henze *et al.*, 1999).

In 1998, the ASM3 model was developed to: (1) create a tool for use in the next generation of activated sludge models (Henze *et al.*, 2000), and (2) overcome some defects in the ASM1 model which became evident when intensive research was performed on the basis of the ASM1. The ASM3 model was initially developed for biological nitrogen removal, with principally the same goal as the ASM1 (Gernaey *et al.*, 2003) but its main objectives remain to correct a number of defects that have appeared during the intensive usage of the ASM1 (Gujer *et al.*, 1999).

In this thesis, the original benchmark simulation model no.1 (Copp, 2002) is considered as a description of the real WWTP. The ASM1 model is selected to describe the biological processes in the activated sludge reactors. This selection is motivated since the BSM1 model is extensively used in the industry. Furthermore, according to Jeppsson and Pons (2004), the benchmark plant is a success as more than hundred scientific publications, in which the model is fully or partially considered (influent files, plant performances evaluations), can be found in literature. In other words, the advantage of using the benchmark plant is that any researcher can perform a comparative study based on the finding. Therefore, the work provided in this thesis could be eventually utilised by others or lead to further investigations.

## IWA/COST Benchmark Simulation Model No.1 (BSM1)

The original benchmark plant, as displayed in Figure (2.5), consists of 5 activated sludge tanks in series (2 anoxic ones + 3 aerobic ones), followed by a secondary settler.

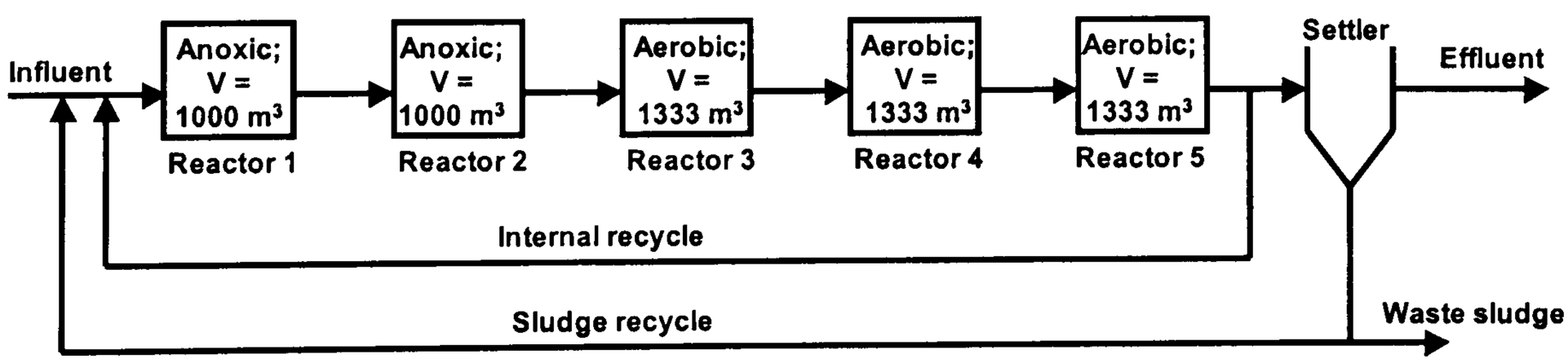


**Figure 2.5** Original benchmark plant considered in the thesis.

There are two recycle streams, one for transport of nitrate rich mixed liquor from the last aerated tank to the first anoxic tank, and one for transport of concentrated sludge from the bottom of the settler to the first anoxic tank. The ASM1 model (Henze *et al.*, 2000), is selected to describe the biological processes in the activated sludge reactors. A ten-layer one-dimensional settler model applying the double-exponential settling velocity function proposed by Takács *et al.* (1991) is chosen to describe the settling process. All simulations are performed on a Matlab/Simulink platform, based on the open-loop benchmark configuration. Figure (2.6) display the three different influent files, which contain 14 days of influent data at 15-minutes intervals, available with the benchmark plant. The constant influent wastewater data file is not represented here for reason of simplifications.

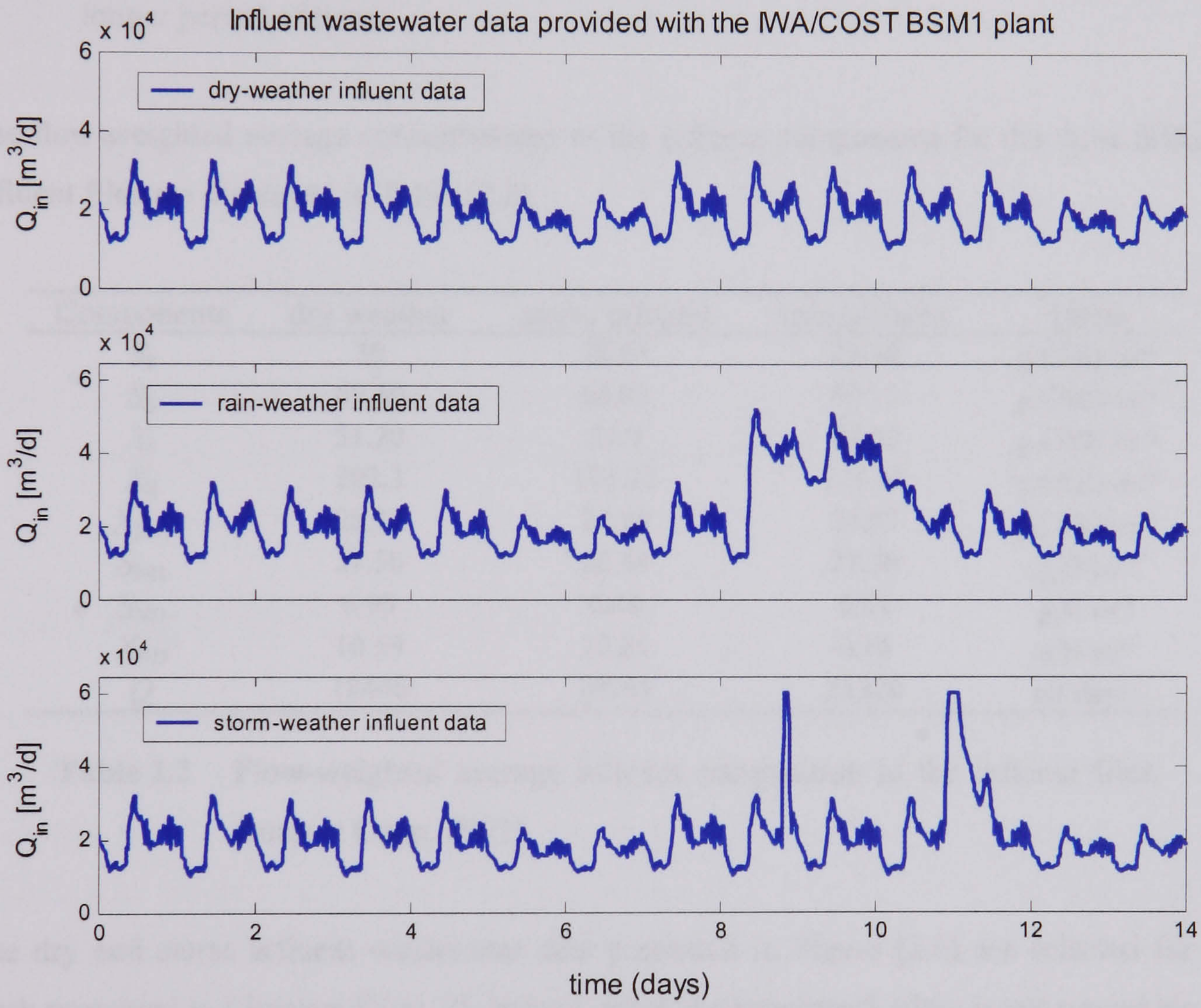


**Figure 2.6** Dry, rain and storm influent wastewater data available within the IWA/COST benchmark simulation model no.1.

These influent wastewater data mimic real wastewater characteristics typical for a plant of the chosen size and are defined as follow (Copp, 2002):

- The 'dry weather' file represents a set of data equivalent to normal diurnal variations in flow and COD load.

- The 'storm influent' is a variation of the 'dry weather' file added with two different storm event. The first one is of high intensity and short duration and is expected to flush the sewer of particulate material, and the second one assumes that the sewer is cleared of particulate matter during the first storm event. Therefore, a small increase in the COD load can be observed during the second storm.

- The rain influent represents a long event where the influent flow does not reach the level attained during the storm events, and where the increase flow is sustained for a longer period of time.

The flow-weighted average concentrations of the influent components for the three different influent files are displayed in Table (2.2).

| Components | dry weather | storm influent | rain influent | Units |
|---|---|---|---|---|
| $S_I$ | 30 | 28.03 | 25.96 | g COD $m^{-3}$ |
| $S_S$ | 69.50 | 64.93 | 60.13 | g COD $m^{-3}$ |
| $X_I$ | 51.20 | 51.9 | 44.30 | g COD $m^{-3}$ |
| $X_S$ | 202.3 | 193.32 | 175.05 | g COD $m^{-3}$ |
| $X_{B,H}$ | 28.17 | 27.25 | 24.37 | g COD $m^{-3}$ |
| $S_{NH}$ | 31.56 | 28.48 | 27.30 | g N $m^{-3}$ |
| $S_{ND}$ | 6.95 | 6.49 | 6.01 | g N $m^{-3}$ |
| $X_{ND}$ | 10.59 | 10.24 | 9.16 | g N $m^{-3}$ |
| $Q$ | 18446 | 19745 | 21320 | $m^3$ $day^{-1}$ |

**Table 2.2** Flow-weighted average influent composition in the influent files. (source: Copp, 2002)

The dry and storm influent wastewater data presented in Figure (2.6) are selected for the work presented in Chapters IV to VI. Indeed, when the benchmark plant is not run within the IUWS, theses files are essential to mimic the influent of the WWTP. For the final case study presented in Chapter VI, where the IUWS is considered, the influent file presented in Gernaey *et al.*, (2006) and discussed in Section (2.3) is considered.

## Sensors available with the BSM1 model

The common sensors that are available with the IWA/COST benchmark plant, as well as an example of their characteristics, which are mainly considered in this work, are summarised in Table (2.3). The benchmark plant is in constant development and the most updated information are available on the COST Action 624 benchmark web site (http://www.ensic.u.nancy.fr/ COSTWWTP/).

| | Delay (minutes) | Low-level detection limit | Sampling time (minutes) |
|---|---|---|---|
| Oxygen ($S_O$) | - | 0.1 | continuous |
| Nitrate and nitrite nitrogen ($S_{NO}$) | 10 | 0.1 | 10 |
| $NH_4^+$ +$NH_3$ nitrogen ($S_{NH}$) | 10 | 0.2 | 10 |
| Total suspended solids (TSS) | - | - | continuous |
| Influent (= effluent) flow rate (Q) | - | - | continuous |
| Readily biodegradable substrate ($S_S$) | 30 | 0.1 | 30 |
| Slowly biodegradable substrate ($X_S$) | 30 | 0.1 | 30 |

**Table 2.3** Typical on-line measurements and off-line analyses ($S_S$ and $X_S$) coefficients that are considered (non-exhaustive) within the BSM1 plant configuration.

Sensor location is not investigated in the scope of this work. For further information on the plant, sensors and control strategies, the reader should refer to Copp (2002).

## Modelling of the river system

Water quality changes in rivers are mainly caused by physical transport and exchange processes (e.g. diffusion/dispersion), and biological, biochemical or physical conversion processes (Zacharof *et al.*, 2003). The historical development of oxygen, nitrogen and phosphorous models, which has become increasingly complex, was initiated with the pioneering work of Streeter and Phelps in 1925. This work contributed to development of the Enhanced Stream Water Quality Model (QUAL2E), which is widely used (Reichert *et al.*, 2001a), and includes nutrient cycling and algae. However, even though the fundamental conversion processes in surface water are similar to the ones in WWT, the model description is incompatible with the ASM models (e.g. ASM1, ASM2, ASM2d, ASM3; Henze *et al.*, 2000), which has severe implication when defining interfaces.

Therefore, the IWA (formerly IWAQ) formed a Task Group on River Water Quality Modelling in 1997 to mainly overcome this compatibility limitation and others defects that are described in Shanahan *et al.*, (1998) and Reichert *et al.*, (2001a). The fundamentals of the model as well as guidelines for selecting the appropriate model structure and hydraulic formulation can be found in Shanahan *et al.*, (2001); Reichert *et al.*, (2001b) and Vanrolleghem *et al.*, (2001).

## River characteristics

The river that is selected for this work is 2560 meters (m) long with a maximum depth H = 10m. The inputs to the river are a constant base flow, the two combined sewer overflows and the WWTP effluent. The constant base flow increases from the beginning of the river and down stream as 0.1728.L, where L is the length position. The river is divided into 9 reaches in which uniform flow is assumed. A truly uniform flow is one in which the velocity is the same in both magnitude and direction at a given instant at every point in the fluid. Each reach is characterised by a constant cross section, as represented in Figure (2.7), and length.

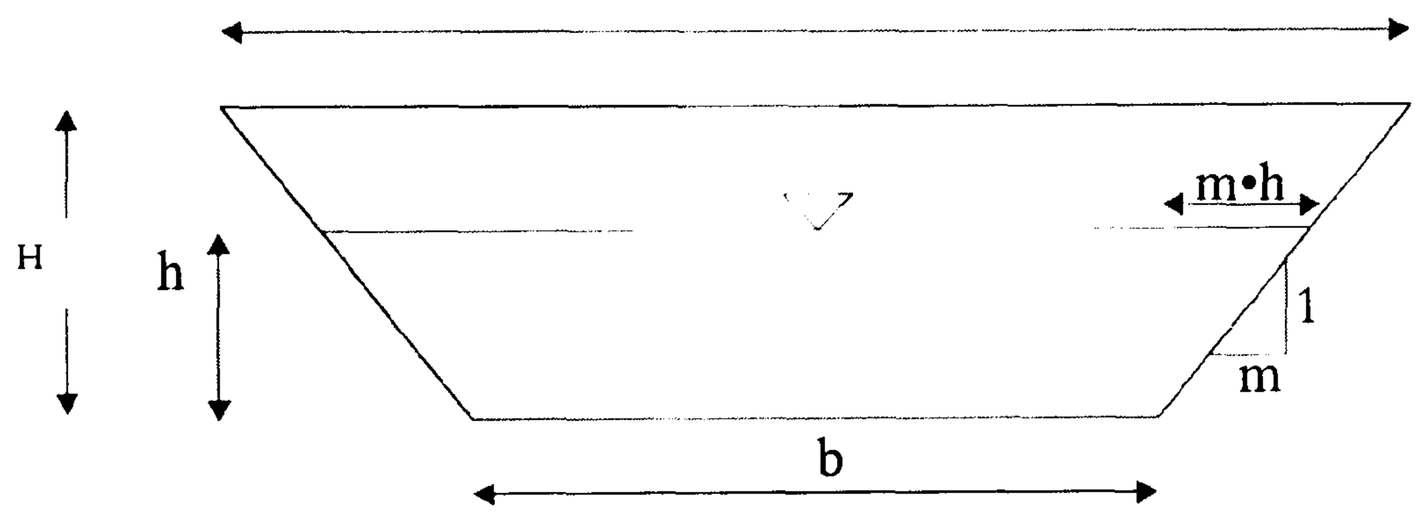


**Figure 2.7** Cross section profile of a river reach.

The most widely used equation for describing the uniform flow in open channels is the Manning formula, which is given by:

$$Q(t) = \frac{1}{\mathrm{n}} A(t) R_{\mathrm{h}}(t)^{2/3} S_0^{1/2} \tag{2.6}$$

where $A(t)$ is the water filled cross sectional area, n is the friction factor, $R_{\mathrm{h}}$ is the hydraulic radius ($A(t)/P(t)$) and $S_0$ is the bed slope. According to Figure (2.7), the water filled cross sectional area (A) is given by:

$$A(t) = \mathrm{b}h(t) + \mathrm{m}h(t)^2 = (\mathrm{b} + \mathrm{m}h(t))h(t) \tag{2.7}$$

where m is section side slope given by:

$$m = \frac{T - b}{2H} \tag{2.8}$$

The wetted parameter P is given by:

$$P(t) = b + 2\sqrt{(1 + m^2)}h(t) \tag{2.9}$$

If the slope and friction factor are assumed to be constant, it can be shown that the flow rate is given uniquely by the water level height *h(t)* as represented in Figure (2.8).

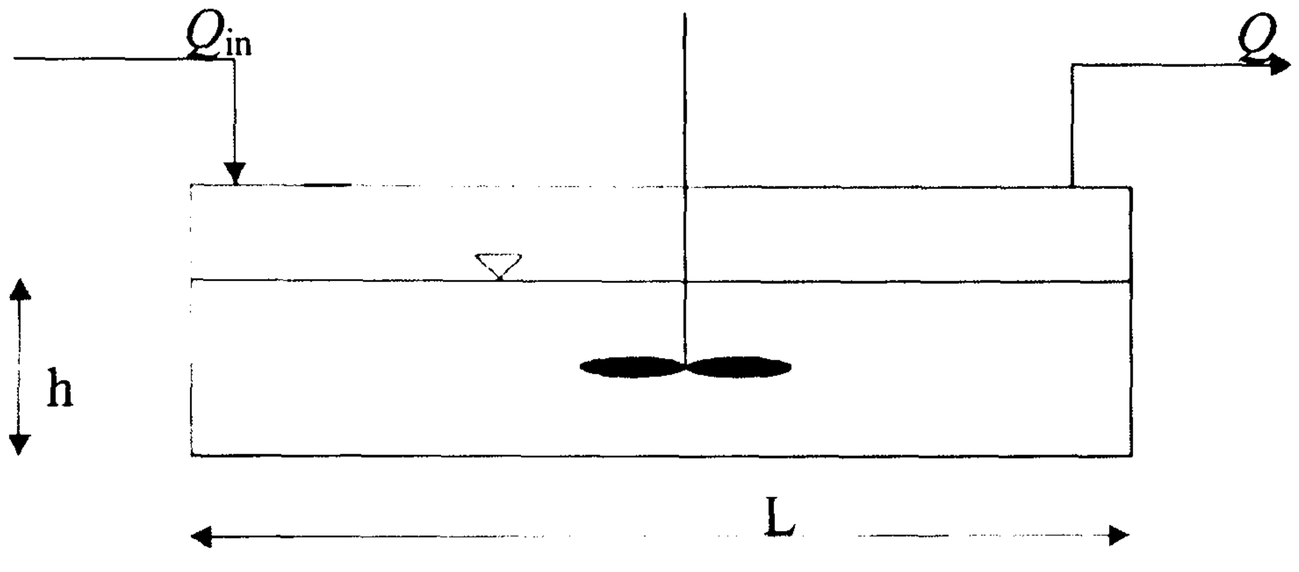


**Figure 2.8** Flow rate dependence on the water level height

The differential equation for one river reach becomes:

$$\frac{dV(t)}{dt} = Q_{in} - Q = Q_{in} - \alpha A(t) R_H(t)^{2/3} \tag{2.10}$$

where $\alpha=(m/R_H)^{0.5}$. Similarly to that of the sewer, the question is how the height is related to the volume? This can be achieved with

$$A(t) = V(t)/L = bh(t) + mh(t)^2 \rightarrow \tag{2.11}$$

$$h(t)^2 + \frac{b}{m}h(t) - \frac{V(t)}{Lm} \quad \rightarrow \quad h(t) = -\frac{b}{2m} \pm \sqrt{\frac{b^2}{4m^2} + \frac{V(t)}{Lm}} \tag{2.12}$$

Thus, for each change in volume, a new water level height is calculated followed by a new outflow, using Equation (2.6). The state variables considered in the river model are displayed in Table B.3 of Appendix B.

## Process reactions

Thirteen processes are considered to describe the biological reactions as described:

1. Aerobic growth of heterotrophs with $NH_4$
2. Aerobic growth of heterotrophs with $NO_3$
3. Aerobic endogenous respiration of heterotrophs
4. Anoxic growth of heterotrophs with $NO_3$
5. Anoxic growth of heterotrophs with $NO_2$
6. Anoxic endogenous respiration of heterotrophs
7. Growth of first stage nitrifiers
8. Aerobic endogenous respiration of first stage nitrifiers
9. Growth of second stage nitrifiers
10. Aerobic endogenous respiration of second stage nitrifiers
11. Hydrolysis
12. Adsorption of phosphate
13. Desorption of phosphate

For further information about the above-mentioned processes, the reader can refer to Reichert *et al.*, (2001b).

## Interactions between the sewer, WWTP and river

There are several interactions between the sewer system, the WWTP and the receiving water. These interactions are important and it is essential to simulate any control strategies on the full-scale urban wastewater system rather than concentrating the efforts individually on each element. The impact of these interactions, such as combined sewer overflow spill or the quality of the effluent from the WWTP, can create harmful levels of pollutants in the receiving water. The first element that interacts with the urban wastewater system is the sewer, which clearly affects the WWTP effluent quality, dependent upon the wastewater quality of the incoming water. Subsequently, a single CSO event, which depends upon the dilution capacity of the receiving water, can contribute to an increase in the pollutant concentration in the river. Furthermore, CSOs play an important role in increasing the oxygen demand in the river, primarily responsible for a decrease in oxygen concentration, which leads to toxic compounds in the receiving water (Meirlaen, 2002). The CSOs flow impact on the receiving water is detailed in next section through a simulation study.

## Simulation study

The IUWS simulations are performed using the Matlab/Simulink platform with a dynamic influent wastewater data (Gernaey *et al.*, 2005). It is initially simulated during 130 days, so that constant daily average loads are established. This approach allows sediments to be concurrently accumulated until reaching equilibrium (i.e. the amount that settles in the sediment storage equals the amount that is resuspended). Wastewater passes through the trunk sewer without any discharges via the two combined sewer overflows. The CSOs effect on the river is displayed in Figure (2.9). A Simulink block diagram representation of the full-scale model is displayed in Figure (2.10) (Linblom *et al.*, 2005a; 2005b).

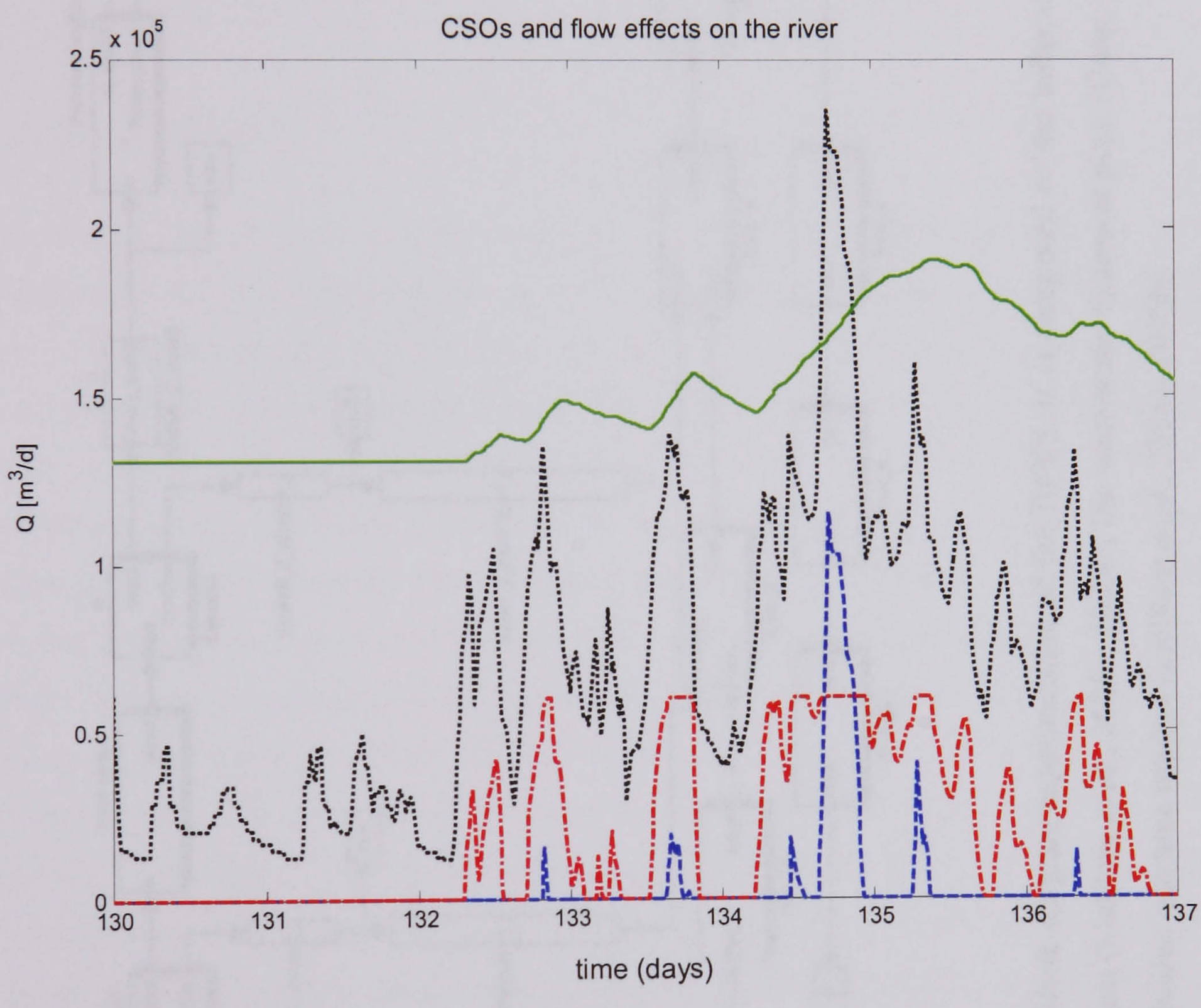


**Figure 2.9** CSOs and flow effects on the river model - (dotted line) dynamic influent wastewater data to the sewer network – (dashed line) CSO1 occurring when the 1st equalisation basin is full – (dotted/dashed line) CSO2 occurring when the 2nd equalisation basin is full – (solid line) effluent at the 4th reach of the river model.

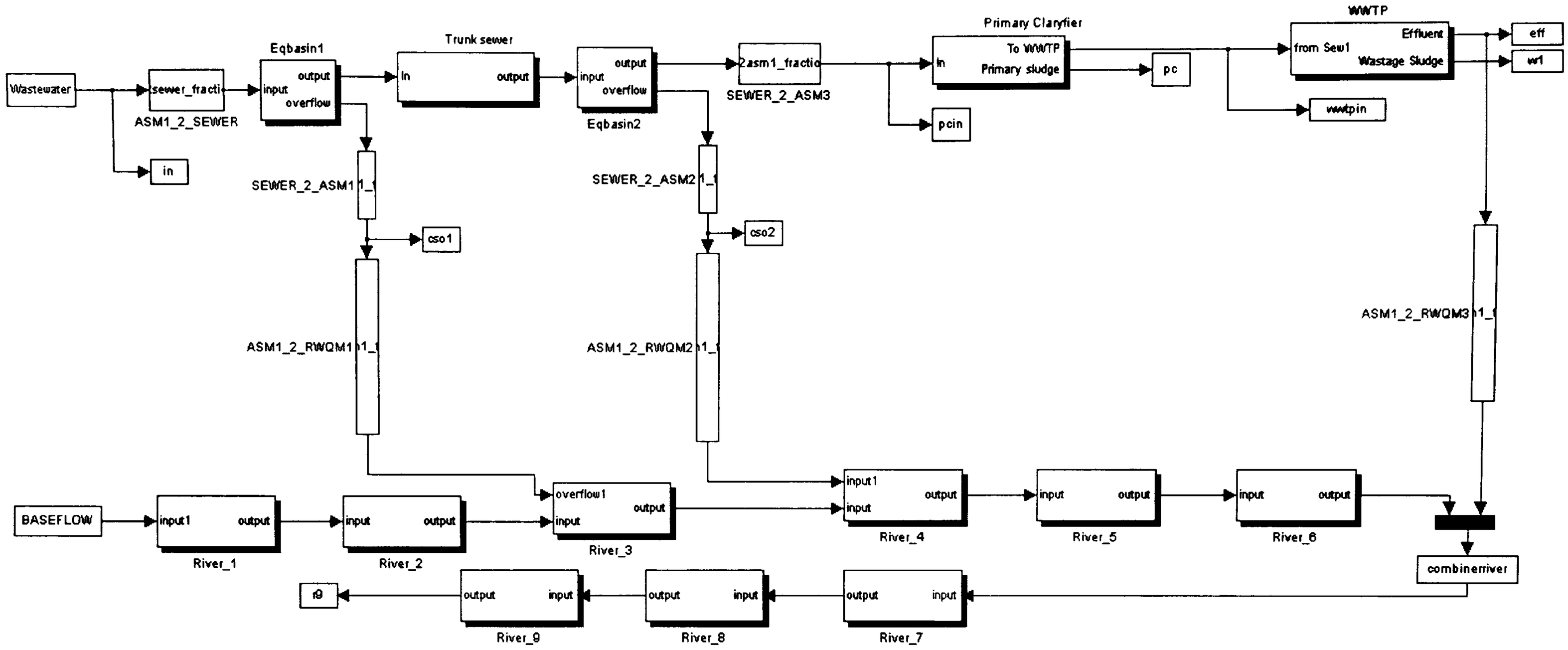


**Figure 2.10** Simulink block diagram representation of the IUWS. It is composed of the influent wastewater (Gernaey *et al.*, 2006), the sewer system (Linblom *et al.*, 2005a; 2005b), the wastewater treatment plant (Coop, 2002) (including a primary clarifier) and the river divided into nine reaches (Linblom *et al.*, 2005a; 2005b).

It can be observed from the simulation results presented in Figure (2.9) that the dry influent flows, entering the sewer network, augment after two days, before increasing intensively to reach its maximum peak after about five days. The CSOs from the second equalisation basin start occurring (after 2.5 days) before the one from the first equalisation basin (after 2.8 days). This is due the capacity of the storage tanks from the 2$^{nd}$ equalisation basin, which is less important than the first one. The CSO spill out the untreated wastewater directly into the river and an increase of the river flow is observed. The effects in the river will lead to oxygen depletion, and increases in levels of ammonia. Further details on the IUWS system are presented in Linblom *et al.*, (2005a; 2005b), as well as some model responses. However, at current time, this model is not further investigated, as the above authors are in the validating phase of the IUWS.

## 2.4) SUMMARY

This Chapter has provided a brief introduction to the integrated urban wastewater system composed of the sewer network, the WWTP and the river. The most common technology utilised in the design of sewer network is the combined one, even taught it is regarded as causing high pollution and hygienic risks. To treat the wastewater entering the plant from the sewer network four stages are generally required: preliminary, primary, secondary and tertiary treatments. The main objective is the reduction of nitrogen, phosphorous, organic matter and suspended solids. The secondary treatment, particularly the activated sludge process, is the most widespread treatment. This aerobic biological treatment is utilised as a culture of bacteria suspended in the wastewater in an aeration tank to absorb, absorb and biodegrade the organic pollutant. Therefore, a particular attention will be devoted to the design of state observer and software sensors on the activated sludge model no.1. The receiving water that is considered in this work is a river, as this is the most common discharge point for effluent from the WWTP and as the CSOs typically spill into rivers. A state of the art review in sensing technologies is also provided for each sub-system, as well as a brief discussion on actuators.

The selected IUWS model is described in this Chapter and concentrates on the sewer network, WWTP and river models. Firstly, the selected influent wastewater data entering the trunk sewer, which reproduces typical phenomena observed in the influent of full-scale WWTPs, is briefly discussed. Secondly, the hydraulics and dimensions, and processes that that are considered for the trunk sewer and the equalisation basins are provided. Thirdly, the

COST simulation benchmark, which is selected as the real plant in this work, as well as the typical sensors that can be eventually modelled, is briefly discussed. Fourthly, the river characteristics and process reactions of the RWQM1 model are described, as it is selected to describe the receiving waters. The interactions between all sub-systems are also briefly discussed. Finally, a simulation study is proposed to illustrate the CSOs flow effects on the river.

# Chapter III

# Non-linear State and Parameter estimation

In this chapter, some theories behind non-linear state and parameter estimation are presented. The historical review of the most common software sensors is initially proposed. The choice of selecting Kalman and $H_\infty$ filtering as the basis for this work is explained as well as the advantages and drawbacks of these techniques. Then, the theories associated with linear and non-linear observability are derived as it represents the fundamental of observer designs. Subsequently, the linear and extended Kalman and $H_\infty$ filters are derived as well as the parameter identification algorithms. These types of software sensors are generally considered as the main tools in achieving joint state and parameter estimation to bioprocesses. Therefore, two examples of activated sludge processes are proposed where on-line observers based-EKF and EHF are applied on simple and augmented models. Results are illustrated through simulation studies. The advantages and drawback of the proposed software sensors are discussed. Parts of the material in this chapter are covered in Benazzi *et al.*, (2003); Benazzi and Katebi, (2004); Benazzi *et al.*, (2005c); Benazzi and Katebi, (2006).

## 3.1) HISTORICAL REVIEW

Estimation problems can be regarded as a subset of the class of approximation problems. The approximation problem can be stated as being the approximation of an unknown quantity from a combination of known quantities. The theory behind estimation date backs since 1632 and is attributed to Galileo Galilei (Wilson, 1972). Methods based on time averaging, which

is generally referred to as a least square estimation method, are essentially deterministic. Even though Legendre, in 1810, first published the least squared method (Legendre, 1810), it is generally attributed to Gauss who, according to Kaillath (1974), first employed the technique in 1795 for the planetary motion estimation problem. The pioneers in the application of the least squares technique to stochastic processes are Kolmogorov (1939, 1941) and Wiener (1949).

Kolmogorov provided a comprehensive treatment of the prediction problem for discrete-time stationary processes (i.e. inexistent time variations of the statistic properties of the random process) but however, didn't develop an explicit formula for the optimum linear predictor. On the other hand, Wiener, who was working independently on anti-aircraft fire-control problems, derived an equation for continuous time. It is known as the Wiener-Hopf integral equation, which is based on a spectral factorisation method. Many extensions and generalisations followed Wiener's work based on stationary cases (e.g. Zadeh and Ragazzini, 1950; Bode and Shannon, 1950) prior to the development of solutions for non-stationary processes (e.g. Darlington, 1958; Shinbrot, 1958). Unfortunately, the application of Wiener's filtering technique is faced by several difficulties, which are summarised as follow (Elsayed, 1988):

1) The Wiener filter is only valid for stationary cases, as non-stationary processes require a new derivation of the integral equation, which is not straightforward.
2) Only the solution to single variable systems is considered with the Wiener filtering approach. Even if generalisation to multivariable cases has been made, new analysis is required and the procedure remains complex.
3) The derivation of the Wiener-Hopf integral equation is not transparent and inappropriate for machine computation from a mathematical viewpoint.

In 1960, R. E. Kalman presented a new approach to the prediction and filtering problem (Kalman, 1960) based on the solution to the Minimum Mean-Square Error (MMSE). Many authors regard Kalman filtering theory as the most significant contribution to the filtering and prediction theory since Wiener' work. Indeed, most of drawbacks encountered with the Wiener filter were eliminated with Kalman's theory. These are summarised as follow (Elsayed, 1988):

1) The linear dynamic system is described by state space form, which makes machine computation and MIMO applications easier.
2) Both stationary and non-stationary random processes, and single-variables and multiple-variables, are treated in a unified framework.

From this time and due to a large evolution in digital computing, research has focused on this filter and its applications, particularly in the area of ships, spacecraft, aircraft and navigation systems. These types of computer-based sensors are called software sensors when performing joint state and parameter estimation on-line. The term 'observer' (or state observer) is sometimes utilised when performing state variables estimation only and 'parameter estimator' when internal model parameter estimation is performed (Bastin and Dochain, 1990).

The extended Kalman filter, which is an extension of the KF originally developed for linear model, is widely utilised to perform state and/or parameter estimations on non-linear dynamic systems. This particular type of algorithm, which is presented later in this chapter, consists of linearised versions (e.g. the linearised tangent model) of the process dynamics, which are computed from Taylor's series expansions of a state space model around some equilibrium points. With such an approach, the linear observer theory can be applied (Bastin and Dochain, 1990). The extended Kalman filter has found applications in (bio)chemical processes (e.g. Stephanopoulos and San, 1984; Caminal *et al.*, 1987; Tsobanakis *et al.*, 1992; Jeppsson, 1996). The success of the extended Kalman filter is the ease of implementation since the algorithm can be directly derived from the state space model. However, it is based on a linearised model, which means that the stability and convergence properties are essentially local and valid around an equilibrium point. Therefore, is it difficult to guarantee its stability over wide ranges of operation. Furthermore, the derivation of the extended Kalman filter is based on some stochastic assumptions on the measurement and process noises, which might be questionable in practice (Perrier *et al.*, 2000).

Kalman filtering also presents a major drawback. For instance, when implemented on bioprocess systems, the accuracy of the estimated concentrations and/or parameter can be very poor. The main reason is illustrated within this thesis but it is assumed that the noise source statistics are known and it is the "average" estimation error that is minimized. What would happen if the process noise source statistic were unknown and/or if the interest would be in minimising the worst-case estimation error? These limitations gave rise to the $H_\infty$

filtering, also known as "minimax" filtering. The '$H_\infty$' symbol stands for H-infinity and will be utilised in the sequel.

$H_\infty$ filtering is an advanced and robust estimation technique that minimizes the worst possible effects of the modelling errors and additive noise on the signal estimation errors by introducing uncertainties in the models. Furthermore, it can deal with nonlinearities through the Extended $H_\infty$ Filter (EHF) feature, from local linearisation occurring at each iteration. In addition, parametric uncertainties can also be accommodated through parameter estimation using an augmented filter, as presented later in this chapter.

Even if $H_\infty$ optimisation can be found in Helton (1976), Zames (1981) is the pioneer in proposing a solution to the feedback controller problem, which consists of minimisation of the effect of a disturbance on the plant output, subject to the constraint of internal stability of the close-loop system. In this theory, the $H_\infty$-norm (maximum modulus) of a weighted sensitivity is minimised in an attempt to reduce the energy of the plant output for the worst disturbances. In Zames (1981) and Zames and Francis (1983), it is argued that the $H_\infty$-norm, as opposed to the $H_2$-norm (square root of the integral of the square of the modulus) of the Wiener-Hopf approach, is ideal for dealing with uncertainties in the plant's frequency response or in the frequency spectrum of the exogenous signal. Different techniques can be employed for the determination of the $H_\infty$ optimal weighted sensitivity function. For further details on these various theories, the reader can refer to Zames and Francis (1983), Francis and Zames (1984), Francis *et al.* (1984), Grimble (1985, 1886). The authors and their respective co-workers implemented $H_\infty$ theory for controller design purposes. A similar theory, based on an extended feature, is employed in this thesis to deal with the design of an optimal non-linear estimator based on $H_\infty$ optimisation. In this case, the main objective is to design an optimal estimator, which minimises the maximum error spectrum (or worst case error) of the error difference between the desired and the estimated signals subject to the constraint of the filter.

This review on filtering has motivated the work presented on Chapter V and VI, where both EKF and EHF are applied to the ASM1 model. However, prior to the design of an observer, it is imperative to investigate if the system under study possesses the observability properties. Indeed, in order to guarantee the exponential convergence of the observer, the process must be locally observable, i.e. the linearised tangent model must be observable and fulfil the classical rank condition.

## 3.2) OBSERVABILITY

Observability is an important structural property of dynamic systems defined as the possibility to infer the state of the system from examining its input and output behaviour. The conditions of observability can govern the existence of a full solution to the monitoring and/or control system design problem. In other words, a system is said to be observable if every of its state variable are influencing some of the process variables. Only in this case, it is possible to design an observer that is able to theoretically reconstruct the time evolution of the unmeasured state variables, after a fine arbitrarily chosen time (Dochain and Vanrolleghem, 2001).

On the other hand, if a system is not observable (also called unobservable), solutions to solve the monitoring and/or control system design may not exist. During the last four decades, this property has continued to be examined since it was first discovered and studied by Kalman in 1960 and later by Kalman *et al.*, in 1962 (Franklin, 2002). Sontag (1979), introduced the concept of algebraic observability for *n*-dimensional polynomial systems. This theory implies the existence of a polynomial expression of the state variables in terms of a finite number of derivatives of the output function. Isidori (1985) developed differential geometric methods in the synthesis of feedback laws for non-linear systems and contributed to outstanding design problems such as feedback linearisation, control, disturbance decoupling, and model matching.

Observer designs are often based on linear observability theory, which affects the acceptability of the proposed results. Only few attempts have been proved on very simple non-linear bioprocess systems, based on reduced models that describe non-linear growth reactions. Delattre *et al.*, (2002), performed an observability analysis of a non-linear tubular reactor that involves one non-linear growth reaction and proved that a finite number of dominant modes are observable under certain conditions. Anguelova (2004), compared two different approaches (differential geometric and algebraic) to test the observability of a kinetic model for *S. cerevisiae* and concluded that there is an upper bound derived for the number of Lie derivatives (for the algebraic approach) that have to be considered in the test for rational systems. Furthermore, Dochain and Vanrolleghem (2001), performed a successful local observability analysis on a two-step nitrification process, and on a simple microbial growth process composed of three state variables. Additionally, Bogaerts and

Vande Wouwer (2004), successfully investigated the global observability properties of a non-linear system (a fed-batch bioprocess) based on the observability map theory.

The ASM1 model, which is composed of thirteen state variables, as originally developed is unobservable. This is explained by the fact that not all state variables influence some of the process variables (e.g. soluble and particulate inert organic matter). Hence many researchers have reformulated or reduced the model based on their understanding of the process without systematically checking the observability properties. Therefore, as observability analysis of reduced-order ASM1 models is investigated in the next chapter, it is important to present the concept of linear and nonlinear observability based on the observability map (Isidori, 1985; Nijmeijer and Van der Schaft, 1990). For further details on this subject, the reader can also refer to Gauthier and Kupka (1994), Dochain and Vanrolleghem (2001), Bastin and Dochain (1990), and Bogaerts and Vande Wouwer (2004).

## Linear observability: the Kalman rank test

The following definitions and results given here for observability of linear systems can be found in standard books (e.g. Gopal, 1993; Tewari, 2002). Throughout this section, the following class of discrete time invariant linear system is considered:

$$\begin{aligned} \dot{\mathbf{x}}(t) &= \mathbf{A}\mathbf{x}(t) + \mathbf{B}\mathbf{u}(t) \\ \mathbf{y}(t) &= \mathbf{C}\mathbf{x}(t) \end{aligned} \tag{3.1}$$

where $\dot{\mathbf{x}}$ is the state variable at time $t$, $\mathbf{u}(t)$ the control input, $\mathbf{y}(t)$ is the observation vector (also called output vector), **A** is the system matrix (also called state evolution matrix), **B** the control gain matrix (also called input vector), and **C** the output matrix. In the time variant case, **A**, **B** and **C** are matrix functions of time with constant parameters. Note that the following linear observability description, also called the Kalman rank test, is also applicable to discrete time systems.

The linear system describe by Equation (3.1) is said to be observable at time step $t_0$ if, for a state $\mathbf{x}(t_0)$, there is a finite $t_1 > t_0$ such that knowledge of the output **y** from $t_0$ to $t_1$ are sufficient to determine the state $t_0$. On the other hand, a system is said to be unobservable when the values of some elements in the state vector at time $t_0$ may not be determined from examining the system outputs regardless of the number of measurements (or observation).

Though, and when possible, additional observations may allow the full state information to be accumulated in order to obtain a complete observable system. The linear time variant system described by Equation (3.1), with state vector **x** of dimension $N$, is said to be observable if the observability matrix $\boldsymbol{O}$, with

$$\boldsymbol{O} = \begin{bmatrix} \mathbf{C} \\ \mathbf{CA} \\ \mathbf{CA}^2 \\ \vdots \\ \mathbf{CA}^{N-1} \end{bmatrix}, \tag{3.2}$$

is full rank. The proof of this test (Gopal, 1993) utilises Equation (3.1) to determine the value of $\mathbf{y}(t)$ for $0 \leq t \leq N\text{-}1$ in terms of $\mathbf{x}(0)$ and the known control input $\mathbf{u}(t)$ during that time period. In other words, the linear stationary system is observable only if

$$rank(\boldsymbol{O}) = N\ . \tag{3.3}$$

This test is only valid for the type of linear systems of the form of Equations (3.1). For non-linear systems, two types of solutions remain possible to solve the observability problem. The first consists of the performance of a non-linear observability analysis and is presented later in this chapter. The last, an alternative solution that is often employed within complex non-linear systems, is the piece-wise linear method.

## Piece-wise linear observability

This approach, which is often used in control engineering to check the observability of non-linear models, consists of using the linear observability theory, piece-wise in time. In other words, one can assume that the non-linear system under study is composed of a linear model at each sampling point. Under this assumption, the Kalman rank test ($[\mathbf{C}\ \mathbf{CA}\ldots\mathbf{CA}^{n-1}]'$) for observability of linear systems can be applied piece-wise in time (at each sampling point). This type of approach is investigated through simulation results in Chapter IV. However, applying the linear theory on non-linear models usually affects the acceptability of the proposed results. Therefore, when deterministic models are not too complex, it is important to perform non-linear observability analyses, for instance based on the Lie derivatives (also called observability map), prior non-linear observer designs and implementations.

# Non-linear observability: the Lie derivatives

Observability is a critical issue in dynamical systems (Dochain and Vanrolleghem, 2001) and particularly with bioprocesses applications. For instance, the implementation of Kalman filters for bioreactors is based on the a priori knowledge of the observability of the process. Unfortunately, observability analysis remains very complex in bioprocesses due to the non-linear aspects of their dynamics. Furthermore, there are large uncertainties in the kinetics of the biochemical reactions and analytical expressions descriptions usually employed make such an approach even more difficult. Very few applications, in which the observability of non-linear biochemical processes is attempted, are available (Dochain and Vanrolleghem, 2001). Consequently, the purpose of this subsection is to provide sufficient theoretical conditions to determine if a system possesses whether or not the local distinguishability property by the so-called "observability rank condition" as established by Hermann and Krener (1977). The following theory is based on Hermann and Krener (1977), Isidori, (1985), and Bogaerts and Vande Wouwer (2004).

Throughout this section, the following class of non-linear systems with outputs (or measurements) is considered

$$\dot{\mathbf{x}} = \mathbf{f}(\mathbf{x}, \mathbf{u}), \quad \text{with} \qquad \mathbf{x}(0) = \mathbf{x}_0 \tag{3.4}$$

$$\mathbf{y}_i = \mathbf{h}_i(\mathbf{x}), \quad 1 \le i \le p, \tag{3.5}$$

where $\mathbf{x}$ is the state vector with $n$ states $x_1,\ldots x_n$, $\mathbf{u}$ is the input vector with $m$ inputs $u_1,\ldots,u_m$, and $\mathbf{y}$ is the output vector or measurements with $p$ outputs $y_1,\ldots,y_p$. It is assumed that $\mathbf{x} \in X$, $\mathbf{u} \in U$, $\mathbf{y} \in Y$, where $X$, $U$ and $Y$ are open subsets of $\mathcal{R}^n$, $\mathcal{R}^m$, $\mathcal{R}^p$, respectively. The map $\mathbf{h}$: $X \rightarrow Y$ corresponds to the vector of $p$ measurements (observation), where $h_i \in C^\infty(X)$, for $1 \le i \le p$ and $\mathbf{h} = (h_1,\ldots h_p)^T$. It is also assumed that the system is complete for every bounded measurable input $\mathbf{u}(t)$ and for every $\mathbf{x}_0 \in X$ there exists a solution to the system (Equation (3.4)) such that $\mathbf{x}(0) = \mathbf{x}_0$ and $\mathbf{x}(t) \in X$ for all $t \in \mathcal{R}$.

The observability property is related to the distinguishability of the initial states location, given only measurements of outputs (and possibly their derivatives) and inputs. Using the

general state space model given by Equations (3.4) and (3.5), the observation space (or observability map), denoted **w**, is given by

$$\mathbf{w}(\mathbf{x}) = \begin{pmatrix} w^1(\mathbf{x}) \\ w^2(\mathbf{x}) \\ \vdots \\ w^p(\mathbf{x}) \end{pmatrix},$$

with

$$\mathbf{w}^i(\mathbf{x}) = \begin{pmatrix} \mathbf{y}_i \\ \dot{\mathbf{y}}_i \\ \vdots \\ \mathbf{y}_i^{(k_i-1)} \end{pmatrix} = \begin{pmatrix} L_f^0 \mathbf{h}_i(\mathbf{x}) \\ L_f^1 \mathbf{h}_i(\mathbf{x}) \\ \vdots \\ L_f^{k_i-1} \mathbf{h}_i(\mathbf{x}) \end{pmatrix},$$

and

$$k = \sum_{i=1}^{p} k_i, \quad k \geq n, \tag{3.6}$$

where $L_f^k h_i$ is the $k$th Lie derivative along the vector field **f** (with $k$ assimilated to the number of state variables for this specific case), which is defined as

$$L_f^k h_i(\mathbf{x}) = \frac{\partial (L_f^{k-1} h_i(\mathbf{x}))}{\partial \mathbf{x}} \mathbf{f}(\mathbf{x}, \mathbf{u}), \qquad k \geq 1,$$

with

$$L_f^0 h_i(\mathbf{x}) = h_i(\mathbf{x}) . \tag{3.7}$$

Following this introduction, the non-linear observability definitions as well as the conditions that must be satisfied for that property are now presented following Hermann and Krener, (1977):

***Definition 1.*** The non-linear system given by Equations (3.4) and (3.5) is *globally observable* if all initial conditions, $\mathbf{x}_0$, can be determined uniquely from $\mathbf{y}(t)$ and $\mathbf{u}(t)$ in the whole domain of definition $\mathbf{x}_0 \in X$, $\forall \mathbf{u} \in U$ (Hermann and Krener, 1977).

This concept can be further supported if the state trajectories progress in a local neighbourhood, leading to *local observability* property. But on the other hand, the notion of global observability can be seen as weakened by requiring that a given initial state is only distinguishable from its neighbours, leading to the *weakly observability* property. Finally, restricting trajectories to lie in a local neighbourhood can further support the last notion:

***Definition 2.*** The non-linear system given by Equations (3.4) and (3.5) is *locally weakly observable* at $\mathbf{x}_0$ if all initial conditions in a neighbourhood, $V$, of $\mathbf{x}_0$, which lead to state trajectories remaining in some open neighbourhood $U$ at $\mathbf{x}_0$ under control action $\mathbf{u}$, can be uniquely determined from $\mathbf{y}(t)$ and $\mathbf{u}(t)$ (Hermann and Krener, 1977).

It is important to observe that these definitions are equivalent for linear systems and in addition, it is worth noting that the linear results are independent of the input trajectory. Finally, we give the conditions for evaluating two of the forms of non-linear observability as follows:

***Condition 1.*** The non-linear system given by Equations (3.4) and (3.5) is *globally observable* if $\mathbf{w}^{\mathrm{I}}(\mathbf{x})$ is uniquely invertible with respect to $\mathbf{x}$ in the whole domain of definition (Hermann and Krener, 1977).

***Condition 2.*** The non-linear system given by Equations (3.4) and (3.5) is *locally weakly observable* if the Jacobian of $\mathbf{w}(\mathrm{x})$ has full rank in the whole domain of definition (Hermann and Krener, 1977).

As defined in Condition (1), the system is said *globally observable* if the inverse $\mathbf{w}^{\mathrm{I}}(\mathbf{x})$ of the observation space exist everywhere (in the state and input space). However, as the solution of Equation (3.6) is not a trivial problem, global observability can be difficult to consider in practice (Bogaerts and Vande Wouwer, 2004). Therefore, the local weak observability theory is mainly considered in chapter IV, which leads to study the local invertibility of the observability map, in the neighbourhood of a point $\mathbf{x}$. Hence, the system is said *locally weakly observable* if its

$$\text{rank } \mathcal{Q}(\mathbf{x}) = n \quad \text{with } \mathcal{Q}(\mathbf{x}) = \frac{\partial \mathbf{w}(\mathbf{x})}{\partial \mathbf{x}} \tag{3.8}$$

and $n$, being the order of the system under consideration. On the other hand, if $\mathcal{Q}(\mathbf{x}) \neq n$, then, the system is said (locally) unobservable. There are different reasons for unobservability, which are almost the same as uncontrollability, and can be stated as follows (Tewari, 2002):

- The use of superfluous state variables in the state space model.
- Pole-zero cancellation in the system transfer matrix.
- Too much symmetry (i.e. infinitely many trajectories for the control system that cannot be distinguished from each other by observing the input-output map).
- Physical unobservability (i.e. selection of an output vector which is physically unaffected by one or more state variables).

If the sub-systems which cause unobservability are stable (capability of a system to come near one of its equilibrium points once displaced from it), it is possible to securely disregard those state variables that do not contribute to the outputs, and design an observer based on the residual state variables.

Global observability analysis of non-linear systems is possible through the introduction of canonical forms. These guarantee the invertibility of the observability map and hence, the global observability of the system. This implies that the system can be written in the following form (Gautier and Kupka, 1994, Bogaerts and Vande Wouwer, 2004):

$$\dot{\mathbf{x}} = \begin{bmatrix} \dot{\mathbf{x}}^1 \\ \cdots \\ \dot{\mathbf{x}}^i \\ \cdots \\ \dot{\mathbf{x}}^{w-1} \\ \dot{\mathbf{x}}^w \end{bmatrix} = \begin{bmatrix} \mathbf{f}^1(\mathbf{x}^1, \mathbf{x}^2, \mathbf{u}) \\ \cdots \\ \mathbf{f}^i(\mathbf{x}^1, \ldots, \mathbf{x}^{i+1}, \mathbf{u}) \\ \cdots \\ \mathbf{f}^{w-1}(\mathbf{x}^1, \ldots, \mathbf{x}^w, \mathbf{u}) \\ \mathbf{f}^w(\mathbf{x}^1, \ldots, \mathbf{x}^w, \mathbf{u}) \end{bmatrix},$$

$$\mathbf{y} = \begin{pmatrix} h_1(x_1^1) \\ h_2(x_1^1, x_2^1) \\ \cdots \\ h_{n1}(x_1^1, \ldots, x_{n1}^1) \end{pmatrix}, \tag{3.9}$$

where

$$\forall i \in \{1, \ldots, w\}, \quad \mathbf{x}^i \in \Re^{n_i}, \quad n_1 \geq n_2 \geq \cdots n_w, \quad \sum_{1 \leq i \leq w} n_i = n \tag{3.10}$$

and

$$\forall j \in \{1, \ldots, n_1\} : \frac{\partial h_j}{\partial x_j^1} \neq 0, \quad \forall i \in \{1, \ldots, w-1\},$$

$$\forall (\mathbf{x}, \mathbf{u}) \in \Re^n \times \Re^m : \text{rank } \frac{\partial \mathbf{f}^i(\mathbf{x}, \mathbf{u})}{\partial \mathbf{x}^{i+1}} = n_{i+1}. \tag{3.11}$$

By Conditions (3.10), it is implied that the first state variables ($n_1$) can be inferred from the measurements, while Conditions (3.11) guarantee the detection in the measurement of any differences in the state trajectory. In other words, by considering two different initial states $\mathbf{x}(0)$ and $\mathbf{x}'(0)$, which differ only by the components $\mathbf{x}^2(0)$ and $\mathbf{x}^{2'}(0)$, the first state variable given in Equation (3.9) show that the state trajectories $\mathbf{x}^1(t)$ and $\mathbf{x}^{1'}(t)$, provided that Condition (3.11) is satisfied for $i = 1$. As it is possible to reconstruct the components of $\mathbf{x}^1(t)$ through inversion of the measurement operator $\mathbf{h}(\mathbf{x})$ utilising Condition (3.10), the deviation between the trajectories $\mathbf{x}^1(t)$ and $\mathbf{x}^{1'}(t)$ will be observable in the output. Similarly, identical reasoning holds for any couple $\mathbf{x}^i(t)$ and $\mathbf{x}^{i'}(t)$ from one set of equations to the preceding one described by the system given in Equation (3.9). For convenience, Condition (3.11) can be rewritten in terms of the square matrices $M_i(\mathbf{x},\mathbf{u})$

$$\forall i \in \{1, \ldots, w-1\}, \quad \forall (\mathbf{x}, \mathbf{u}) \in \Re^n \times \Re^m : \text{rank } M_i(\mathbf{x}, \mathbf{u}) = n_{i+1}. \tag{3.12}$$

with

$$M_i(\mathbf{x},\mathbf{u}) = \left( \frac{\partial \mathbf{f}^i(\mathbf{x},\mathbf{u})}{\partial \mathbf{x}^{i+1}} \right)^T \left( \frac{\partial \mathbf{f}^i(\mathbf{x},\mathbf{u})}{\partial \mathbf{x}^{i+1}} \right) \in \Re^{n_{i+1}} \times \Re^{n_{i+1}}. \tag{3.13}$$

The above-mentioned conditions are sufficient to state whether or not a non-linear system possesses the local weak or global observability properties. Once verified, it is possible to design a state observer or software sensor for state and parameter estimation, respectively. However, it should be kept in mind that the observability conditions are restrictive to many practical applications and may account for the failure of software sensors (e.g. extended Kalman filter) to find widespread application.

## 3.3) KALMAN AND $H_\infty$ FILTERING TECHNIQUES

As mentioned previously, non-linear filtering techniques consist of an algorithm for the on-line estimation of the state variables and parameters, which are not measured in real-time, on the basis of related measurements that are more easily accessible (Bastin and Dochain, 1990). For further details on linear and non-linear filtering, the reader can refer to Bastin and Dochain (1990), Dochain and Vanrolleghem (2001), Welch and Bishop (2002), Brown and Hwang (1997), Katebi and Grimble (1998), and Nagpal and Khargonekar (1991).

### Kalman filtering

Since Kalman published a solution for the Minimum Mean-Square Error (MMSE), which is described by a state space formulation, the KF provides a recursive solution to the linear optimal filtering problem. The solution is recursive, which means that each update estimate of the state is calculated from the previous estimate and the new input data. Therefore, only the previous estimate value needs to be stored instead of storing the entire past observed data. As a result, the KF is also convenient for online real-time processing because of the minimal storage data required.

One of the major problems in the area of linear systems is called the observer design problem. It consists of determining (or estimating) the internal states of a linear system, having an access only to the measurements (or outputs). In others words, it is the same as having a "black box" where access to the inputs and outputs is available, without having the ability to observe what's inside the box. One of the approaches to this problem is based on state space model, which can be described by the following linear stochastic difference equation:

$$\mathbf{x}_k = \mathbf{\Phi x}_{k-1} + \boldsymbol{\psi}\mathbf{u}_k + \mathbf{w}_{k-1} \tag{3.14}$$

In addition, the outputs of the system, which illustrate the relationship between the process state and the measurements, are generally represented by the following linear equation:

$$\mathbf{y}_k = \mathbf{H}\mathbf{x}_k + \mathbf{v}_k \tag{3.15}$$

where $\mathbf{\Phi} = \mathbf{A}$, $\boldsymbol{\psi} = \mathbf{B}$ and $\mathbf{H} = \mathbf{C}$ are the terms similar to those presented in Equation (3.1), within the previous section discussing observability. In addition, $w_k$ and $v_k$ are random variables representing the process and measurement noise with noise sequences of zero means and covariance **Q** and **R**, respectively. Note that for the entire process model considered in this work, the white noise will be generated utilising the Gaussian random number function (normal distribution) under Matlab/Simulink. This block generates regularly distributed random numbers over a specific interval, corresponding to the sampling time, with zero mean and the following variance noise and covariance:

$$\begin{aligned} \mathbf{E}\{\mathbf{ww}'\} &= \mathbf{Q} \\ \mathbf{E}\{\mathbf{vv}'\} &= \mathbf{R} \\ \mathbf{E}\{\mathbf{wv}'\} &= \mathbf{NN} = 0. \end{aligned} \tag{3.16}$$

Hence, the process covariance matrix, which is tuned by trial and errors, and the measurement noise vector considered in the rest of the thesis are defined as follows:

$$\mathbf{Q} = \begin{bmatrix} pctq.X & & \\ & \ddots & 0 \\ 0 & & \ddots \\ & & pctq.X^{n-1} \end{bmatrix},$$

and

$$\mathbf{R} = \begin{bmatrix} pctr.X \\ \vdots \\ \vdots \\ pctr.X^{n-1} \end{bmatrix}, \tag{3.17}$$

with '*pctq*' and '*pctr*' representing percentage values with range in a range between 2 to 20% of the steady state concentrations (e.g. the state variable) under study ($X$). To illustrate the magnitude of the chosen noise distribution added to the (measured) state variables of the ASP model presented in Section (3.4), the dissolved oxygen and substrate corrupted measurements are shown in Figure (3.1).

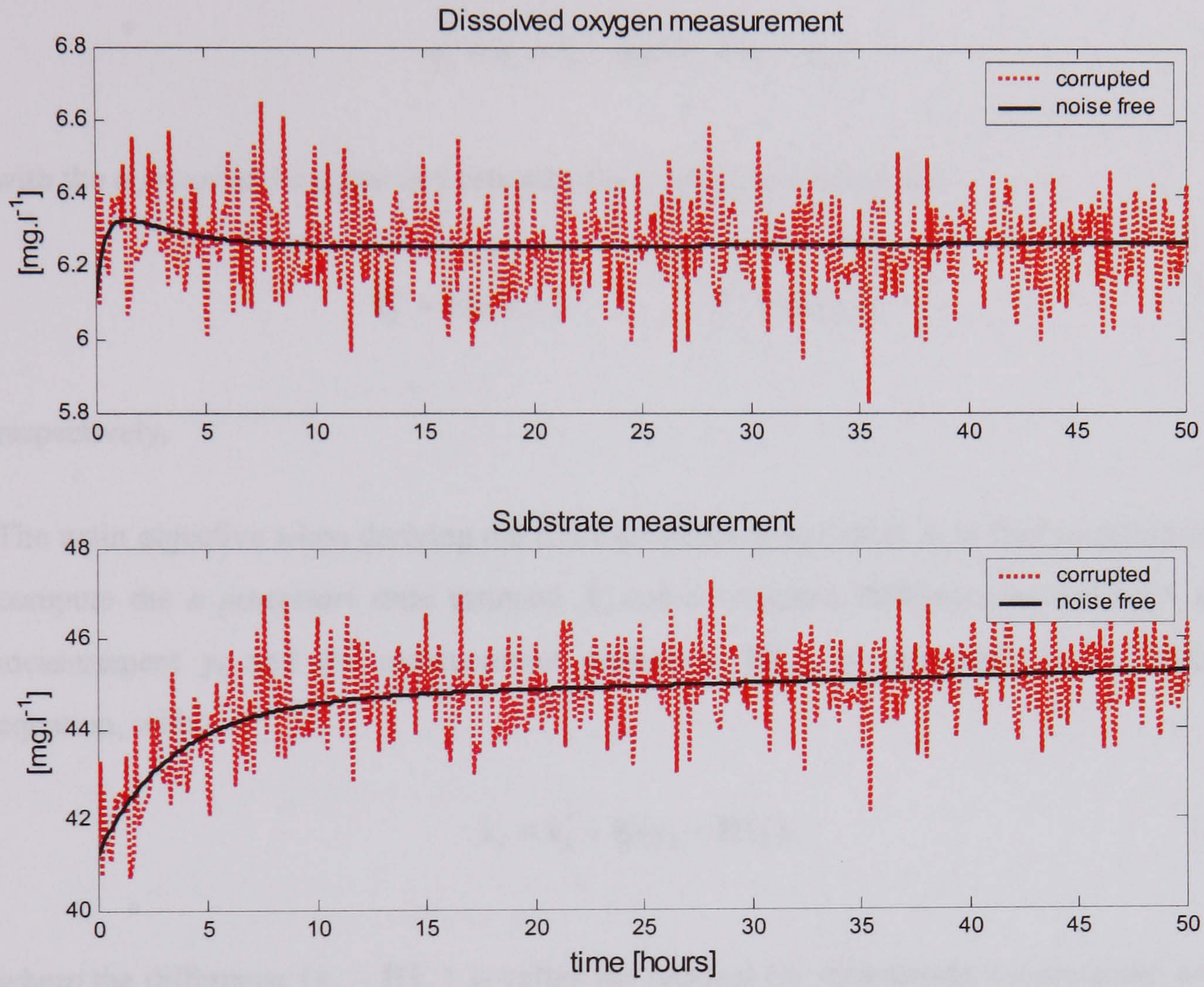


**Figure 3.1** Illustration example of the magnitude utilised for the noise distribution of the dissolved oxygen and substrate measurements, with the ASP model presented in Section (3.4).

The on-line measurements are corrupted by an additive white Gaussian signal with a mean value of zero and a standard deviation that is 10% of the actual value of the state variable. It also illustrates the possible difficulty the identification algorithm has to deal with when a parametric estimation is performed. Furthermore, real measurements are often affected by noise with non-zero mean and changing variance, trends, outliers, sensor failures etc. However, these extra difficulties are not considered in this thesis.

The Kalman filter derivation requires the definition of the estimated state $\hat{\mathbf{x}}_k^- \in \Re^n$ (the 'super minus') defined as the *a priori* state estimate at time step k, given knowledge of the process prior to step k, and $\hat{\mathbf{x}}_k \in \Re^n$ to be the *a posteriori* state estimate at time step k given measurements $\mathbf{y}_k$. The *a priori* and *a posteriori* error are given by (Welch and Bishop, 2002)

$$e_k^- \equiv \mathbf{x}_k - \hat{\mathbf{x}}_k^-, \text{ and } e_k \equiv \mathbf{x}_k - \hat{\mathbf{x}}_k, \tag{3.18}$$

with the *a priori* and *a posteriori* estimate error covariance are given by

$$\mathbf{P}_k^- = E[e_k^- e_k^{-T}], \qquad \mathbf{P}_k^- = E[e_k e_k^T], \tag{3.19}$$

respectively.

The main objective when deriving the Kalman observer algorithm is to find an equation that compute the *a posteriori* state estimate $\hat{\mathbf{x}}_k^-$ and a weighted difference between the actual measurement $\mathbf{y_k}$ and the measurement prediction $\mathbf{H}\hat{\mathbf{x}}_k^-$, as presented in the following equation, with

$$\hat{\mathbf{x}}_k = \hat{\mathbf{x}}_k^- + \mathbf{K}(\mathbf{y}_k - \mathbf{H}\hat{\mathbf{x}}_k^-), \tag{3.20}$$

where the difference $(\mathbf{y}_k - \mathbf{H}\hat{\mathbf{x}}_k^-)$ is called the residual (or measurement innovation) and the n × m matrix **K** is the Kalman gain (also called the blending factor) that minimizes the *a posteriori* error covariance given in Equation (3.15). One form of the equation that is required in minimizing the error is given by (Welch and Bishop, 2002)

$$\mathbf{K}_k = \mathbf{P}_k^- \mathbf{H}^T (\mathbf{H}\mathbf{P}_k^- \mathbf{H}^T + \mathbf{R})^{-1}, \tag{3.21}$$

where **P** is the solution of the following Riccati equation

$$\mathbf{P}_k^- = \mathbf{\Phi}_k \mathbf{P}_{k-1} \mathbf{\Phi}_k^T + \mathbf{Q}_k \tag{3.22}$$

The computation of the discrete Kalman algorithm is summarised in Figure (3.2). It is differentiated in two groups of equations: (1) the time update equations (prediction) and (2)

the measurement update equations (correction). This representation, proposed by Brown *et al.*, (1997), is given in a loop form, which can be seen as a computer algorithm.

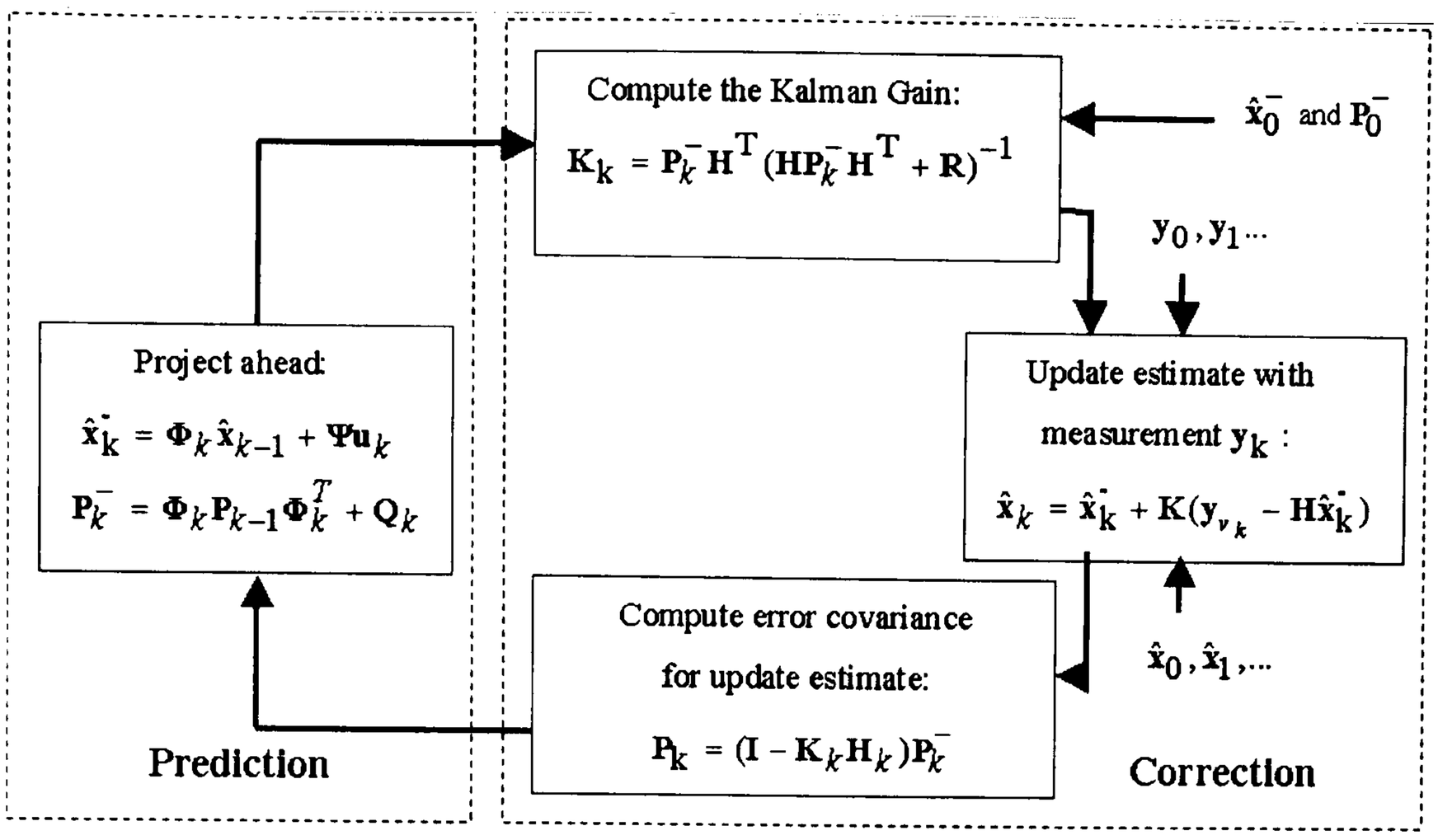


**Figure 3.2** Kalman Filter loop including the prediction and correction phases (source: Brown and Hwang, 1997)

Note that both the discrete and continuous filters are implemented in this work. The continuous KF is proposed in Figure (3.3).

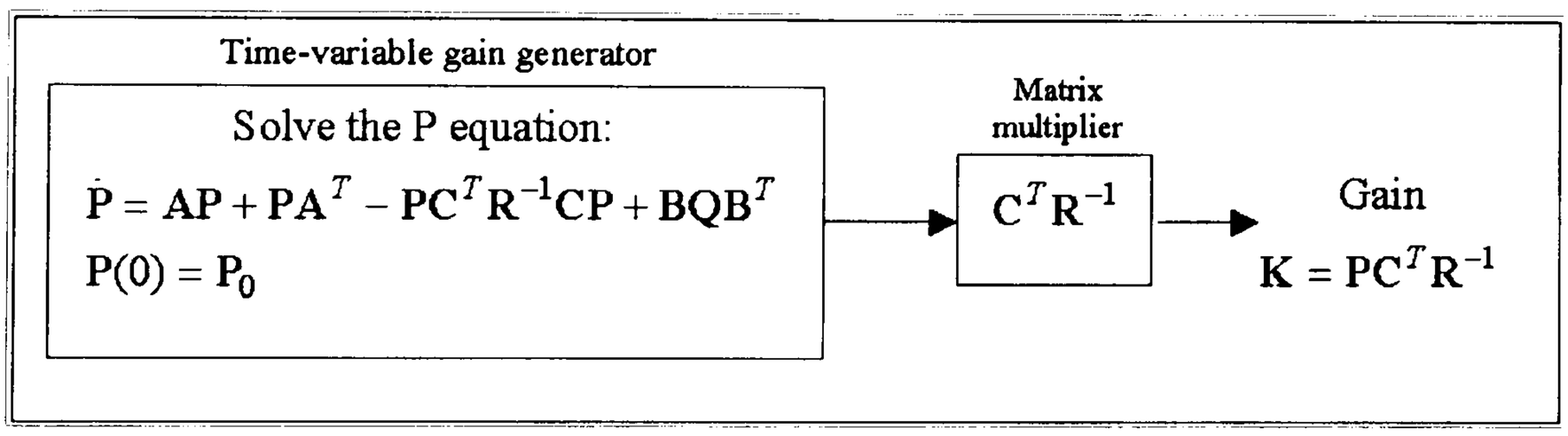


**Figure 3.3** The Kalman Gain Generator for the continuous case where the matrix coefficient **A**, **B**, and **C** are equivalent to **Φ**, **Ψ** and **H** in the discrete case, respectively (source: Brown and Hwang, 1997)

It has a similar structure to that of the discrete case, however the solution to the Riccati equation (**P**) and the blending factor (**K**) differs slightly. The proof of this algorithm can be found in Brown and Hwang, (1997). The linear KF is limited to linear systems. In addition, it can provide an estimate of non-linear state variables if the inputs of the system are constant

or slightly perturbed. However, with such approach and for the proposed ASP model ending this chapter, the convergence of the estimate toward the true state is not guarantee if the inputs are perturbed for more than 25% from their original values. The implementation of an extended feature remains the best solution (to a certain extent) to overcome the non-linearity problems generated for instance by the influent wastewater entering the treatment plant.

## The extended Kalman filter

Most of physical systems are described by non-linear equations, with a non-linear continuous (or discrete) state space model of the form

$$\dot{\mathbf{x}}(t) = \mathbf{f}(x,t) + \mathbf{G}(t)\mathbf{w}(t) \tag{3.23}$$

$$\mathbf{y}(t) = \mathbf{C}(x,t) + \mathbf{v}(t) \tag{3.24}$$

where $\mathbf{x} \in \mathcal{R}^n$, $\mathbf{w} \in \mathcal{R}^m$, $\mathbf{D} \in \mathcal{R}^{n \times m}$, $\mathbf{v}$ and $\mathbf{y} \in \mathcal{R}^r$, and $\mathbf{f}$ and $\mathbf{C}$ are non-linear functions, of appropriate dimension, replacing the linear system described by Equation (3.14) and the measurement model given by Equation (3.15). Similar assumptions as that proposed in the case of the linear Kalman filter are made about the process and measurement noises statistic.

One of the solutions to successfully utilise the above-mentioned Kalman filtering theory is the removal of the non-linearities of the dynamic equations describing the system and the output equations. This can be achieved with a small change model of the non-linear differential equations by linearising the system about the state trajectory. The linearised Kalman filter has the advantage that the filter gains are independent of the states and can be computed a priori based on a nominal solution to the non-linear differential equation. However, significant model error and filter divergence can occur, especially in bioprocesses applications where the influent wastewater data are highly non-linear. The EKF can often (but not always) prevent this divergence by estimating the state variables on-line. This approach consists of linearising around the most recent estimates in the attempt to minimise the covariance of the estimation error, assuming that the system under consideration is exactly known, as well as the noise source statistics. A summary of the EKF algorithm is presented in Table (3.1), which serve as a basis for the various applications presented in Chapter V and VI. The full derivation of the extended Kalman filter is provided in Appendix C.

| Steps | Equations |
|---|---|
| System model | $\dot{\mathbf{x}}(t) = \mathbf{f}(x,t) + \mathbf{G}(t)\mathbf{w}(t)$ |
| Measurement model | $\mathbf{y}(t) = \mathbf{C}(x,t) + \mathbf{v}(t)$ |
| Initial conditions | $E\left[\mathbf{x}(0)\right] = \bar{\mathbf{x}}(0)$ |
| | $\mathrm{cov}\left[\left(\mathbf{x}(0) - \bar{\mathbf{x}}(0)\right) - \left(\mathbf{x}(0) - \bar{\mathbf{x}}(0)\right)\right] = \mathbf{P}(0)$ |
| Estimator (observer) | $\dot{\hat{\mathbf{x}}}(t) = \mathbf{f}(\mathbf{x},t) + \mathbf{K}(t)\left[\mathbf{y}(t) - \mathbf{C}(t)\hat{\mathbf{x}}(t)\right]$ |
| Covariance matrix | $\dot{\mathbf{P}}(t) = \mathbf{F}\mathbf{P}(t) + \mathbf{P}(t)\mathbf{F}^T(t) + \mathbf{D}(t)\mathbf{Q}(t)\mathbf{D}^T(t) - \mathbf{K}(t)\mathbf{R}(t)\mathbf{K}^T(t)$ |
| Gain Matrix | $\mathbf{K}(t) = \mathbf{P}(t)\mathbf{C}^T(t)\mathbf{R}^{-1}(t)$ |
| Linearised system matrix | $\mathbf{F} = \left.\frac{\partial \mathbf{f}}{\partial \mathbf{x}}\right\|_{\mathbf{x}=\hat{\mathbf{x}}}$ and $\mathbf{C} = \left.\frac{\partial \mathbf{C}}{\partial \mathbf{x}}\right\|_{\mathbf{x}=\hat{\mathbf{x}}}$ |

**Table 3.1** Summary of the continuous extended Kalman filter algorithm utilised to perform state estimation.

## Parameter estimation with an extended Kalman filter

The extended Kalman filter can be utilised either for state estimation, parameter estimation or joint state and parameter estimation (Dochain and Vanrolleghem, 2001; Bastin and Dochain, 1990, Jeppsson, 1996). Parameter estimation can only be achieved with the aid of experimental data, which contributes in determining the "optimum" values of the parameters that arise in a mathematical description, assuming that the relationships between the variables and the parameters are explicitly known.

Various conventional techniques (e.g. Bayesian, maximum likelihood, weighted least squares and least square estimations) are generally used for parameter estimation and it is important to initially conduct certain analyses in selecting the identifiable linear or non-linear subset of parameters. For instance, structural, practical and sensitivity analyses are key tools for the parametric estimation problems. These criteria, which are clearly presented in Jeppsson (1996) and Dochain and Vanrolleghem (2001), are not investigated in this work for two reasons: (1) parameter estimation has been extensively covered within the bioprocess (including the ASM1 model) research community and (2) because real or experimental data, which are the basis for parameter identification, are not available at current time.
Successful applications are presented in Jeppsson (1996), Weijers (2000), Dochain and Vanrolleghem (2001), Bastin and Dochain, (1990), Ayesa *et al.* (1991) and Kabouris and Georgakakos (1995). However, the corresponding authors and co-workers investigations remain theoretical as unrealistic assumptions are sometimes considered. For instance, Ayesa

*et al.*, (1991) and Kabouris and Georgakakos (1995) performed parameter and state estimations of an ASP model assuming that all state variables (nine and eleven, respectively) were measured. Farza *et al.*, (1997), proposed on-line estimation of the kinetic growth rate in a fermentation process where both major state variables (biomass and substrate) were assumed to be measured. Jeppsson (1996), assumed on-line measurements of the heterotrophic and autotrophic biomass concentrations, which is a theoretical approach due to the fact that such measurements are (still) not available on-line. All these theoretical approaches are defendable because the parametric estimation with biological system is still an open problem for practical applicability, as stated by Bastin and Dochain (1990):

"*Unfortunately, numerous studies devoted to parameter estimation in biological models have shown that, in practice, the identifiability of the kinetic coefficients is far from being guaranteed and may even be an insuperable difficulty in most applications*"

In addition to the realistic parametric estimation problems, they also concluded that the stability and convergence properties of the EKF algorithm are extremely difficult to analyse, and remain an open problem. Furthermore, Ljung (1979) concluded that an EKF estimator may give bias estimates or may even diverge if not properly initialised. Therefore, the selected parameters that are considered in this thesis (e.g. chapter V and VI) are similar to the one studied by Jeppsson (1996), in which a successful identifiability analysis on the ASM1 model has been already performed. The difference with Jeppsson is that the estimation of the selected parameters is performed with both an EKF feature and a robust non-linear filter, namely, the EHF. For further information on system identification and parameter estimation, the reader can refer to Jeppsson (1996), Ljung (1989) and Bohlin (1991).

The augmented algorithm (augmented with the additional parameters) selected for the estimation is now presented. Considering the following discrete augmented state space model:

$$\dot{\mathbf{x}}(t) = \mathbf{f}(t)(\mathbf{x}(t), \mathbf{u}(t), \boldsymbol{\theta}) + \mathbf{G}(t)(\mathbf{x}(t), \boldsymbol{\theta})\mathbf{w}(t) \tag{3.25}$$

$$\mathbf{y}(t) = \mathbf{h}(t)(\mathbf{x}(t), \boldsymbol{\theta}) + \mathbf{v}(t), \tag{3.26}$$

where the usual assumptions about the noise statistics must be made as for the linear and extended Kalman filters. In order to estimate on-line the vector parameter $\boldsymbol{\theta}$, an augmented model is designed, in which $\boldsymbol{\theta}$ is augmented to the initial state vector $\mathbf{x}_k$. Consequently, the non-linear model described by Equations (3.25) and (3.26) is rewritten in the following form:

$$\begin{bmatrix} \dot{\mathbf{x}}(t) \\ \dot{\boldsymbol{\theta}}(t) \end{bmatrix} = \begin{bmatrix} \mathbf{f}(t)(\mathbf{x}(t), \mathbf{u}(t), \boldsymbol{\theta}) \\ \boldsymbol{\theta}(t) \end{bmatrix} + \begin{bmatrix} \mathbf{G}(t)(\mathbf{x}(t), \boldsymbol{\theta}) & 0 \\ 0 & \boldsymbol{I} \end{bmatrix} \begin{bmatrix} \mathbf{w}(t) \\ \zeta(t) \end{bmatrix} \tag{3.27}$$

$$\mathbf{y}(t) = \mathbf{h}(t)(\mathbf{x}(t), \boldsymbol{\theta}) + \mathbf{v}(t) \tag{3.28}$$

where $\boldsymbol{I}$ is an identity matrix, $\boldsymbol{\theta}(t)$ is considered as a random constant vector ($\dot{\boldsymbol{\theta}}(t) = \boldsymbol{\theta}(t) + \zeta(t)$) and $\zeta(t)$ is a white Gaussian noise sequence with zero mean and uncorrelated with $\mathbf{w}(t)$ (Chui and Chen, 1991). The adaptive capabilities of the filter are achieved with the covariance of the signal $\zeta(t)$ and the identification of the selected parameters requires an initialisation of the augmented covariance matrix $\tilde{\mathbf{P}}_0$, which is similar to the one described in Table (3.1). The only difference is that an augmented system is considered, rather than the standard one. The augmented state variables and process noise vectors can be written in the following form

$$\tilde{\mathbf{x}}(t) = \begin{bmatrix} \mathbf{x}(t) \\ \boldsymbol{\theta}(t) \end{bmatrix} \text{ and } \qquad \tilde{\mathbf{w}}(t) = \begin{bmatrix} \mathbf{w}(t) \\ \zeta(t) \end{bmatrix}, \tag{3.29}$$

respectively. The model described by equations (3.25) and (3.26) can be written in the following form:

$$\dot{\tilde{\mathbf{x}}}(t) = \tilde{\mathbf{f}}(t)(\tilde{\mathbf{x}}(t), \tilde{\mathbf{u}}(t)) + \tilde{\mathbf{G}}(t)(\tilde{\mathbf{x}}(t))\tilde{\mathbf{w}}(t) \tag{3.30}$$

$$\tilde{\mathbf{y}}(t) = \tilde{\mathbf{h}}(t)(\tilde{\mathbf{x}}(t)) + \mathbf{v}(t) \tag{3.31}$$

The augmented model described by equations (3.30) and (3.31) has an identical structure to the standard model given by Equations (3.23) and (3.24). However, with an augmented system, an accurate initial guess of the parameter vector $\boldsymbol{\theta}(t)$ and the initial augmented state vector $\tilde{\mathbf{x}}(t)$ must be supplied to the algorithm. As stated previously, this initial guess must

be as close as possible from the real value (at least for biological applications), which may not be possible in practice. However, for grey box model, the initial guess for the states and parameters are usually available, which make the identification procedure relatively easy in comparison to that for black-box identification. Furthermore, the measurement noise covariance, usually supplied by the sensor manufacture, and the process noise covariance, which reflect the confidence in the model structure accuracy, must be known. This covariance adjustment is often performed by trial and error, which can be time consuming because of the high number of experiments that need to be performed.

## Extended H-infinity filtering

As stated previously, the KF and EKF present disadvantages (e.g. requirements of an accurate initialisation, stability and convergence properties not guaranteed, knowledge of the noise source properties is required), which can lead to unsuccessful applications when applied upon biological processes (and within other fields). Therefore, the extended $H_\infty$ filtering algorithm, which is a pre-requisite to overcome these drawbacks, is presented in the following section. The design of $H_\infty$ filters can be considered as a dual problem to the design of $H_\infty$ controllers. Therefore, a similar philosophy used in the controller design proposed by Katebi and Grimble (1998), and Nagpal and Khargonekar (1991) is followed here but in the case of the estimator design. Consider the following class of linear system given by:

$$\begin{cases} \dot{\mathbf{x}}(t) = \mathbf{A}(t)\mathbf{x}(t) + \mathbf{B}(t)\mathbf{u}(t) + \mathbf{G}_1(t)\mathbf{w}(t) \\ \mathbf{y}(t) = \mathbf{C}_1(t)\mathbf{x}(t) + \mathbf{G}_2(t)\mathbf{v}(t) \\ \mathbf{z}(t) = \mathbf{C}_2(t)\mathbf{x}(t) \end{cases} \tag{3.32}$$

where **x**, **u** and **y** are similar to those described by Equation (3.4) and (3.5), and **z** is the estimated output vector with $q$ outputs $(q_1,\ldots,q_p)^T$. $\mathbf{G_1}(t)\mathbf{w}(k)$ and $\mathbf{G_2}\mathbf{v}(t)$ represent the process and measurement noise with noise sequences of zero means and covariance **Q** and **R**, respectively. The filtering problem is thus one of finding an estimate $\hat{\mathbf{z}}(t)$ of $\mathbf{z}(t)$ using the measurements $\mathbf{y}(t)$. The filter has to minimize the following cost function (Nagpal and Khargonekar, 1991):

$$J = \sup_{\mathbf{w}\in L_2[0,\infty]} \frac{\|\tilde{\mathbf{z}}\|_2^2}{\|\mathbf{w}\|_2^2} < \gamma^2 \tag{3.33}$$

with

$$\tilde{\mathbf{z}}(t) = \mathbf{z}(t) - \hat{\mathbf{z}}(t) \text{ and for } \gamma > 0, \tag{3.34}$$

where gamma ($\gamma$) is the pre-specified $H_\infty$ performance. Considering the following assumptions (Doyle *et al.*, 1989)

(i) $(\mathbf{A},\mathbf{B})$ is stabilisable and $(\mathbf{C}_1,\mathbf{A})$ is detectable

(ii) $(\mathbf{A},\mathbf{G}_1)$ is stabilisable and $(\mathbf{C}_2,\mathbf{A})$ is detectable ,

the solution of the following $H_\infty$ Riccati equation (Doyle *et al.*, 1989; Nagpal and Khargonekar, 1991):

$$\begin{aligned}\mathbf{A}(t)\mathbf{P}(t) + \mathbf{P}(t)\mathbf{A}^T(t) - \mathbf{P}(t)(\gamma^{-2}\mathbf{C}_2{}^T(t)\mathbf{C}_2(t) - \\ \mathbf{C}_1{}^T(t)\mathbf{R}^{-1}(t)\mathbf{C}_1(t))\mathbf{P}(k) + \mathbf{G}_1(t)\mathbf{Q}\mathbf{G}_1^T(t) = 0,\end{aligned} \tag{3.35}$$

must be solved in order to calculate the $H_\infty$ filter gain given by

$$\mathbf{K}_h = \mathbf{P}(t)\mathbf{C}_1^T(t)\mathbf{R}^{-1}(t). \tag{3.36}$$

The filtering problem can be stated as minimising the cost function $J$ in Equation (3.33) for a known value of $\gamma > 0$. For the time invariant systems, the optimal value of $\gamma$ can be found by selecting a large value of $\gamma$ and solving the algebraic Riccati equation in Equation (3.35) in order to calculate the filter gain given by Equation (3.36). The value of $\gamma$ can then be reduced in the usual manner until one of the eigenvalues of the system becomes imaginary or negative (Katebi and Grimble, 1998).

The extended $H_\infty$ filter is an extension of the linear $H_\infty$ filter. The EHF is used to estimate the states of the non-linear reduced-order system, by linearising the system equations around a nominal operating point. Consider the class of non-linear systems defined by

$$\begin{aligned}\dot{\mathbf{x}}(t) &= f(\mathbf{x}(t),t) + \mathbf{K}(\mathbf{x}(t),t) + \mathbf{G}(\mathbf{x}(t),t)\mathbf{w}(t) \\ \mathbf{y}(t) &= h(\mathbf{x}(t),t) + \mathbf{v}(t)\end{aligned}, \tag{3.37}$$

and assuming that the conditional-mean estimate $\hat{\mathbf{x}}(t)$ is known and used to expand the system and measurement models in a Taylor series about $\mathbf{x}(t) = \hat{\mathbf{x}}(t)$. The state space system described by Equation (3.32) is a linearised system with matrices defined by (Katebi and Grimble, 1998)

$$\mathbf{A}(t) = \frac{\partial f[\hat{\mathbf{x}}(t),t)]}{\partial \hat{\mathbf{x}}(t)} \text{ , } \mathbf{B}(t)=\mathbf{K}[\hat{\mathbf{x}}(t),t)]$$

$$\mathbf{G}_1(t)=\mathbf{G}_1[\hat{\mathbf{x}}(t),t)] \text{ , } \mathbf{C}_2(t) = \frac{\partial h[\hat{\mathbf{x}}(t),t)]}{\partial \hat{\mathbf{x}}(t)} . \tag{3.38}$$

The determination of the $H_\infty$ Riccati equation and filter gain are similar to Equations (3.35) and (3.36), respectively. The extended $H_\infty$ filter is summarised in Table (3.2)

| Step | Equations |
|---|---|
| Initial conditions | $\hat{\mathbf{x}}(t_0) = x_0, \mathbf{P}(t_0) = 0$ |
| System matrices | $\mathbf{A}(t) = \frac{\partial f[\hat{\mathbf{x}}(t),t)]}{\partial \hat{\mathbf{x}}(t)}$ , $\mathbf{B}(t)=\mathbf{K}[\hat{\mathbf{x}}(t),t)]$ |
| | $\mathbf{G}_1(t)=\mathbf{G}_1[\hat{\mathbf{x}}(t),t)]$ , $\mathbf{C}_2(t) = \frac{\partial h[\hat{\mathbf{x}}(t),t)]}{\partial \hat{\mathbf{x}}(t)}$ |
| Filter algorithm | $\dot{\hat{x}}(t) = \mathbf{A}(t)\hat{\mathbf{x}}(t) + \mathbf{B}(t)\mathbf{u}(t) + \mathbf{K}_h[\mathbf{y}(t) - \mathbf{C}_2(t)\hat{\mathbf{x}}(t)]$ |
| Filter gain | $\mathbf{K}_h = \mathbf{P}(t)\mathbf{C}_1^T(t)\mathbf{R}^{-1}(t)$ |
| Estimated states | $\mathbf{z}(t) = \mathbf{C}_2\hat{\mathbf{x}}(t)$ |
| $H_\infty$ error variance | $\mathbf{A}(t)\mathbf{P}(t) + \mathbf{P}(t)\mathbf{A}^T(t) - \mathbf{P}(t)(\gamma^{-2}\mathbf{C}_2{}^T(t)\mathbf{C}_2(t) - \mathbf{C}_1^T(t)\mathbf{R}^{-1}(t)\mathbf{C}_1(t))\mathbf{P}(k) + \mathbf{G}_1(t)\mathbf{Q}\mathbf{G}_1^T(t) = 0$ |

**Table 3.2** A summary of the continuous extended $H_\infty$ filter algorithm utilised to perform state estimation (Katebi and Grimble, 1998).

The state vector may be partitioned so that the parameter can be simultaneously estimated. This is achieved by augmented the state space model, which is of the form:

$$\tilde{\mathbf{x}}(t) = \begin{bmatrix}\mathbf{x}(t) & \boldsymbol{\theta}(t)\end{bmatrix} \tag{3.39}$$

In addition,

$$f(x,t)=\begin{bmatrix} f_1(\theta,t) & 0 \\ 0 & 0 \end{bmatrix}\begin{bmatrix} x \\ \theta \end{bmatrix} \tag{3.40}$$

and

$$\tilde{\mathbf{G}}_1=\begin{bmatrix} \mathbf{G}_1 & 0 \\ 0 & G_\theta \end{bmatrix}, \tilde{\mathbf{C}}_1=\begin{bmatrix} \mathbf{C}_1 & 0 \end{bmatrix} \tag{3.41}$$

The proposed extended $H_\infty$ filter for the augmented system can now be defined, as presented in Table (3.3). Similar to the augmented extended Kalman filter algorithm presented above, the parameters are modelled as integrators that are driven by white noise and augmented to the system states.

| Steps | Equations |
|---|---|
| Initial conditions | $\tilde{\hat{\mathbf{x}}}(t_0)=\tilde{\mathbf{x}}_0, \tilde{\mathbf{P}}(t_0)=0$ |
| System matrices | $\mathbf{\Phi}=\partial\left[\frac{f(\mathbf{x},t)}{\partial\mathbf{x}}\right]\Big\|_{x=\bar{x}}=\begin{bmatrix} f_1(\theta) & \Phi_{12} \\ 0 & 0 \end{bmatrix}$ <br> where $\Phi_{12}=\partial\left[\frac{f_1(\theta)x}{\partial x_2}\right]\Big\|_{\mathbf{x}=\bar{\mathbf{x}}}$ |
| Filter algorithm | $\dot{\tilde{\hat{\mathbf{x}}}}(t)=f(\tilde{\hat{\mathbf{x}}},t)+\tilde{\mathbf{K}}_h[y(t)-\tilde{\mathbf{C}}_2\tilde{\hat{\mathbf{x}}}(t)]$ |
| Filter gain | $\tilde{\mathbf{K}}_h=\tilde{\mathbf{P}}(t)\tilde{\mathbf{C}}_1^T(t)\mathbf{R}^{-1}(t),$ |
| Estimated states | $\tilde{\mathbf{z}}(t)=\tilde{\mathbf{C}}_2\tilde{\hat{\mathbf{x}}}(t)$ |
| $H_\infty$ error variance | $\dot{\tilde{\mathbf{P}}}(t)=\mathbf{\Phi}(t)\tilde{\mathbf{P}}(t)+\tilde{\mathbf{P}}(t)\mathbf{\Phi}^T(t)-\tilde{\mathbf{P}}(t)(\gamma^{-2}\tilde{\mathbf{C}}_2{}^T(t)\tilde{\mathbf{C}}_2(t)-\tilde{\mathbf{C}}_1^T(t)\mathbf{R}^{-1}(t)\tilde{\mathbf{C}}_1(t))\tilde{\mathbf{P}}(t)+\tilde{\mathbf{G}}_1(t)\tilde{\mathbf{Q}}\tilde{\mathbf{G}}_1^T(t)=0$ |

**Table 3.3** A summary of the continuous augmented extended $H_\infty$ filter algorithm utilised to perform joint state and parameter estimation (Katebi and Grimble, 1998).

# 3.4) SOFTWARE SENSORS EXAMPLES BASED KALMAN AND $H_\infty$ FILTERING

In order to exemplify a few of the problems discussed in the previous sections, two examples are presented. The first one aims at demonstrating both the extended Kalman filter performances and drawbacks when applied to a simple bioprocess. The second illustrates the extended $H_\infty$ filter performances when applied to a stochastic model. The biological system is an activated sludge process model, which consists of a series of activated sludge tanks in which different conditions (anaerobic, anoxic and aerobic) are used to promote the nutrient removal process. The ASPs allow removal of pollutants from the wastewater, principally those that are in soluble form and those that are biodegradable in a period that is technologically acceptable. As displayed in Figure (3.4), it comprises an aeration tank and a secondary clarifier that is necessary for the settling of the biomass and its recycling.

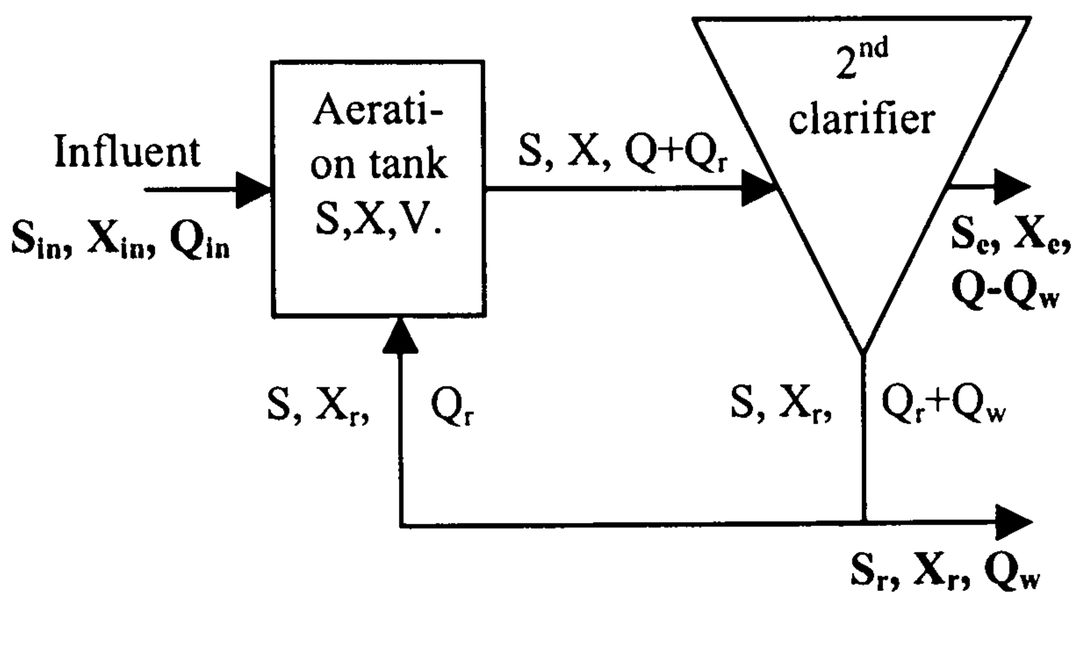


**Figure 3.4** Activated sludge reactor used for joint state and parameter estimation.

where Q represents the secondary influent flow rate; $Q_r$ the return sludge flow rate; $Q_w$ the waste activated-sludge flow rate and $X_e$ the effluent suspended solids. The mass balance on the aerator and the settler are described by the set of non-linear differential Equations (3.42) to (3.45), similar to Nejjari *et al.*, (1999):

$$\dot{X}(t) = \mu(t)X(t) - D(t)(1+r)X(t) + rD(t)X_r(t) \tag{3.42}$$

$$\dot{S}(t) = -\frac{\mu(t)}{Y}X(t) - D(t)(1+r)S(t) + D(t)S_{in} \tag{3.43}$$

$$\dot{C}(t) = -\frac{K_0 \mu(t) X(t)}{Y} - D(t)(1+r)C(t) + K_L a(C_S - C(t)) + D(t)C_{in} \qquad (3.44)$$

$$\dot{X}_r(t) = D(t).(1+r).X(t) - D(t).(\beta + r)X_r(t) \qquad (3.45)$$

where $X$(t), $S$(t), $C$(t) and $X_r$(t) are the states representing the biomass, the substrate, the dissolved oxygen and the recycled biomass concentrations, respectively. The parameters $r$ ($r$=$Q_r$/Q) and $\beta$ ($\beta$=$Q_w$/Q; with Q, $Q_r$ and $Q_w$) represent the ratio of recycled flow to influent flow and the ratio of waste flow to the influent flow, respectively. $S_{in}$ corresponds to the substrate in the feed stream. The biomass growth is described by the specific growth rate, $\mu$ ($\mu$=$r_g$/X) and the yield of cell mass, $Y$. The constants $C_S$, and $K_L$a, represent the dissolved oxygen saturation concentration and the oxygen transfer rate coefficient ($K_L$a = $\alpha$.W with $\alpha$>0 and W=air flow rate), and $K_O$ is a switching constant (DO switch). The kinetic model is similar to one proposed by Olsson (1976) with:

$$\mu(t) = \mu_{max} \frac{S(t)}{K_s + S(t)} * \frac{C(t)}{K_c + C(t)} \qquad (3.46)$$

where $\mu_{max}$ is the maximum specific growth rate, $K_S$ the affinity constant and $K_C$, the saturation constant. For further details on the model description, the reader is referred to Nejjari *et al.*, (1999).

## Software sensor based-EKF

The software sensor implementation is based on an EKF structure. Two measurements (e.g. substrate and dissolved oxygen), which are corrupted by 2% white Gaussian noise, are considered as inputs of the software sensor, as well as the air flow rate ($W$) and the dilution rate ($D$). The dynamic augmented observer utilised for the joint state and parameter estimation example is of the form

$$\begin{aligned} \dot{\tilde{\mathbf{X}}}(t) &= \tilde{\mathbf{A}}(t)\tilde{\mathbf{X}}(t) + \tilde{\mathbf{B}}(t)\tilde{\mathbf{u}}(t) + \tilde{\mathbf{K}}_f(\mathbf{y}(t) - \tilde{\mathbf{z}}(t)) \\ \mathbf{y}(t) &= \mathbf{C}(t)\mathbf{X}(t) + \mathbf{v}(t) \\ \tilde{\mathbf{z}}(t) &= \tilde{\mathbf{C}}(t)\tilde{\mathbf{X}}(t) \end{aligned} \qquad (3.47)$$

The additional state variables (e.g. $X$, $S$, $C$ and $X_r$) are augmented to the initial model to estimate some model parameters. The augmented state vector and inputs given in Equation (3.47) are of the form

$$\tilde{\mathbf{X}}(t) = \begin{bmatrix} X(t) & S(t) & C(t) & X_r(t) & \mu_{\max}(t) & K_S(t) & K_C(t) \end{bmatrix}^T, \tag{3.48}$$

$$\tilde{\mathbf{u}}(t) = \begin{bmatrix} D_{in}(t) & W_{in}(t) & \zeta_{1,in}(t) & \zeta_{2,in}(t) & \zeta_{3,in}(t) \end{bmatrix}^T, \tag{3.49}$$

respectively, where $\zeta_1$, $\zeta_2$ and $\zeta_3$ are white Gaussian noise sequences with zero mean and uncorrelated from each other, where the adaptive capabilities of the filter are achieved with the covariance of the signal $\zeta_{1,2,3}(k)$. Note that the noise sequences are augmented to the initial input vector. However, in the applications presented in Chapter V and VI, these noise sequences will be separated from the deterministic inputs. The system output is of the form

$$\tilde{\mathbf{z}}(t) = \begin{bmatrix} X_{ef}(t) & S_{ef}(t) & C_{ef}(t) & X_{r,ef}(t) & \mu_{\max,ef}(t) & K_{s,ef}(t) & K_{c,ef}(t) \end{bmatrix}^T, \tag{3.50}$$

and the system matrices are define by

$$\tilde{\mathbf{A}}(t) = \left[ \frac{\partial f(\tilde{\mathbf{X}}(t), \boldsymbol{\theta}(t))}{\tilde{\mathbf{X}}(t)} \right]_{\tilde{\mathbf{X}}=\hat{\tilde{\mathbf{X}}}} = \begin{bmatrix} \mathbf{A}(t) & \left[ \frac{\partial \mathbf{X}(t)}{\partial \boldsymbol{\theta}(t)} \right]_{\tilde{\mathbf{X}}=\hat{\tilde{\mathbf{X}}}} \\ 0 & I \end{bmatrix},$$

$$\tilde{\mathbf{B}}(t) = \begin{bmatrix} \mathbf{B}(t) & \vdots & 0 \\ \cdots & \cdots & \cdots \\ 0 & \vdots & I \end{bmatrix}, \quad \tilde{\mathbf{C}}(t) = \begin{bmatrix} \mathbf{C}(t) & \vdots & 0 \end{bmatrix}. \tag{3.51}$$

Simulations results are presented in Figure (3.5) where it appears that the software sensor converges toward the real state with good tracking performances. This type of configuration, which presents great advantages, allows the augmented observer to (1) estimate on-line the concentrations that are hypothetically measured on-line (e.g. dissolved oxygen and substrate) at the same time as filtering the measurement noise created by the physical sensors, (2) to estimate the state variables that are not available in real WWTPs (e.g. biomass and recycled biomass), and (3) to estimate some model parameters.

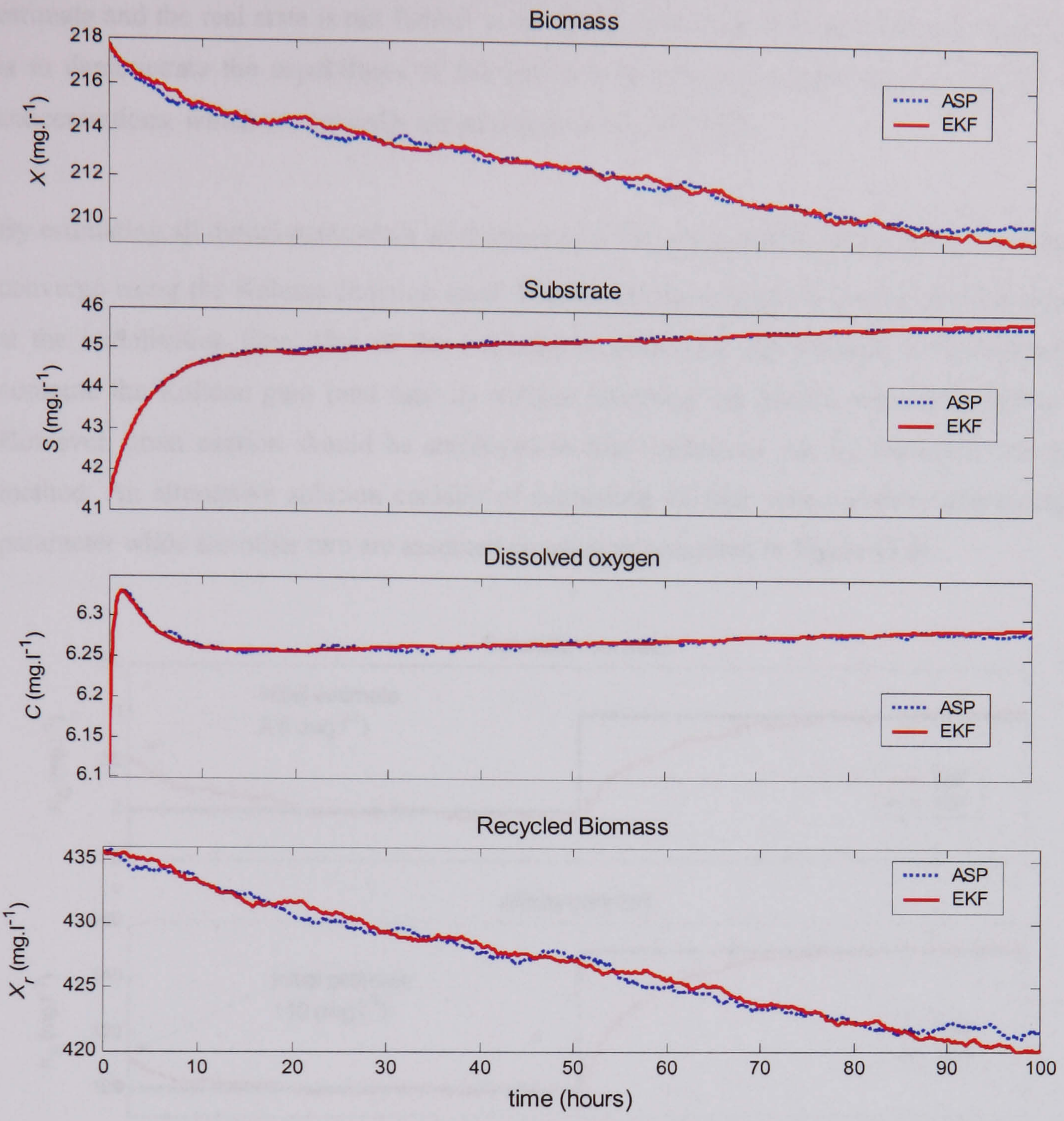


**Figure 3.5** Comparison between the state variables resulting from simulation with the ASP model and the state variables estimated by the software sensor based-EKF. On-line measurement (S and C) are corrupted by an additive white Gaussian signal with a standard deviation that is 2% of the actual value of the state variable. Furthermore, 2% of process noise is also considered.

In this particular case, the main benefit is to estimate the biomasses ($X$ and $X_r$) on-line as it provides an idea of the total weight of the living microorganisms. However, the biomasses estimation presented in Figure (3.5) are 10 to 20 times lower than one would expect in a true process. This is mainly due to the high simplicity of the model and can be overcome by considering the ASM1 model for instance, as presented in Chapter V. The error between the

estimate and the real state is not further investigated in this case because the main objective is to demonstrate the capabilities of the observer to estimate on-line the non-measurable concentrations, which are typically not available in real WWTPs.

By estimating all model parameters simultaneously, the augmented Kalman gain ( $\underline{\tilde{K}}$ ) cannot converge using the Kalman function under Matlab/Simulink because the system is unstable at the initialisation time. One of the solutions to overcome this problem is to eventually compute the Kalman gain (and tune it) without involving the Matlab command 'kalman'. However, great caution should be employed as bias estimation can be achieved with this method. An alternative solution consists of estimating all four state variables and a single parameter while the other two are assumed constant as presented in Figure (3.6).

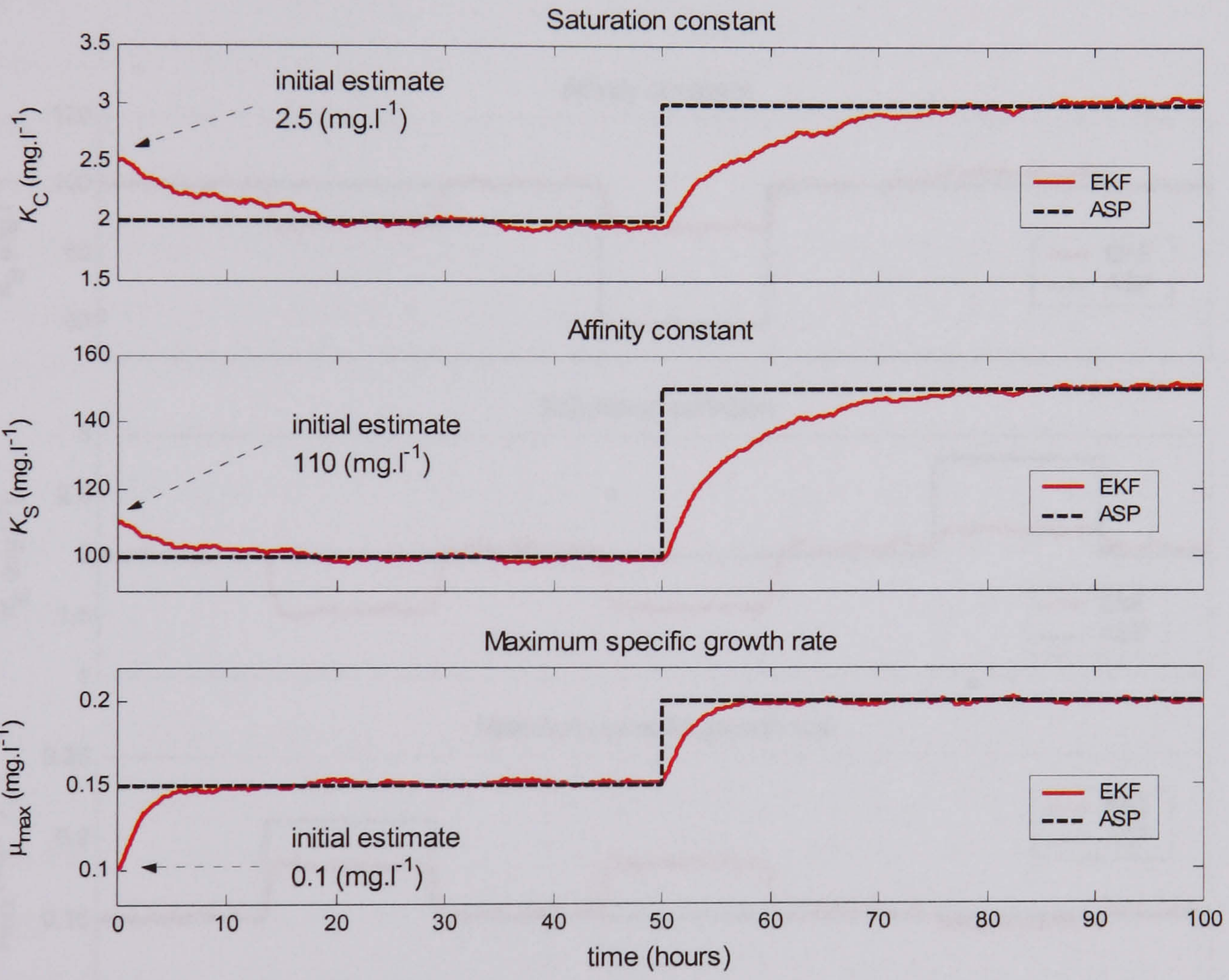


**Figure 3.6** Comparison between the real parameters and the estimated parameters separately. Saturation constant ($K_C$): when $\mu_{max}$ and $K_S$ are known; affinity constant ($K_S$) when $\mu_{max}$ and $K_C$ are known; maximum specific growth rate ($\mu_{max}$) when $K_C$ and $K_S$ are known.

It can observed from these last simulation results that the profiles show the reaction to changes due to abrupt jumps of the kinetic parameters of the plant. Changes of 50% and 40% occur after fifty hours for the saturation constant, the affinity constant and the maximum specific growth rate, respectively. The estimation algorithm converges toward the true parameters in less than twenty hours and shows good tracking performances when two of the parameters are known. The convergence performances of the estimated parameters towards the real ones can be tuned with the covariance of the signal $\zeta(t)$ described in Equation (3.27).

The proposed configuration is not realistic, since in real WWTPs models parameters are rarely constant. Therefore, a cascaded software sensors configuration is proposed to overcome the convergence estimation bias when estimating simultaneously all model parameters.

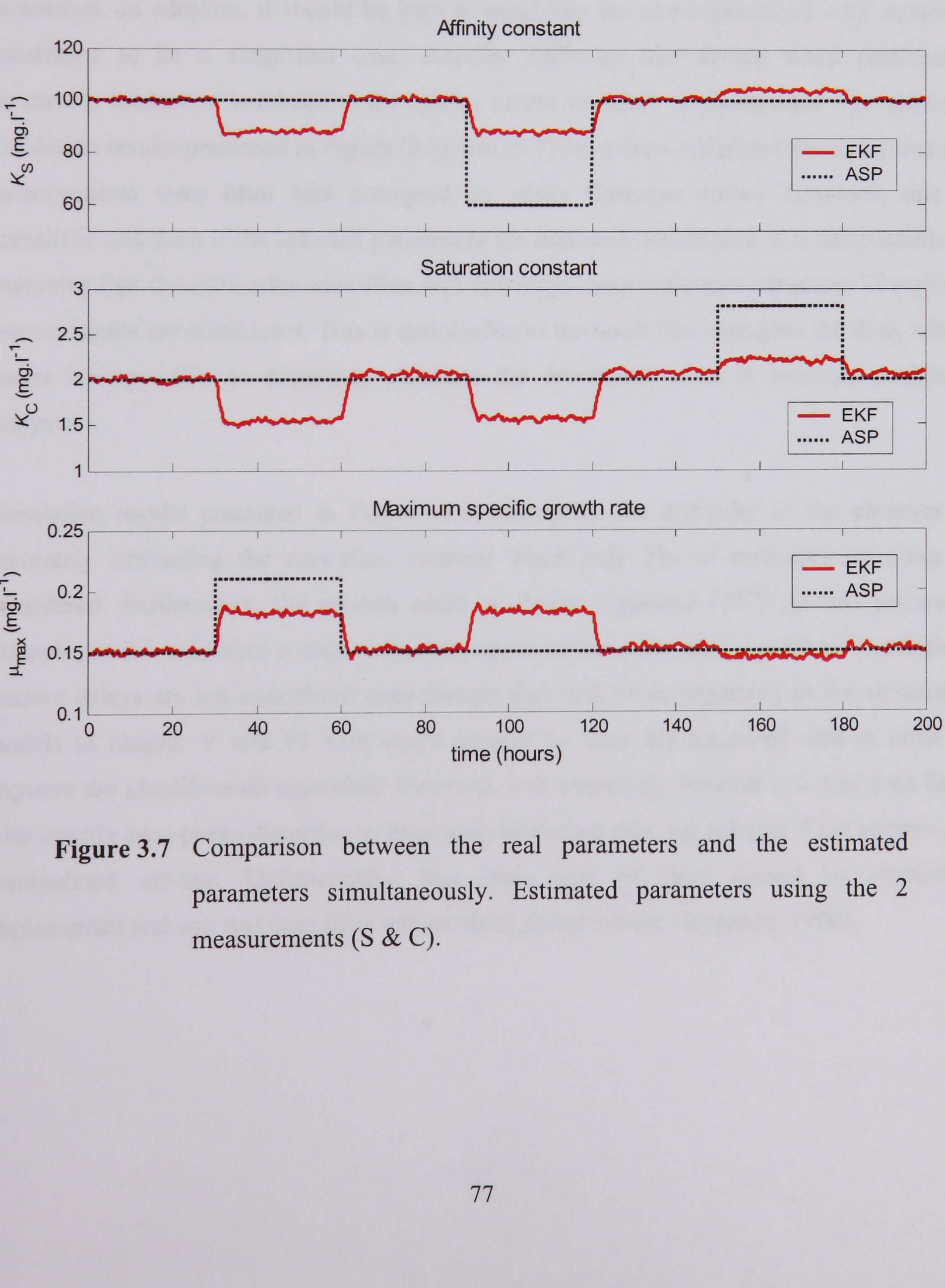


**Figure 3.7** Comparison between the real parameters and the estimated parameters simultaneously. Estimated parameters using the 2 measurements (S & C).

It consists of three local software sensors that individually estimate a single and distinct parameters that are forwarded to a master filter, which is composed on the input of three unknown parameters ($K_C$, $K_C$ and $\mu_{max}$), two measurements (S and C) and two manipulated inputs (D and W), utilised for the multiple-parameters estimation. Simulation results are presented in Figure (3.7) where the kinetic parameters converge to biased values. This is due to (1) the correlation between each parameter in the Monod model, which is a formulation of the growth of bacterial cultures that is extensively applied to ASPs, described in Equation (3.46), and (2) the insufficient persistent excitation of the system even though a Pseudorandom Random Binary Signal (PRBS) was used to excite the system inputs. Furthermore, such design requires knowledge of the parameters at the initialisation time (+/- 1%), which can be difficult in practice.

The bias result from Figure (3.7) clearly illustrates the difficulty when estimating multiple parameters. In addition, it should be kept in mind that the above-described ASP model is considered to be a simplified case. Another difficulty that occurs when performing parametric estimation is related to the quality of the available measurements. The previous simulation results presented in Figure (3.6) and (3.7) have been computed assuming that the measurements were ideal (not corrupted by white Gaussian noise). However, this is unrealistic and even if the selected parameters are assumed identifiable, it is not possible to guarantee that the estimation algorithm will converge toward the true parameter if realistic measurements are considered. This is mainly due to the noise that corrupted the data, which makes it impossible to accurately calculate the derivatives used in eventual analytical analyses.

Simulation results presented in Figure (3.8) exemplify the difficulty of the observer in accurately estimating the saturation constant when only 2% of measurement noise is considered. Furthermore, the process noise is almost neglected ($10^{-4}$) for this particular example, as it would have a major negative impact on the estimation algorithm. In addition, sensors delays are not considered even though they will be incorporated in the simulation models of chapter V and VI. One could propose to filter the measured data in order to improve the identification algorithm. However, it is eventually possible (i.e. low-pass filter with exactly zero-phase distortion to overcome undesired time lag effects) if the outputs are manipulated off-line. Unfortunately, this ideal type of filter cannot be physically implemented and any real time filter will produce poorer results (Jeppsson, 1996).

This case study demonstrated some of the difficulties when performing joint state and parameter estimation online based on an EKF algorithm. It is now possible with this example to draw an idea of some of the difficulties that need to be overcome in the non-linear filtering of bioprocesses applications. Furthermore, it also motivates the need to develop robust estimation algorithm. Therefore, the second example concentrates on software sensor based extended $H_\infty$ filter.

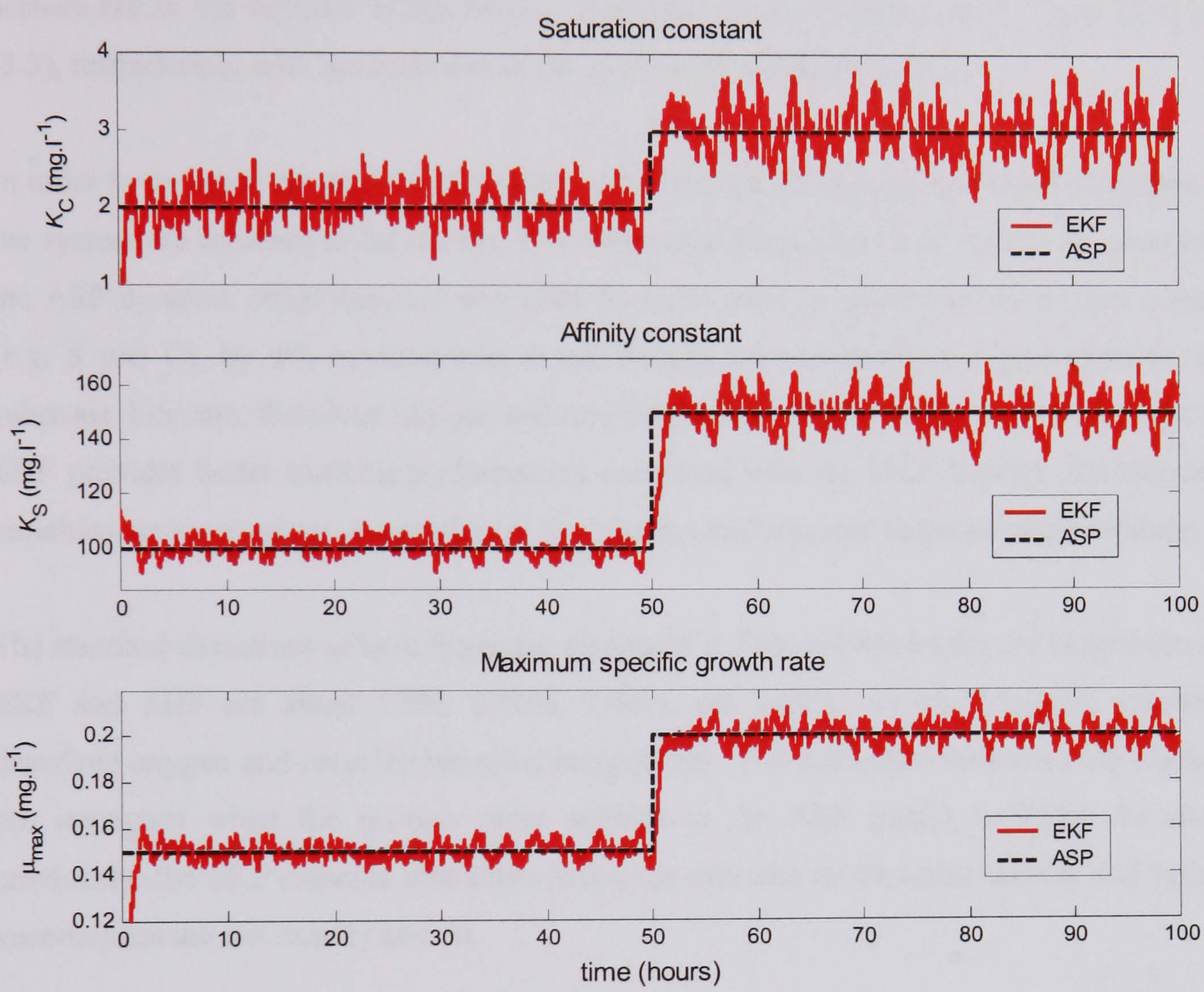


**Figure 3.8** Comparison between the real parameters and the estimated parameters by the software sensor. Saturation constant ($K_C$): when $\mu_{max}$ and $K_S$ are known; affinity constant ($K_S$) when $\mu_{max}$ and $K_C$ are known; maximum specific growth rate ($\mu_{max}$) when $K_C$ and $K_S$ are known. The on-line measurement (S and C) are corrupted by an additive white Gaussian signal with a standard deviation that is 2% of the actual value of the state variable. The process noise in neglected.

## Software sensor based-EHF

The main objective of this example is the presentation of a comparative study between observers based on extended Kalman filtering and extended $H_\infty$ filtering approaches. These observers are implemented on the activated sludge process presented previously and their performances are compared when performing state and joint state and parameter estimations where the EHF algorithm is similar to the EKF one. The difference between both software sensors are in the solution of the Riccati equation, which are displayed in Table (3.1) and (3.3), respectively, with the inclusion of the pre-specified $H_\infty$ performance.

In order to compare the performance of the EHF with the EKF ones, the initial conditions of the system are assumed to be known. The differential Equations (3.42) to (3.45), describing the ASP dynamic behaviour, are corrupted by 0.2% process noise and the on-line sensors (e.g. S and C), by 2% measurement noise. Results are presented in Figure (3.9) for the substrate, biomass, dissolved oxygen and recycled biomass where it can be observed that the EHF provides better tracking performances compared with the EKF. Indeed, the estimated variables are more robust, especially for the biomass and recycled biomass concentrations.

The standard deviations of both filters are displayed in Table (3.4) and the errors between the EKF and EHF are about 1.5%, 0.46%, 1.36% and 0.89%, for the biomass, substrate, dissolved oxygen and recycled biomass, respectively. The difference between both filters is not important when the process noise applied to the ASP model is 0.2%. As stated previously, the EKF presents limitations when the statistics of the noise sources and system uncertainties are not exactly known.

| | $X$ (mg $l^{-1}$) | $S$ (mg $l^{-1}$) | $C$ (mg $l^{-1}$) | $X_r$ (mg $l^{-1}$) |
|---|---|---|---|---|
| Extended Kalman filter | 2.042 | 0.648 | 0.0147 | 4.47 |
| Extended $H_\infty$ filter | 2.013 | 0.645 | 0.0145 | 4.43 |

**Table 3.4** Comparison of the standard deviations between the EKF and the EHF for $X$, $S$, $C$ and $X_r$ concentrations when the model is corrupted with 0.2% process noise and 2 % measurement noise.

Therefore, the process noise of the system is increased to 0.5% in order to compare the filters responses. Results are presented in Figure (3.10), where it can be seen that the EKF scarcely tracked the concentrations. As displayed in Table (3.5) with the standard deviations, the EHF

produced more accurate and robust tracking performance when comparing with the EKF. This time, the errors between the EKF and EHF are about 10%, 2.2%, 14.2% and 12%, for the biomass, substrate, dissolved oxygen and recycled biomass, respectively.

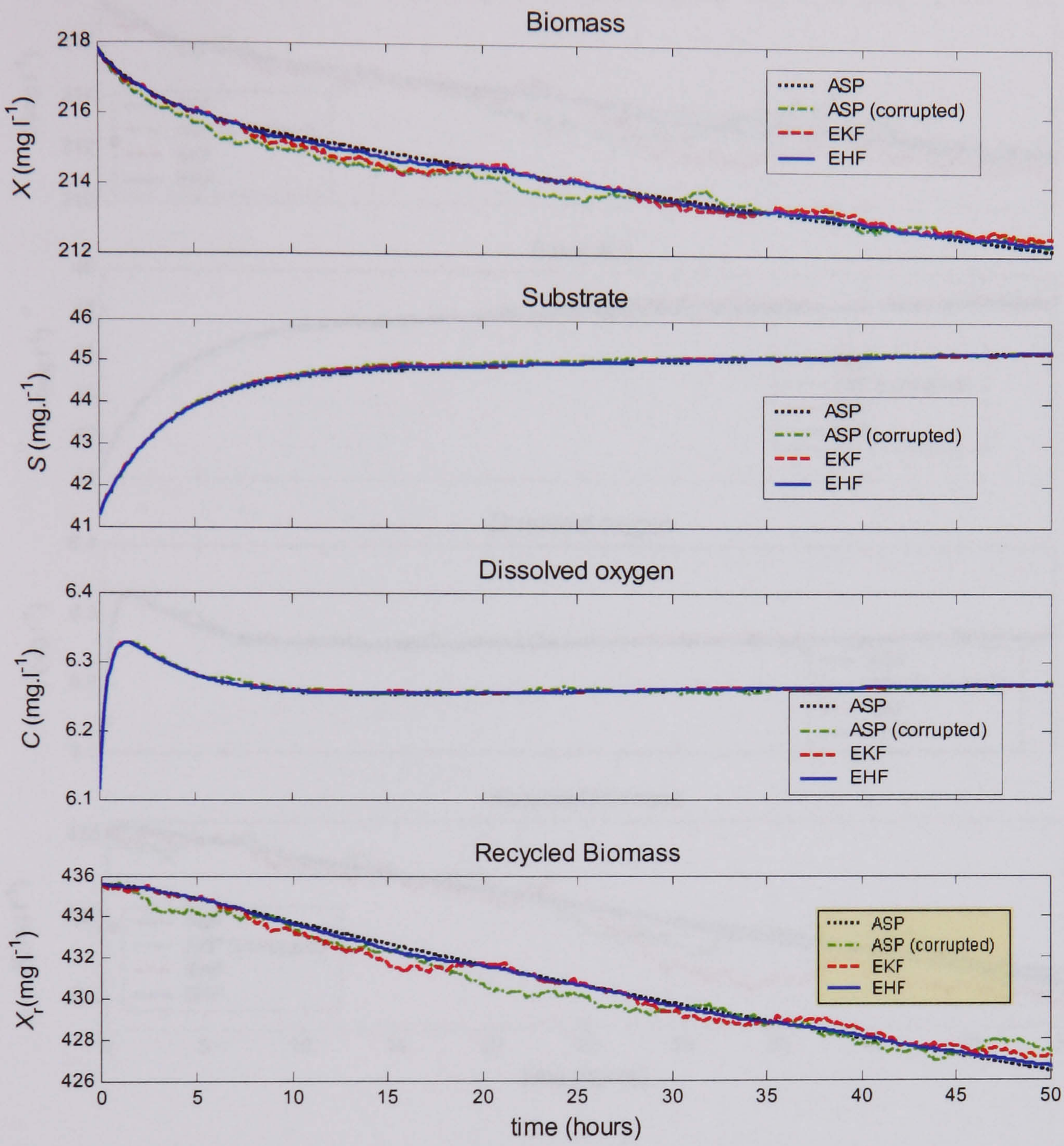


**Figure 3.9** State estimation comparisons of the original ASP model with the ASP model corrupted by 0.2% process noise, the EKF and the EHF algorithms.

This failure from the EKF to produce better tracking performances is related to the 0.5% process noise sources. This confirms that the EHF is more robust than the EKF when dealing with systems without exact knowledge of process noise signals and uncertainties. Simulation

results also illustrated that the EKF and EHF produced similar tracking performances when estimating the measured concentrations (e.g. *S* and *C*).

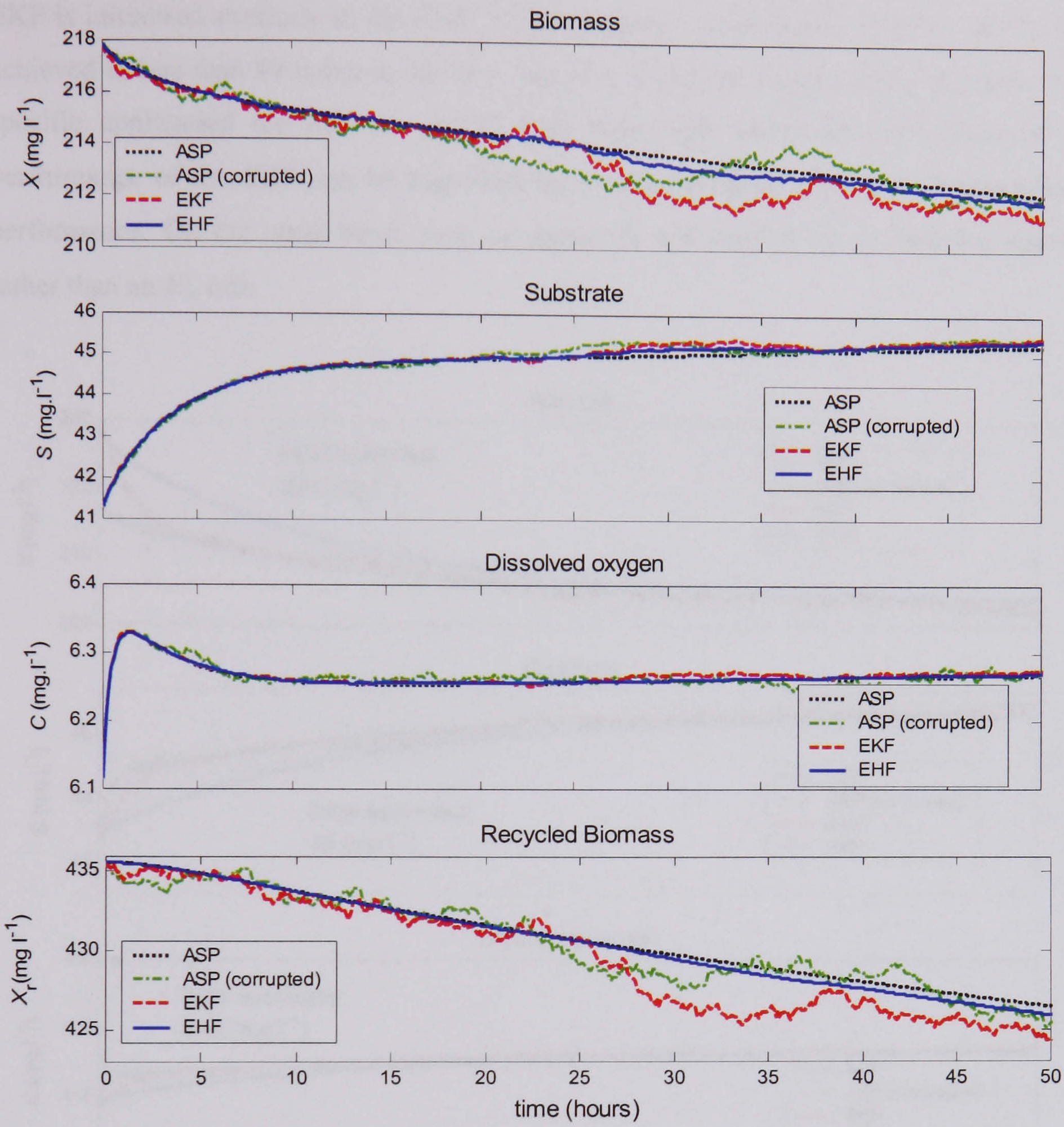


**Figure 3.10** State estimation comparison of the original ASP with the model corrupted by 0.5% process noise, the EKF and the EHF algorithms.

| | $X$ (mg $l^{-1}$) | $S$ (mg $l^{-1}$) | $C$ (mg $l^{-1}$) | $X_r$ (mg $l^{-1}$) |
|---|---|---|---|---|
| Extended Kalman filter | 1.99 | 0.645 | 0.014 | 4.51 |
| Extended $H_\infty$ filter | 1.79 | 0.631 | 0.012 | 3.97 |

**Table 3.5** Comparison of the standard deviations between the EKF and the EHF for $X$, $S$, $C$ and $X_r$ concentrations when the model is corrupted with 0.5% process noise and 2 % measurement noise.

To check the convergence properties of the EHF, the initial conditions are not assumed to be exactly known. Results are presented in Figure (3.11) where it can be observed that the EHF converges toward the real state in approximately less than 500 hours. Furthermore, when the EKF is initialised similarly to the EHF, the convergence properties toward the real state are achieved in less than 80 hours in the best case (e.g. dissolved oxygen concentration). In this specific application the EKF is around 85% time faster than the EHF. However, the performance of the EHF can be improved by increasing gamma ($\gamma$), the pre-specified $H_\infty$ performance. On the other hand, such an approach will lead to an $H_2$ filtering approach rather than an $H_\infty$ one.

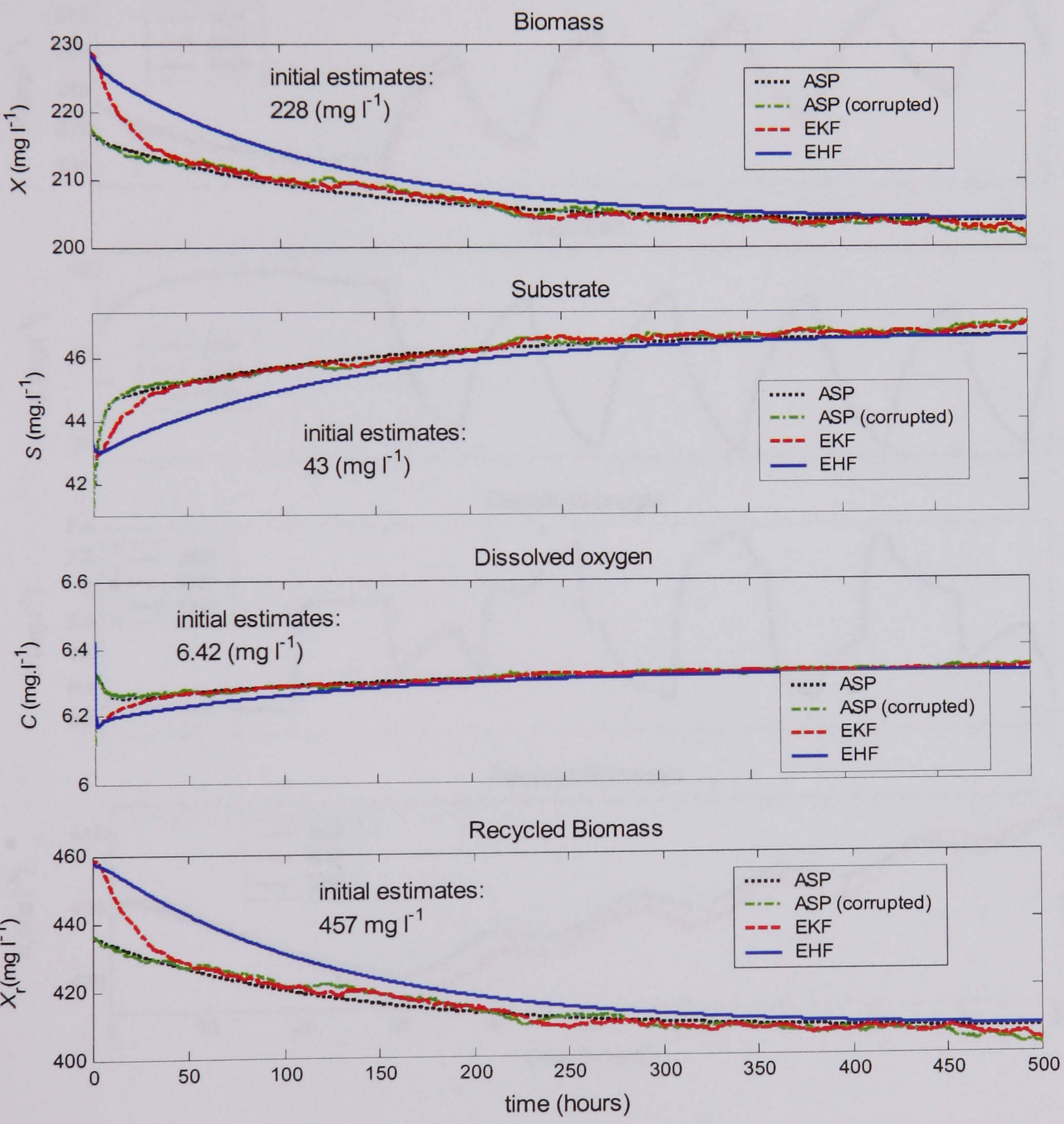


**Figure 3.11** Comparison between the EHF and EKF convergence performances when the initial conditions are not exactly known.

The performances of the EHF are also tested and compared with the EKF by applying pulses on the inputs of the system (e.g. dilution rate and air flow rate). Note that for clarity reasons, the process noise is almost neglected ($10^{-4}$) in this application. Results are presented in Figure (3.12) where it can be seen that the EHF, when estimating the unmeasured states (e.g. biomass and recycled biomass), provides closer tracking performances toward the true state with a standard deviation of 2.55 $mg.l^{-1}$ for the biomass and 2.74 $mg.l^{-1}$ for the recycled biomass, while the EKF demonstrates poorer tracking performances with standard deviations of 2.65 $mg.l^{-1}$ and 3.29 $mg.l^{-1}$, respectively.

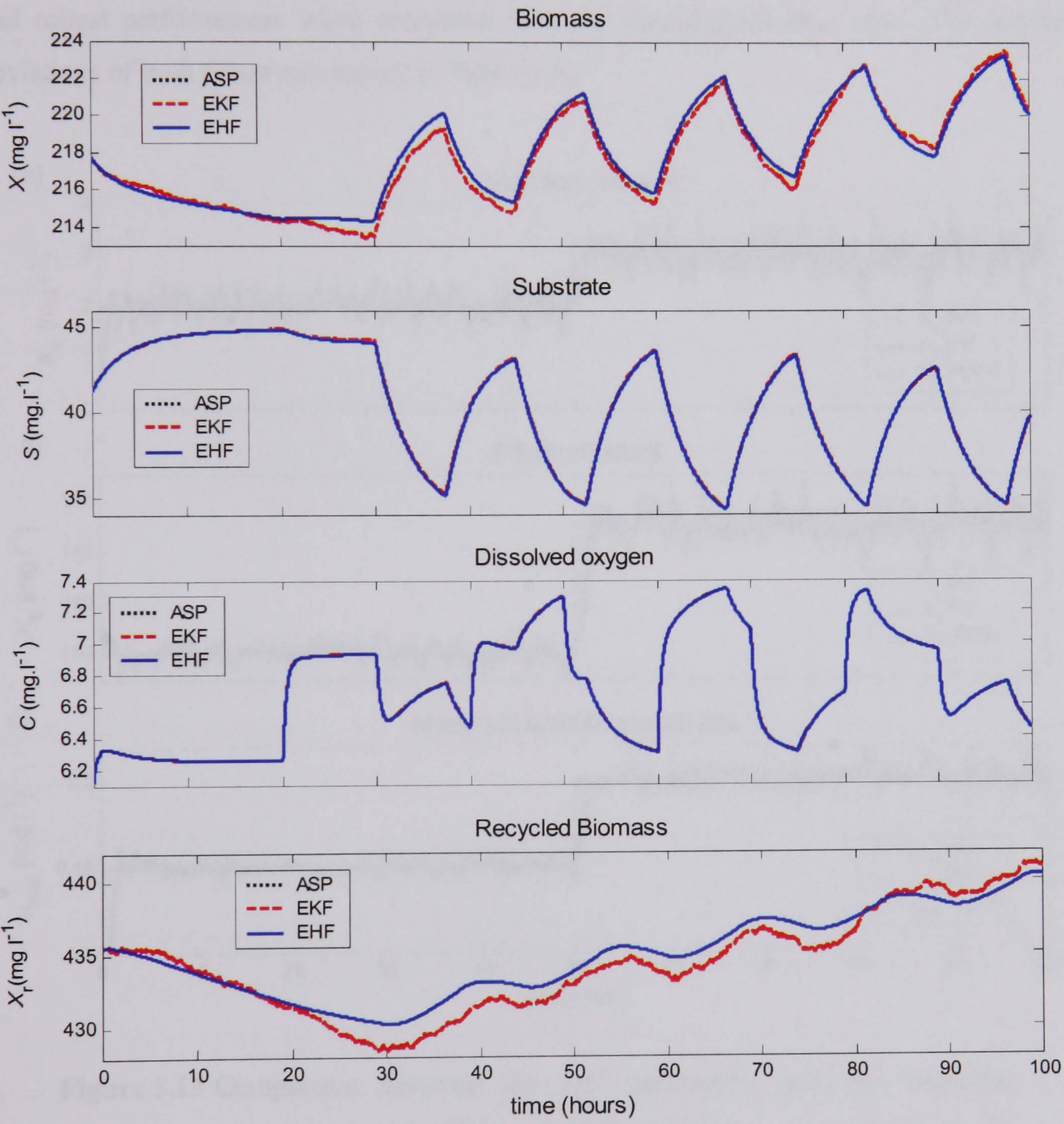


**Figure 3.12** Comparison between the EHF and EKF when pulses are applied on the inputs of the system, which are the dilution rate (-25% pulses) and airflow rate (+25% pulses).

When the concentrations are measured on-line (DO and S), similar and accurate tracking performances toward the real states are achieved with both observers. Therefore, their standard deviations errors, which are neglectable, are not presented here.

For the final example, a joint state and parameter estimation algorithm is produced in order to check the observer performances when the system parameters are augmented as additional states to the system's state vector describe by Equations (3.42) to (3.45). The EHF algorithm is similar to the EKF one, given by Equations (3.47) to (3.51). Results are presented in Figure (3.13) where it can be observed that the extended $H_\infty$ filter provides better tracking and robust performances when compared with the extended Kalman filter. The standard deviations of both filters are display in Table (3.6).

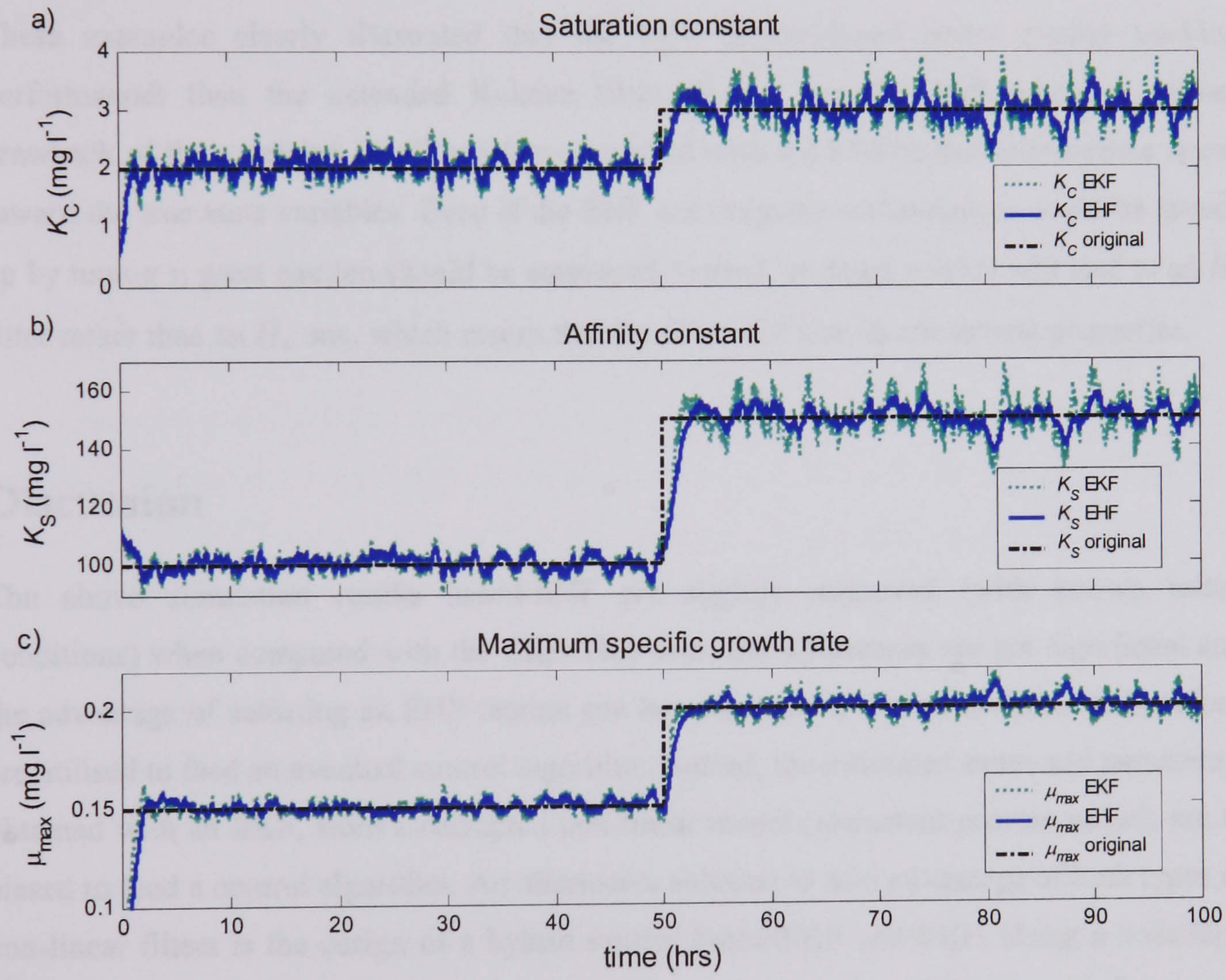


**Figure 3.13** Comparison between the real parameters and the estimated parameters by the EHF and EKF algorithms , respectively. (a) $K_C$ when $\mu_{max}$ and $K_S$ are known; (b) $K_S$ when $\mu_{max}$ and $K_C$ are known; (c) $\mu_{max}$ when $K_C$ and $K_S$ are known.

| | $K_C$ ($mg.l^{-1}$) | $K_S$ ($mg.l^{-1}$) | $\mu_{max}$ ($h^{-1}$) |
|---|---|---|---|
| Extended Kalman filter | 0.572 | 25.12 | 0.02742 |
| Extended $H_\infty$ filter | 0.539 | 24.72 | 0.02704 |

**Table 3.6** Comparison of the standard deviations between the EKF and the EHF for $K_C$, $K_S$ and $\mu_{max}$ model parameters when the system is corrupted with 0.2% process noise and 2 % measurement noise.

The errors, as presented in the above table, in terms of standard deviations, between the extended Kalman filter and the extended $H_\infty$ filter, are improved by 5.8%, 1.6% and 1.4% for the saturation constant, affinity constant and maximum specific growth rate parameters, respectively, with the EHF feature.

These examples clearly illustrated that the EHF demonstrated better overall tracking performances than the extended Kalman filter on this specific ASP model. A minor drawback of the extended $H_\infty$ filter when compared with the EKF is the convergence speed toward the true state variables. Even if the EHF convergence performances could be speed-up by tuning $\gamma$, great caution should be employed. Indeed, an large $\gamma$ value will lead to an $H_2$ filter rather than an $H_\infty$ one, which means that the filter will lose its robustness properties.

## Discussion

The above simulation results based-EHF are slightly improved (with known initial conditions) when compared with the EKF. However, the differences are not significant and the advantage of selecting an EHF feature can be motivated if the estimated concentrations are utilised to feed an eventual control algorithm. Indeed, the estimated states and parameters obtained with an EKF, from a corrupted non-linear model (important process noise), are to biased to feed a control algorithm. An alternative solution to take advantage of both types of non-linear filters is the design of a hybrid system based-EKF and EHF. Using a switching technique, an eventual EKF could provide fast convergence and tracking performances toward the true states before switching on an EHF, which could take over the EKF for control purposes.

## 3.5) SUMMARY

This chapter has provided a brief historical review of the most common linear and non-linear filtering techniques. The choice for selecting the Kalman and $H_\infty$ filtering features, as the basis for this work, is motivated by the many drawbacks the Wiener filter presented (e.g. only valid for stationary cases, application to multivariable systems remain complex, the derivation of Wiener-Hopf integral is not transparent). The Kalman filter overcomes most of these problems and is suitable in many engineering applications as well as its extended feature, which is mainly employed with non-linear systems. The EKF is extensively utilised and further investigated in Chapter V and VI. However, it cannot be considered as the perfect filter when applied to bioprocesses, as the noise source statistics and the initial parameters values must be known. Furthermore, the convergence and stability properties are not guaranteed and still remain an open problem. All these drawbacks have motivated the choice of selecting the $H_\infty$ filtering technique, which is further investigated in the Chapter VI.

The proposed examples pointed out a few of the problems discussed in this Chapter. It has consisted of applying software sensors based-EKF and EHF on an ASP model. The proposed simulations studies demonstrated the multiple-parametric estimation problems in addition to the measurement noise effect on the estimation. The robustness performances of the EHF were also illustrated through simulation studies, and compared with the standard EKF. The uncertainty of any estimated results from a true process is not guaranteed if it is taken into account that models used to describe WWT processes are much more complex. Furthermore, the model parameters are usually time varying and functions of temperature, pH (which are considered in the BSM1 model) etc., measurements are not often continuously available and many of the state variables are not measurable at all. As the ASM1 model is too complex to design efficient software sensors, an attempt to reduce it is proposed in the next chapter, where various reduced-order models are proposed even if some model parameters may be lost.

# Part II

# Monitoring of the Urban Wastewater System

# Chapter IV

# Non-linear observability of WWTP models

The original ASM1 model developed by the IWA task group is not fully observable and its parameters are not all identifiable. The objective of this Chapter is to develop a set of observable reduced models and to study their properties. The differential equations of the original ASM1 model are first introduced as a reminder of its complexity. Three reduced-order models for the activated sludge process are presented, as well as the simplifying assumptions. A comparison of the dynamic behaviour of these reduced models with the ASM1 model is performed. The linear piece-wise observability property is investigated prior to the non-linear observability theory. Both methodologies are compared with each other. Finally, a general procedure for model reduction and software sensor implementation is proposed. Parts of the material in this Chapter are covered in Benazzi and Katebi (2005), Benazzi *et al.*, (2005a, 2005b, 2005c, 2005d, 2005e), Benazzi *et al.*, (2006)

## 4.1 SIMPLIFICATION OF THE ASM1 MODEL

As mentioned in Section (2.3), the WWTP considered in this work is the IWA/COST benchmark simulation model No.1. Within this plant configuration, the ASM1 model (Henze *et al.*, 2000) is selected to describe the biological processes in the activated sludge reactors. This complex model, initially developed by the International Association on Water Quality (IWAQ, formerly IAWPRC), is represented in a matrix format, as displayed in Appendix D. It is composed of thirteen state variables, nineteen parameters and incorporates eight processes, as described in Henze *et al.*, (2000). The model complexity is often hidden when

using the matrix format, which illustrates the stoichiometric relationships that relate the state variables to the process rate equations. Therefore, to emphasise on these complexities, the full set of differential equations describing the ASM1 model and utilised in the sequel, is discussed and formulated in the following subsections.

## Initial ASM1 model formulation

The ASM1 model is extensively utilised to describe carbon removal and nitrification-denitrification processes. The full descriptions of the ASM1 model, as well as the processes that are involved, are given in (Henze *et al.*, 2000). The ASM1 is composed of 13 components or state variables that are listed (with their associated symbols and state variable units) in Table B2 of Appendix B. The different processes included in the ASM1 model are

$P_1$: Aerobic growth of heterotrophs;

$P_2$: Anoxic growth of heterotrophs;

$P_3$: Aerobic growth of autotrophs;

$P_4$: Decay of heterotrophs;

$P_5$: Decay of autotrophs;

$P_6$: Ammonification of soluble organic nitrogen;

$P_7$: Hydrolysis of entrapped organic materials;

$P_8$: Hydrolysis of entrapped organic nitrogen.

The matrix representation showing the process kinetics and stoichiometric relationship that relate the state variables to the process rate equations is displayed in Appendix D. The stoichiometric and kinetic parameters (as well as their corresponding values) are given in Appendix B, Tables B2.1 and B2.2. From the matrix notation, it is possible to obtain the complete set of differential equations for all 13 state variables. The basic equation for a mass balance within any system boundary (e.g. a completely mixed reactor) is of the form:

$$\text{Input} - \text{Output} + \text{Reaction} = \text{Accumulation}. \tag{4.1}$$

The input and output terms, which are considered as transport terms, depend upon the physical characteristics of the system that is modelled (e.g. the flow and the volume of the tank). The reaction term is obtained by summing the process rate expression and the product of the stoichiometric coefficients provided with the matrix notation (Appendix D). For the following differential equations describing the original ASM1 model, the mass balance formula of Equation (4.1) is utilised for the first aerobic tank for each of the 13 concentrations (or accumulations). Note that this mass balance will be slightly different for the first anoxic tank as the internal recycled flow would be included. However, it is not incorporated in the following differential equations description as the study concentrates on aerobic conditions.

The soluble inert organic matter ($S_I$) and particulate inert organic matter ($X_I$) mass balances are not presented here because they are not involved in any reaction process. Therefore, only 11 of the differential equations are presented instead of the original 13. Furthermore, the restrictions, simplifications and assumptions (e.g. the system operates at constant temperature, changes in the wastewater character cannot be properly handled by the model, etc.) associated with the ASM1 model are provided in details in Henze *et al.*, (2000) and summarised in Jeppsson (1996).

The dynamic behaviour of the readily biodegradable substrate concentration, which is removed by growth of heterotrophic bacteria (either in aerobic or anoxic condition) and could be increased by hydrolysis of slowly biodegradable substrate, is described by:

$$\frac{dS_S}{dt} = Q\frac{S_{S,in} - S_S}{V} + \left\{ -\frac{\mu_{mH}}{Y_H} \times \left(\frac{S_S}{K_S + S_S}\right) \times \left[ \left(\frac{S_O}{K_{O,H} + S_O}\right) + \eta_g \times \left(\frac{K_{O,H}}{K_{O,H} + S_O}\right)\left(\frac{S_{NO}}{K_{NO} + S_{NO}}\right) \right] + K_h \times \frac{X_S / X_{B,H}}{K_X + \left(X_S / X_{B,H}\right)} \times \left[ \left(\frac{S_O}{K_{O,H} + S_O}\right) + \eta_h \times \left(\frac{K_{O,H}}{K_{O,H} + S_O}\right)\left(\frac{S_{NO}}{K_{NO} + S_{NO}}\right) \right] \right\} \times X_{B,H} \qquad (4.2)$$

The term $V$ and $Q$ (with $Q_{in} = Q_{ef}$) from Equation (4.2) to (4.12), denote the volume (assumed constant to a level of 1333 $m^3$) of the first aerobic compartment and the flow, respectively. The $S_S$ reaction from the mass balance of Equation (4.1) involves three

processes: aerobic growth of heterotrophs ($P_1$), anoxic growth of heterotrophs ($P_2$) and hydrolysis of entrapped organic materials ($P_7$).

The concentration of slowly biodegradable substrate is removed by hydrolysis and formed by decay of both the heterotrophic and autotrophic biomass according to

$$\frac{dX_S}{dt} = Q\frac{X_{S,in} - X_S}{V} + \left\{ (1-f_p)\times(b_H \times X_{B,H})\times(b_A \times X_{B,A}) - K_h \times \frac{X_S / X_{B,H}}{K_X + (X_S / X_{B,H})} \times \left[ \left( \frac{S_O}{K_{O,H} + S_O} \right) + \eta_h \times \left( \frac{K_{O,H}}{K_{O,H} + S_O} \right)\left( \frac{S_{NO}}{K_{O,H} + S_{NO}} \right) \right] \right\} \times X_{B,H} \quad (4.3)$$

The $X_S$ reaction from the mass balance of Equation (4.1) involves three processes: decay of heterotrophs ($P_4$), decay of autotrophs ($P_5$) and the hydrolysis of entrapped organic materials ($P_7$).

The active heterotrophic biomass concentration, which is formed by growth under either an aerobic or anoxic condition, is given by

$$\frac{dX_{B,H}}{dt} = Q\frac{X_{B,H,in} - X_{B,H}}{V} + \left\{ \mu_{mH} \times \left( \frac{S_S}{K_S + S_S} \right) \times \left[ \left( \frac{S_O}{K_{O,H} + S_O} \right) + n_g \times \left( \frac{K_{O,H}}{K_{O,H} + S_O} \right)\left( \frac{S_{NO}}{K_{NO} + S_{NO}} \right) \right] - b_H \right\} \times X_{B,H} \quad (4.4)$$

The $X_{B,H}$ reaction from the mass balance of Equation (4.1) involves three processes: aerobic growth of heterotrophs ($P_1$), anoxic growth of heterotrophs ($P_2$) and decay of heterotrophs ($P_4$).

The description of the active autotrophic biomass concentration, which is much simpler since the autotrophs growth only occurs under aerobic conditions, is described by the following differential equation

$$\frac{dX_{B,A}}{dt} = Q\frac{X_{B,A,in} - X_{B,A}}{V} + \left[\mu_{mA} \times \left(\frac{S_{NH}}{K_{NH} + S_{NH}}\right)\left(\frac{S_O}{K_{O,H} + S_O}\right) - b_A\right] \times X_{B,A} \qquad (4.5)$$

The $X_{B,A}$ reaction from the mass balance of Equation (4.1) involves two processes: aerobic growth of autotrophs ($P_3$) and decay of autotrophs ($P_5$).

The inert particulate product arising from biomass decay is formed by decay of both the heterotrophic and autotrophic biomass, according to

$$\frac{dX_P}{dt} = Q\frac{X_{P,in} - X_P}{V} + f_p\left(b_H \times X_{B,H}\right) \times \left(b_A \times X_{B,A}\right) \qquad (4.6)$$

The $X_P$ reaction from the mass balance of Equation (4.1) involves two processes: decay of heterotrophs ($P_4$) and decay of autotrophs ($P_5$).

The concentration of dissolved oxygen in the wastewater is associated only with aerobic growth of the heterotrophic and autotrophic biomass. The dynamic equation describing this is given by

$$\frac{dS_O}{dt} = Q\frac{S_{O,in} - S_O}{V} + \left\{-\mu_{mH} \times \left(\frac{1 - Y_H}{Y_H}\right)\left(\frac{S_S}{K_S + S_S}\right)\left(\frac{S_O}{K_{O,H} + S_O}\right) \times X_{B,H} - \mu_{mA} \times \left(\frac{4.57 - Y_A}{Y_A}\right) \times \left(\frac{S_{NH}}{K_{NH} + S_{NH}}\right)\left(\frac{S_O}{K_{O,A} + S_O}\right) \times X_{B,A}\right\} + K_L a.(S_{O,SAT} - S_O) \qquad (4.7)$$

The $S_O$ reaction from the mass balance of Equation (4.1) involves two processes: aerobic growth of heterotrophs ($P_1$) and aerobic growth of autotrophs ($P_2$). The value 4.57 in the stoichiometric expression for aerobic growth of autotrophs is the theoretical oxygen demand associated with the oxidation of ammonia nitrogen to nitrate nitrogen. $K_La$ is the oxygen transfer function (assumed to be linear), which is supposed constant to a level of 10 $hr^{-1}$ in the first aerated tank, and is dependent on the airflow that is produced by the aeration blowers. The oxygen saturation concentration ($S_{O,SAT}$) is set to a level of 8 g $O_2$ $m^{-3}$.

The concentration of nitrate is produced by aerobic growth of the autotrophic bacteria and removed during anoxic growth of the heterotrophic biomass, according to

$$\frac{dS_{NO}}{dt} = Q\frac{S_{NO,in} - S_{NO}}{V} + \left\{-\mu_{mH}\eta_g \times \left(\frac{1-Y_H}{2.86.Y_H}\right)\left(\frac{S_S}{K_S + S_S}\right)\left(\frac{K_{O,H}}{K_{O,H} + S_O}\right)\left(\frac{S_{NO}}{K_{NO} + S_{NO}}\right)\times\right.$$

$$\left. X_{B,H} + \frac{\mu_{mA}}{Y_A} \times \left(\frac{S_{NH}}{K_{NH} + S_{NH}}\right)\left(\frac{S_O}{K_{O,A} + S_O}\right) \times X_{B,A}\right\} \quad (4.8)$$

The $S_{NO}$ reaction from the mass balance of Equation (4.1) involves two processes: anoxic growth of heterotrophs ($P_2$) and aerobic growth of autotrophs ($P_3$). The 2.86 factor in the stoichiometric expression for anoxic growth of heterotrophic biomass, which is included to maintain consistent unit on a COD basis, is the oxygen equivalence for conversion of nitrate nitrogen to nitrogen gas.

The ammonia concentration, which is assumed to be the sum of the ionised (ammonium) and un-ionised (ammonia) forms, decreases as a result of the nitrification process and increases as a result of ammonification of soluble organic nitrogen. The dynamic equation describing this is given by

$$\frac{dS_{NH}}{dt} = Q\frac{S_{NH,in} - S_{NH}}{V} + \left\{-i_{XB}\mu_{mH} \times \left(\frac{S_S}{K_S + S_S}\right)\left[\left(\frac{S_O}{K_{O,H} + S_O}\right) + n_g \times\right.\right.$$

$$\left.\left.\left(\frac{K_{O,H}}{K_{O,H} + S_O}\right) \times \left(\frac{S_{NO}}{K_{NO} + S_{NO}}\right)\right] + k_a \times S_{ND}\right\} \times X_{B,H} - \mu_{mA}\left(i_{XB} + \frac{1}{Y_A}\right) \times$$

$$\left(\frac{S_{NH}}{K_{NH} + S_{NH}}\right)\left(\frac{S_O}{K_{O,A} + S_O}\right) \times X_{B,A} \quad (4.9)$$

The $S_{NH}$ reaction from the mass balance of Equation (4.1) involves three processes: aerobic growth of heterotrophs ($P_1$), anoxic growth of heterotrophs ($P_2$) and aerobic growth of autotrophs ($P_3$).

The soluble biodegradable organic nitrogen concentration, which is converted to ammonia nitrogen by ammonification and formed by hydrolysis of particulate organic nitrogen, is given by

$$\frac{dS_{ND}}{dt} = Q\frac{S_{ND,in} - S_{ND}}{V} + \left\{-k_A \times S_{ND} + K_h \times \frac{X_{ND}/X_{B,H}}{K_X + \left(X_S/X_{B,H}\right)} \times\right.$$

$$\left[\left(\frac{S_O}{K_{O,H}+S_O}\right)+\eta_h\times\left(\frac{K_{O,H}}{K_{O,H}+S_O}\right)\left(\frac{S_{NO}}{K_{NO}+S_{NO}}\right)\right]\times X_{B,H} \qquad (4.10)$$

The $S_{ND}$ reaction from the mass balance of Equation (4.1) involves two processes: ammonification of soluble organic nitrogen ($P_6$) and hydrolysis of entrapped organic nitrogen ($P_8$).

The particulate biodegradable organic nitrogen concentration is increased from decay of both the heterotrophic and autotrophic biomass and decreased by the hydrolysis process. The dynamic differential equation describing this is given by

$$\frac{dX_{ND}}{dt}=Q\frac{X_{ND,in}-X_{ND}}{V}+\left\{\left(i_{XB}-f_p\times i_{XP}\right)\left(b_H\times X_{B,H}\right)*\left(b_A\times X_{B,A}\right)-K_h\times\frac{X_{ND}/X_{B,H}}{K_X+\left(X_S/X_{B,H}\right)}\times\right.$$

$$\left.\left[\left(\frac{S_O}{K_{O,H}+S_O}\right)+\eta_h\times\left(\frac{K_{O,H}}{K_{O,H}+S_O}\right)\left(\frac{S_{NO}}{K_{NO}+S_{NO}}\right)\right]\right\}\times X_{B,H} \qquad (4.11)$$

The $X_{ND}$ reaction from the mass balance of Equation (4.1) involves three processes: decay of heterotrophs ($P_4$), decay of autotrophs ($P_5$) and hydrolysis of entrapped organic nitrogen ($P_8$).

The alkalinity, which provides information by which undue changes in pH can be predicted, is given by

$$\frac{dS_{ALK}}{dt}=Q\frac{S_{ALK,in}-S_{ALK}}{V}+\left\{\frac{1}{14}\times k_a\times S_{ND}+\mu_{mH}\times\left(\frac{S_S}{K_S+S_S}\right)\times\left[-\frac{i_{XB}}{14}\times\left(\frac{S_O}{K_{O,H}+S_O}\right)\right.\right.$$

$$\left.\left.+n_g\times\left(\frac{1-Y_H}{14\times 2.86\times Y_H}-\frac{i_{XB}}{14}\right)\left(\frac{K_{O,H}}{K_{O,H}+S_O}\right)\left(\frac{S_{NO}}{K_{NO}+S_{NO}}\right)\right]\right\}\times X_{B,H}-$$

$$\mu_{mA}\times\left(\frac{i_{XB}}{14}+\frac{1}{7\times Y_A}\right)*\left(\frac{S_{NH}}{K_{NH}+S_{NH}}\right)\left(\frac{S_O}{K_{O,A}+S_O}\right)\times X_{B,A} \qquad (4.12)$$

The $S_{ALK}$ reaction from the mass balance of Equation (4.1) involves four processes: aerobic growth of heterotrophs ($P_1$), anoxic growth of heterotrophs ($P_2$), aerobic growth of autotrophs ($P_3$) and ammonification of soluble organic nitrogen ($P_6$). The nitrification rate,

which has the largest impact on alkalinity, can decrease if the pH level is too low, meaning that corrosive, aggressive effluent and bulking problems can occur.

The differential Equations (4.2) to (4.12) clearly illustrate the complex mass balance descriptions of the original ASM1 model, which is not obvious within the matrix format presented in Appendix D. A simplified schematic representation of the original ASM1 model, which is considered with the benchmark plant, is proposed in Figure (4.1).

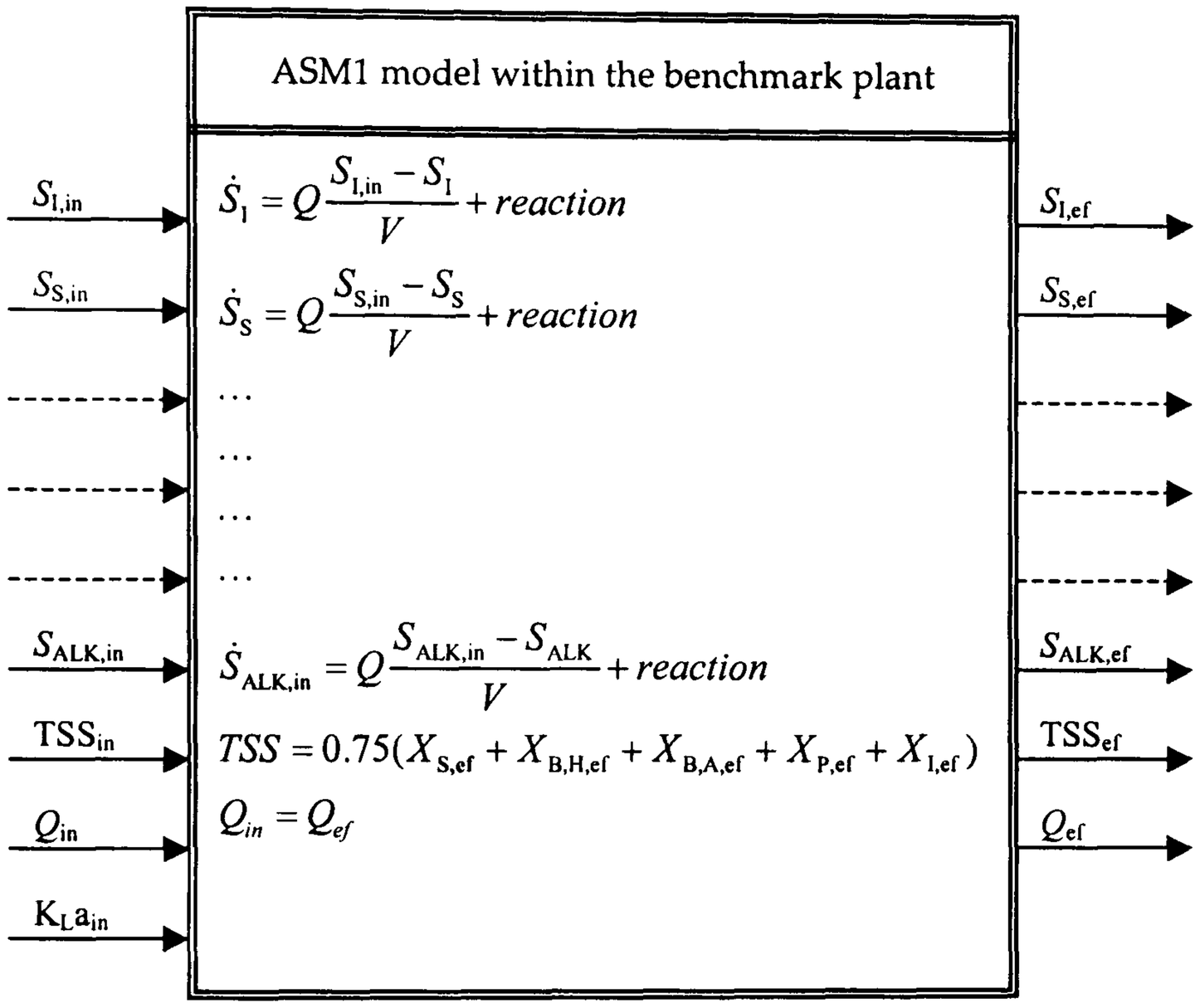


**Figure 4.1** Simplified schematic representation of the ASM1 model composed of 13 state variable, 15 inputs and 16 outputs, within the benchmark plant configuration.

The Total Suspended Solid (TSS) concentration is obtained by a summing fraction of $X_S$, $X_{B,H}$, $X_{B,A}$, $X_P$ and $X_I$ concentrations. Note that influent and effluent flows are identical. Furthermore, it should be emphasised that the activated sludge process model considered within the benchmark plant (BSM1), is the ASM1 model described by Equation (4.2) to (4.12) added with $S_I$ and $X_I$ concentrations. The benchmark plant consists of 5 activated sludge tanks (also called reactor) in series (2 anoxic ones + 3 aerobic ones). The entire work presented in the sequel concentrate on the 1st aerobic reactor. The choice of this specific location is motivated by two points: (1) aerobic conditions are of main interest, and (2) the non-linearities of the plant are at a maximum at this location, which is a prerequisite when

implementing software sensors. Indeed, non-linear filtering algorithm performances are improved when the excitement of the system is significant. The description of the original ASM1 model in term of state variables, inputs, eventual state variables that can be directly measured, etc. are detailed in Table (4.1).

| | |
|---|---|
| State variables (13) | $S_I$, $S_S$, $X_I$, $X_S$, $X_{B,H}$, $X_{B,A}$, $X_P$, $S_O$, $S_{NO}$, $S_{NH}$, $S_{ND}$, $X_{ND}$, $S_{ALK}$ |
| Inputs (16) | $S_{I,in}$, $S_{S,in}$, $X_{I,in}$, $X_{S,in}$, $X_{B,H,in}$, $X_{B,A,in}$, $X_{P,in}$, $S_{O,in}$, $S_{NO,in}$, $S_{NH,in}$, $S_{ND,in}$, $X_{ND,in}$, $S_{ALK,in}$, $TSS_{in}$, $Q_{in}$, $K_La_{in}$ |
| Outputs (15) | $S_{I,ef}$, $S_{S,ef}$, $X_{I,ef}$, $X_{S,ef}$, $X_{B,H,ef}$, $X_{B,A,ef}$, $X_{P,ef}$, $S_{O,ef}$, $S_{NO,ef}$, $S_{NH,ef}$, $S_{ND,ef}$, $X_{ND,ef}$, $S_{ALK,ef}$, $TSS_{ef}$, $Q_{ef}$ |
| Parameters (19) | $\mu_{mH}$, $K_S$, $K_{OH}$, $K_{NO}$, $b_H$, $\eta_g$, $\eta_h$, $K_h$, $K_X$, $\mu_{mA}$, $K_{NH}$, $b_A$, $K_{OA}$, $k_a$, $Y_A$, $Y_H$, $f_p$, $i_{XB}$, $i_{XP}$ |
| Processes involved (8) | $P_1$, $P_2$, $P_3$, $P_4$, $P_5$, $P_6$, $P_7$, $P_8$ |
| Eventual measurements | $Q$, $S_O$, $S_{NO}$, $S_{NH}$, $S_{ALK}$, TSS (on-line) |
| | $S_S$, $X_S$ (off-line, via respirometer) |

**Table 4.1** Original ASM1 model description associated the benchmark plant. The state variables and parameters definitions are presented in Appendix B, Table B.2, B2.1 and B2.2.

A brief description of the BSM1 plant configuration is proposed in Chapter II and for further information on the plant the reader should refer to Copp (2002). Following this introduction of the original ASM1 model, a reduced-order model formulation is now proposed.

## Reduced-order models formulation

The original ASM1 model considers state variables that are measurable ($S_O$, $S_{NO}$, $S_{NH}$, $S_{ALK}$) as well as those that are not accessible in real wastewater treatment plants (e.g. $S_I$, $S_S$, $X_I$, $X_S$, $X_{B,H}$, $X_{B,A}$, $X_P$, $S_{ND}$ and $X_{ND}$). Therefore, it is important to produce observable reduced order models prior to the implementation of the software sensors, in order to (1) reduce the model complexity for on-line monitoring purposes, (2) utilise the estimated concentrations to feed an eventual control algorithm, and (3) enhance the practical applicability of the proposed applications. Consequently, three reduced models are derived for various case studies presented in Chapter V and VI. The reducing techniques are based on a matrix decoupling method, which is detailed in Section (4.3), and personal experience. The considerations

required in order to produce the reduced models, using the ASM1 as a starting point, are also discussed for each case. Therefore, all comparisons between the reduced models and the ASM1 model are performed with the benchmark plant described in Chapter II. Prior to the presentation of the reduced-order models, it is important to briefly discuss the simulation procedure, which is identical for all the applications proposed in the sequel.

## Simulation procedure

All simulations are executed within the Matlab/Simulink platform, based on the defined open-loop benchmark configuration. Furthermore, the default benchmark plant physical values, given in Copp (2002), are selected (e.g. the volume of the 1$^{st}$ aerated reactor ($V_3$) and the air flow rate ($K_La$) are set to 1333 $m^3$ and 10 $hr^{-1}$, respectively). In order to guarantee a reliable application of the ASM1 and to ensure that similar analyses are done on the output data; a two-step simulation procedure involving simulations to steady state followed by dynamic simulations using the different influent files (presented in Chapter II) is required (Copp, 2002).

The steady state simulation procedure involves the simulation of the system under study (for 200 days) using an influent of constant flow and composition. Note that dynamic simulations should always follow a steady state simulation to ensure a consistent starting point and to eliminate the influence of starting conditions on the generated dynamics outputs (Copp, 2002). The dynamic simulations should be lead by a steady state simulation. Then, using the dry weather influent file as dynamic input, another simulation has to be run for 14 days and the resulting state variable must be saved. The starting point for evaluating the dynamic response of the plant to each of the influent disturbances files will be those last (saved) state variables. From these dynamic simulations, only the data generated during the last 7 days are of interest (Copp, 2002).

Table (4.2) summarises the simulation procedure that is applied prior any reduced model implementation, in order to compare the dynamics outputs with those available in benchmark manual. Simulation results should be presented for a period of 7 days, between the 7$^{th}$ and 14$^{th}$ day (Copp, 2002) to include variations in the design hydraulic loading during a weekend. However, for simplification reasons, simulation results are eventually presented for a single day or two to three days (from the 7$^{th}$ day) in the sequel.

| | steady state simulation (constant influent file) | dry weather simulation | corresponding influent file | units |
|---|---|---|---|---|
| Dry Weather (DW) | 200 | 14 | (DW) 14 | days |
| Storm Influent (SI) | 200 | 14 | (ST) 14 | days |
| Rain Influent (RI) | 200 | 14 | (RI) 14 | days |

**Table 4.2** Simulation procedure to perform with the benchmark plant. The data of interest correspond the last seven days of the simulation procedure.

## Reduced-order 'Model A'

The main objective in the development of the following model (named 'Model A') is to estimate on-line the autotrophic biomass concentration and the heterotrophic biomass concentration, as presented in Chapter V. To do so, it is not necessary to consider the full-scale ASM1 model. Therefore, the following considerations were required in order to produce the reduced-order 'Model A'. Soluble inert organic matter ($S_I$) contributes to the effluent chemical oxygen demand (COD), and particulate inert organic matter ($X_I$) becomes a component of the total suspended solids in the Activated Sludge System (ASS). In other words, the $S_I$ fraction passes through the ASS without resulting in any effects, whilst $X_I$ is utilised to predict the total amount of sludge in the system, which contributes in determination of the waste and recirculation rates. Therefore, both $S_I$ and $X_I$ are excluded from the reduced model because they do not contribute to any other reactions and are not actively involved in any conversion processes.

Inclusion of the particulate products arising from biomass decay ($X_P$) in the ASM1 is an approach to account for the fact that not all biomass in the activated sludge system is active (Henze *et al.*, 2000). Description of alkalinity ($S_{ALK}$) in the ASM1 is not essential (no impact on biological transformations), although its incorporation is sometimes advantageous because it provides information by which excessive change in pH can be predicted (Henze *et al.*, 2000). Therefore, these two components are also excluded from the reduced models. The soluble biodegradable organic nitrogen ($S_{ND}$) and particulate biodegradable organic nitrogen ($X_{ND}$) are also neglected even though, indirectly, they will slightly affect some concentrations estimated by the software sensors. However, this model will be employed to design observers that can estimate the heterotrophic biomass ($X_{B,H}$) and the autotrophic biomass ($X_{B,A}$) concentrations, and later, the heterotrophic yield ($Y_H$), which are not directly correlated with $S_{ND}$ and $X_{ND}$. The readily biodegradable substrate ($S_S$) and the ammonia ($S_{NH}$)

concentrations are assumed constant to a steady state level (given in Copp, 2002) of 1.5 g COD $m^{-3}$ and 5.548 g N $m^{-3}$, respectively. Because the $S_S$ concentration is assumed constant, the hydrolysis mechanism cannot occur, which means that the $X_S$ concentration is also removed from the system. Note that $S_S$ and $S_{ND}$ concentrations are assumed constant because if removed from the reduced model, the system correlation between the four state variables describing the reduced model would not exist. In other words, there would exist no dependence between each state variable, which would lead to an incorrect reduced-model.

Consequently, the reduced-order 'Model A', which includes four state variables, which are: $X_{B,H}$ and $X_{B,A}$, dissolved oxygen ($S_O$) and nitrate and nitrite nitrogen ($S_{NO}$) concentrations, is of the form

$$\frac{dX_{B,H}}{dt} = Q\frac{X_{B,H,in} - X_{B,H}}{V} + \left\{\mu_{mh} \times 0.13 \times \left[\left(\frac{S_O}{K_{O,H} + S_O}\right) + n_g \times \left(\frac{K_{O,H}}{K_{O,H} + S_O}\right)\left(\frac{S_{NO}}{K_{NO} + S_{NO}}\right)\right] - b_H\right\} \times X_{B,H} \tag{4.13}$$

$$\frac{dX_{B,A}}{dt} = Q\frac{X_{B,A,in} - X_{B,A}}{V} + \left[\mu_{mA} \times 0.85 \times \left(\frac{S_O}{K_{O,H} + S_O}\right) - b_A\right] X_{B,A} \tag{4.14}$$

$$\frac{dS_O}{dt} = Q\frac{S_{O,in} - S_O}{V} + \left\{-\mu_{mH} \times \left(\frac{1 - Y_H}{Y_H}\right) \times 0.13 \times \left(\frac{S_O}{K_{O,H} + S_O}\right) \times X_{B,H} - \mu_{mA} \times \left(\frac{4.57 - Y_A}{Y_A}\right) \times 0.85 \times \left(\frac{S_O}{K_{O,A} + S_O}\right) \times X_{B,A}\right\} + K_L a.(S_{O,SAT} - S_O) \tag{4.15}$$

$$\frac{dS_{NO}}{dt} = Q\frac{S_{NO,in} - S_{NO}}{V} + \left\{-\mu_{mH}\eta_g \times \left(\frac{1 - Y_H}{2.86 \times Y_H}\right) \times 0.13 \times \left(\frac{K_{O,H}}{K_{O,H} + S_O}\right) \times \left(\frac{S_{NO}}{K_{NO} + S_{NO}}\right) \times X_{B,H} + \frac{\mu_{mA}}{Y_A} \times 0.85 \times \left(\frac{S_O}{K_{O,A} + S_O}\right) \times X_{B,A}\right\} \tag{4.16}$$

The description of the reduced 'Model A' in term of state variables, inputs, processes etc. is detailed in Table (4.3).

| | |
|---|---|
| State variables (4) | $X_{B,H}$, $X_{B,A}$, $S_O$, $S_{NO}$ |
| Inputs (6) | $X_{B,H,in}$, $X_{B,A,in}$, $S_{O,in}$, $S_{NO,in}$, $Q_{in}$, $K_La_{in}$ |
| Outputs (4) | $X_{B,H,ef}$, $X_{B,A,ef}$, $S_{O,ef}$, $S_{NO,ef}$ |
| Parameters (10) | $\mu_{mH}$, $K_{OH}$, $K_{NO}$, $b_H$, $\eta_g$, $\mu_{mA}$, $b_A$, $K_{OA}$, $Y_A$, $Y_H$ |
| Processes involved (5) | $P_1$, $P_2$, $P_3$, $P_4$, $P_5$ |
| Eventual measurements (2) | $S_O$, $S_{NO}$, TSS (on-line) |

**Table 4.3** Reduced-order 'Model A' description. The state variables and parameter definitions are presented in Appendix B, Table B.2, B2.1 and B2.2.

To enhance the understanding of the dynamic behaviour of any reduced model, it is important to compare it with the original one (e.g. the ASM1). Therefore, the reduced 'Model A' is implemented in parallel with the benchmark plant, as presented in Figure (4.2).

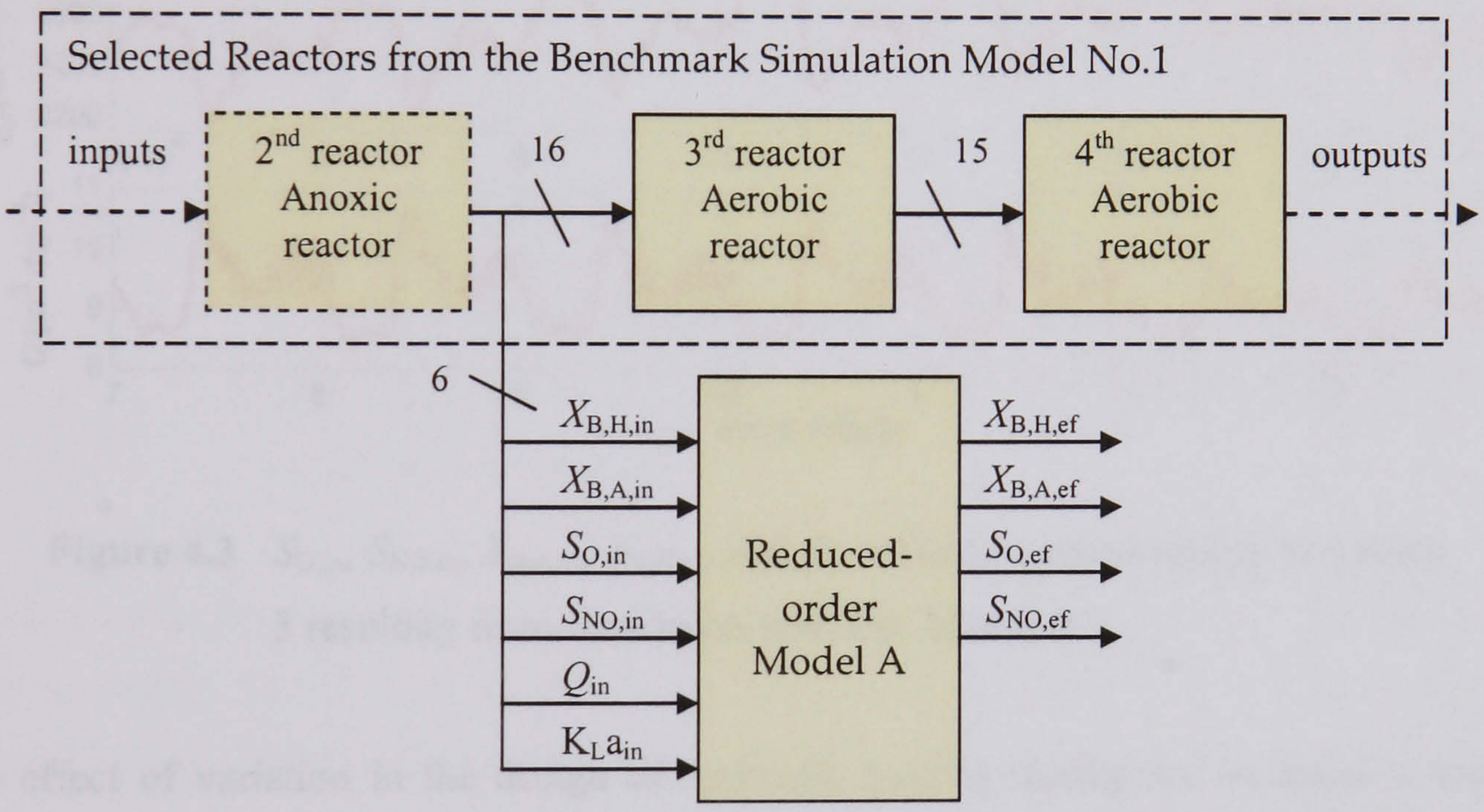


**Figure 4.2** Schematic representation of the 'Model A', implemented in parallel with the benchmark plant.

Note that even if $X_{B,H,in}$ and $X_{B,A,in}$ are not physically available on the influent of the 3rd reactor, they are considered in the reduced model, similar to the original ASM1 model. For the state observer applications, these influent concentrations will be considered either constant or available from fractions of TSS measurement. This work, which is not covered within this Chapter, is presented in Chapter V. The dry influent wastewater data file, which is available with the benchmark plant, is used to characterize the influent wastewater for the

models. The dynamic behaviours of the influent concentrations with the reduced 'Model A' are presented in Figure (4.3). $K_La_{in}$, which is set to a constant level of 10 $hr^{-1}$ for this model and in the sequel, is not illustrated.

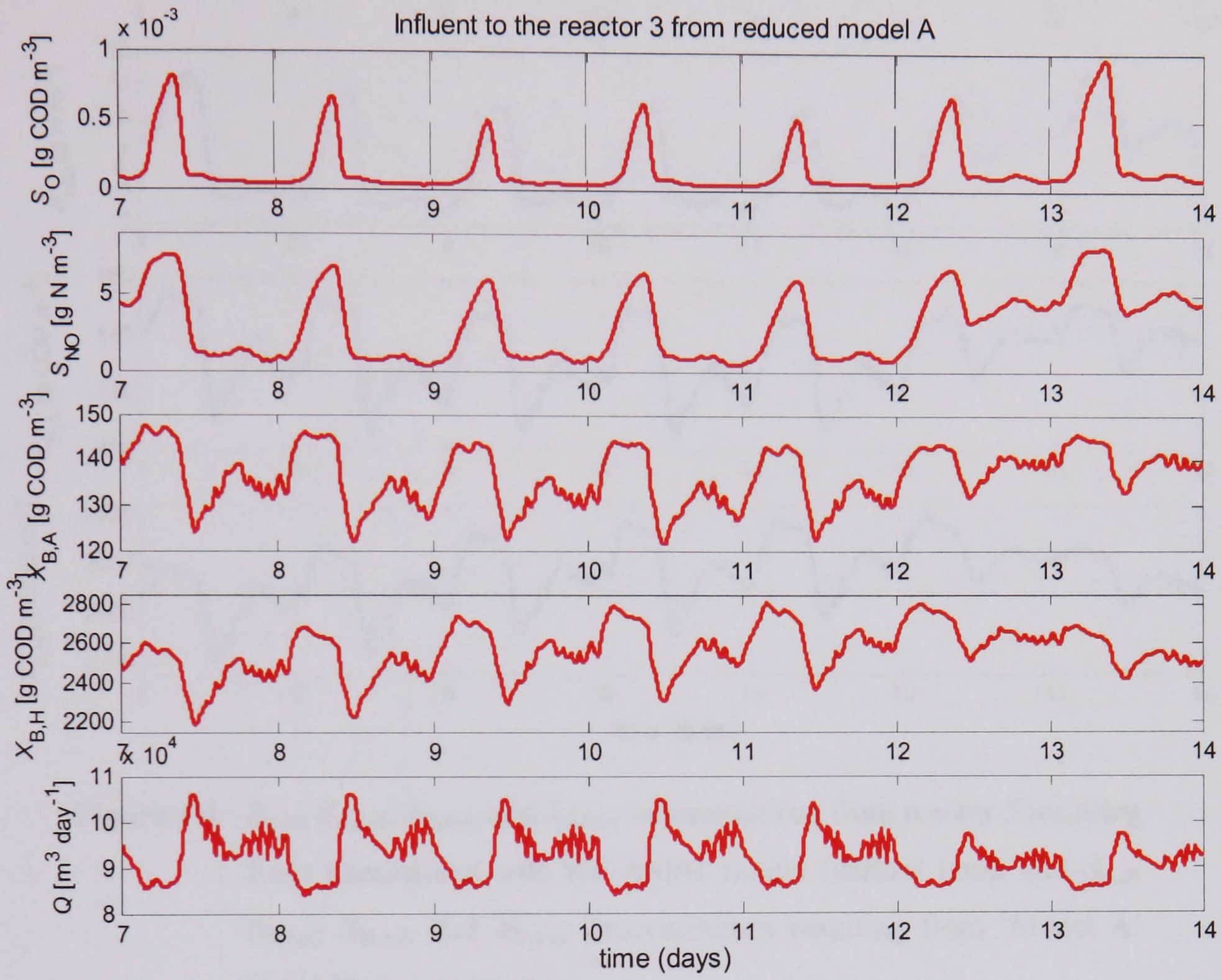


**Figure 4.3** $S_{O,in}$, $S_{NO,in}$, $X_{B,A,in}$, $X_{B,H,in}$, and $Q_{in}$ influent concentrations to reactor 3 resulting from simulation with the 'Model A'.

The effect of variation in the design of hydraulic loading during the weekend is clearly illustrated between the 12th and 14th day. The daily period of the expected trends in weekly data is represented for the dissolved oxygen concentration, which motivates the previous discussion on displaying the data during 1 to 3 days. Furthermore, the DO influent variations are close to zero because it corresponds to the effluent of the anoxic reactor (oxygen free).

Simulation results from the effluent of the reduced 'Model A' and the corresponding concentrations from the original ASM1 model are presented in Figure (4.4). It is obvious from the graph that the behaviour of $S_{NO}$, $X_{B,A}$ and $X_{B,H}$ concentrations resulting from the reduced 'Model A' are similar to the ASM1 model.

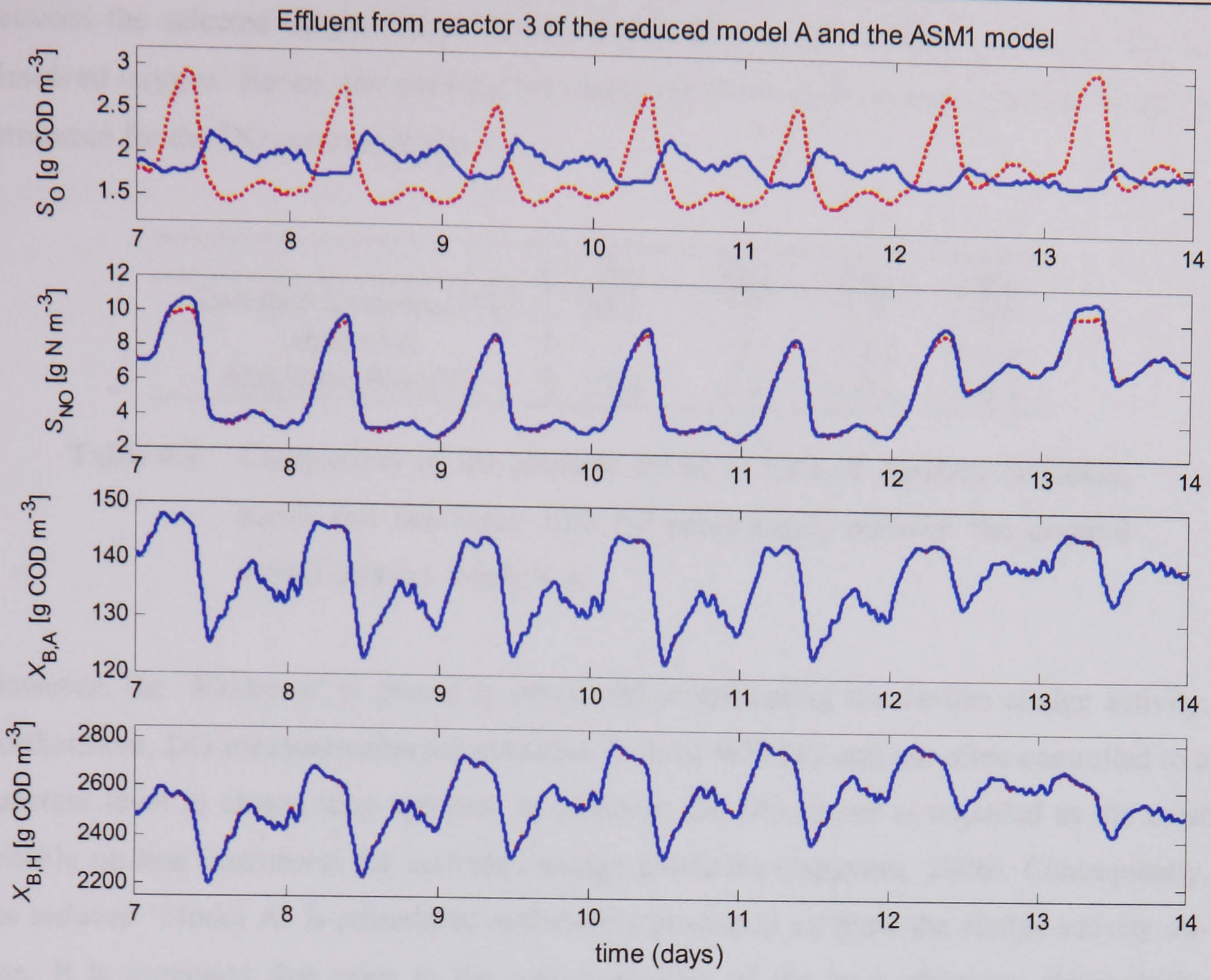


**Figure 4.4** $S_{O,ef}$, $S_{NO,ef}$, $X_{B,A,ef}$ and $X_{B,H,ef}$ concentrations from reactor 3 resulting from simulations with the ASM1 model (dashed line), and $S_{O,ef}$, $S_{NO,ef}$, $X_{B,A,ef}$ and $X_{B,H,ef}$ concentrations resulting from 'Model A' (solid line), respectively.

However, important biases occur for the dissolved oxygen, which is probably caused by two reasons. Firstly, the DO is not affected by the hydrolysis process of entrapped organics materials ($S_S$ assumed constant and $X_S$ removed from the reduced model) and entrapped organic nitrogen ($S_{ND}$ and $X_{ND}$ are excluded from the reduced model). Secondly, the ammonia ($S_{NH}$), which increases as a result of ammonification of soluble biodegradable organic nitrogen ($S_{ND}$ excluded), is also removed from the reduced model.

The differences between the selected outputs resulting from simulations with the benchmark plant and the reduced 'Model A' are expressed in terms of absolute errors. For each concentration, the standard deviations, means and maximum biases are obtained with the data statistic tools provided within Matlab. Then, the absolute errors between the original ASM1 model and the reduced model are calculated in percentage for each concentration. Results are summarised in Table (4.4) where it can be observed that the maximum disparities

between the selected outputs from the benchmark plant and the 'Model A' occur for the dissolved oxygen. Hence, the tracking performances of an eventual state observer might be erroneous for the DO concentrations.

| | $S_O$ | $S_{NO}$ | $X_{B,H}$ | $X_{B,A}$ |
|---|---|---|---|---|
| *Standard Deviation* (%) | 68.6 | 3.7 | 1.7 | 0.5 |
| *Mean* (%) | 1 | 1 | < 0.1 | < 0.1 |
| *Maximum Bias* (%) | 27.3 | 5.9 | < 0.1 | < 0.1 |

**Table 4.4** Comparison of the absolute errors in term of standard deviation, mean and maximum bias (in percentage), between the original ASM1 and the 'Models A'.

However, the 'Model A' is primarily employed in estimating the on-line sludge activity. Furthermore, DO measurements are available in most WWTPs and are often controlled to a constant level in closed loop systems. In addition, the DO sensor is regarded as the most reliable on-line instrument for activated sludge processes (Jeppsson, 1996). Consequently, the reduced 'Model A' is considered sufficiently precise to estimate the sludge activity on-line. It is reminded that prior to the implementation of the state observer, observability analysis of this reduced model is required. For simplification reasons, this work is presented in next section, as the reduced-order 'Model B' and 'Model C' are introduced.

## Reduced-order 'Model B'

The main objective in producing a reduced-order model (separated into two similar models named 'Model Ba' and 'Model Bb') is (1) to perform on-line estimation and detection of abnormal substrate concentration in WWTPs using a software sensor based-EKF (based on 'Model Ba') and (2) to present a joint state and parameter estimation application where a software sensor based-EKF is implemented to estimate on-line the biomass concentrations and the heterotrophic yield (based on 'Model Bb'). The only difference between these models is that in the 'Model Ba', the heterotrophic and autotrophic biomass concentrations are assumed constant, while in 'Model Bb', the differential equations describing the biomass activity are included in the reduced model.

### 'Model Ba'

The assumption of constant biomasses is similar to that proposed by Ingildsen (2002), who assumed the slowly changing variables to be constant. Therefore, the $X_{B,H}$ and $X_{B,A}$

concentrations are kept constant in the reduced model, as the variations in the amount of sludge in the system is a slow process. Consequently, the $X_{ND}$ concentration, which is generated from decay of both $X_{B,H}$ and $X_{B,A}$, and $S_{ND}$ concentrations, which is formed by hydrolysis of $X_{ND}$, is also neglected in the 'Model Ba'. Identical assumptions as those presented for 'Model A' hold for $S_I$, $X_I$, $X_P$ and $S_{ALK}$ concentrations for the following reduced models (including the 'Model Bb'and 'Model C'). Therefore, the 'Model Ba' includes five state variables of the form

$$\frac{dS_S}{dt} = Q\frac{S_{S,in} - S_S}{V} + \left\{ -\frac{\mu_{mH}}{Y_H} \times \left(\frac{S_S}{K_S + S_S}\right) \times \left[ \left(\frac{S_O}{K_{O,H} + S_O}\right) + \eta_g \times \left(\frac{K_{O,H}}{K_{O,H} + S_O}\right) \times \left(\frac{S_{NO}}{K_{NO} + S_{NO}}\right) + K_h \times \frac{X_S/2561}{K_X + \left(X_S/2561\right)} \times \left[ \left(\frac{S_O}{K_{O,H} + S_O}\right) + \eta_h \times \left(\frac{K_{O,H}}{K_{O,H} + S_O}\right) \times \left(\frac{S_{NO}}{K_{NO} + S_{NO}}\right) \right] \right] \right\} \times 2561 \tag{4.17}$$

$$\frac{dX_S}{dt} = Q\frac{X_{S,in} - X_S}{V} + \left\{ \left(1 - f_p\right) \times \left(b_H \times 2561\right) \times \left(b_A \times 135\right) - K_h \times \frac{X_S/2561}{K_X + \left(X_S/2561\right)} \times \left[ \left(\frac{S_O}{K_{O,H} + S_O}\right) + \eta_h \times \left(\frac{K_{O,H}}{K_{O,H} + S_O}\right)\left(\frac{S_{NO}}{K_{O,H} + S_{NO}}\right) \right] \right\} \times 2561 \tag{4.18}$$

$$\frac{dS_O}{dt} = Q\frac{S_{O,in} - S_O}{V} + \left\{ -\mu_{mH} \times \left(\frac{1 - Y_H}{Y_H}\right)\left(\frac{S_S}{K_S + S_S}\right)\left(\frac{S_O}{K_{O,H} + S_O}\right) \times 2561 - \mu_{mA} \times \left(\frac{4.57 - Y_A}{Y_A}\right) \times \left(\frac{S_{NH}}{K_{NH} + S_{NH}}\right)\left(\frac{S_O}{K_{O,A} + S_O}\right) \times 135 \right\} + K_L a \times (S_{O,SAT} - S_O) \tag{4.19}$$

$$\frac{dS_{NO}}{dt} = Q\frac{S_{NO,in} - S_{NO}}{V} + \left\{ -\mu_{mH} \times \eta_g \times \left(\frac{1 - Y_H}{2.86 \times Y_H}\right)\left(\frac{S_S}{K_S + S_S}\right)\left(\frac{K_{O,H}}{K_{O,H} + S_O}\right)\left(\frac{S_{NO}}{K_{NO} + S_{NO}}\right) \times 2561 + \frac{\mu_{mA}}{Y_A} \times \left(\frac{S_{NH}}{K_{NH} + S_{NH}}\right)\left(\frac{S_O}{K_{O,A} + S_O}\right) \times 135 \right\} \tag{4.20}$$

$$\frac{dS_{NH}}{dt} = Q\frac{S_{NH,in} - S_{NH}}{V} + \left\{-i_{XB}\mu_{mH} \times \left(\frac{S_S}{K_S + S_S}\right)\left[\left(\frac{S_O}{K_{O,H} + S_O}\right) + n_g \times \right.\right.$$

$$\left.\left.\left(\frac{K_{O,H}}{K_{O,H} + S_O}\right) \times \left(\frac{S_{NO}}{K_{NO} + S_{NO}}\right)\right] + k_a \times S_{ND}\right\} \times 2561 - \mu_{mA}\left(i_{XB} + \frac{1}{Y_A}\right) \times$$

$$\left(\frac{S_{NH}}{K_{NH} + S_{NH}}\right)\left(\frac{S_O}{K_{O,A} + S_O}\right) \times 135 \qquad (4.21)$$

Note that $X_{B,H}$ and $X_{B,A}$ concentrations are assumed constant to a level 2561 and 135 g COD $m^{-3}$, respectively. These biomasses levels represent the steady state values of the theoretical data available with the BSM1 model. The description of the 'Model Ba' in term of state variables, inputs, processes etc. is detailed in Table (4.5). Its dynamic behaviour is compared with the ASM1 model, as presented in the schematic overview of Figure (4.5).

| State variables (5) | $S_S$, $X_S$, $S_O$, $S_{NO}$, $S_{NH}$ |
|---|---|
| Inputs (7) | $S_{S,in}$, $X_{S,in}$, $S_{O,in}$, $S_{NO,in}$, $S_{NH,in}$, $Q_{in}$, $K_La_{in}$ |
| Outputs (5) | $S_{S,ef}$, $X_{S,ef}$, $S_{O,ef}$, $S_{NO,ef}$, $S_{NH,ef}$ |
| Parameters (18) | $\mu_{mH}$, $K_S$, $K_{OH}$, $K_{NO}$, $b_H$, $\eta_g$, $\eta_h$, $K_h$, $K_X$, $\mu_{mA}$, $K_{NH}$, $b_A$, $K_{OA}$, $k_a$, $Y_A$, $Y_H$, $f_p$, $i_{XB}$ |
| Processes involved (7) | $P_1$, $P_2$, $P_3$, $P_4$, $P_5$, $P_6$, $P_7$ |
| Measurements (5) | $S_O$, $S_{NO}$, $S_{NH}$ (on-line) \| $S_S$, $X_S$ (off-line) |

**Table 4.5** Reduced 'Model Ba' description. The state variables, parameter etc., are displayed in Appendix B, Table B.2, B2.1 and B2.2.

Similar to the 'Model A', the dry influent wastewater data are used to characterize the influent wastewater for the models. The dynamic behaviours of the influent concentrations to the 'Model Ba' are presented in Figure (4.6) for $S_{S,in}$, $X_{S,in}$ and $S_{NH,in}$ concentrations. $S_{O,in}$, $S_{NO,in}$ and $Q_{in}$ influent concentrations are not illustrated here because they are identical to those presented in Figure (4.3).

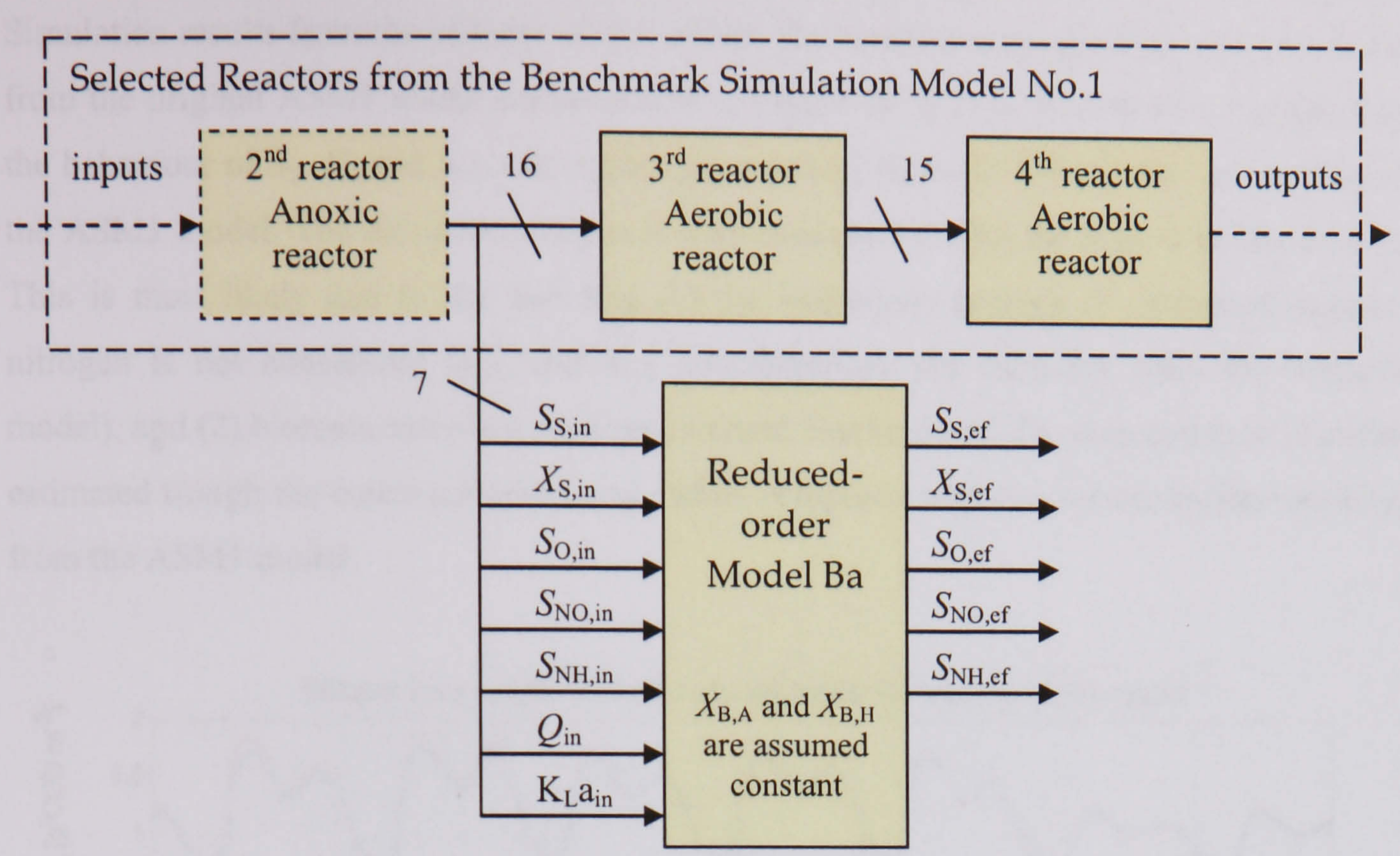


**Figure 4.5** Schematic representation of the 'Model Ba', implemented in parallel with the benchmark plant.

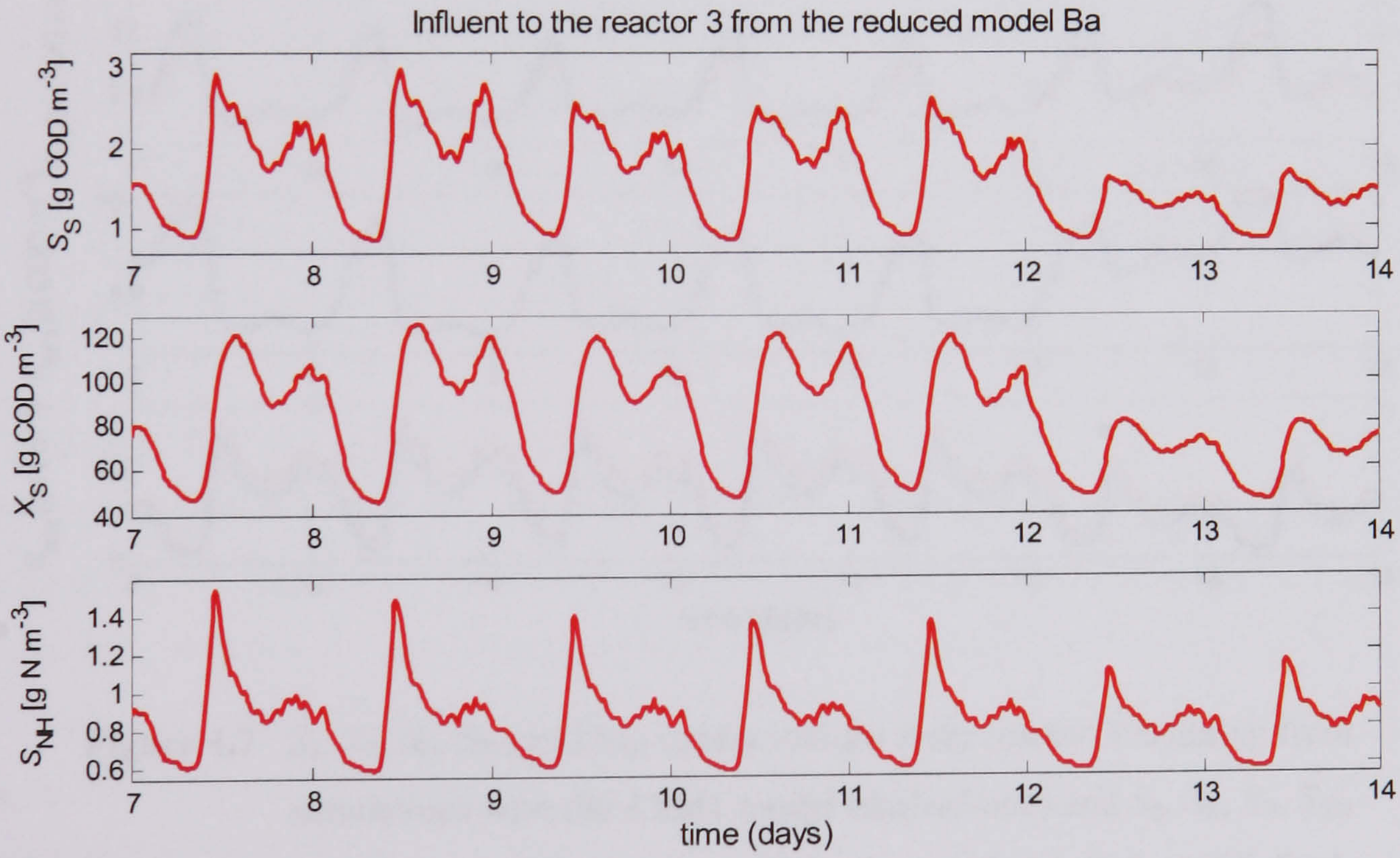


**Figure 4.6** $S_{S,in}$, $X_{S,in}$, $S_{NH,in}$ influent concentrations to reactor 3 resulting from simulation with the reduced-order 'Model Ba'.

Simulation results from the effluent of the 'Model Ba' and the corresponding concentrations from the original ASM1 model are presented in Figure (4.7). It is clear from the graph that the behaviour of $S_S$, $X_S$ and $S_{NO}$ concentrations resulting from the 'Model Ba' are similar to the ASM1 model. The dissolved oxygen is over estimated during the high intensity events. This is most likely due to the fact that (1) the hydrolysis process of entrapped organic nitrogen is not considered ($S_{ND}$ and $X_{ND}$ concentrations are excluded from the reduced model), and (2) biomass activities are kept constant. Furthermore, $S_{NH}$ concentration is under estimated trough the entire period of time, when compared with $S_{NH}$ concentration resulting from the ASM1 model.

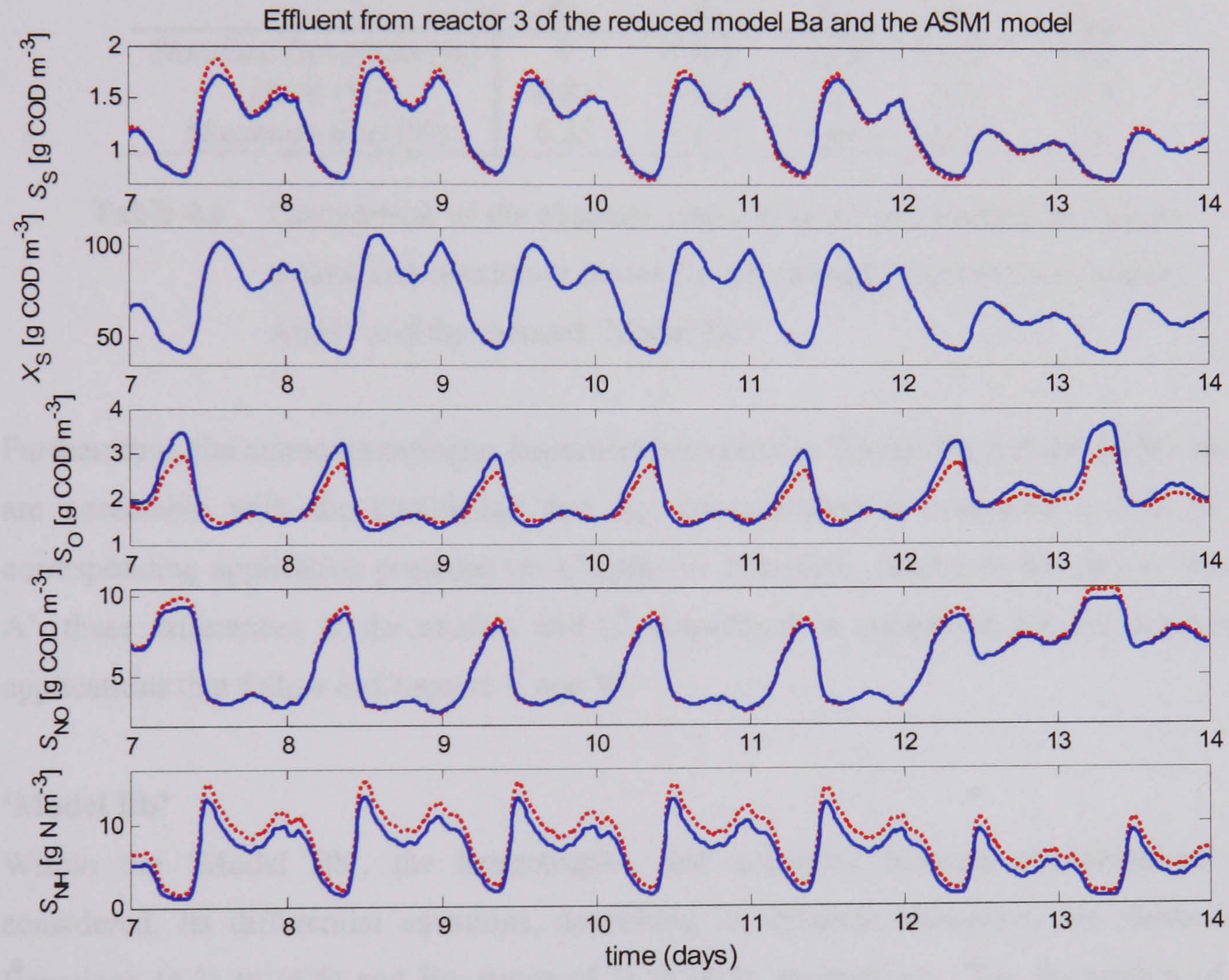


**Figure 4.7** $S_S$, $X_S$, $S_O$, $S_{NO}$ and $S_{NH}$ concentrations from reactor 3 resulting from simulations with the ASM1 model (dashed line) and $S_S$, $X_S$, $S_O$, $S_{NO}$ and $S_{NH}$ concentrations resulting from 'Model Ba' (solid line), respectively.

This phenomena is most likely due to the constant levels of $X_{B,A}$ and $X_{B,H}$ concentrations considered in the reduced model. Indeed, by keeping the heterotrophic biomass and

autotrophic biomass concentrations constant, the anoxic growth of heterotrophs and aerobic growth of autotrophs processes cannot occur.

Similarly to 'Model A', the absolute errors between the original ASM1 model and the 'Model Ba' are calculated in terms of standard deviations, means and maximum biases, for each concentration. Results are summarised in Table (4.6) were it can be observed that the maximum discrepancies occur for $S_S$, $S_O$, $S_{NO}$ and $S_{NH}$ concentrations with a maximum standard deviation error occurring for the dissolved oxygen (30.8%) for the reasons explained earlier.

| | $S_S$ | $X_S$ | $S_O$ | $S_{NO}$ | $S_{NH}$ |
|---|---|---|---|---|---|
| *Standard Deviation* (%) | 9 | < 0.1 | 30.8 | 6.84 | 9.75 |
| *Mean* (%) | 0.81 | < 0.1 | 5 | 1.96 | 18.4 |
| *Maximum Bias* (%) | 6.35 | < 0.1 | 15.6 | 5.82 | 12 |

**Table 4.6** Comparison of the absolute errors in terms of standard deviations, means and maximum biases (in percentage), between the original ASM1 and the reduced 'Model Ba'.

Furthermore, the ammonia nitrogen disparities between the 'Model Ba'and the ASM1 model are acceptable with the knowledge that $S_{NH}$ concentration is measured on-line in the corresponding application presented in Chapter V. Therefore, similar to the case in 'Model A', these differences in the models will be considered as acceptable for the monitoring applications that follow in Chapters V and VI.

**'Model Bb'**

Within the 'Model Bb', the heterotrophic and autrophic biomass concentrations are considered. Its differential equations, describing its dynamic behaviour, are identical to Equations (4.2) to (4.5) and Equations (4.7) to (4.9), respectively. The description of the 'Model Bb' in term of state variables, inputs, processes etc. is detailed in Table (4.7). Its dynamic behaviour is compared with the ASM1 model, as presented in the schematic overview of Figure (4.8).

Similar to the 'Model A' and 'Model Ba', the dry influent wastewater data are used to characterize the influent wastewater for the models. The dynamic behaviours of the influent concentrations to the 'Model Bb' are not represented here because they are identical to those displayed in Figure (4.3) and (4.6).

| | |
|---|---|
| State variables (7) | $S_S$, $X_S$, $X_{B,H}$, $X_{B,A}$, $S_O$, $S_{NO}$, $S_{NH}$ |
| Inputs (9) | $S_{S,in}$, $X_{S,in}$, $X_{B,H,in}$, $X_{B,A,in}$, $S_{O,in}$, $S_{NO,in}$, $S_{NH,in}$, $Q_{in}$, $K_La_{in}$ |
| Outputs (7) | $S_{S,ef}$, $X_{S,ef}$, $X_{B,H,ef}$, $X_{B,A,ef}$, $S_{O,ef}$, $S_{NO,ef}$, $S_{NH,ef}$ |
| Parameters (18) | $\mu_{mH}$, $K_S$, $K_{OH}$, $K_{NO}$, $b_H$, $\eta_g$, $\eta_h$, $K_h$, $K_X$, $\mu_{mA}$, $K_{NH}$, $b_A$, $K_{OA}$, $k_a$, $Y_A$, $Y_H$, $f_p$, $i_{XB}$ |
| Processes involved (7) | $P_1$, $P_2$, $P_3$, $P_4$, $P_5$, $P_6$, $P_7$ |
| Eventual measurements (5) | $S_O$, $S_{NO}$, $S_{NH}$ (on-line)<br>$S_S$, $X_S$ (off-line) |

**Table 4.7** Reduced-order 'Model Bb' description. The state variables and parameter definitions are presented in Appendix B, Table B.2, B2.1 and B2.2.

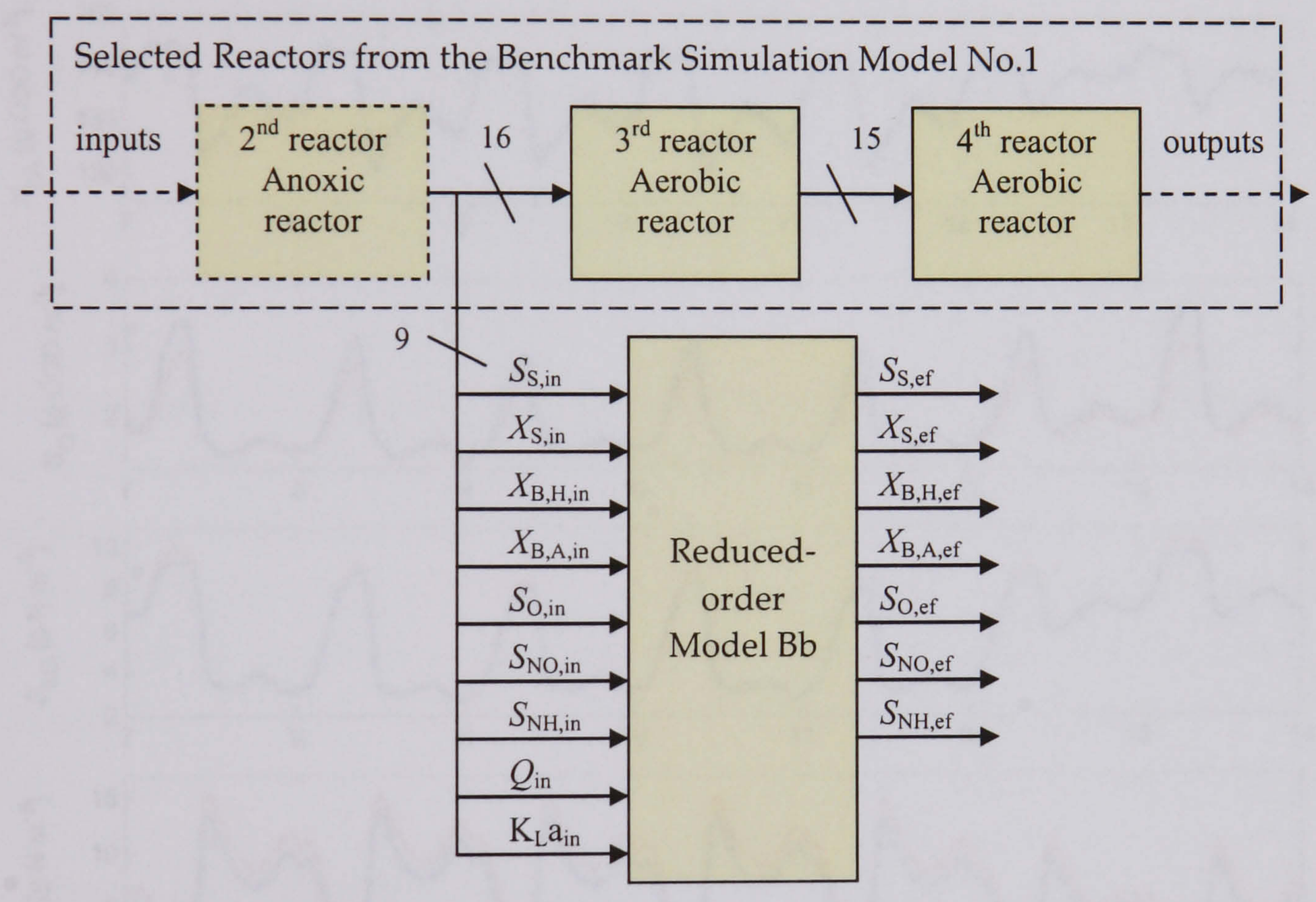


**Figure 4.8** Schematic representation of the 'Model Bb', implemented in parallel with the benchmark plant.

The difference between the original ASM1 and the 'Model Bb' are presented in Figure (4.9). Comparing these results with the ones presented in Figure (4.7), it can be observed that the constant biomasses levels do not affect the slowly biodegradable substrate. Furthermore, $S_S$, $S_O$, $S_{NO}$ and $S_{NH}$ concentrations are closer to the original ASM1 model in comparison to the reduced 'Model Ba'.

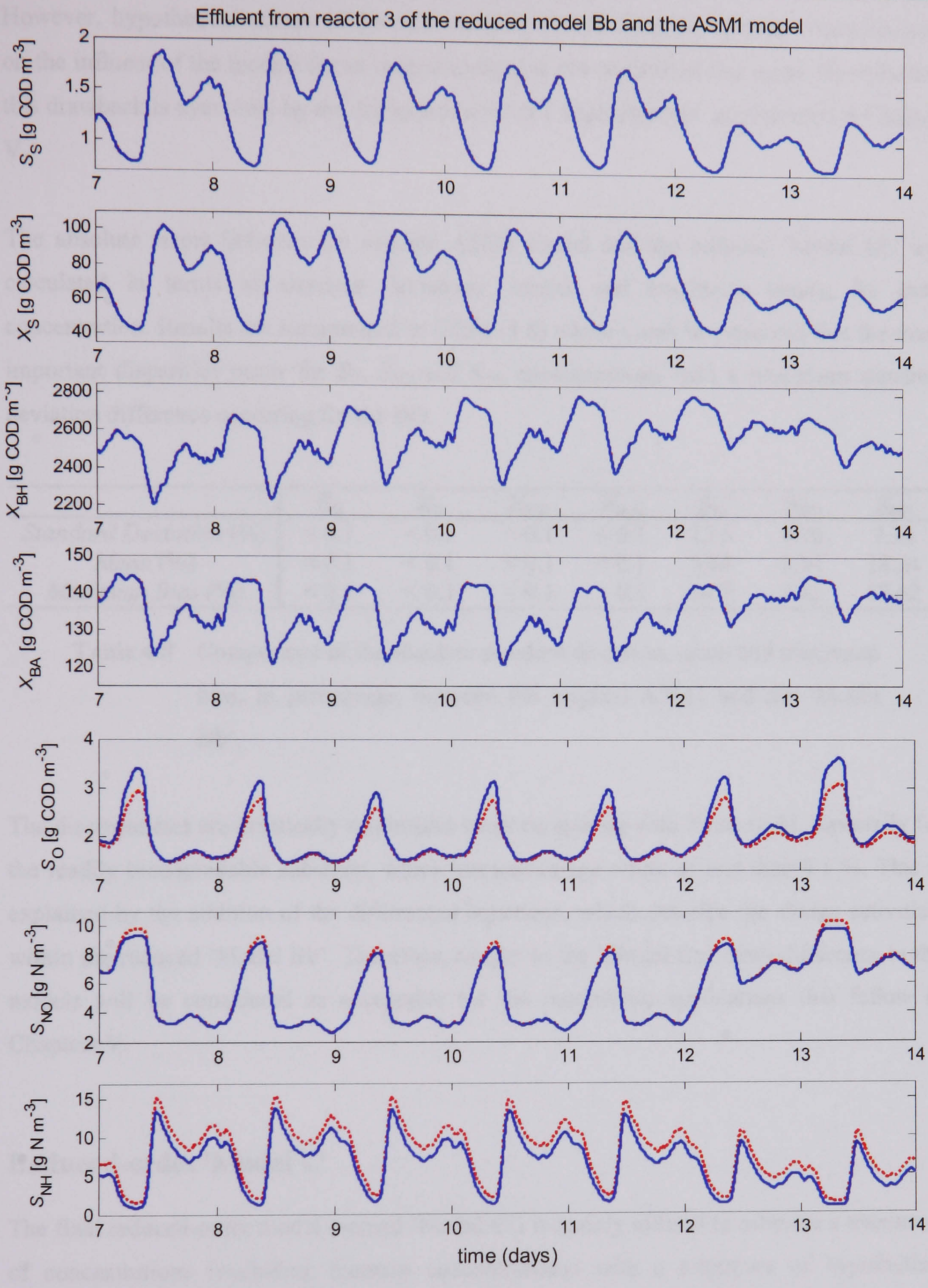


**Figure 4.9** $S_S$, $X_S$, $X_{B,H}$, $X_{B,A}$, $S_O$, $S_{NO}$ and $S_{NH}$ concentrations from reactor 3 resulting from simulations with the ASM1 model (dashed line) and $S_S$, $X_S$, $X_{B,H}$, $X_{B,A}$, $S_O$, $S_{NO}$ and $S_{NH}$ concentrations resulting from 'Model Bb' (solid line), respectively.

However, hypothetical access of the heterotrophic and autotrophic biomass concentrations on the influent of the models (or as measurements) is not realistic at this stage. Nevertheless this drawback is overcome by the implementation of a state observer, as presented in Chapter V.

The absolute errors between the original ASM1 model and the reduced 'Model Bb' are calculated in terms of standard deviations, means and maximum biases, for each concentration. Results are summarised in Table (4.8) where it can be observed that the most important disparities occur for $S_O$, $S_{NO}$ and $S_{NH}$ concentrations with a maximum standard deviation difference occurring for the DO.

| | $S_S$ | $X_S$ | $X_{B,H}$ | $X_{B,A}$ | $S_O$ | $S_{NO}$ | $S_{NH}$ |
|---|---|---|---|---|---|---|---|
| *Standard Deviation* (%) | < 0.1 | < 0.1 | < 0.1 | < 0.1 | 23.5 | 4.90 | 7.24 |
| *Mean* (%) | < 0.1 | < 0.1 | < 0.1 | < 0.1 | 5.64 | 2.14 | 18.24 |
| *Maximum Bias* (%) | < 0.1 | < 0.1 | < 0.1 | < 0.1 | 14.7 | 5.43 | 10.62 |

**Table 4.8** Comparison of the absolute standard deviation, mean and maximum bias, in percentage, between the original ASM1 and the 'Model Bb'.

The discrepancies are drastically minimised when comparing with Table (4.6), especially for the readily biodegradable substrate, which has percentage errors of less than 0.1 %. This is explained by the addition of the differential equations, which describe the sludge activities, within the reduced 'Model Bb'. Therefore, similar to the 'Model Ba', such difference in the models will be considered as acceptable for the monitoring applications that follow in Chapters V.

## Reduced-order 'Model C'

The final reduced-order model (named 'Model C') is mainly utilised to estimate a maximum of concentrations (excluding biomass concentrations) with a minimum of hypothetical available measurements. Therefore, the same assumptions as the 'Model Ba' are held but the particulate biodegradable organic nitrogen ($X_{ND}$) and soluble biodegradable organic nitrogen ($S_{ND}$) concentrations are also included in the reduced model. The differential equations describing the reduced 'Model C' are identical to the 'Model Ba' ones, which is described by Equations (4.17) to (4.21). Note that $X_{B,H}$ and $X_{B,A}$ concentrations are kept constant. In addition the following two differential equations are also considered:

$$\frac{dS_{ND}}{dt} = Q\frac{S_{ND,in} - S_{ND}}{V} + \left\{ -k_a \times S_{ND} + K_h \times \frac{X_{ND}/2561}{K_X + \left(X_S/2561\right)} \times \left[ \left( \frac{S_O}{K_{O,H} + S_O} \right) + \eta_h \times \left( \frac{K_{O,H}}{K_{O,H} + S_O} \right) \left( \frac{S_{NO}}{K_{NO} + S_{NO}} \right) \right] \right\} \times 135 \quad (4.22)$$

$$\frac{dX_{ND}}{dt} = Q\frac{X_{ND,in} - X_{ND}}{V} + \left\{ \left(i_{XB} - f_p \times i_{XP}\right)\left(b_H \times 2561\right) \times \left(b_A \times 135\right) - K_h \times \frac{X_{ND}/2561}{K_X + \left(X_S/2561\right)} \times \left[ \left( \frac{S_O}{K_{O,H} + S_O} \right) + \eta_h \times \left( \frac{K_{O,H}}{K_{O,H} + S_O} \right) \left( \frac{S_{NO}}{K_{NO} + S_{NO}} \right) \right] \right\} \times 2561 \quad (4.23)$$

The description of the 'Model C' in term of state variables, inputs, processes etc. is detailed in Table (4.9). It can be observed that seven state variables and outputs are considered, while five measurements (two on-line and three off-line sensors) can hypothetically be available with this specific configuration.

| | |
|---|---|
| State variables (7) | $S_S$, $X_S$, $S_O$, $S_{NO}$, $S_{NH}$, $S_{ND}$, $X_{ND}$ |
| Inputs (9) | $S_{S,in}$, $X_{S,in}$, $S_{O,in}$, $S_{NO,in}$, $S_{NH,in}$, $S_{ND,in}$, $X_{ND,in}$, $Q_{in}$, $K_La_{in}$ |
| Outputs (7) | $S_{S,ef}$, $X_{S,ef}$, $S_{O,ef}$, $S_{NO,ef}$, $S_{NH,ef}$, $S_{ND,ef}$, $X_{ND,ef}$ |
| Parameters (19) | $\mu_{mH}$, $K_S$, $K_{OH}$, $K_{NO}$, $b_H$, $\eta_g$, $\eta_h$, $K_h$, $K_X$, $\mu_{mA}$, $K_{NH}$, $b_A$, $K_{OA}$, $k_a$, $Y_A$, $Y_H$, $f_p$, $i_{XB}$, $i_{XP}$ |
| Processes involved (8) | $P_1$, $P_2$, $P_3$, $P_4$, $P_5$, $P_6$ $P_7$, $P_8$ |
| Measurements (5) | $S_O$, $S_{NO}$, $S_{NH}$ (on-line) \| $S_S$, $X_S$ (off-line) |

**Table 4.9** Reduced-order 'Model C' description. The state variables and parameter definitions are presented in Appendix B, Table B.2, B2.1 and B2.2.

Its dynamic behaviour is compared with the ASM1 model, as presented in the schematic overview of Figure (4.10). Similarly to the case of the reduced 'Model A' and the 'Model B', the dry influent wastewater data file is used to characterize the influent wastewater for the models.

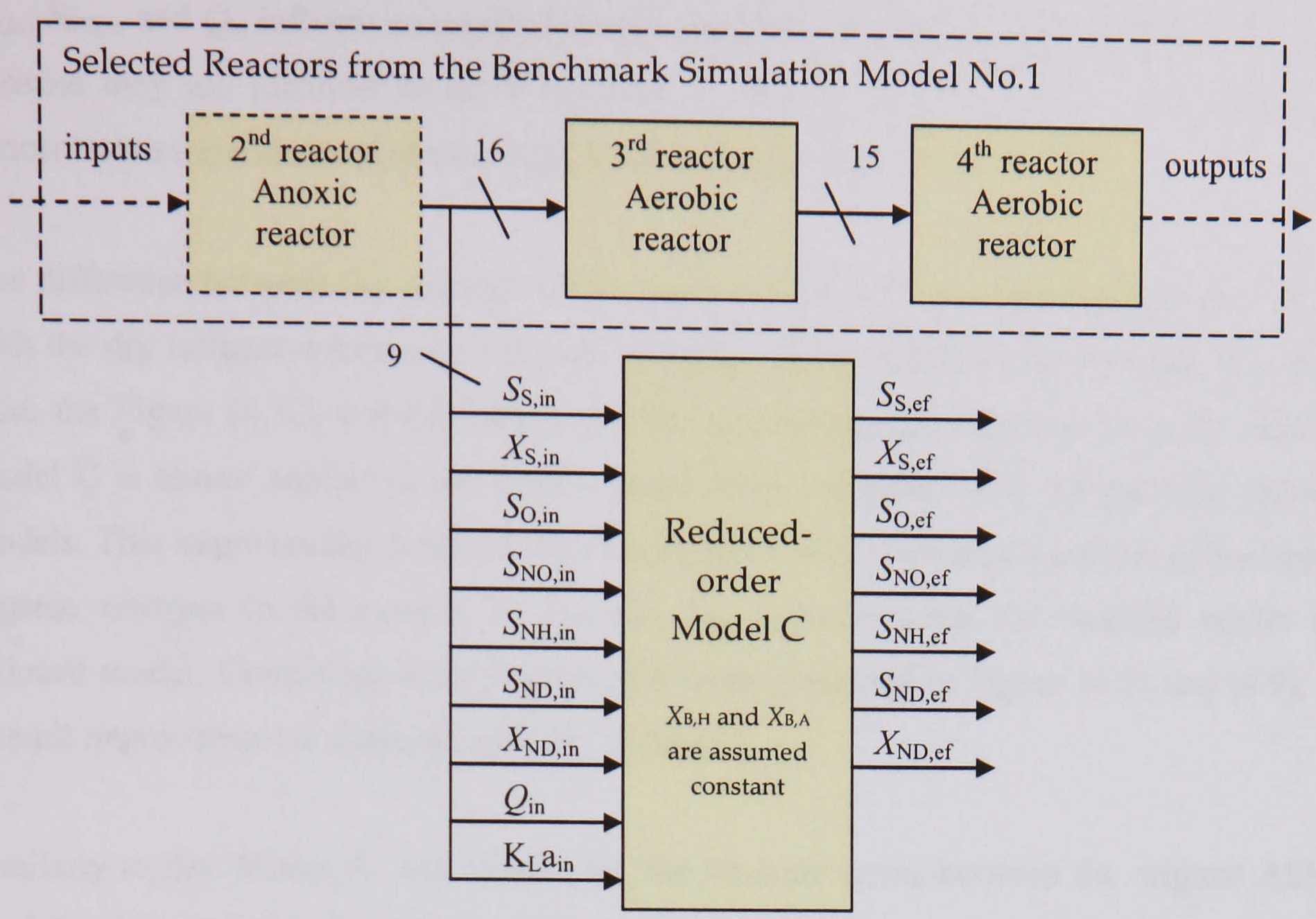


**Figure 4.10** Schematic representation of the reduced-order 'Model C', implemented in parallel with the benchmark plant.

The dynamic behaviours of the influent concentrations to the 'Model C' are presented in Figure (4.11) for $S_{ND,in}$ and $X_{ND,in}$ concentrations.

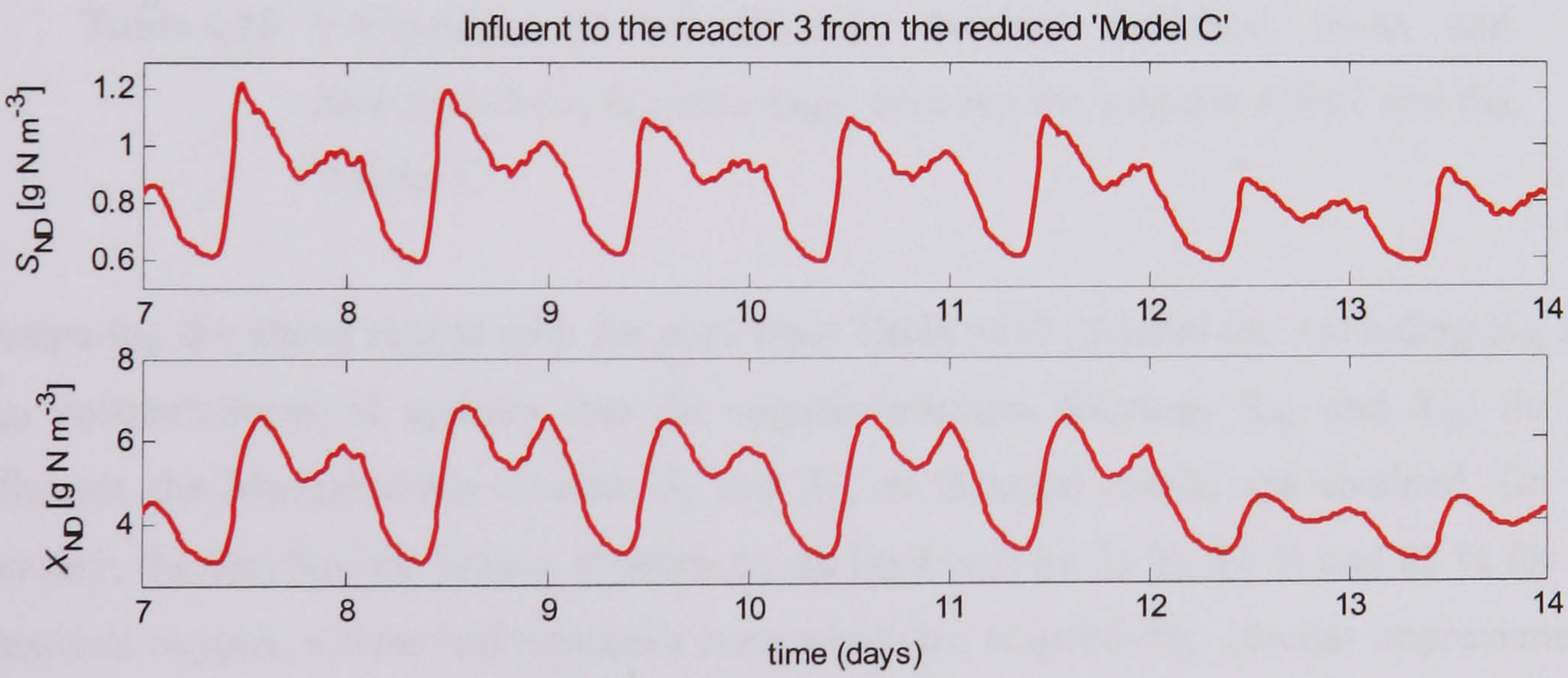


**Figure 4.11** $S_{ND,in}$, and $X_{ND,in}$, influent concentrations to reactor 3 resulting from simulation with the reduced-order 'Model C'.

$S_{O,in}$, $S_{NO,in}$ and $Q_{in}$ influent concentrations and the flow, respectively, are not illustrated here because they are identical to those presented in Figure (4.3) while $S_{S,in}$, $X_{S,in}$ and $S_{NH,in}$ concentrations are identical to those displayed in Figure (4.6).

The difference between the original ASM1 and the 'Model C' is presented in Figure (4.12) with the dry influent wastewater data and in Figure (4.13) with the storm events. It is clear from the Figure (4.12) that the behaviour of $S_{NH}$ concentration resulting from the reduced model C is almost similar to the ASM1 model when compared with the previous reduced models. This improvement confirms the consideration of the hydrolysis process of entrapped organic nitrogen in the system, as $S_{ND}$ and $X_{ND}$ concentrations are included within the reduced model. Comparing these results with those presented in Figure (4.7) and (4.9), an overall improvement is achieved with the 'Model C'.

Similarly to the 'Model A' and 'Model B', the absolute errors between the original ASM1 model and the 'Model C' are presented in terms of standard deviations, means and maximum biases, for each concentration. Results are summarised in Table (4.10) where it can be observed that the maximum discrepancy still occurs for $S_O$.

| | $S_S$ | $X_S$ | $S_O$ | $S_{NO}$ | $S_{NH}$ | $S_{ND}$ | $X_{ND}$ |
|---|---|---|---|---|---|---|---|
| *Standard Deviation* (%) | 9 | < 0.1 | 14.6 | 2.56 | 1.7 | 10.3 | < 0.1 |
| *Mean* (%) | 0.81 | < 0.1 | 0.53 | < 0.1 | < 0.1 | < 0.1 | < 0.1 |
| *Maximum Bias* (%) | 6.35 | < 0.1 | 9.8 | 3.29 | 5 | 6.5 | < 0.1 |

**Table 4.10** Comparison of the absolute standard deviation, mean and maximum bias, in percentage, between the original ASM1 and the 'Model C'.

Comparing the above results with the ones from Table (4.6) ('Model Ba' excluding $S_{ND}$ and $X_{ND}$ concentrations) it appears that the organic nitrogen fractions $S_{ND}$ and $X_{ND}$ do not influence the biodegradable fraction $S_S$ and $X_S$, as identical results are obtained. On the contrary, the standard deviations differences are improved by 51 %, 62 % and 82 % for the dissolved oxygen, nitrate and ammonia concentrations, respectively. Similar improvements are achieved with the means and maximum biases.

Hypothetical accesses to nitrogen and ammonia concentrations on the influent of the models (or as measurements) are not realistic at this stage.

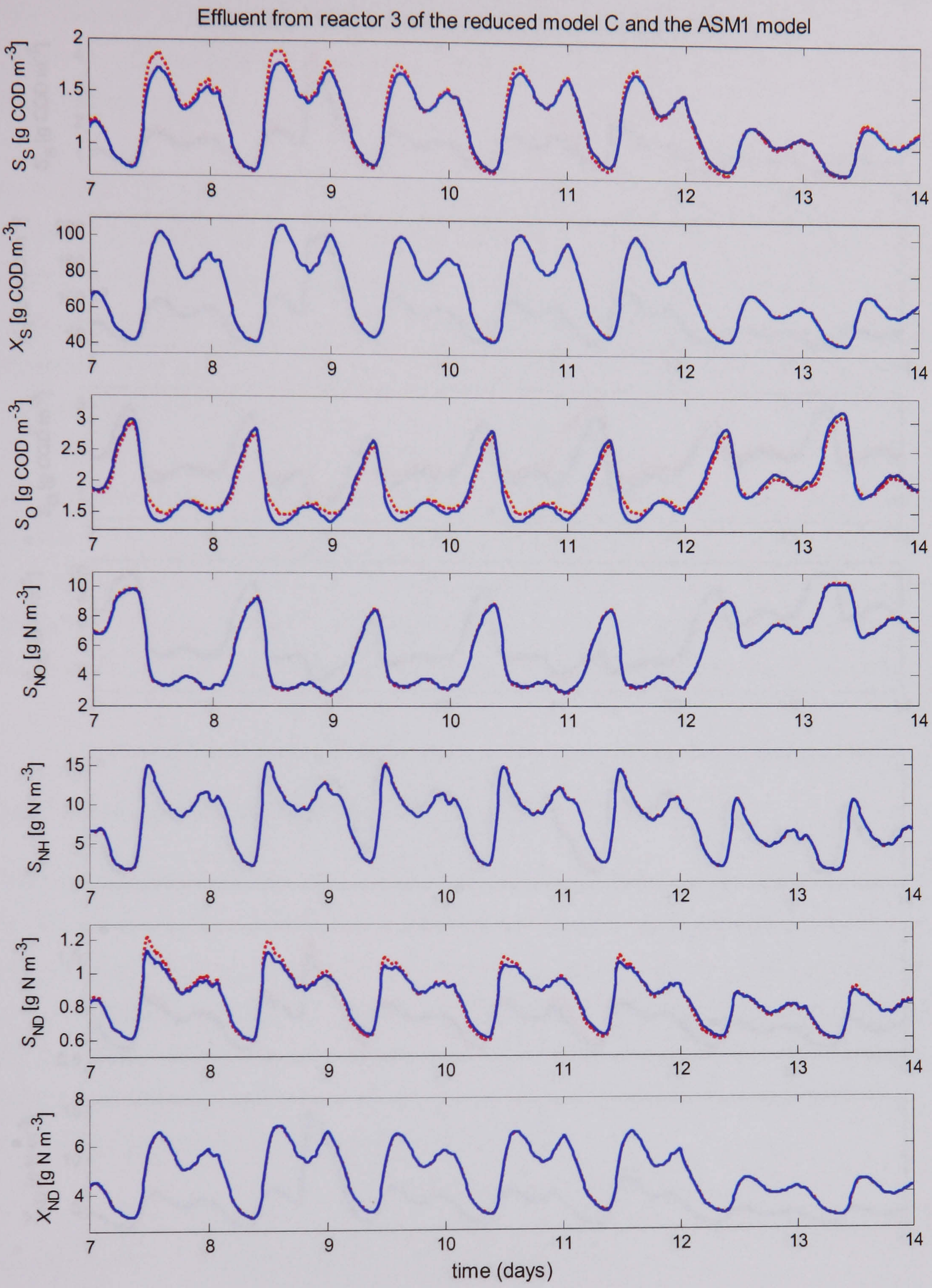


**Figure 4.12** $S_S$, $X_S$, $S_O$, $S_{NO}$, $S_{NH}$, $S_{ND}$ and $X_{ND}$ concentrations from reactor 3 resulting from simulations with the ASM1 model (dashed line) and $S_S$, $X_S$, $S_O$, $S_{NO}$, $S_{NH}$, $S_{ND}$ and $X_{ND}$ concentrations resulting from 'Model C' (solid line), respectively. The dry influent wastewater data are considered.

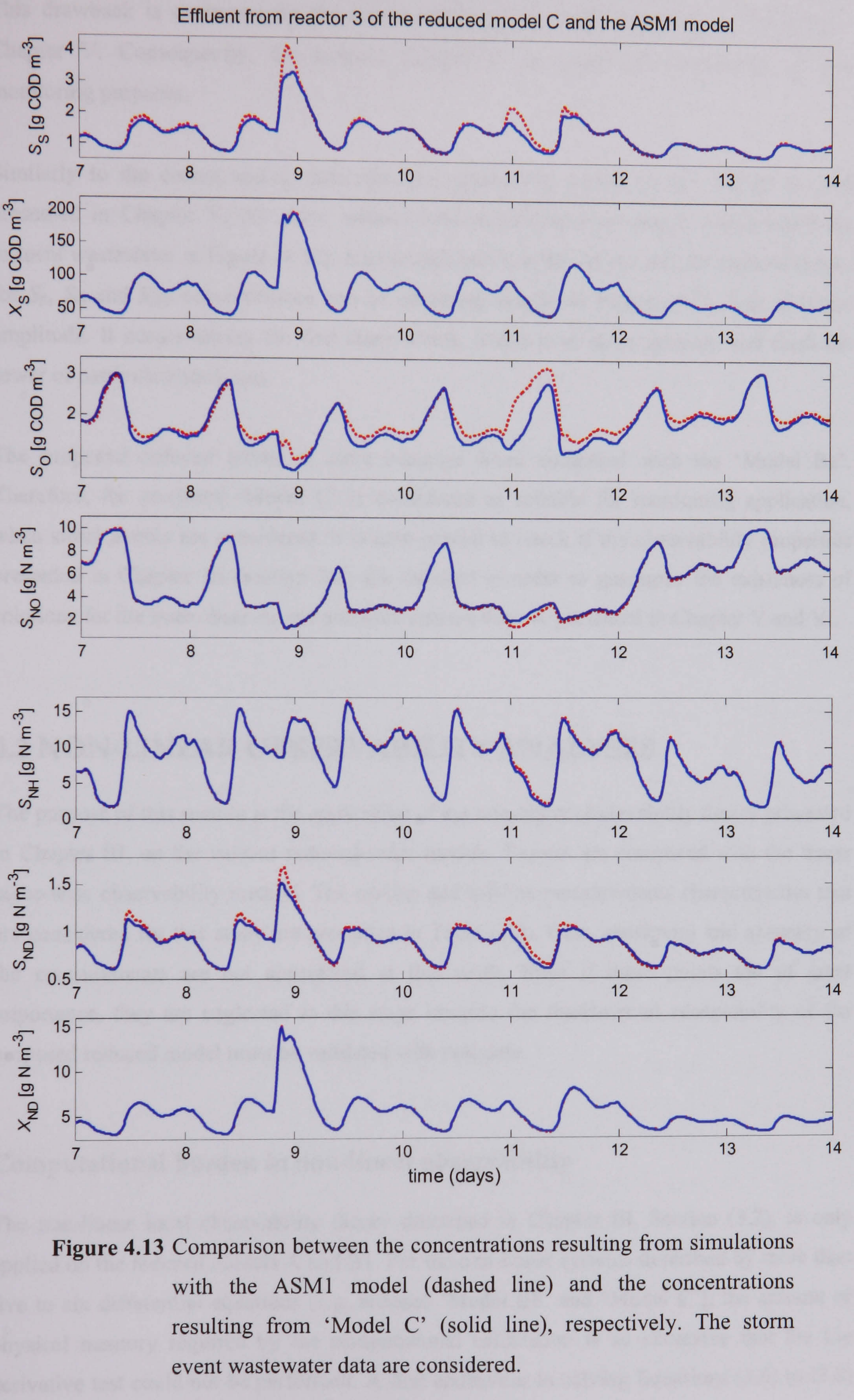


**Figure 4.13** Comparison between the concentrations resulting from simulations with the ASM1 model (dashed line) and the concentrations resulting from 'Model C' (solid line), respectively. The storm event wastewater data are considered.

This drawback is overcome by the implementation of a state observer, as presented in Chapter V. Consequently, the reduced 'Model C' is considered sufficiently precise monitoring purposes.

Similarly to the corresponding state observer application, based on the 'Model C' and presented in Chapter V, the storm influent wastewater data are used to characterise the influent wastewater in Figure (4.13). A mismatch between the ASM1 and the reduced model for $S_S$, $S_O$ and $S_{ND}$ concentrations can be observed, similar to Figure (4.12), but of larger amplitude. It occurs during the first storm event, which is of short duration and flush the sewer of particulate materials.

The proposed reduced model is more accurate when compared with the 'Model Ba'. Therefore, the proposed 'Model C' is considered as suitable for monitoring application, when storm events are considered. It is now crucial to check if the observability properties presented in Chapter III (section 2.2) are satisfied in order to guarantee the existences of solutions for the state observer and software sensors that are presented in Chapter V and VI.

## 4.2 NON-LINEAR OBSERVABILITY ANALYSES

The purpose of this section is the application of the non-linear observability theory presented in Chapter III, on the various reduced-order models. Results are compared with the linear piece-wise observability method. The on-line and off-line measurements characteristics that are considered for this study are presented in Table (2.2). Cost, sensitivity and accuracy of the measurements are not considered in this work. Even if these points are of great importance, they are neglected at this stage because the fundamental acceptability of the proposed reduced model must be validated with real data.

### Computational burden in non-linear observability

The non-linear local observability theory described in Chapter III, Section (3.2), is only applied on the reduced models A and B1. For the non-linear systems described by more than five to six differential equations (e.g. reduced 'Model Bb' and 'Model C'), the amount of physical memory required by the computational calculation is so excessive that the Lie derivative test could not be performed. A first endeavour in solving Equations (3.6) to (3.8)

has been unsuccessfully attempted with Matlab, using a symbolic form of the ASM1 model. A simple calculation, based on single Lie derivatives workspace memory storage, clearly confirmed that for a ninth order system, 200GB of memory would be required.

This significant memory requirement has motivated the use of Maple, which is more efficient for such symbolic calculations. However, a similar problem occurred for sixth order non-linear systems. This computational burden is due to each Lie derivatives calculation, which requires storage of the previous calculations in the memory when computing the observation space $\mathbf{w}(x)$ given in Equation (3.6). Furthermore, a symbolic form of the expressions is initially required before substituting the numerical operating conditions in the model. Therefore, even with a 4 GHz processor equipped with 2GB of memory and 4095MB of virtual memory, the computational analysis of the observation space and the rank failed. Consequently, the adopted solution for investigating the observability of the reduced 'Model Bb' and 'Model C', is the piece-wise linear approach. This technique as been briefly discussed in Chapter II and further investigated in this Chapter.

## Observability analysis of 'Model A'

### Linear piece-wise observability analysis

The 'Model A' under study, which is defined in the form of Equations (3.4) and (3.5), is assumed stable. The linear piece-wise approach, presented in Chapter III, is initially investigated. The dynamic non-linear system described by Equations (4.12) to (4.15) is assumed to be composed of a linear model at each sampling point. Under this assumption, the Kalman rank test ($[\mathbf{C\ CA}\ldots\mathbf{CA}^{n-1}]'$) for observability of linear systems is applied piece-wise in time at each sampling point (also called operating points or conditions in this work).

Results are presented in Figure (4.14) were it can be observed that the rank (*rk*) test succeeded at all operating points (e.g. 43673) when $S_O$ is considered as the only measurement. All operating conditions are obtained by running the reduced model in parallel with the benchmark plant over a fourteen days period. To confirm these results, the non-linear observability theory, also presented in Chapter III, is investigated.

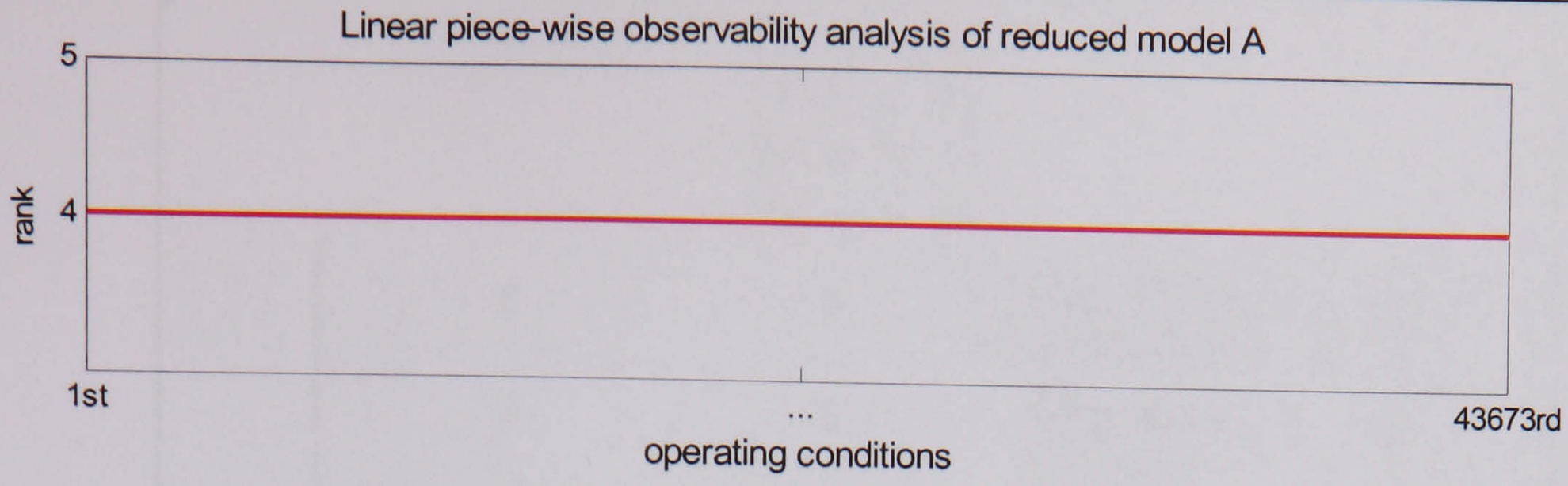


**Figure 4.14** Linear piece-wise observability analysis applied on the reduced 'Model A', achieved with a single measurement ($S_O$).

**Non-linear observability analysis**

The non-linear reduced 'Model A' is selected to perform the non-linear observability analysis. The observation space given by Equation (3.6) has been initially computed, up to $k$=4 (e.g. the order of the system). This computation involved Lie derivatives along the vector field **f** described by Equation (3.7). The implicit observability map is of the form

$$\mathbf{w}(\mathbf{x})=\begin{pmatrix} \dfrac{-1.5\times\mu_H\times(1-Y_H)\times S_O\times X_{B,H}}{(Y_H\times(K_S+1.5)\times(K_{O,H}+S_O))}-\dfrac{5.548\times\mu_A\times(4.47-Y_A)\times S_O\times X_{B,A}}{(Y_A\times(K_{NH}+5.548)\times(K_{O,A}+S_O))}+\cdots \\ -\dfrac{1.5\times\mu_H\times(1-Y_H)\times S_O\times\dfrac{1.5\times\mu_H\times\dfrac{S_O}{K_{O,H}+S_O}+\dfrac{ng\times K_{O,H}\times S_{NO}}{(K_{O,H}+S_O)\times(K_{NO}+S_{NO})}}{K_S+1.5}-b_H\times X_{B,H}}{(Y_H\times(K_S+1.5))\times(K_{O,H}+S_O)}-\cdots \\ -\dfrac{1.5\times\mu_H\times(1-Y_H)\times S_O\times\dfrac{1.5\times\mu_H\times\dfrac{S_O}{K_{O,H}+S_O}+\dfrac{ng\times K_{O,H}\times S_{NO}}{(K_{O,H}+S_O)\times(K_{NO}+S_{NO})}}{K_S+1.5}-b_H\times X_{B,H}}{(Y_H\times(K_S+1.5))\times(K_{O,H}+S_O)}+\cdots \\ \dfrac{3\times\left(\dfrac{1.5\times\mu_H\times(1-Y_H)}{(Y_H\times(K_S+1.5))\times(K_{O,H}+S_O)}+\dfrac{1.5\times\mu_H\times(1-Y_H)S_O}{(Y_H\times(K_S+1.5))\times(K_{O,H}+S_O)^2}\right)\cdots}{(Y_H\times(K_S+1.5))\times(K_{O,H}+S_O)}+\cdots \end{pmatrix}, \tag{4.24}$$

Note that for simplification reasons the transport terms of Equation (4.1), the entire observation space as well as its invertibility matrix ($\mathcal{Q}(\mathbf{x})$) are not represented here. Then, the computation of the local invertibility of the observability map has been computed, which is given by $\mathcal{Q}(\mathbf{x})$ of the implicit form given by

$$\mathcal{Q}(\mathbf{x}) = \begin{bmatrix} \begin{bmatrix} 0 & 0 & 0 & 0 \\ 0 & 0 & 0 & 0 \\ 0 & 0 & 0 & 0 \\ 0 & 0 & 0 & 0 \end{bmatrix} & & \\ \begin{bmatrix} 0 & 0 & \left(\frac{1.5\times\mu_H\times(1-Y_H)}{(Y_H\times(K_S+\ldots)\times\ldots}+\ldots\right) & 0 \\ 0 & 0 & \frac{5.548\times\mu_A\times\ldots}{Y_A\times(K_{NH}+\ldots}+\ldots & 0 \\ \frac{1.5\times\mu_H\times(1-Y_H)}{(Y_H\times(K_S+1.5))\times\ldots}+\ldots & \frac{5.548\times\mu_A\times\cdots}{Y_A\times(K_{NH}+} & \frac{3\times\mu_H\times(1-Y_H)\times\ldots}{(Y_H\times\ldots)\times(K_{O,H}\ldots} & 0 \\ 0 & 0 & 0 & 0 \end{bmatrix} & \\ \begin{bmatrix} 3\times\frac{-1.5\ldots}{(Y_H\times(K_S+\ldots}-\frac{}{Y_H\times(K_S+\ldots}+\ldots & 1.5\times\frac{-5.548\times\ldots}{(Y_H\times(K_S+\ldots}-\frac{}{Y_H\times(K_S+\ldots}+\ldots & 1.5\times\frac{-5.548\times\mu_H\times\ldots}{(Y_H\times(K_S+\ldots}+\ldots & -1.5\times\mu_H\ldots \\ \vdots & \vdots & \vdots & \vdots \\ \frac{2.25\times\mu_H{}^2}{\ldots}\times\ldots & 0 & \frac{2.25\times\mu_H{}^2\times(1-\ldots}{\ldots}\times\ldots & \frac{2.25\times\ldots}{\ldots}\times\ldots \end{bmatrix} & \\ \begin{bmatrix} 6\times\frac{-1.5\ldots}{(Y_H\times(K_S+\ldots}-\frac{}{Y_H\times(K_S+\ldots}+\ldots & 1.5\times\frac{-5.548\times\ldots}{(Y_A\times(K_{NH}+\ldots}-\frac{}{Y_H\times(K_S+\ldots}+\ldots & 3\times\frac{3\mu_H\ldots}{(Y_H\times(K_S+\ldots}-\frac{}{Y_H\times(K_S+\ldots}-\ldots & \frac{4.5\times\ldots}{Y_H\times\ldots}+\ldots \\ \vdots & \vdots & \vdots & \vdots \end{bmatrix} \end{bmatrix} \tag{4.25}$$

Finally, based on the observation space and the local invertibility of the observability map, the rank of the reduced model has been investigated in the neighbourhood of various operating points.

Simulation results presented in Figure (4.15) are achieved at each of the operating conditions displayed in Table (4.11). Again, for abbreviation reasons, the entire table is not displayed. The selected points, for which the dry influent wastewater data are used to characterize the influent wastewater for the reduced-order model, cover a period of twenty-four hours between the seventh and eighth days of the benchmark plant output data. It can be observed from Figure (4.15) that a single measurement ($S_O$) is also sufficient to achieve the local observability properties around the neighbourhood of the ten operating conditions.

However, caution should be considered, as the non-linear properties have been investigated only for few operating points.

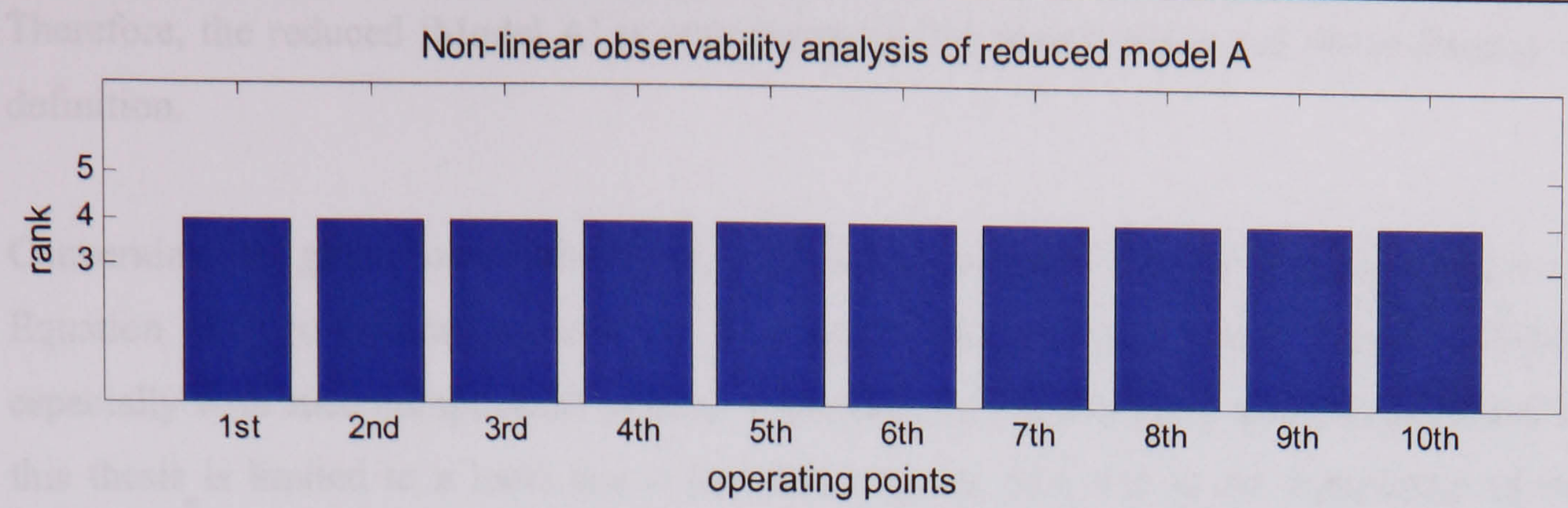


**Figure 4.15** Non-linear observability analyses based on the Lie derivative, achieved with a single measurement ($S_O$). The three first and last operating points are displayed in Table (4.11)

Over a period of 24 hours, there are more than three thousand operating conditions, while for a 14 days simulation period, these increases to about 44,000, as displayed on the x-axis on Figure (4.14). To be consistent, the non-linear observability properties should be investigated (if possible) for the whole domain of definition, similarly to the linear piece-wise case, to guarantee the local observability.

| OC / In. Out. | 1 | 2 | 3 | … | … | 8 | 9 | 10 |
|---|---|---|---|---|---|---|---|---|
| $Q_{in=ef}$ | 95251 | 93754 | 86886 | … | … | 93284 | 95899 | 99122 |
| $X_{B,H,in}$ | 2498.5 | 2500.4 | 2579.9 | … | … | 2480.8 | 2456.6 | 2442.6 |
| $X_{B,H}$ | 2499.4 | 2499.4 | 2593.3 | | | 2475.9 | 2487.9 | 2451.5 |
| $X_{B,A,in}$ | 141 | 146.04 | 146.6 | … | … | 137 | 135.1 | 133.7 |
| $X_{B,A}$ | 141.4 | 146.54 | 147.6 | | | 137.3 | 137.3 | 134.7 |
| $S_{O,in}$ | $1e^{-4}$ | $1e^{-4}$ | $2e^{-4}$ | … | … | $4e^{-5}$ | $4e^{-5}$ | $3e^{-5}$ |
| $S_O$ | 1.84 | 1.705 | 1.74 | | | 1.92 | 1.90 | 1.95 |
| $S_{NO,in}$ | 4.43 | 1.143 | 6.75 | … | … | 1.02 | 1.27 | 0.79 |
| $S_{NO}$ | 7.16 | 5.96 | 9.43 | | | 3.71 | 3.97 | 3.43 |

**Table 4.11** Operating conditions (OC), which represent the x-axis of Figure (4.15), used to investigate the non-linear observability of the reduced-order 'Model A'. The y-axis (Q: $m^3/d$ unit; from $X_{B,H}$ to $S_O$: g COD $m^{-3}$ units; and $S_{NO}$ g N $m^{-3}$ units) represent the inputs (In.) and outputs of the reduced 'Model A' (Out.).

In other words, the rank test should be performed at all possible times (smaller than the time step from the solver) rather than for a few operating conditions. The proposed results demonstrated similarities between the linear piece-wise approach and the non-linear one.

Therefore, the reduced 'Model A' is considered locally observable in the whole domain of definition.

Concerning the global observability, it is important to bear in mind that the solution of Equation (3.6) is difficult to consider in practice (Bogaerts and Vande Wouwer, 2004), especially with such complicated models. Therefore, the observability analyses presented in this thesis is limited to a local one rather than a global one, due to the complexity of the reduced models. It should also be emphasised that global observability, which is not often considered, is mainly performed on simple second order model.

## Observability analysis of model B (Ba and Bb)

### Model Ba: Linear piece-wise observability analysis

The reduced 'Model Ba' under study, which is described by Equations (4.16) to (4.20), is assumed stable. A similar linear piece-wise observability, as the one performed for 'Model A', has been investigated. Simulation results are presented in Figure (4.16) where it can be observed that the rank (denoted *rk*) test failed (*rk* = 4) at a set of operating points (e.g. the 41514$^{th}$) when $S_O$ was considered as the only measurement. The system matrix of the linear model at the 41514$^{th}$ point, where a loss of observability occurred, is of the form

$$\mathbf{A} = \begin{bmatrix} -1305.45 & 21.976 & -0.0209 & -0.00128 & 0 \\ 0 & -21.976 & -3.551 & -0.217 & 0 \\ -413.28 & 0 & -18.645 & 0 & -333.56 \\ -6.1247 & 0 & 4.4786 & -0.0252 & 77.0346 \\ -69.9723 & 0 & -3.4209 & -0.0117 & -78.5136 \end{bmatrix}. \quad (4.26)$$

This matrix is singular ($\mathbf{A}.\mathbf{A}^{-1} \neq \mathbf{I}$) and has a non zero determinant (close to zero: 8.2e-10). This implies that all columns (and/or rows) are not independent, which results in a non-observable system ($rk \neq 5$ instead of $rk = 5$). Consequently, the linear model, at the selected operating condition, is not valid when the dissolved oxygen measurement is considered. The set of operating conditions causing the lost of observability is presented in the next subsection. Note that all operating points (e.g. 43648$^{th}$) are obtained by running the reduced model in parallel with the benchmark plant over a fourteen days period.

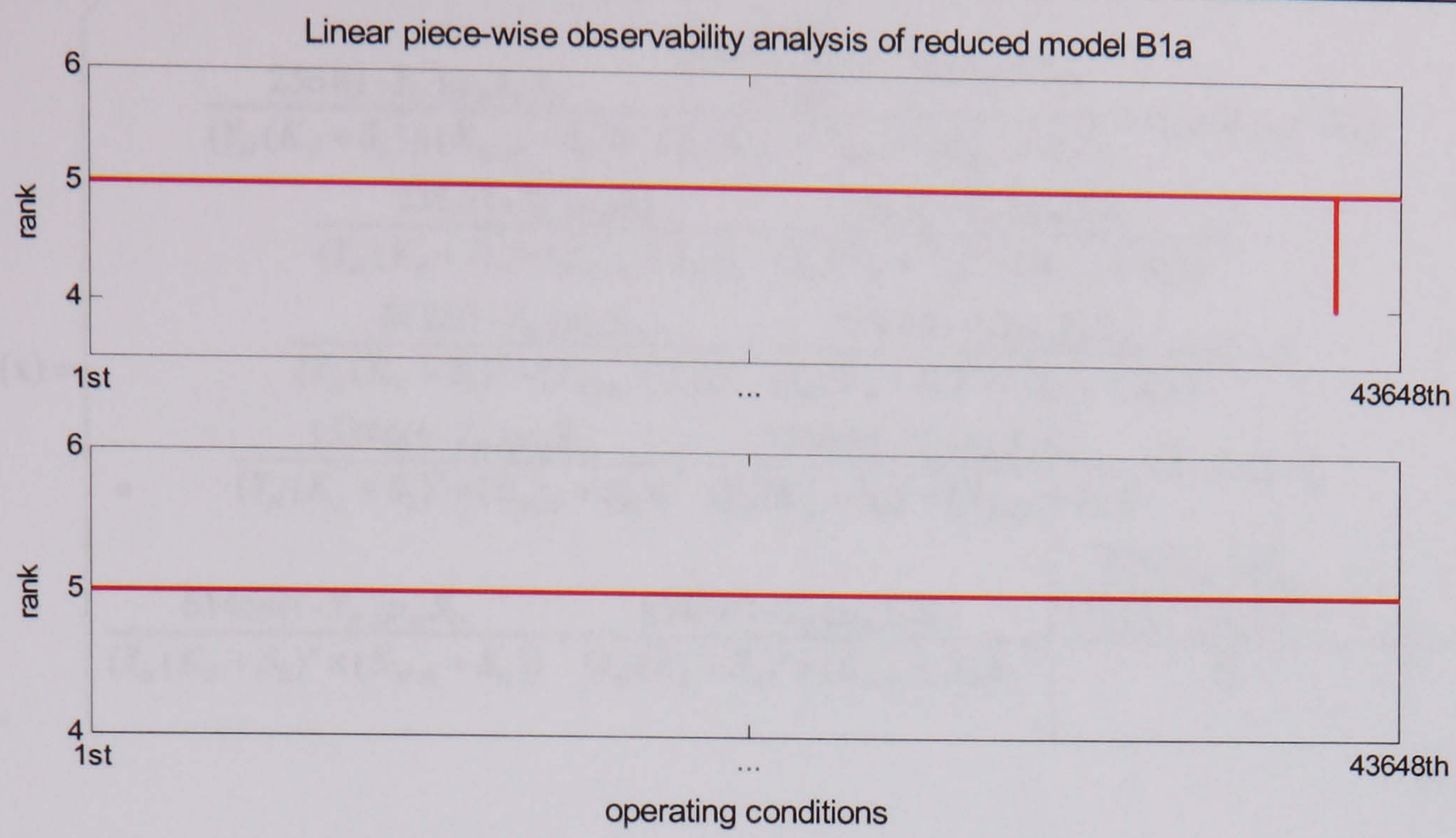


**Figure 4.16** Linear piece-wise observability analysis applied on the 'Model Ba'. (top plot) $S_O$ measurement is considered. (bottom plot) $S_O$ and $S_{NO}$ measurements are considered.

By increasing the (hypothetically) available sensors number to two (e.g. $S_O$ and $S_{NO}$), the rank of the reduced model is equivalent to the order of the non-linear system ($rk = 5$). Therefore, the linear piece-wise analysis, which is applied over a fourteen days period at every sampling point (e.g. 43618 points), demonstrated that the reduced 'Model Ba' is observable in the whole domain of definition with two measurments. To confirm these results, a non-linear observability analysis is investigated.

**Model Ba: non-linear observability analysis**

The non-linear reduced 'Model Ba' is selected to perform the non-linear observability analysis. The observation space given by Equation (3.6) has been initially computed, up to $k$=5 (e.g. the order of the system). This computation involved Lie derivatives along the vector field **f** described by Equation (3.7). The implicit observability map and its invertibility are presented in Equation (4.27) and (4.28), respectively. Similarly to the reduced 'Model A', the transport terms of Equation (4.1), the entire observation space as well as its invertibility matrix ($\mathcal{Q}(\mathbf{x})$) are not represented here.

$$\mathbf{w}(\mathbf{x})=\begin{pmatrix}
\dfrac{2561(1-Y_H)\mu_H S_S S_O}{(Y_H(K_S+S_S)\times(K_{O,H}+S_O))}-\dfrac{135\times\left(\dfrac{457}{100}-Y_A\right)\mu_A S_O\times S_{NH}}{(Y_A(K_{NH}+S_{NH})\times(K_{O,A}+S_O))}+K_L a(S_{O,sat}-S_O) \\
\dfrac{2561(1-Y_H)\mu_H S_O}{(Y_H(K_S+S_S)\times(K_{O,H}+S_O))}-\dfrac{2561(1-Y_H)\mu_H S_S S_O}{(Y_H(K_S+S_S)^2\times(K_{O,H}+S_O))}\times\cdots \\
\dfrac{5122(1-Y_H)\mu_H S_O}{(Y_H(K_S+S_S)^2\times(K_{O,H}+S_O))}+\dfrac{5122(1-Y_H)\mu_H S_S S_O}{(Y_H(K_S+S_S)^3\times(K_{O,H}+S_O))}\times\{\cdots\} \\
\dfrac{15366(1-Y_H)\mu_H S_O}{(Y_H(K_S+S_S)^3\times(K_{O,H}+S_O))}+\dfrac{15366(1-Y_H)\mu_H S_S S_O}{(Y_H(K_S+S_S)^4\times(K_{O,H}+S_O))}\times\{\cdots\}\times\{\cdots\}\cdots \\
\dfrac{61464(1-Y_H)\mu_H S_O}{(Y_H(K_S+S_S)^4\times(K_{O,H}+S_O))}+\dfrac{61464(1-Y_H)\mu_H S_S S_O}{(Y_H(K_S+S_S)^5\times(K_{O,H}+S_O))}\times\left\{\dfrac{\dfrac{2561\mu_H S_S S_O}{(Y_H(K_S+S_S)\times\cdots}-\cdots}{Y_H}\right\}\times\cdots
\end{pmatrix}, \tag{4.27}$$

The local invertibility of the observability map ($\mathcal{Q}(\mathbf{x})$), is employed to investigate the rank of the non-linear model at the selected operating conditions displayed in Table (4.12). Simulation results are presented Figure (4.17) where it can be observed that a single measurement ($S_O$) is sufficient to achieve the local observability properties around the neighbourhood of the operating conditions. Indeed, the rank of the system is equal to five, the order of the model, at the selected operating conditions.

$$\mathcal{Q}(\mathbf{x}) = \begin{bmatrix} \begin{bmatrix} \frac{5122(1-\cdots}{(Y_H(K_S+S\cdots} + \cdots & 0 & \frac{2561(1-Y_H)\cdots}{Y_H\times\cdots} - \cdots & 0 & 0 \\ 0 & 0 & 0 & 0 & 0 \\ \frac{2561(1-Y_H)\cdots}{(Y_H(K_S+\cdots} - \cdots & 0 & -\frac{5122\times\cdots}{(Y_H(K_S+\cdots} + \cdots & 0 & -\frac{135\times\left(\frac{457}{100}-\cdots\right)\cdots}{(Y_A(K_{NH}+\cdots} \\ 0 & 0 & 0 & 0 & 0 \\ 0 & 0 & & 0 & \end{bmatrix} & \begin{bmatrix} 0 & \cdots & 0 \\ & 0 & \\ \vdots & \ddots & \vdots \\ & 0 & \\ 0 & \vdots & 0 \end{bmatrix} \\ \begin{bmatrix} -\frac{5122(1-\cdots}{(Y_H(K_S+S\cdots} & \frac{2561(1-Y_H)\cdots}{(Y_H(K_S+\cdots} - \cdots & \cdots & \cdots & -\frac{135\times\left(\frac{457}{100}-\cdots\right)\cdots}{(Y_A(K_{NH}+\cdots} \\ \vdots & \vdots & \vdots & \vdots & \vdots \\ \vdots & \vdots & \vdots & \vdots & \vdots \end{bmatrix} & \begin{bmatrix} \\ \\ \vdots \\ \\ \end{bmatrix} \\ \begin{bmatrix} \\ \\ \vdots \\ \\ \end{bmatrix} & \begin{bmatrix} \\ \\ \vdots \\ \\ \end{bmatrix} \end{bmatrix} \tag{4.28}$$

Furthermore, the 9th operating condition, displayed in Table (4.12), which created a loss of observability concerning the linear model described by the system matrix in Equation (4.26), has been successfully computed with the non-linear observability theory. These results imply that the proposed reduced-order 'Model Ba' is locally observable with a single measurement

and that there is no requirement in increasing the number of available sensors to two, as demonstrated by the linear piece-wise approach. However, the same conclusion as that discussed for 'Model A' should be applied regarding the application of the rank test at all possible times rather than for a few operating conditions.

| OC / In. Out. | 1 | 2 | 3 | … | … | 8 | 9 | 10 |
|---|---|---|---|---|---|---|---|---|
| $Q_{in=ef}$ | 95237 | 90180 | 86886 | … | … | 93287 | **85621** | 99111 |
| $S_{S,in}$ | 1.48 | 1.43 | 1.03 | … | … | 1.97 | **0.846** | 2.21 |
| $S_S$ | 1.12 | 1.16 | 0.9 | | | 1.5 | **0.75** | 1.43 |
| $X_{S,in}$ | 75.24 | 76.2 | 56.12 | … | … | 102.5 | **46.27** | 97.32 |
| $X_S$ | 63.27 | 65.52 | 49.91 | | | 87.89 | **41.22** | 81.34 |
| $S_{O,in}$ | $1e^{-4}$ | $1e^{-4}$ | $2e^{-4}$ | … | … | $4e^{-5}$ | **$8.49e^{-4}$** | $3e^{-5}$ |
| $S_O$ | 1.96 | 1.93 | 2.69 | | | 1.55 | **3.58** | 1.56 |
| $S_{NO,in}$ | 4.32 | 4.16 | 6.62 | … | … | 0.97 | **7.97** | 0.73 |
| $S_{NO}$ | 6.94 | 6.77 | 8.76 | | | 3.51 | **9.66** | 3.35 |
| $S_{NH,in}$ | 9 | 9.49 | 5.02 | … | … | 11.79 | **3.47** | 13.35 |
| $S_{NH}$ | 5.19 | 5.35 | 1.91 | | | 7.46 | **0.81** | 8.83 |

**Table 4.12** Operating conditions (OC), which represent selected operating points from the x-axis of Figure (4.17), used to test the non-linear weak observability of the reduced-order 'Model Ba' during dry weather conditions. The y-axis (Q: $m^3/d$ unit; from $S_S$ to $S_O$: g COD $m^{-3}$ units; and $S_{NO}$ g N $m^{-3}$ units) represents the inputs (In.) and outputs (Out.) of the reduced 'Model Ba'.

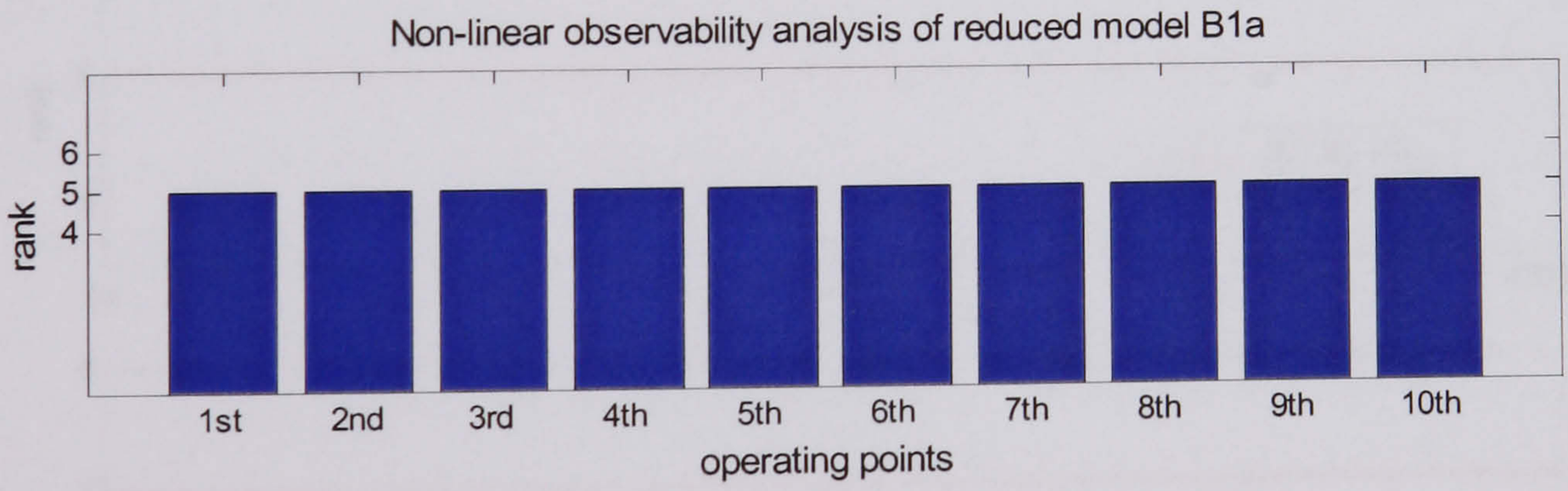


**Figure 4.17** Non-linear observability analyses based on the Lie derivative, achieved with a single measurement ($S_O$).

**Model Bb**

The reduced 'Model Bb' under study, which is described by Equations (4.1) to (4.4) and (4.6) to (4.8), is also assumed stable. The linear piece-wise observability approach has been successfully investigated. Simulation results are displayed in Figure (4.18).

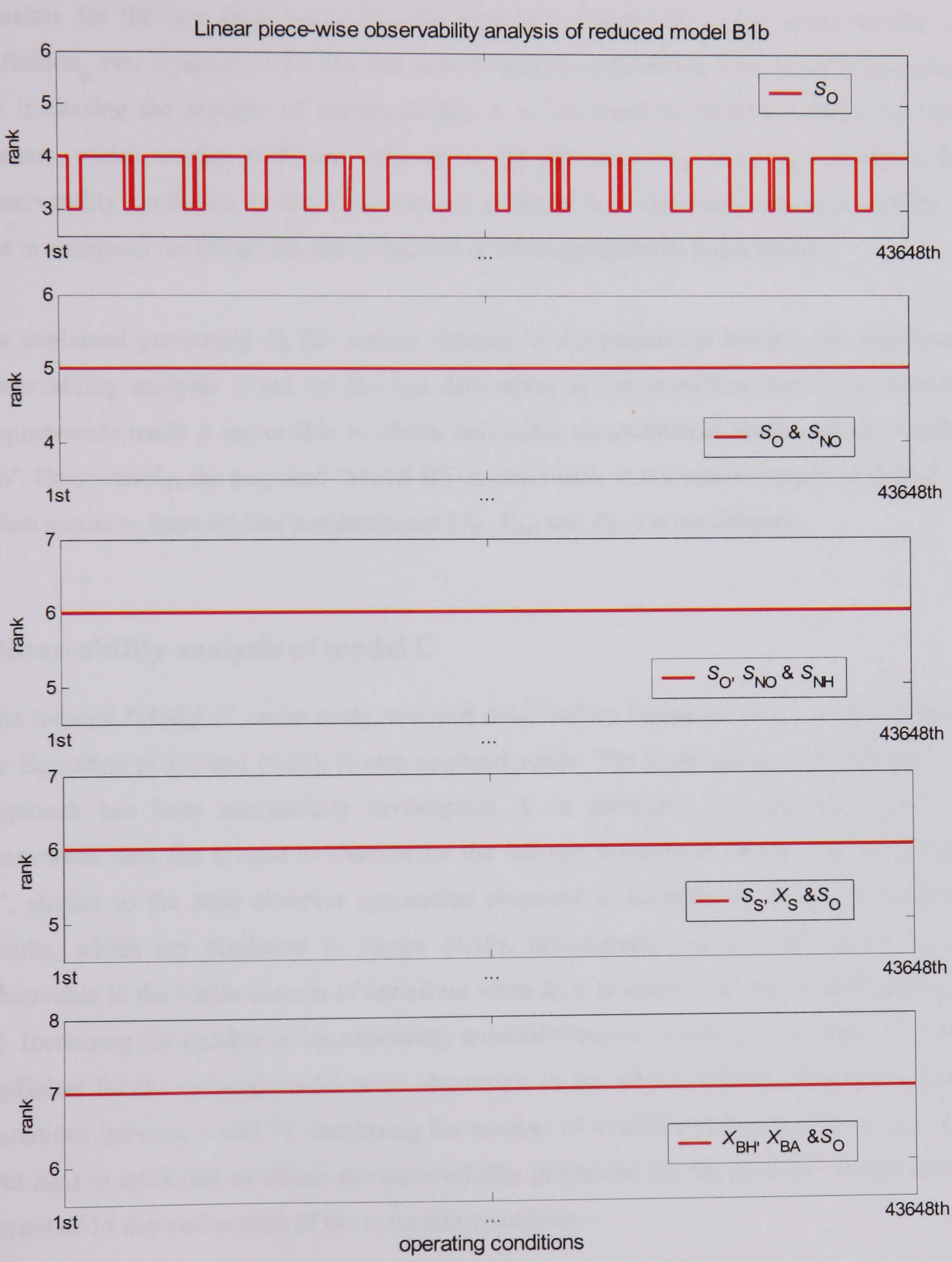


**Figure 4.18** Linear piece-wise observability theory analysis applied on the reduced 'Model Bb'.

This graph demonstrates that 'Model Bb' is not observable in the whole domain of definition when the DO sensor is exclusively assumed available. Increasing the number of hypothetical available measurements to two ($S_O$ and $S_{NO}$) or even three ($S_O$, $S_{NO}$ and $S_{NH}$) is still not sufficient in obtaining the local observability properties for the reduced model. However, when $S_O$, $X_{B,H}$ and $X_{B,A}$ measurements are assumed available on-line (which is not physically possible for the two latter variables), the system is observable in the entire domain of definition, over a period of 14 day and at each operating condition. This result implies that by increasing the number of measurements, it is important to carefully select the right sensors, which contain sufficient information (in this case $X_{B,H}$ and $X_{B,A}$) to obtain the observability conditions in the whole domain of definition. The non-linear observability is not investigated for Model Bb and C because of the computational requirements.

As explained previously in the section relating to computational burden, the non-linear observability analysis based on the Lie derivatives is not presented here. The memory requirements made it impossible to obtain successful computational results for the 'Model Bb'. Conclusively, the proposed 'Model Bb' is observable in the whole domain of definition when access to three on-line measurements ($S_O$, $X_{B,H}$ and $X_{B,A}$) is considered.

## Observability analysis of model C

The reduced 'Model C' under study, which is described by Equations (4.17) to (4.21) added by Equations (4.22) and (4.23), is also assumed stable. The linear piece-wise observability approach has been successfully investigated. It is reminded that the storm influent wastewater data file is used to characterise the influent wastewater for the reduced 'Model C', similar to the state observer application proposed in Chapters V and VI. Simulation results, which are displayed in Figure (4.19), demonstrate that the 'Model C' is not observable in the whole domain of definition when $S_O$ is uniquely assumed available (rank = 4). Increasing the number of hypothetically available sensors to two (e.g. $S_O$ and $S_{NO}$) is not sufficient for the reduced model to be observable in the whole domain of definition (rank variations between 6 and 7). Increasing the number of available measurements to ($S_O$, $S_{NO}$ and $S_{NH}$) is sufficient to obtain the observability properties for the reduced model, over a period of 14 day and at each of the operating conditions.

Similar to the previous case (e.g. reduced 'Model Bb'), the non-linear observability analysis based on the Lie derivatives is not performed here. The memory requirements made it

impossible to obtain successful computational results for the reduced 'Model C'. Consequently, the proposed reduced-order 'Model C' is observable in the whole domain of definition when access to three on-line measurements ($S_O$, $S_{NO}$ and $S_{NH}$) is considered.

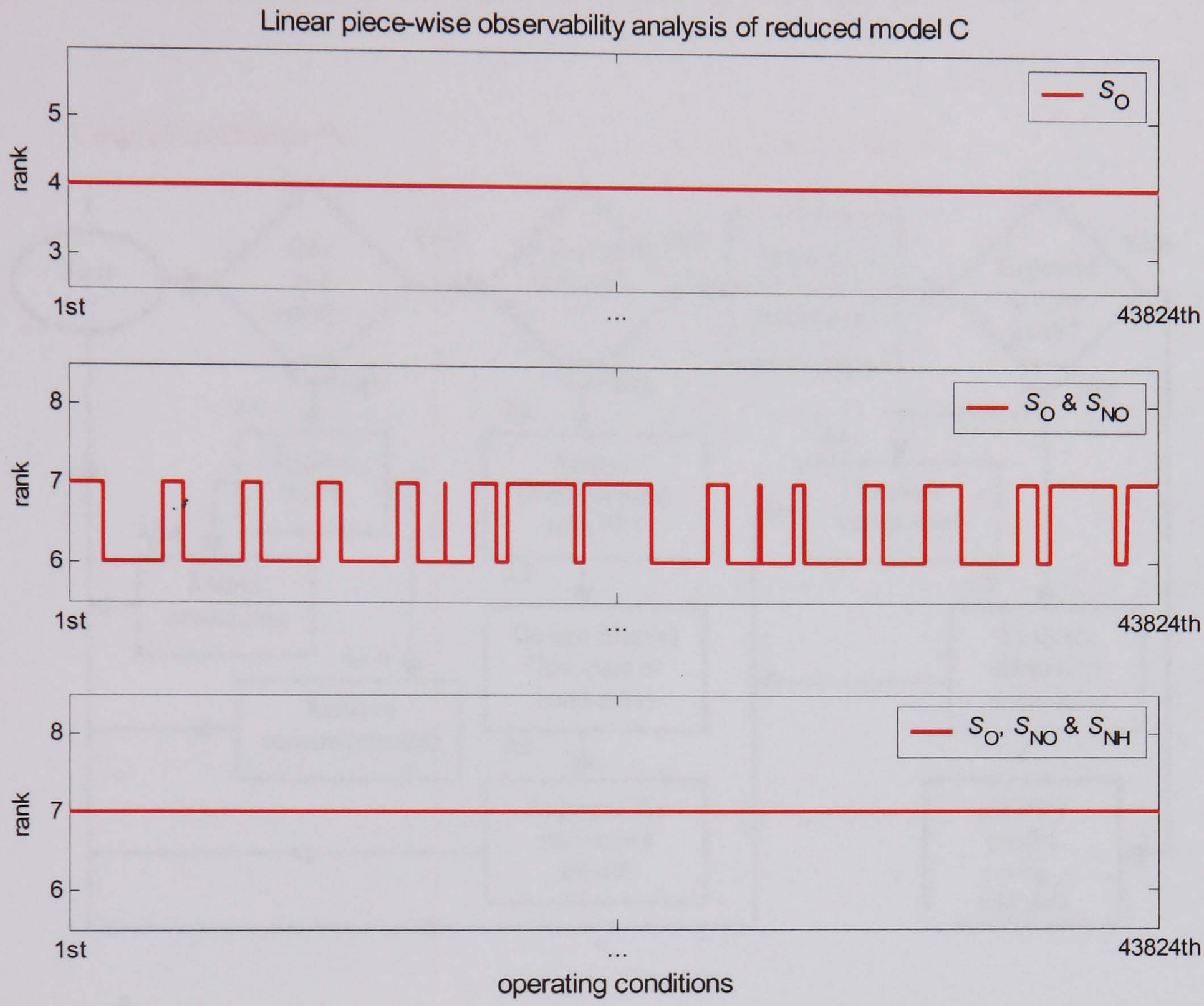


**Figure 4.19** Linear piece-wise observability theory analysis applied on the reduced 'Model C'. (bottom plot) $S_O$, $S_{NO}$ and $S_{NH}$ measurements are considered to achieve linear piece-wise observability in the whole domain of definition.

## 4.3 GENERAL PROCEDURE FOR OBSERVERS DESIGN

This section aims at providing a general procedure for model reduction and software sensor design for WWTPs. However, discussion and results based on software sensor implementation are further demonstrated through simulation studies in the next Chapter.

## Design procedure

The flow chart diagram presented in Figure (4.20) illustrates the general procedure for model reduction and software sensor design of activated sludge processes. With reference to the numbers given in the blocks of this figure, the procedure is detailed as follows:

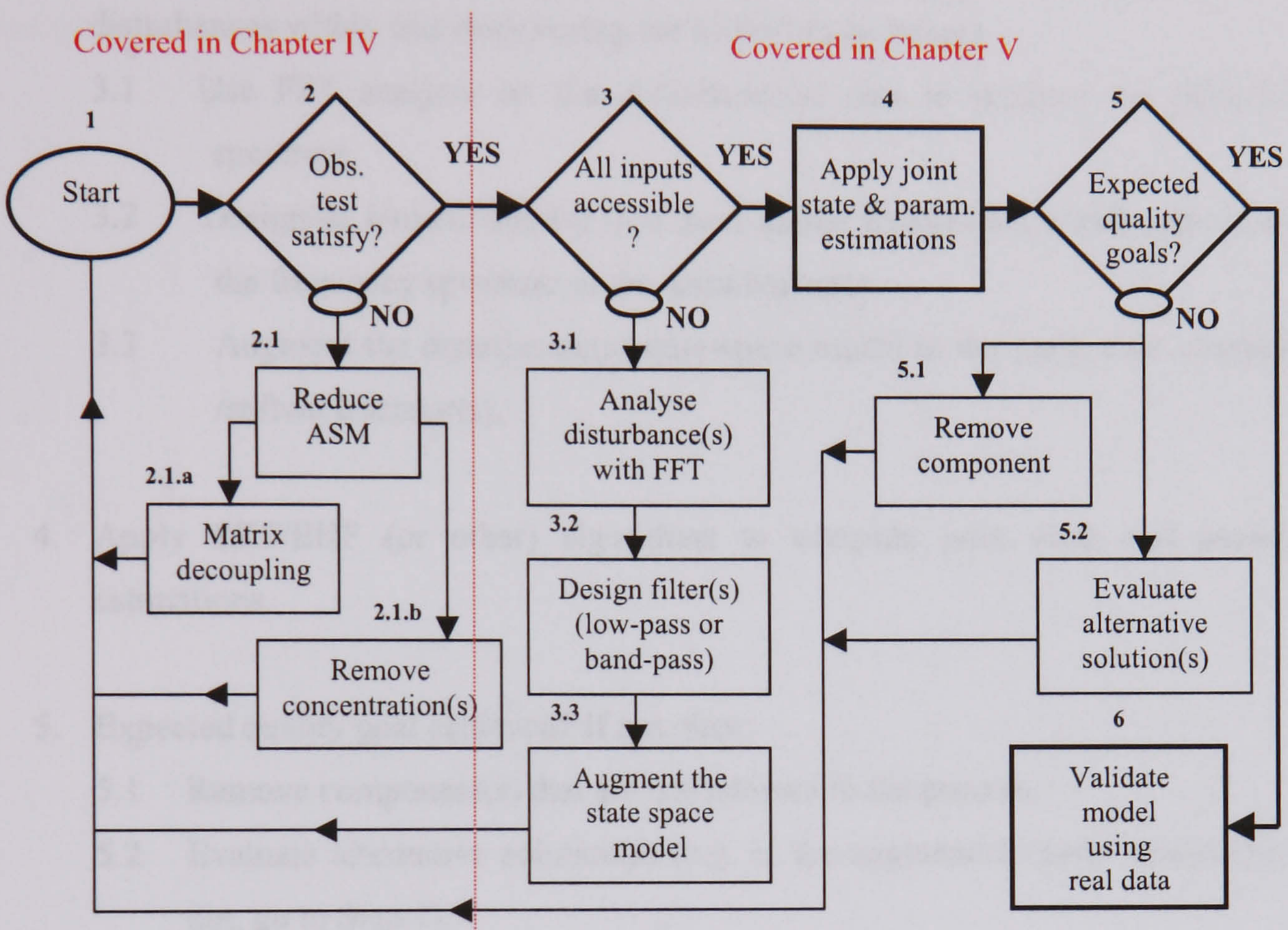


**Figure 4.20** General procedure for model reduction and to design software sensor(s) based on an EKF and/or EHF. The left section is covered in Chapter IV while the right section of the procedure is covered in Chapter V.

1. Select an appropriate ASM model (initialise and calibrate it) and evaluate the effluent quality goal to be achieved.

2. Is the model globally observable (all initial conditions must be determined uniquely from the output(s) and input(s) in the whole domain of definition)? Or
   Is the model locally weakly observable (full rank in the whole domain of definition)?
   If not, then:
   2.1 Reduce the ASM following one of the two different techniques:

2.1a Use a matrix decoupling technique, which allows the user to identify which component(s) is/are not affecting the model.

2.1b Remove non-essential state variable(s) that is/are not relevant within the specific process (based on experience).

3. Are all plant inputs accessible? If not, model the unknown input(s) (also called disturbances within this work) using the following technique:

   3.1 Use FFT analysis on the disturbance(s) data to produce the disturbance spectrum.

   3.2 Design/fit a/some filter(s) (low pass and/or band-pass), which approximates the frequency spectrum of the disturbance(s).

   3.3 Augment the disturbance(s) state-space model to the main state observer(s) /software sensor(s).

4. Apply EKF/EHF (or other) algorithms to compute joint state and parameter estimations.

5. Expected quality goal achieved? If not, then:

   5.1 Remove component(s) that are not relevant to the process.

   5.2 Evaluate alternative solution(s) (e.g. is the augmented model observable? If not, go to Step 1).

6. Validate the model using real data.

In step 1, it is required that the model be initialised and calibrated. This work is not presented here but has been performed for the benchmark plant to ensure consistent comparison of process behaviour and when applicable, consistent comparison of control strategies. It is important to duplicate the steady states and dynamics (and obtain the same results) given within the benchmark manual to make sure that the simulator is tuned in an appropriate way, as proposed by Copp, (2002).

In step 2, a procedure to reduce the model is described. The model reduction technique that has been employed previously is based on step 2.1b. The method described by step 2.1a consists of decoupling a linear model through investigation of the coupling system matrix (denoted **A**), which for instance is of the form of Equation (4.29). The zero coefficients are

denoted by $X$ in Equation (4.29) and the vector **x** represents the thirteen state variables of the original ASM1. Even if this model is highly non-linear, it is possible to obtain a linear model at a random operating point. The decoupling technique consists of studying the coefficient of the system matrix. Since each coefficient represents the level of correlation between the different states, this gives a qualified indication of which states can be left out of the system description. For instance, the system matrix **A** clearly illustrates that $S_I$, $X_I$ and $S_{ALK}$ are decoupled from the rest of the system, as their coupling coefficients are zeros.

$$\mathbf{Ax} = \begin{bmatrix} a_{11} & X & X & X & X & X & X & X & X & X & X & X & X \\ X & a_{22} & X & a_{24} & a_{25} & a_{26} & X & a_{28} & a_{29} & a_{210} & a_{211} & a_{212} & X \\ X & X & a_{33} & X & X & X & X & X & X & X & X & X & X \\ X & a_{42} & X & a_{44} & a_{45} & a_{46} & X & a_{48} & a_{49} & a_{410} & a_{411} & a_{412} & X \\ X & a_{52} & X & a_{54} & a_{55} & 0 & X & a_{58} & a_{59} & a_{510} & a_{511} & a_{512} & X \\ X & a_{62} & X & a_{64} & a_{65} & a_{66} & X & a_{68} & a_{69} & a_{610} & a_{611} & a_{612} & X \\ X & X & X & X & a_{75} & a_{76} & a_{77} & X & X & X & X & X & X \\ X & a_{82} & X & a_{84} & a_{85} & a_{86} & X & a_{88} & a_{89} & a_{810} & a_{811} & a_{812} & X \\ X & a_{92} & X & a_{94} & a_{95} & a_{96} & X & a_{98} & a_{99} & a_{910} & a_{911} & a_{912} & X \\ X & a_{102} & X & a_{104} & a_{105} & a_{106} & X & a_{108} & a_{109} & a_{1010} & a_{1011} & a_{1012} & X \\ X & a_{112} & X & a_{114} & a_{115} & a_{116} & X & a_{118} & a_{119} & a_{1110} & a_{1111} & a_{1112} & X \\ X & a_{122} & X & a_{124} & a_{125} & a_{126} & X & a_{128} & a_{129} & a_{1210} & a_{1211} & a_{1212} & X \\ X & a_{132} & X & a_{134} & a_{135} & a_{136} & X & a_{138} & a_{139} & a_{1310} & a_{1311} & a_{1312} & a_{1313} \end{bmatrix} * \begin{bmatrix} S_I \\ S_S \\ X_I \\ X_S \\ X_{B,H} \\ X_{B,A} \\ X_P \\ S_O \\ S_{NO} \\ S_{NH} \\ S_{ND} \\ X_{ND} \\ S_{ALK} \end{bmatrix} \quad (4.29)$$

This technique can also provide information as to which states have the strongest influence upon the model (e.g. $S_S$, $X_S$) by investigating the values of the coefficients. However, this method can only give a rough idea of the relationship between the state variables. Furthermore, the best technique of model reduction still remains the personal experience of the researcher/engineer.

The remainder of the procedure (e.g. step 3 to 6), which is based on solutions for modelling unknown inputs based on Fast Fourier Transform (FFT) and software sensor design for joint state and parameter estimation, is detailed in next Chapter.

## 4.4 CONCLUSIONS

The proposed reduced-order models (e.g. 'Model A', 'Model Ba', 'Model Bb' and 'Model C'), which are considered sufficiently accurate for the monitoring applications proposed in

Chapters V and VI, have been compared with the original ASM1 model. The linear piece-wise and non-linear observability theories applied to the reduced 'Model A' demonstrated similar successful results. Therefore, a state observer can be designed with this specific reduced model assuming access only to the dissolved oxygen measurement.

The reduced 'Model Ba' is observable with (1) two measurements (e.g. $S_O$ and $S_{NO}$) when applying the linear piece-wise approach, and (2) a single measurement (e.g. $S_O$) when applying the non-linear observability theory. These results implied the existence of a linear reduced model, which is not valid, when applying the rank condition in the whole domain of definition. However, from the non-linear observability approach, the non-linear reduced 'Model Ba' is observable at the selected operating conditions. Consequently, the use of two measurements should be considered as a safe solution in this case, when designing software sensors, which are often based on linearised models (e.g. the extended Kalman filter). The observability of the reduced 'Model Bb' and 'Model C' is achieved with three measurements, which are $X_{B,H}$, $X_{B,A}$, $S_O$ and $S_O$, $S_{NO}$, $S_{NH}$, respectively, based on the linear piece-wise approach. Note that even if $X_{B,H}$ and $X_{B,A}$ measurements are not physically available, a state observer is proposed in Chapter V to overcome this drawback.

The non-linear approach is not investigated for the two latter reduced models because of the computational burden involved. The Lie derivative technique is probably most reliable when applied to non-linear systems, but however, the memory and time requirements in performing such analysis are significant for models of order greater than fifth order. It can be concluded that for highly complex non-linear systems, the linear piece-wise approach remains probably the best solution to ensure the local observability of the reduced models on the whole domain of definition. A general procedure for model reduction and software sensor design is proposed to end this Chapter and is further investigated in Chapter V.

# Chapter V

# Non-linear filtering based-extended Kalman filters

In this Chapter, three software sensor applications, based on the extended Kalman filter, are demonstrated to overcome the lack of instrumentation in WWTPs. Initially, the design of an augmented state observer is proposed, in estimating the concentrations based on the reduced 'Model C'. The disturbances are modelled using fast Fourier transform and spectral analysis. Subsequently, a state observer is designed to detect abnormal substrate concentrations in WWTPs, due for instance to substrate shock load. Finally, the last sensor is designed for monitoring the sludge activity in WWTPs. Two case studies are proposed to (1) realistically estimate on-line the heterotrophic biomass and autotrophic biomass concentrations, and (2) estimate on-line the heterotrophic yield, based on a joint state and parameter estimator. Simulation results are presented to demonstrate the performance of the proposed software sensors. Parts of the material in this Chapter are covered in Benazzi *et al.*, (2005a, 2005b. 2005c, 2005d, 2005e).

## 5.1) MODELLING THE DISTURBANCES THROUGH AN AUGMENTED OBSERVER

This application, which is based on the reduced-order 'Model C' presented in Chapter IV, Section (4.1), is first introduced in further expansion of Step 3 to 6 of the general procedure presented in Chapter IV. The augmented state observer that follows present the advantage of

modelling the disturbances (also called unknown inputs) in the frequency domain, using fast Fourier transform (FFT) and spectral analysis. The term 'augmented' is employed because the original reduced 'Model C' is supplemented by extra states variables, which recreates the unknown concentrations. On-line monitoring of activated sludge processes is proposed during wet-weather conditions (storm events), which correspond to the 'worst' scenario available with the benchmark plant.

It is not always possible, and often difficult, to design an estimation algorithm that converges quickly and accurately towards the true values of the process variables. The convergence rate depends on the available knowledge about the process, the data quality and the sampling frequency from the available sensors (or measurements). Mathematical models are key tools in defining the performance of software sensors, because they describe the implicit knowledge, quality and validity of the process (Chéruy, 1996). However, even in the presence of reliable and accurate mathematical models, other complications may arise. For instance, all inputs of the models are not often physically available. In other words, the historic data of the influent substrate (and others) is not physically accessible in practice. In this case, it is possible to model theses disturbances using spectral analysis, as briefly discussed in Step 3 of the general procedure presented in Chapter IV.

## Augmented observer based EKF for state estimation

The unknown inputs are analysed using FFT and spectral analysis techniques prior to the state observer implementation. This method is based on designing filter(s), which cover the frequency spectrum of the disturbances. A typical data for the analysis is shown in Figure (5.1a). Firstly, $S_{ND}$ concentration profiles are obtained in the time domain by simulating the benchmark plant for a period of seven days, as displayed in Figure (5.1a). Note that only a period of one day is required to capture the diurnal influent wastewater data dynamics. Secondly, on the resulting influent data (into the first aerobic reactor), FFT is used to convert the set of uniform space points from the time domain to the frequency domain in order to obtain the spectral content of the signal, and to design the appropriate filter. It consists of designing a first-order transfer function and properly tuned it, to cover the energy of $S_{ND}$ concentration. The first order transfer function is of the form

$$HS_{ND}(s) = \frac{K_{SND}}{\tau_{SND}s + 1}\zeta_{SND}, \text{ with } \tau_{SND} = \frac{1}{\omega_{c,SND}} \tag{5.1}$$

By substituting $\tau_{SND}$ in Equation (5.1), the first order transfer function is of the form

$$HS_{ND}(s) = K_{SND}\frac{\omega_{c,SND}}{s+\omega_{c,SND}}\zeta_{SND} \tag{5.2}$$

where $K_{SND}$ is the gain ($K_{SND} = 100$), $\tau_{SND}$ the time constant ($\tau_{SND} \approx 3.92$), $\omega_{c,SND}$ the cut-off frequency ($\omega_{c,SND} = 0.255$) and $\zeta_{SND}$ the input, which is a white Gaussian noise sequence with a variance ($\sigma_{SND}$) equal to 0.01. Then, the transfer function given in Equation (5.2) is converted to the state space form, which is given by

$$\begin{aligned} \dot{XS}_{ND}(t) &= \left[-\omega_{c,SND}\right] XS_{ND}(t) + \zeta_{SND}(t) \\ \underset{\sim}{y}_{SND}(t) &= \left[K_{SND}\omega_{c,SND}\right] XS_{ND}(t) \end{aligned} \tag{5.3}$$

where the system coefficient of the state space model given by Equation (5.3) are used as augmented state of the 'Model C'. The output coefficient of Equation (5.3) is utilised only to tune the 1st order transfer function, which cover the energy $S_{NH}$ concentration, as displayed in Figure (5.1b). Note that the cut-off frequency is obtained by trial and error. The frequency response in the semilog Cartesian coordinate system of the transfer function given by Equation (5.3) is displayed in Figure (5.2).

For the following application results, the above-described technique is also utilised for the $S_S$ concentration. The first order state space transfer function is of the form

$$\begin{aligned} \dot{XS}_S(t) &= \left[-\omega_{c,SS}\right] XS_S(t) + \zeta_{SS}(t) \\ \underset{\sim}{y}_{SS}(t) &= \left[K_{SS}\omega_{c,SS}\right] XS_S(t) \end{aligned} \tag{5.4}$$

with $K_{SS} = 100$, $\tau_{SS} \approx 3.84$, $\omega_{c,SS} = 0.260$ and $\zeta_{SS}$ is a white Gaussian noise sequence with a variance ($\sigma_{SS}$) equal to 0.01. The profile of $S_S$ concentration, the 1st order transfer function and the frequency response in the semilog Cartesian coordinate system are not represented here, as they are similar to Figure (5.1a), (5.1b) and (5.2), respectively.

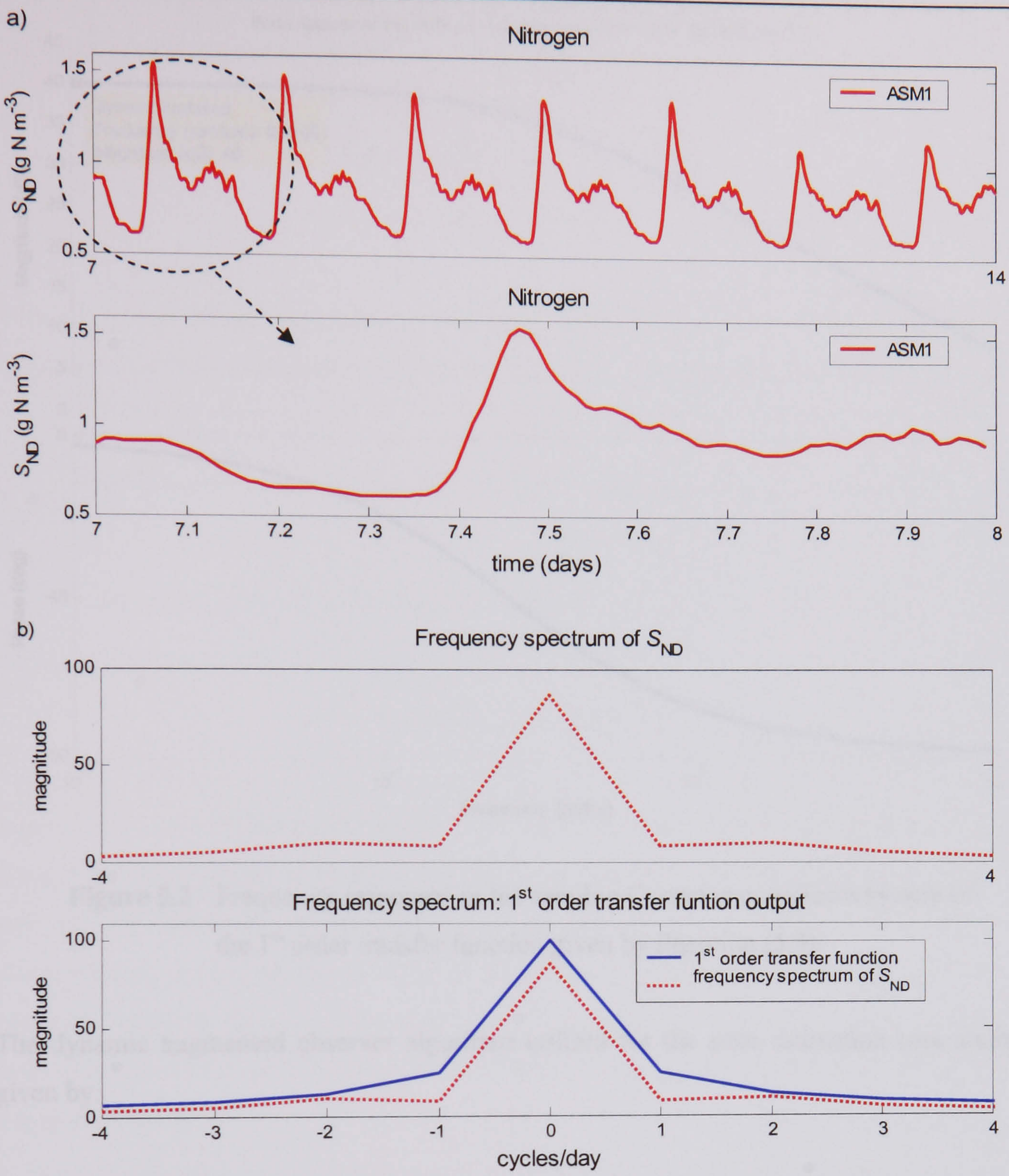


**Figure 5.1** (5.1a) $S_{ND}$ concentration resulting from simulations with the ASM1 model. (5.1b) Disturbances filter design using FFT technique. FFT of $S_{ND}$ concentration (dotted line).

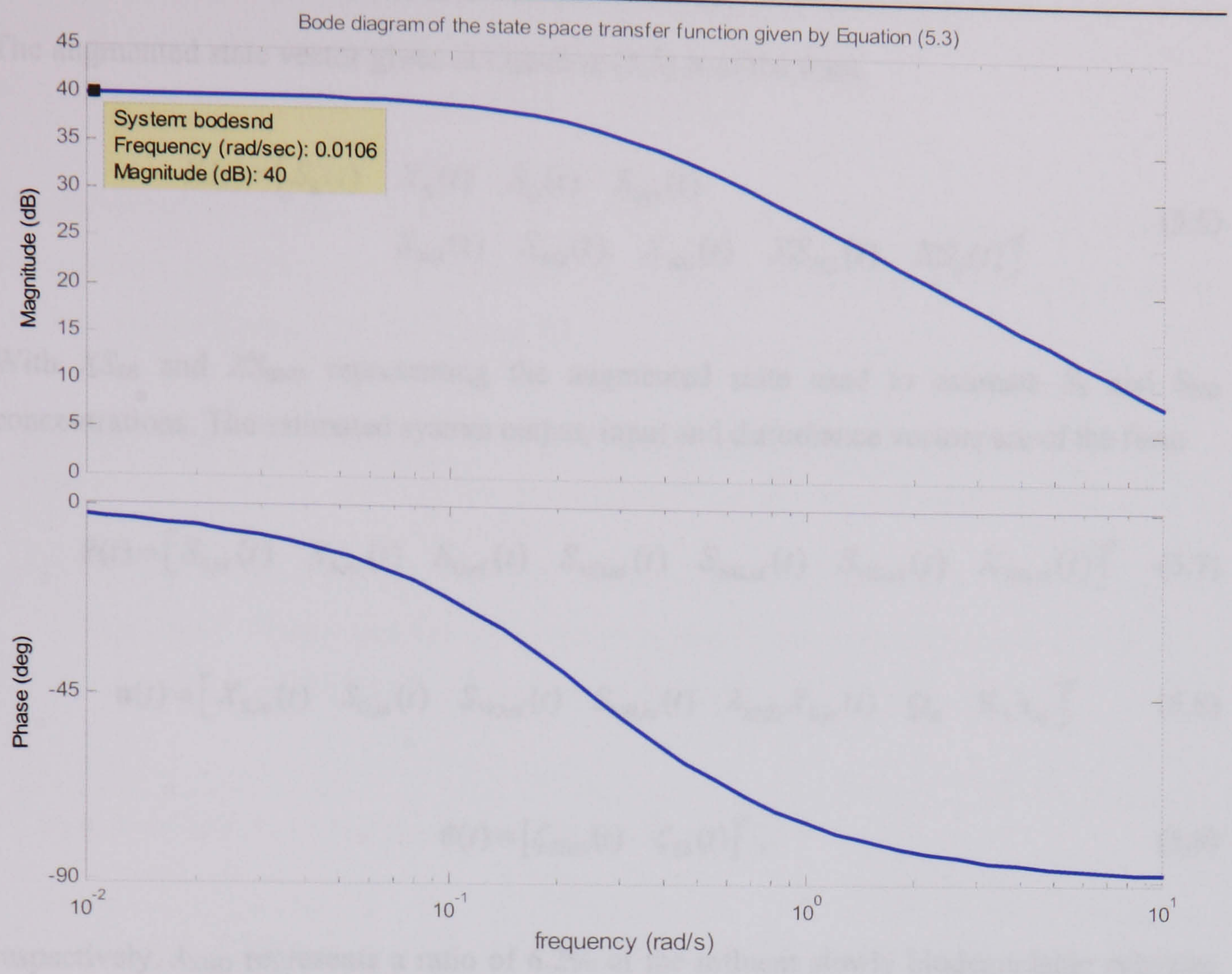


**Figure 5.2** Frequency responses in the semilog Cartesian coordinate system of the 1st order transfer function given by Equation (5.3).

The dynamic augmented observer algorithm utilised for the state estimation case study is given by:

$$\begin{aligned}\dot{\tilde{\mathbf{X}}}(t) &= \tilde{\mathbf{f}}(\mathbf{x}(t),\mathbf{u}(t)) + \tilde{\mathbf{A}}(t)\tilde{\mathbf{X}}(t) + \tilde{\mathbf{B}}(t)\mathbf{u}(t) + \tilde{\mathbf{K}}(\mathbf{y}(t) - \tilde{\mathbf{z}}(t)) + \tilde{\mathbf{D}}(t)\mathbf{d}(t)\\ \mathbf{y}(t) &= \mathbf{C}(t)\mathbf{X}(t) + \mathbf{v}(t)\\ \tilde{\mathbf{z}}(t) &= \tilde{\mathbf{C}}(t)\tilde{\mathbf{X}}(t)\end{aligned} \tag{5.5}$$

where $\mathbf{v}(t)$ is the measurement noise and $\tilde{\mathbf{K}}$ is the Kalman gain deduced from the properties of the augmented state space model to minimise the variance of the estimation error. Note that the Kalman filter is a linear observer and therefore, the extended model must be linearised with respect to augmented states, as described in Chapter III. $\tilde{\mathbf{f}}(\mathbf{x}(t),\mathbf{u}(t))$ is the linearised system, which is described by the differential Equations (4.17) to (4.22). However, it is reminded that the influent concentrations $S_{S,in}$ and $S_{ND,in}$ are replaced in 'Model C' by the additional state variables $XS_S$ and $XS_{ND}$, respectively.

The augmented state vector given in Equation (5.5) is of the form

$$\tilde{\dot{\mathbf{X}}}(t) = \begin{bmatrix} S_S(t) & X_S(t) & S_O(t) & S_{NO}(t) \\ & S_{NH}(t) & S_{ND}(t) & X_{ND}(t) & XS_{ND}(t) & XS_S(t) \end{bmatrix}^T \tag{5.6}$$

With $XS_{SS}$ and $XS_{SND}$ representing the augmented state used to estimate $S_S$ and $S_{ND}$ concentrations. The estimated system output, input and disturbance vectors are of the form

$$\tilde{\mathbf{z}}(t) = \begin{bmatrix} S_{S,ef}(t) & X_{S,ef}(t) & S_{O,ef}(t) & S_{NO,ef}(t) & S_{NH,ef}(t) & S_{ND,ef}(t) & X_{ND,ef}(t) \end{bmatrix}^T \tag{5.7}$$

$$\mathbf{u}(t) = \begin{bmatrix} X_{S,in}(t) & S_{O,in}(t) & S_{NO,in}(t) & S_{NH,in}(t) & \lambda_{XND} X_{S,in}(t) & Q_{in} & K_L a_{in} \end{bmatrix}^T \tag{5.8}$$

$$\mathbf{d}(t) = \begin{bmatrix} \zeta_{SND}(t) & \zeta_{SS}(t) \end{bmatrix}^T, \tag{5.9}$$

respectively. $\lambda_{XND}$ represents a ratio of 6.2% of the influent slowly biodegradable substrate ($\lambda_{XND}$ = 0.062), utilised to estimate the particulate organic nitrogen concentration. Indeed, one of the objectives of the proposed application is to estimate non-measurable concentrations based on fractions of those measurable concentrations. $\zeta_{SND}$ and $\zeta_{SS}$ are uncorrelated white Gaussian noise sequences (e.g. $\sigma_{SND}$ = 0.01 and $\sigma_{SS}$ = 0.01), which are used to excite the inputs of their respective transfer functions. $\mathbf{D}(k)$ is the disturbance matrix, which is of the form

$$\tilde{\mathbf{D}}(t) = \begin{bmatrix} 0 & \cdots & 0 & | & 1 & 0 \\ 0 & \cdots & 0 & | & 0 & 1 \end{bmatrix}^T. \tag{5.10}$$

The system, input and output matrices, which are proposed in Equation (5.5), are defined by

$$\tilde{\mathbf{A}}(t) = \begin{bmatrix} \mathbf{A}(t) & \vdots & 0 & 0 \\ \cdots & \cdots & \cdots & \cdots \\ 0 & \vdots & -\omega_{c,SS} & 0 \\ 0 & \vdots & 0 & -\omega_{c,SND} \end{bmatrix} \quad \tilde{\mathbf{B}}(t) = \begin{bmatrix} \mathbf{B}(t) & \vdots & 0 \\ \cdots & \cdots & \cdots \\ 0 & \vdots & I \end{bmatrix} \tag{5.11}$$

$$\tilde{\mathbf{C}}(k) = \begin{bmatrix} \mathbf{C}(k) & | & 0 & 0 \end{bmatrix} \tag{5.12}$$

Note that the input matrices are not represented in the sequel because this work concentrate on monitoring application based on an open-loop model.

The characteristics of the selected model are described in Table (5.1), in terms of inputs, disturbances and selected measurements. A schematic overview of the state observer implementation is presented in Figure (5.3).

| Selected model | 'Model C' + 2 state variable ($XS_S$, $XS_{SND}$) |
|---|---|
| Inputs (8) | $X_{S,in}$, $S_{O,in}$, $S_{NO,in}$, $S_{NH,in}$, $Q_{in}$, $K_La_{in}$, $\zeta_{SS}$, $\zeta_{SND}$ |
| Disturbances (2) | $S_S$, $S_{ND}$ |
| Measurements (3) | $S_O$, $S_{NO}$, $S_{NH}$ |

**Table 5.1** Model description, which is utilised by the state observer based on the 'Model C', described in Chapter IV.

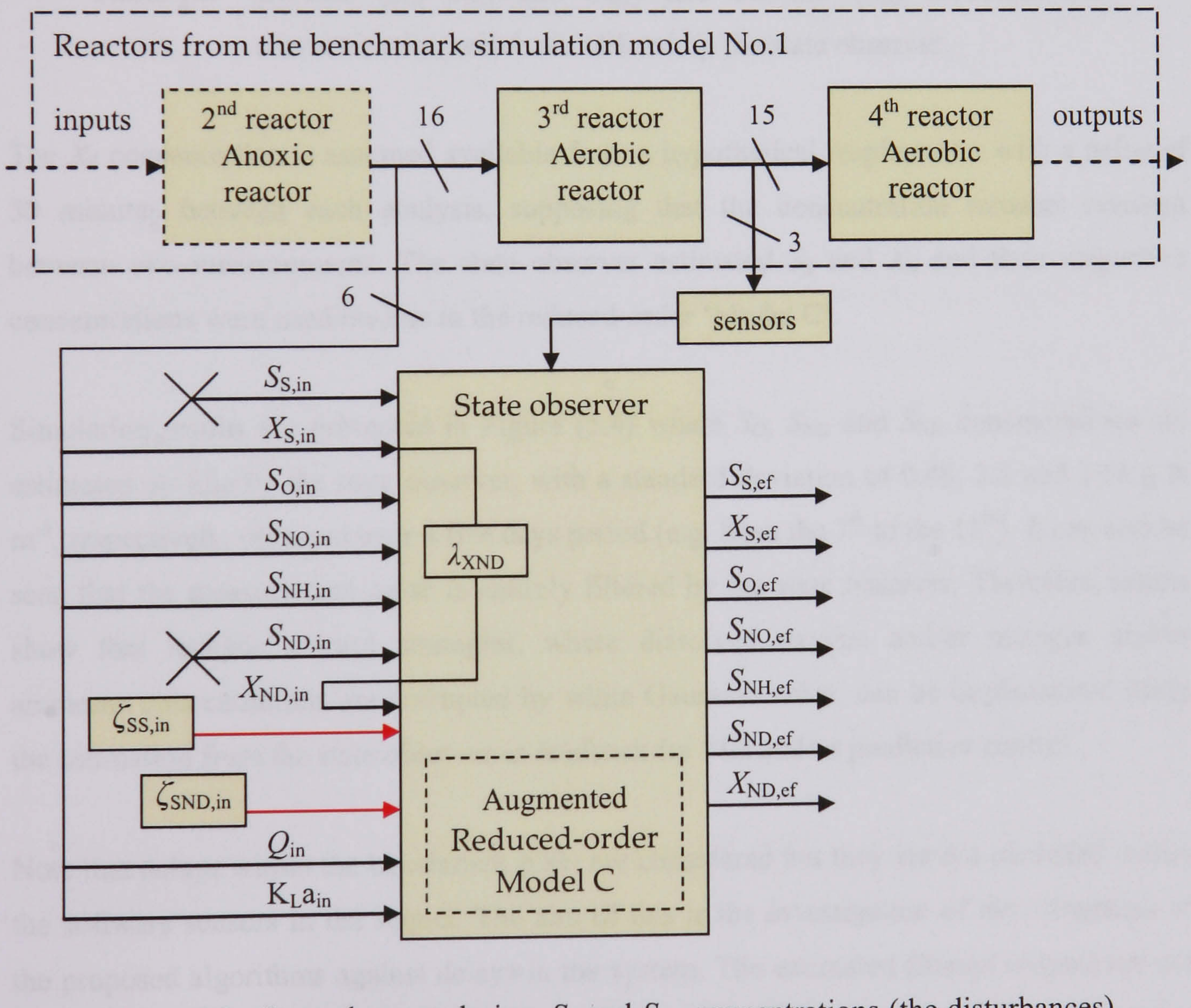


**Figure 5.3** State observer design. $S_S$ and $S_{ND}$ concentrations (the disturbances) are analysed using FFT and spectral analysis techniques prior to the state observer design.

It includes all concentrations estimated by the state observer, including state variables that are measured on-line as well as state variables that are not available (e.g. $S_S$, $S_{ND}$). This configuration has been successfully implemented within Matlab/Simulink platform, in parallel with the benchmark plant. On-line measurements are corrupted by an additive noisy signal with a variance equal to 10% of the corrupted concentrations (e.g. steady state value available in COST benchmark manual). Characteristics of the on-line measurements and off-line analysis are described in Table (5.2).

| | Variance ($\sigma$) | Delay (min.) | Low-level detec. limit | Sampling time (min.) |
|---|---|---|---|---|
| Oxygen ($S_{O,ef}$) | 0.172 | - | 0.1 | continuous |
| Nitrate and nitrite nitrogen ($S_{NO,ef}$) | 0.654 | 10 | 0.1 | 10 |
| $NH_4^+$ +$NH_3$ nitrogen ($S_{NH,ef}$) | 0.555 | 10 | 0.2 | 10 |
| Slowly bio. substrate ($X_{S,in}$) | - | 30 | 0.1 | 30 |

**Table 5.2** On-line ($S_O$, $S_{NO}$ and $S_{NH}$) and off-line ($X_S$) measurements characteristics, which are utilised by the state observer.

The $X_S$ concentration is assumed available from a hypothetical respirometer with a delay of 30 minutes between each analysis, supposing that the concentration remains constant between two measurements. The state observer estimated $S_S$ and $X_S$ and their respective concentrations were used on-line in the reduced-order 'Model C'.

Simulation results are presented in Figure (5.4) where $S_O$, $S_{NO}$ and $S_{NH}$ concentrations are estimated on-line by the state observer, with a standard deviation of 0.48, 2.2 and 3.56 g N $m^{-3}$, respectively, obtained over a five days period (e.g. from the $7^{th}$ to the $11^{th}$). It can also be seen that the measurement noise is entirely filtered by the state observer. Therefore, results show that realistic control strategies, where dissolved oxygen and/or nitrogen and/or ammonia concentrations are corrupted by white Gaussian noise, can be implemented using the estimation from the state observer as feedback for PID and/or predictive control.

Note that delays within the benchmark plant are considered but they are not modelled within the software sensors in the sequel. The aim of this is the investigation of the robustness of the proposed algorithms against delays in the system. The estimated filtered outputs are not presented in the remaining applications, as the main benefit in designing observers remains the estimation of non-measurable state variable. To do so, as mentioned earlier, particulate nitrogen estimation was obtained assuming a ratio of $X_{ND}$ to $X_S$ of 6.2%.

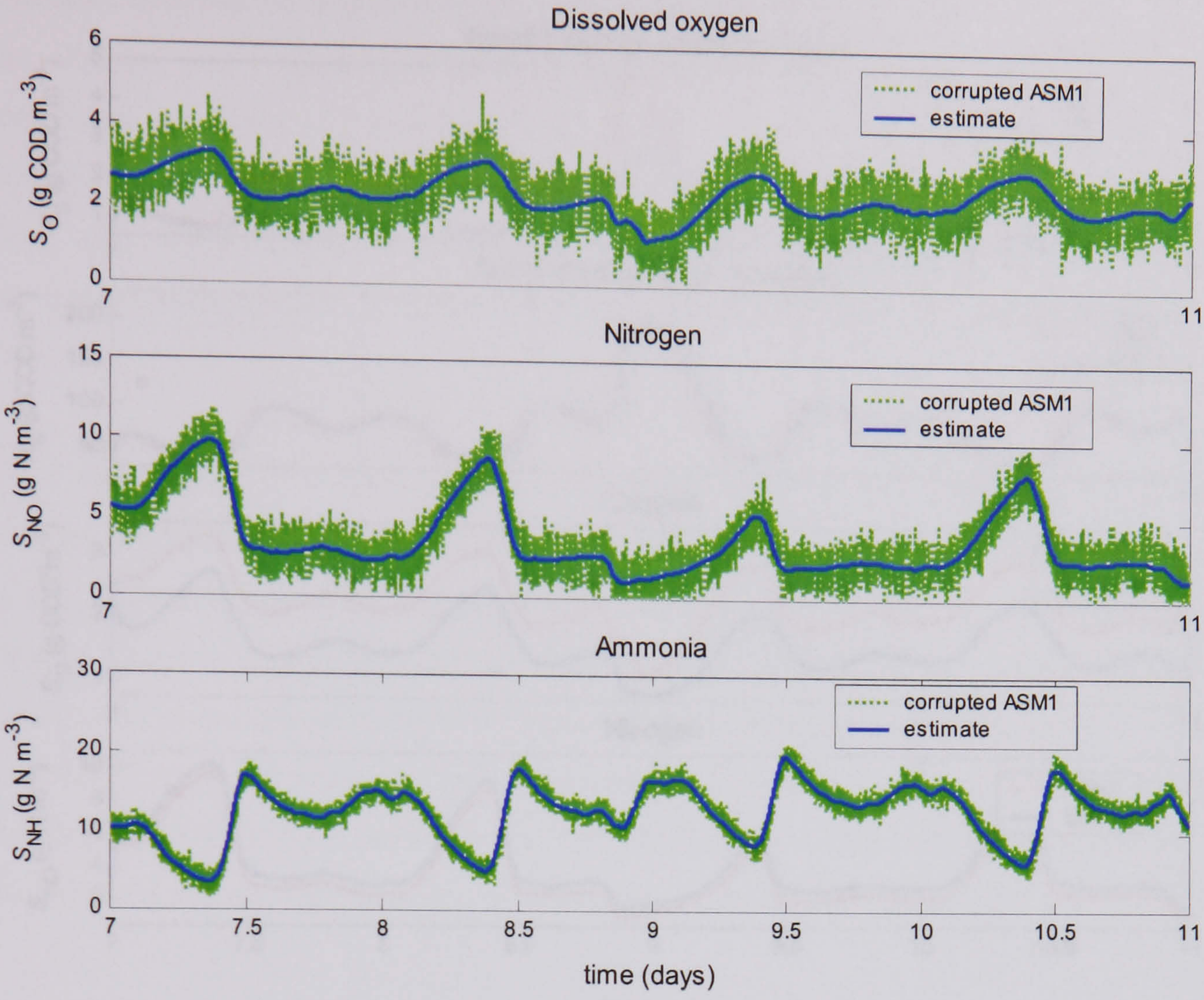


**Figure 5.4** Comparison between $S_O$, $S_{NO}$ and $S_{NH}$ concentrations resulting from simulations with the ASM1 model corrupted by white Gaussian noise and $S_O$, $S_{NO}$ and $S_{NH}$ estimated by the state observer based EKF.

Results displayed in Figure (5.5) show that all concentrations from the reduced 'Model C' are estimated considering three on-line sensors and a hypothetical respirometer. It can be observed that the proposed extended Kalman filter is sufficiently robust against delays in the system. Furthermore, in particular, $S_S$, $S_{ND}$ and $X_{ND}$ concentrations are estimated on-line by the state observer with absolute errors in term of standard deviation of 20%, 12.8% and 18.2 % from the 7$^{th}$ until the 11$^{th}$ days, and maximum bias of 54.1%, 11% and 16.9 % occurring during the high intensity event, respectively.

$S_O$ concentration is under estimated with an absolute mean error of 59.9 %, which is probably caused by the $S_S$ concentration mismatch. The state observer also successfully estimated the remaining concentrations (e.g. $X_S$, $S_{NO}$ and $S_{NH}$), similar to the response in Figure (4.13), which correspond to the reduced model outputs.

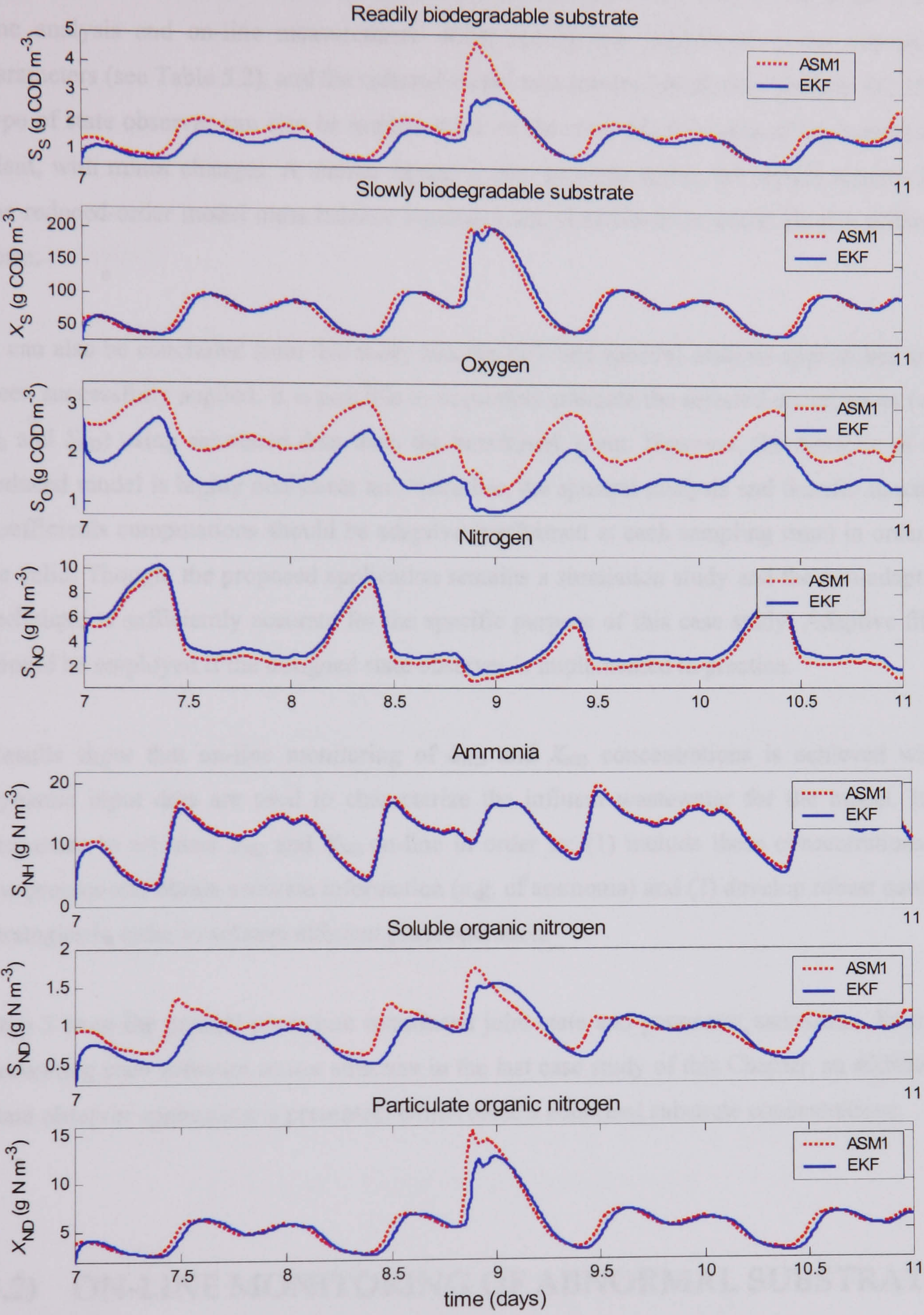


**Figure 5.5** Comparison between the concentrations resulting from simulations with the ASM1 model and the concentrations estimated by the state observer based EKF.

The delay between the true state values and the state observer estimates are attributed to off-line analysis and on-line measurements delay coefficients introduced in the simulation parameters (see Table 5.2), and the reduced model mismatches (detailed in Chapter IV). This type of state observer can also be implemented on the other aerobic tanks of the benchmark plant, with minor changes. A similar design is also possible within the anoxic reactors but the reduced-order model mass balance equations and state observer would be of a different form.

It can also be concluded from this study that the FFT and spectral analysis approaches have been successfully applied. It is possible to accurately estimate the selected disturbances (e.g. $S_S$ and $S_{ND}$) using simulated data from the benchmark plant. However, the dynamic of the reduced model is highly non-linear and therefore, the spectral analysis and transfer function coefficients computations should be adaptive (performed at each sampling time) in order to be valid. Though, the proposed application remains a simulation study and the non-adaptive technique is sufficiently accurate for the specific purpose of this case study. Adaptive filter should be employed if the designed state observer is implemented in practice.

Results show that on-line monitoring of $S_{ND}$ and $X_{ND}$ concentrations is achieved when dynamic input data are used to characterize the influent wastewater for the model. It is important to estimate $S_{ND}$ and $X_{ND}$ on-line in order to: (1) include these concentrations in the process and obtain accurate information (e.g. of ammonia) and (2) develop robust control strategies in order to achieve efficient plant operation.

Step 3 from the general procedure introduced joint state and parameter estimation. Prior to presenting such software sensor structure in the last case study of this Chapter, an additional state observer application is presented, which detects abnormal substrate concentrations.

## 5.2) ON-LINE MONITORING OF ABNORMAL SUBSTRATE CONCENTRATIONS

This application concentrates on a new approach for the on-line monitoring and detection of abnormal readily biodegradable substrate ($S_S$) and slowly biodegradable substrate ($X_S$) concentrations, for example due to the input of toxic loads from the sewer, or due to

substrate shock load. Off-line measurements of $S_S$ and $X_S$ in the activated sludge tanks are not available in a real WWTP. Therefore, the $S_S|X_S$ sensor presented in this case study is designed to detect these abnormal substrate concentrations and eventually activate an alarm with a fast response time.

## Plant layout

'Model Ba', described in Chapter IV, is selected to represent the biological process. The original benchmark plant is considered to be the real plant and the state observer is implemented on the first aerated reactor. A general overview of the state observer location is given in Figure (5.6). A detailed schematic of the $S_S|X_S$ state observer implementation is presented in Figure (5.13).

Three case studies are described in the following subsections. The first illustrates the fast and accurate convergence of the EKF algorithm, as well as the estimated concentration from the reduced 'Model Ba'. The second depicts the difficulties to estimate $X_S$ when off-line analysis is not available. The final demonstrates the $S_S|X_S$ state observer performances when no measurements of $S_S$ and $X_S$ are available.

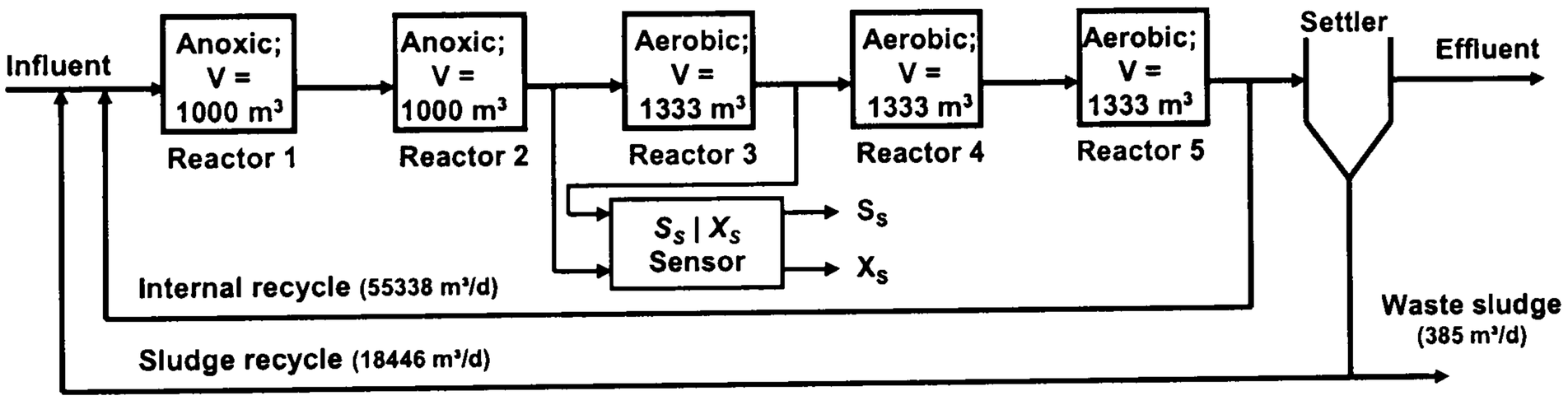


**Figure 5.6** Original benchmark plant including the $S_S|X_S$ state observer implemented in parallel of the 1st aerobic reactor.

### Case (5.2a): $S_S|X_S$ sensor when off-line analyses are available

In the first case study, simulations are performed to check the convergence of the algorithm and the performance of the state observer, which is given by:

$$\begin{aligned}\dot{\mathbf{X}}(t) &= \mathbf{A}(t)\mathbf{X}(t) + \mathbf{B}(t)\mathbf{u}(t) + \mathbf{K}(\mathbf{y}(t) - \mathbf{z}(t)) \\ \mathbf{y}(t) &= \mathbf{C}(t)\mathbf{X}(t) + \mathbf{v}(t) \\ \mathbf{z}(t) &= \mathbf{C}(t)\mathbf{X}(t)\end{aligned}, \tag{5.13}$$

with the state and input vectors of the form

$$\mathbf{X}(t) = \begin{bmatrix} S_S(t) & X_S(t) & S_O(t) & S_{NO}(t) & S_{NH}(t) \end{bmatrix}^T \tag{5.14}$$

$$\mathbf{u}(t) = \begin{bmatrix} S_{S,in}(t) & X_{S,in}(t) & S_{O,in}(t) & S_{NO,in}(t) & S_{NH,in}(t) & Q_{in} & K_L a_{in} \end{bmatrix}^T \tag{5.15}$$

The estimated system output, which is identical to the output vector $\mathbf{y}(t)$ given in Equation (5.13), without the added measurement noise signal $\mathbf{v}(t)$, is of the form

$$\mathbf{z}(t) = \begin{bmatrix} S_{S,ef}(t) & X_{S,ef}(t) & S_{O,ef}(t) & S_{NO,ef}(t) & S_{NH,ef}(t) \end{bmatrix}^T \tag{5.16}$$

The system and output matrices of Equation (5.13) are of the form:

$$\mathbf{A}(t)\mathbf{X}(t) = \begin{bmatrix} \frac{\partial S_S(t)}{\partial S_S(t)} & \frac{\partial S_S(t)}{\partial X_S(t)} & \cdots & \cdots & \frac{\partial S_S(t)}{\partial S_{SNH}(t)} \\ \vdots & & \ddots & & \vdots \\ \frac{\partial S_{SNH}(t)}{\partial S_S(t)} & \cdots & & \cdots & \frac{\partial S_{SNH}(t)}{\partial S_{SNH}(t)} \end{bmatrix} \times \begin{bmatrix} S_S(t) \\ X_S(t) \\ S_{SO}(t) \\ S_{SO}(t) \\ S_{SNH}(t) \end{bmatrix}, \tag{5.17}$$

$$\mathbf{C}(t)\mathbf{X}(t) = \begin{bmatrix} \ddots & & 0 \\ & I & \\ 0 & & \ddots \end{bmatrix} \times \begin{bmatrix} S_S(t) \\ X_S(t) \\ S_{SO}(t) \\ S_{SO}(t) \\ S_{SNH}(t) \end{bmatrix} \tag{5.18}$$

Note that the input matrices are not represented in the sequel because this work concentrates on the monitoring application based on an open-loop model. Therefore, the manipulated inputs do not affect the estimated concentrations. The characteristics of the selected model are described in Table (5.3).

| Selected model | 'Model Ba' |
|---|---|
| Inputs (7) | $S_{S,in}$, $X_{S,in}$, $S_{O,in}$, $S_{NO,in}$, $S_{NH,in}$, $Q_{in}$, $K_La_{in}$ |
| Disturbances (0) | - |
| Measurements (3) | $S_O$ (on-line), $S_S$, $X_S$ (off line) |

**Table 5.3** Model description, which is utilised by the state observer. The dynamics are presented in Chapter IV, Section (4.1).

Characteristics of the on-line measurement and off-line analysis are described in Table (5.4). The on-line measurement is corrupted by an additive noisy signal with a variance equal to 10% of the corrupted concentrations.

| | Variance ($\sigma$) | Delay (min.) | Low-level detection limit | Sampling time (min.) |
|---|---|---|---|---|
| Oxygen ($S_{O,ef}$) | 0.35 | - | 0.1 | continuous |
| Readily biodegradable substrate ($S_S$) | - | 30 | 0.1 | 30 |
| Slowly biodegradable substrate ($X_S$) | - | 30 | 0.1 | 30 |

**Table 5.4** On-line measurements (selected from the effluent of the 1st aerated tank) and off line analyses ($S_S$ and $X_S$) coefficients that are considered for this specific case study.

A single on-line measurement ($S_O$) is assumed available and off-line analyses of $S_S$ and $X_S$ are also (hypothetically) assumed to be known (from respirometer), at the influent of the reduced model. A delay of 30 minutes between each analysis, assuming that the concentrations are constant between two measurements, is considered.

Simulation results are presented in Figure (5.7) for $S_S$ and $X_S$ concentrations. It can be observed that the respective concentrations converge toward their true state values in about two hours. Satisfactory tracking results are also obtained even if the estimated state variables from the state observer are underestimated during periods of high concentration and overestimated when low concentration occur, with maximum biases of 7% and 3%, and standard deviations of 0.29 and 18.7 g COD/m$^3$, respectively. Note that the biases occured after half a day and that the standard deviations are obtained over a single days period (e.g. from the 7$^{th}$ to the 8$^{th}$ days). The biases are caused by the simplifying assumptions that are considered to produce the reduced model. For instance, it's interesting to compare the estimated concentration from Figure (5.7) with results from the reduced model displayed in Figure (4.7), as it confirms that the biases (e.g. $S_S$ and $X_S$ concentrations) are due to the mismatch between the reduced-order model and the original ASM1 model.

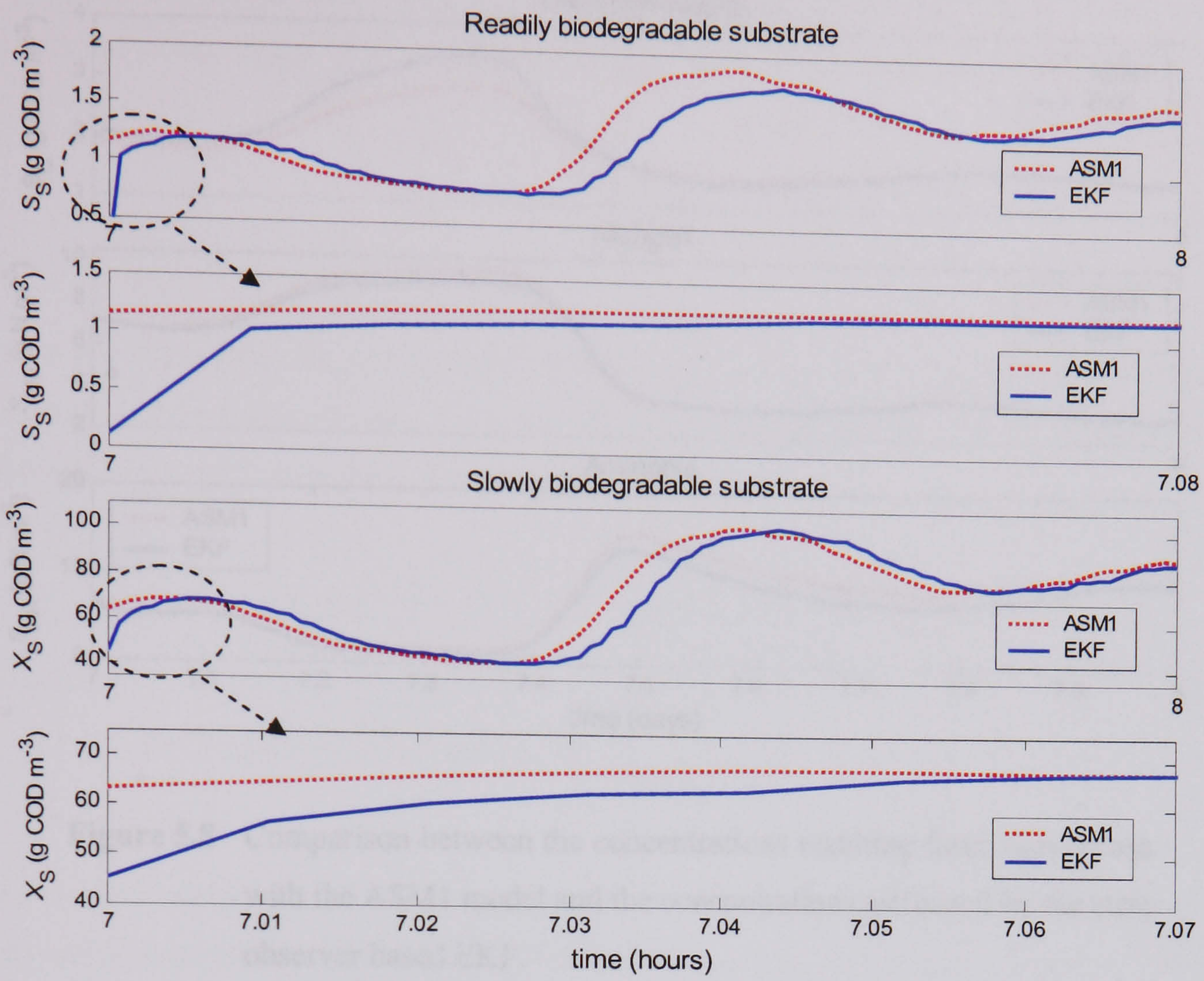


**Figure 5.7** Tracking and convergence performances of the EKF towards the real concentrations resulting from simulation with the ASM1 model.

Delays between the true state values and the state observer estimates are attributed to off-line and on-line measurements delay coefficients introduced in the simulation parameters. It demonstrates that the proposed extended Kalman filter is sufficiently robust against delays in the system. The remaining concentrations ($S_O$, $S_{NO}$ and $S_{NH}$) estimated by the software sensor are presented in Figure (5.8). It can be observed, as expected when comparing with Figure (4.7) from Chapter IV (e.g. $S_O$, $S_{NO}$ and $S_{NH}$ concentrations), that the algorithm based-EKF converges accurately toward the real states.

The biases between the real concentrations and the estimation are also due to the simplifying assumptions detailed in Chapter IV. This case study illustrates the state observer performance assuming $S_S$ and $X_S$ on the influent of the reduced model. However, such assumption implies the use of a respirometer, which can be relatively expensive. Therefore, it is important to consider applications were $S_S$ and/or $X_S$ are not available at the influent of the observer, as proposed in the following case study.

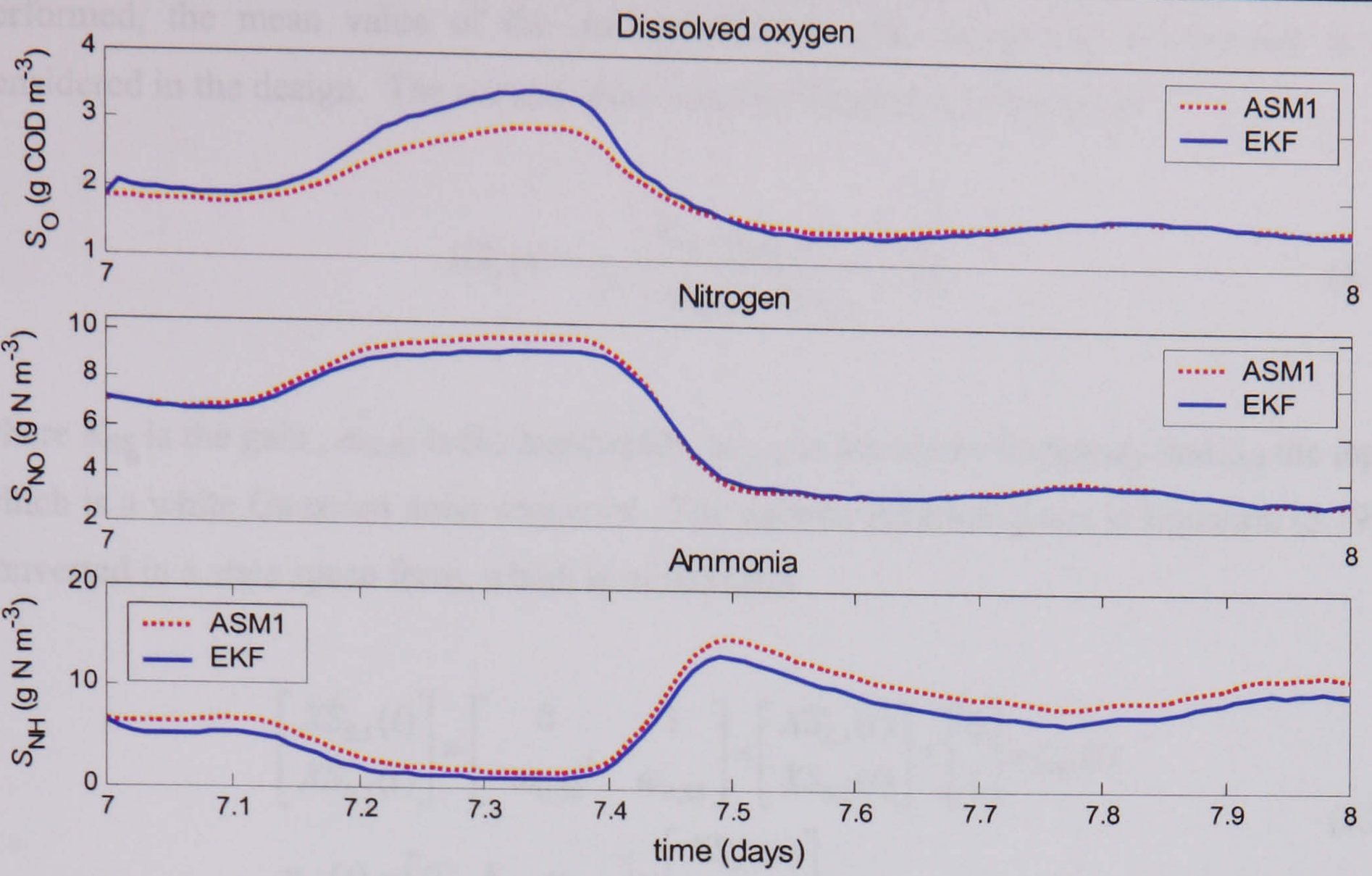


**Figure 5.8** Comparison between the concentrations resulting from simulations with the ASM1 model and the concentrations estimated by the state observer based EKF.

## Case (5.2b): $S_S$ and $X_S$ correlation

In the second case study, two different models ('Model Ba.1' and 'Model Ba.2') are implemented to investigate the correlation between $S_S$ and $X_S$ concentrations.

**Model Ba.1**

In 'Model Ba.1', it is assumed that measurements of $X_S$ concentration are available (from off-line analysis) and a state estimation of $S_S$ concentration, based on disturbance modelling, is performed. The disturbances are analysed using FFT and spectral analysis techniques, prior to the state observer implementation. Dynamic $S_S$ concentrations profiles are obtained in the time domain by simulating the benchmark plant, as presented in Figure (5.9a). On the resulting influent data, FFTs are applied to obtain the spectral content of the signal, and to design the appropriate transfer functions. The difference in applying this technique when compared with the previous application in Section (5.1) is that a 2$^{nd}$ order transfer function is considered to cover the energy of the theoretical data ($S_S$) in the frequency domain, instead of a 1$^{st}$ order transfer function. Note that when a second order transfer function design is

performed, the mean value of the theoretical data (also called DC component) is not considered in the design. The second order transfer function is of the form

$$HS_{\mathrm{S}}(s)=\frac{K_{\mathrm{SS}}.\omega_{\mathrm{B,SS}}.s}{s^2+\omega_{\mathrm{B,SS}}.s+\omega_{\mathrm{O,SS}}}\times\zeta_{\mathrm{SS}} \tag{5.19}$$

where $K_{SS}$ is the gain , $\omega_{B,SS}$ is the bandwidth , $\omega_{O,SS}$ is the centre frequency and $\zeta_{SS}$ the input, which is a white Gaussian noise sequence . The transfer function given in Equation (5.19) is converted in a state space form, which is of the form

$$\begin{aligned}\begin{bmatrix}\dot{XS}_{\mathrm{S},1}(t)\\ \dot{XS}_{\mathrm{S},2}(t)\end{bmatrix}&=\begin{bmatrix}0 & 1\\ -\omega_{\mathrm{O,SS}}{}^2 & \omega_{\mathrm{B,SS}}\end{bmatrix}\times\begin{bmatrix}XS_{\mathrm{S},1}(t)\\ XS_{\mathrm{S},2}(t)\end{bmatrix}+\begin{bmatrix}0\\ 1\end{bmatrix}\times\zeta_{\mathrm{SS}}(t)\\ \underset{\sim}{y}_{\mathrm{SS}}(t)&=\begin{bmatrix}0 & K_{\mathrm{SS}}.\omega_{\mathrm{B,SS}}\end{bmatrix}\times\begin{bmatrix}XS_{\mathrm{S},1}(t)\\ XS_{\mathrm{S},2}(t)\end{bmatrix}\end{aligned} \tag{5.20}$$

The system coefficient of the state space model given by Equation (5.20) are used as augmented state of the 'Model Ba.1', with $K_{SS}$ = 18, $\omega_{B,SS}$ = 1.1, $\omega_{O,SS}$ = 1 and a variance ($\sigma_{SS}$) equal to 0.001. The output coefficients of Equation (5.20) are only utilised to tune the 2nd order transfer function, which covers the energy of the $S_S$ concentration, as displayed in Figure (5.9b). Note that the bandwidth and centre frequency are obtained by trial and error. The frequency response in the semilog Cartesian coordinate system of the transfer function given by Equation (5.20) is displayed in Figure (5.10). These results demonstrate that this technique slightly differs from the one presented in Figure (5.1b) and Figure (5.3b).

The observer algorithm structure is identical to that described by Equations (5.5), with an augmented state vector of the form

$$\tilde{\mathbf{X}}(t)=\begin{bmatrix}S_{\mathrm{S}}(t) & X_{\mathrm{S}}(t) & S_{\mathrm{O}}(t) & S_{\mathrm{NO}}(t) & S_{\mathrm{NH}}(t) & XS_{\mathrm{S},1}(t) & XS_{\mathrm{S},2}(t)\end{bmatrix}^T, \tag{5.21}$$

with $XS_{S,1}$ and $XS_{S,2}$ from Equation (5.21) representing the augmented state used to estimate the $S_S$ concentration. The estimated output vector is of the form

$$\tilde{\mathbf{z}}(t)=\begin{bmatrix}S_{\mathrm{S,ef}}(t) & X_{\mathrm{S,ef}}(t) & S_{\mathrm{O,ef}}(t) & S_{\mathrm{NO,ef}}(t) & S_{\mathrm{NH,ef}}(t)\end{bmatrix}^T \tag{5.22}$$

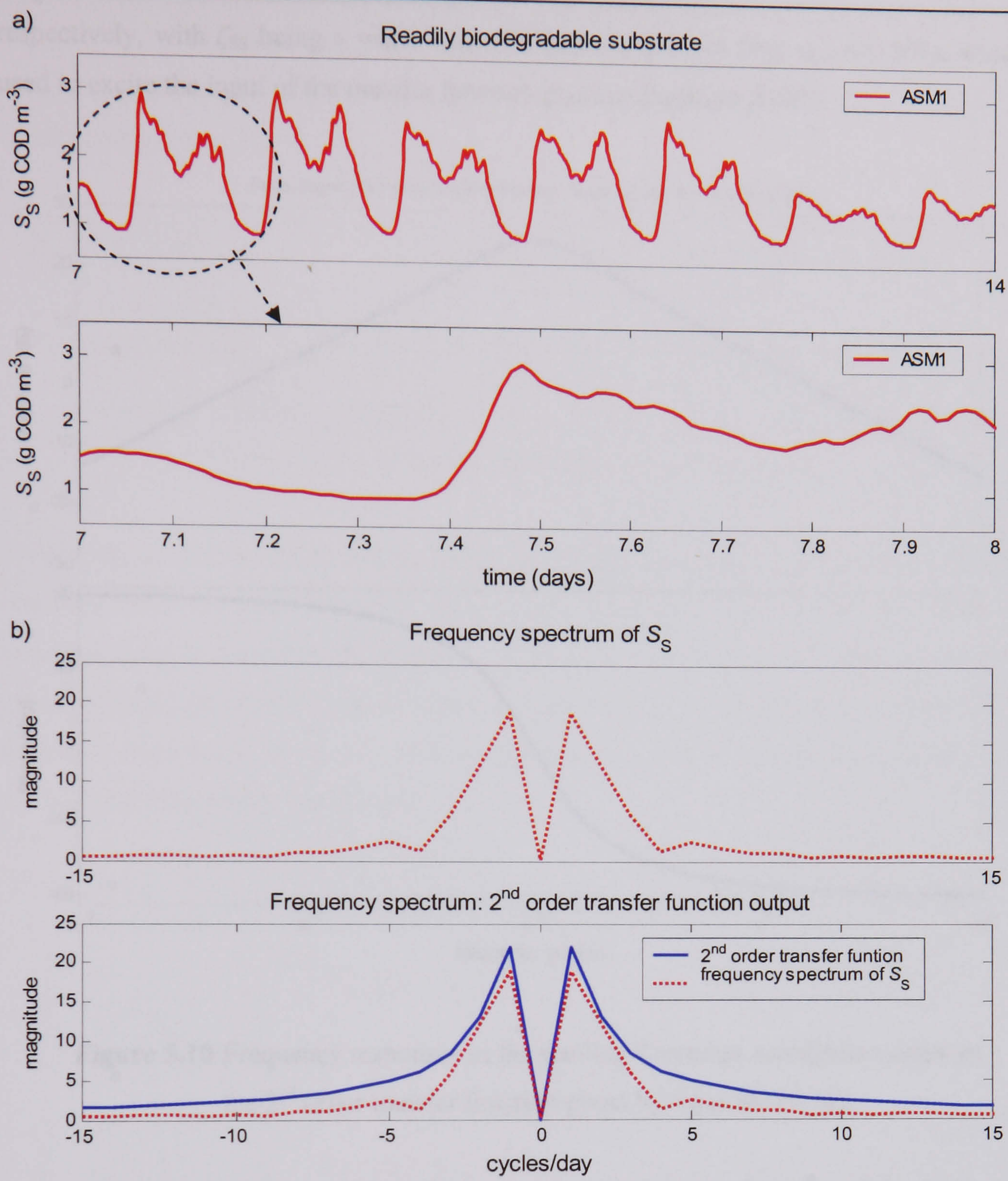


**Figure 5.9** (5.9a) $S_S$ concentration on the influent of the first aerobic tank of the benchmark plant resulting from simulations with the ASM1 model. (5.9b) Disturbances filter design using FFT technique.

The input and disturbances vectors are of the form

$$\mathbf{u}(t) = \begin{bmatrix} X_{S,in}(t) & S_{O,in}(t) & S_{NO,in}(t) & S_{NH,in}(t) & Q_{in} & K_L a_{in} \end{bmatrix}^T \tag{5.23}$$

$$\tilde{\mathbf{D}}(t)\mathbf{d}(t) = \begin{bmatrix} 0 & \cdots & 0 & | & 0 & 1 \end{bmatrix}^T \zeta_{SS}(t)s\,, \tag{5.24}$$

respectively, with $\zeta_{SS}$ being a white Gaussian noise sequences (e.g. $\sigma_{SS} = 0.001$), which is used to excite the input of the transfer function given in Equation (5.20).

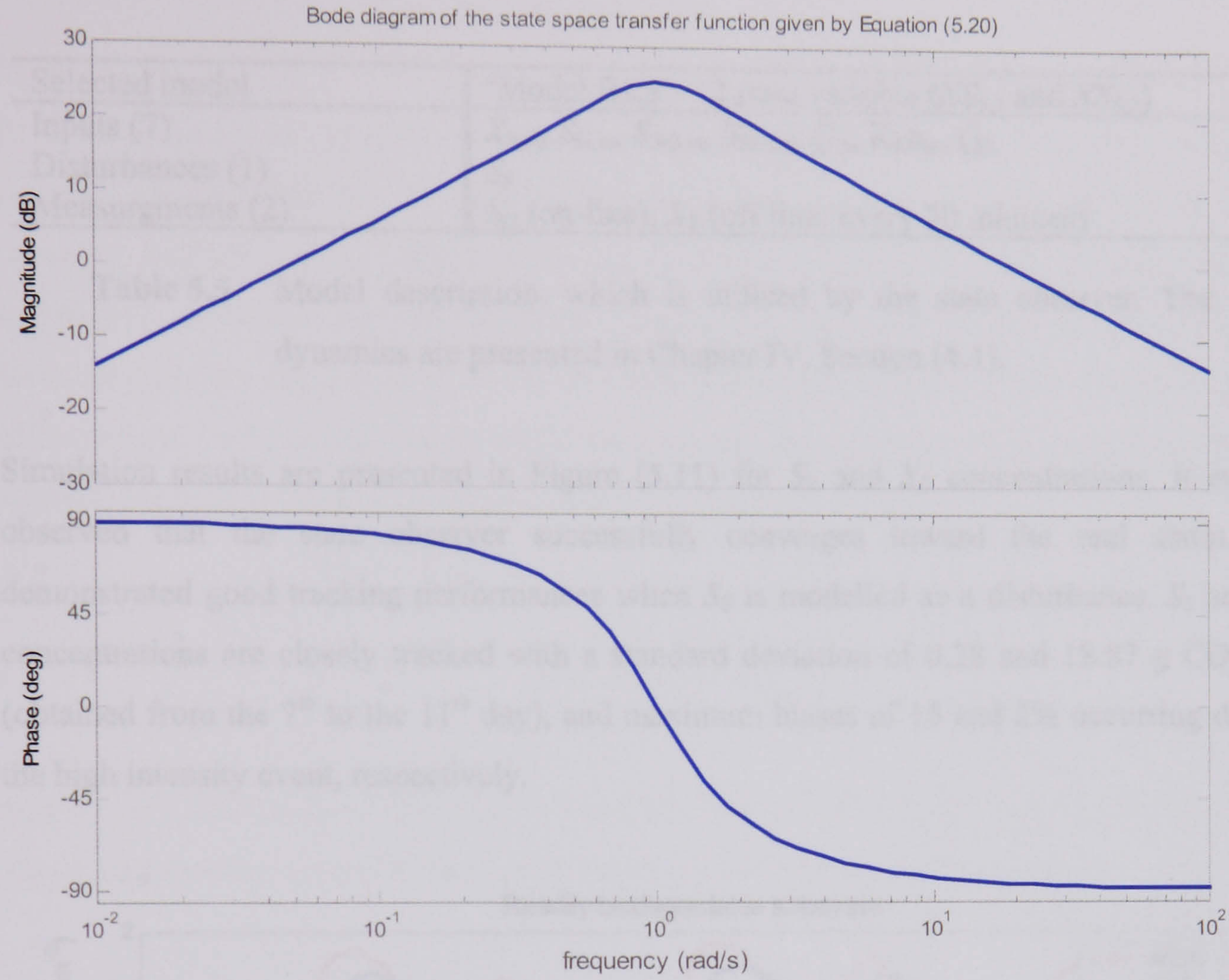


**Figure 5.10** Frequency responses in the semilog Cartesian coordinate system of the 2nd order transfer function given by Equation (5.20).

The system and output matrices, which are proposed in Equation (5.5), are defined by

$$\tilde{\mathbf{A}}(t) = \begin{bmatrix} \mathbf{A}(t) & \vdots & 0 & 0 \\ \cdots & \cdots & \cdots & \cdots \\ 0 & \vdots & 0 & 1 \\ 0 & \vdots & -\omega_{O,SS}{}^{2} & \omega_{B,SS} \end{bmatrix} \tag{5.25}$$

$$\tilde{\mathbf{C}}(t) = \begin{bmatrix} \mathbf{C}(t) & \vdots & 0 & 0 \end{bmatrix} \tag{5.26}$$

The characteristics of the selected model are described in Table (5.5). A single on-line measurement ($S_O$) is assumed available and off-line analyses of $X_S$ are also (hypothetically)

assumed to be known (from respirometer), at the influent of the reduced model. All the remaining assumptions (e.g. on-line and off-line measurement characteristics) are identical to the previous case (5.2a).

| Selected model | 'Model B1.a' + 2 state variable ($XS_{S,1}$ and $XS_{S,2}$) |
|---|---|
| Inputs (7) | $X_{S,in}$, $S_{O,in}$, $S_{NO,in}$, $S_{NH,in}$, $Q_{in}$, $K_La_{in}$, $\zeta_{SS}$ |
| Disturbances (1) | $S_S$ |
| Measurements (2) | $S_O$ (on-line), $X_S$ (off line: every 30 minutes) |

**Table 5.5** Model description, which is utilised by the state observer. The dynamics are presented in Chapter IV, Section (4.1).

Simulation results are presented in Figure (5.11) for $S_S$ and $X_S$ concentrations. It can be observed that the state observer successfully converges toward the real states and demonstrated good tracking performances when $S_S$ is modelled as a disturbance. $S_S$ and $X_S$ concentrations are closely tracked with a standard deviation of 0.28 and 18.87 g COD/m$^3$ (obtained from the 7$^{th}$ to the 11$^{th}$ day), and maximum biases of 15 and 2% occurring during the high intensity event, respectively.

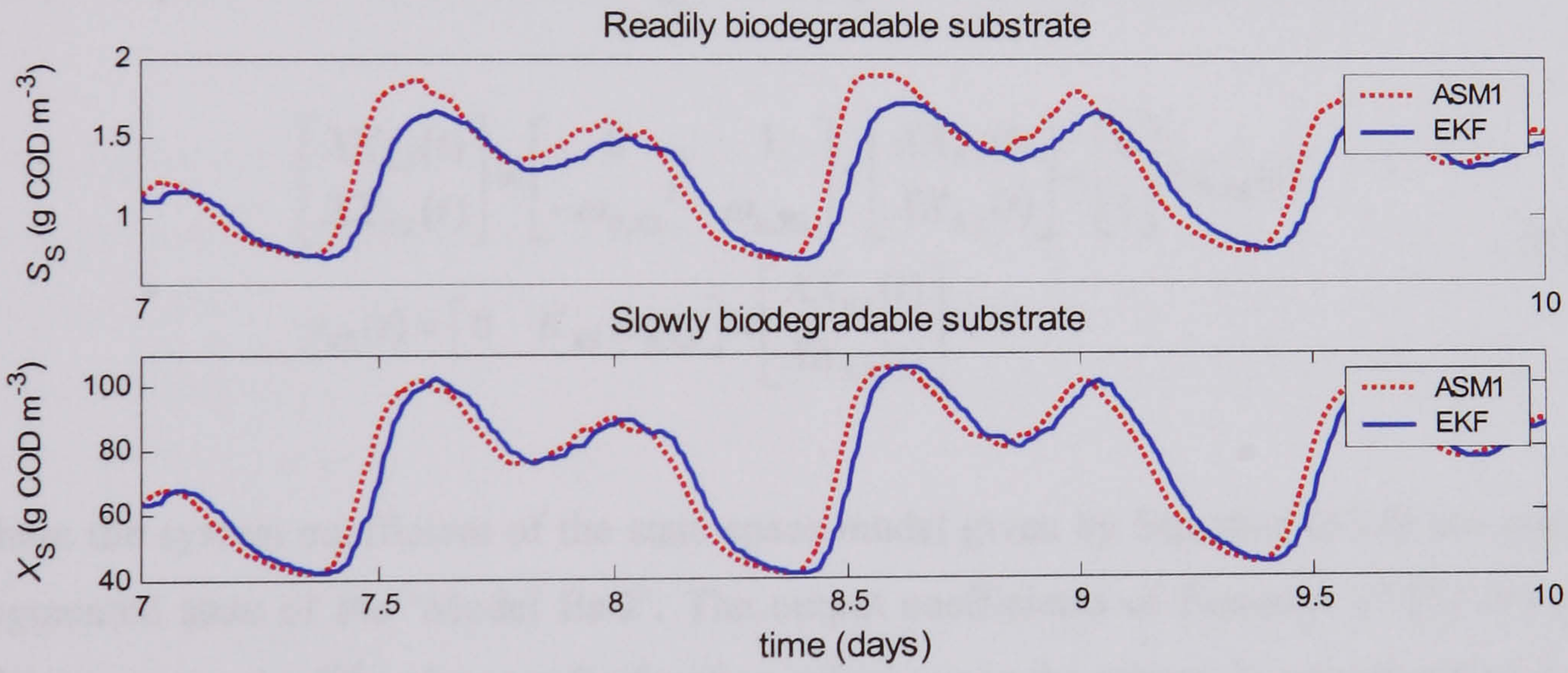


**Figure 5.11** Concentrations comparison resulting from simulation with the original benchmark plant (dotted line) the state observer, based on an EKF, were $S_{S,in}$ is modelled as a disturbance.

This clearly implies that: (1) $S_S$ concentration can be estimated by the state observer when $X_S$ concentration is available from off-line analysis and (2) further development can be considered for on-line monitoring purposes. Note that $S_O$, $S_{NO}$ and $S_{NH}$ concentrations are not represented here because they are identical to those presented in Figure (5.8).

The objective of the following case is to check if whether or not similar assumptions can be considered when $X_S$ concentration is modelled as a disturbance and $S_S$ measurements available trough a hypothetical respirometer.

**Model Ba.2**

In 'Model Ba.2', the inverse assumption is made: measurements of $S_S$ concentration are assumed available and the $X_S$ concentration is modelled as a disturbance. Similarly to the previous application, the disturbances are analysed using FFT and spectral analysis techniques. Dynamic $X_S$ concentrations profiles are obtained in the time domain by simulating the benchmark plant, similar to results presented in Figure (5.9a). On the resulting influent data, FFTs are applied to obtain the spectral content of the signal, and to design the appropriate filters. The second order transfer function is of the form

$$HX_S(s) = \frac{K_{XS}.\omega_{B,XS}.s}{s^2 + \omega_{B,XS}.s + \omega_{O,XS}} \times \zeta_{XS} \tag{5.27}$$

with $K_{XS} = 1320$, $\omega_{B,XS} = 1.09$, $\omega_{O,XS} = 1$ and the variance of the noisy input $\zeta_{XS}$ is: $\sigma_{XS} = 0.1$. The state space form transfer function given in Equation (5.27) is of the form

$$\begin{aligned} \begin{bmatrix} \dot{XX}_{S,1}(t) \\ \dot{XX}_{S,2}(t) \end{bmatrix} &= \begin{bmatrix} 0 & 1 \\ -\omega_{O,XS}{}^2 & \omega_{B,XS} \end{bmatrix} \times \begin{bmatrix} XX_{S,1}(t) \\ XX_{S,2}(t) \end{bmatrix} + \begin{bmatrix} 0 \\ 1 \end{bmatrix} \times \zeta_{XS}(t) \\ \underset{\sim}{y}_{XS}(t) &= \begin{bmatrix} 0 & K_{XS}.\omega_{B,XS} \end{bmatrix} \times \begin{bmatrix} XX_{S,1}(t) \\ XX_{S,2}(t) \end{bmatrix} \end{aligned} \tag{5.28}$$

where the system coefficient of the state space model given by Equation (5.28) are used as augmented state of the 'Model Ba.2'. The output coefficients of Equation (5.28) are only utilised to tune the 2nd order transfer function, which cover the energy $X_S$ concentration in the frequency domain. The profile of $X_S$ concentration, the 2nd order transfer function and the frequency response in the semilog Cartesian coordinate system are not represented here, as they are similar to Figure (5.9a), (5.9b) and (5.10), respectively. The observer algorithm structure is identical to the one described by Equations (5.5), with an augmented state vector given by

$$\tilde{\mathbf{X}}(t) = \begin{bmatrix} S_S(t) & X_S(t) & S_O(t) & S_{NO}(t) & S_{NH}(t) & XX_{S,1}(t) & XX_{S,2}(t) \end{bmatrix}^T, \tag{5.29}$$

with $XX_{S,1}$ and $XX_{S,2}$ representing the augmented state used to estimate $X_S$ concentration. The estimated output vector is of the form

$$\tilde{\mathbf{z}}(t) = \begin{bmatrix} S_{S,ef}(t) & X_{S,ef}(t) & S_{O,ef}(t) & S_{NO,ef}(t) & S_{NH,ef}(t) \end{bmatrix}^T \tag{5.30}$$

The input and disturbances vectors are of the form

$$\mathbf{u}(t) = \begin{bmatrix} S_{S,in}(t) & S_{O,in}(t) & S_{NO,in}(t) & S_{NH,in}(t) & Q_{in} & K_L a_{in} \end{bmatrix}^T \tag{5.31}$$

$$\tilde{\mathbf{D}}(t)\mathbf{d}(t) = \begin{bmatrix} 0 & \cdots & 0 & | & 0 & 1 \end{bmatrix}^T \zeta_{XS}(t). \tag{5.32}$$

The system and output matrices, which are proposed in Equation (5.5), are defined by

$$\tilde{\mathbf{A}}(t) = \begin{bmatrix} \mathbf{A}(t) & \vdots & 0 & 0 \\ \cdots & \cdots & \cdots & \cdots \\ 0 & \vdots & 0 & 1 \\ 0 & \vdots & -\omega_{O,XS}{}^2 & \omega_{B,XS} \end{bmatrix} \qquad \tilde{\mathbf{C}}(t) = \begin{bmatrix} \mathbf{C}(t) & \vdots & 0 & 0 \end{bmatrix} \tag{5.33}$$

The characteristics of the selected model are described in Table (5.6). A single on-line measurement ($S_O$) is assumed available and off-line analyses of $S_S$ are also (hypothetically) assumed available (from respirometer), at the influent of the reduced model. All the remaining assumptions (e.g. on-line and off-line measurement characteristics) are also identical to the previous case (5.2a)

| Selected model | 'Model Ba' + 2 state variable ($XX_{XS,1}$ and $XX_{XS,2}$) |
|---|---|
| Inputs (7) | $S_{S,in}$, $S_{O,in}$, $S_{NO,in}$, $S_{NH,in}$, $Q_{in}$, $K_L a_{in}$, $\zeta_{XS}$ |
| Disturbances (1) | $X_S$ |
| Measurements (2) | $S_O$ (on-line), $S_S$ (off line: every 30 minutes) |

**Table 5.6** Model description, which is utilised by the state observer. The dynamics of the reduced-model are presented in Chapter IV, Section (4.1).

Simulation results from 'Model Ba.2', displayed in Figure (5.12), show poor estimate and tracking results even though the possibility of off-line analysis of $S_S$ is considered. The absolute errors between the original ASM1 model and the modified reduced 'Model Ba.2'

are calculated in terms of standard deviations, means and maximum biases, for each concentration, over a period of 3 days.

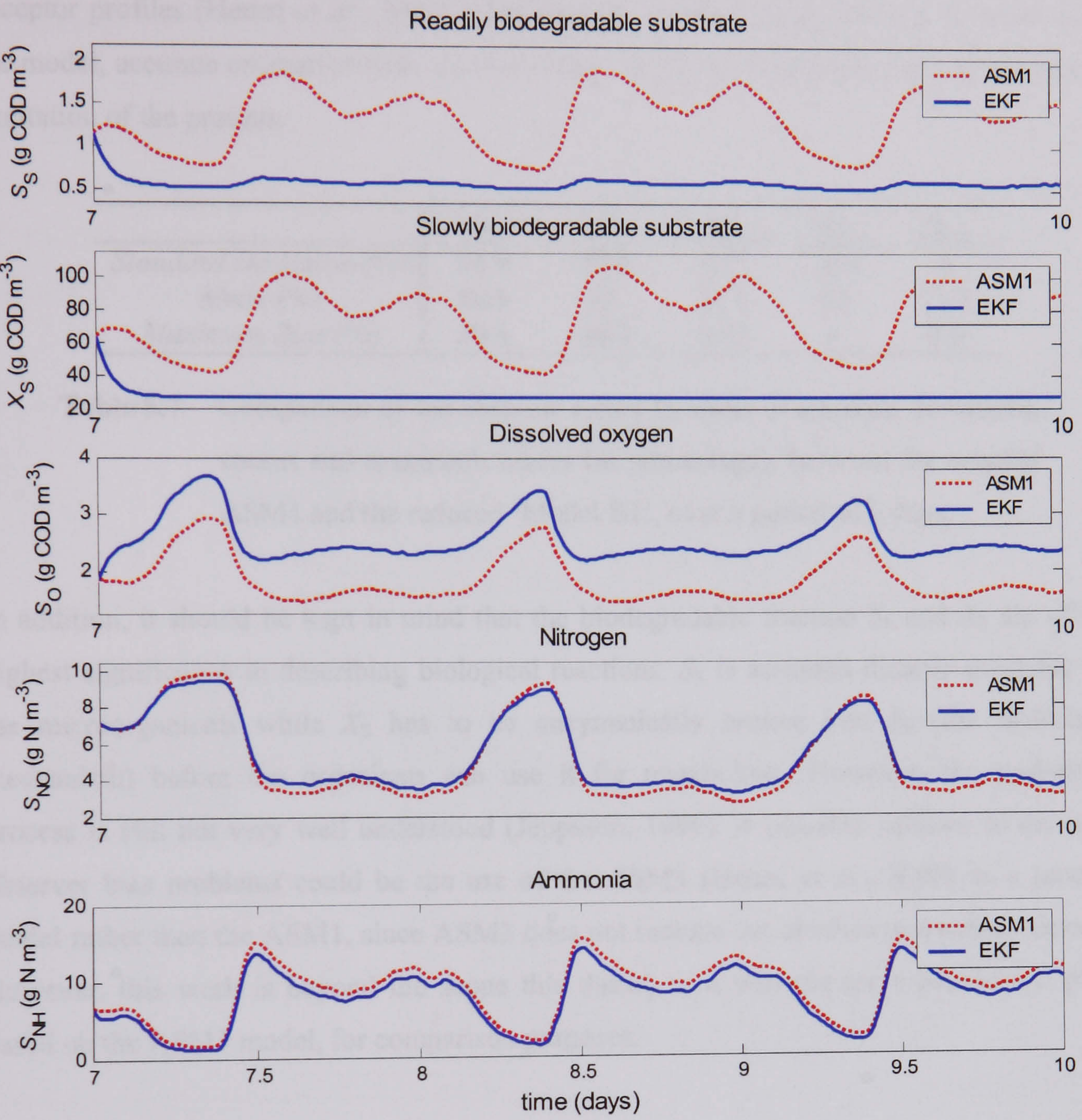


**Figure 5.12** Concentrations comparison resulting from simulation with the original benchmark plant and the state observer based on a EKF, where $X_{S,in}$ is modelled as a disturbance.

Results are summarised in Table (5.7) where it can be observed that the maximum discrepancies occur for $S_S$ and $X_S$ concentrations with maximum standard deviation errors of about 80%. This significant estimation bias is probably attributed to the original mathematical description of the ASM1 model. Indeed, it is based on a circular (growth-decay-growth) relationship, also called the *death-regeneration* concept (Henze *et al.*, 2000),

where the slowly biodegradable substrate is removed by hydrolysis (and formed by decay of both heterotrophic and autotrophic biomass). Therefore, $X_S$ is a crucial variable primarily responsible for the attainment of realistic space-time and real time dependent electron acceptor profiles (Henze *et al.*, 2000). Consequently, if this concentration is removed from the model, accurate estimation from the state observer cannot be achieved, due to the lack of excitation of the process.

| | $S_S$ | $X_S$ | $S_O$ | $S_{NO}$ | $S_{NH}$ |
|---|---|---|---|---|---|
| *Standard Deviation* (%) | **81.9** | **79.8** | 5.7 | 12.4 | 6 |
| *Mean* (%) | **56.8** | **63** | 28.1 | 4.8 | 11.7 |
| *Maximum Bias* (%) | **39.6** | **40.4** | 20.2 | 4 | 8.9 |

**Table 5.7** Comparison of the absolute errors in terms of standard deviations, means and maximum biases (in percentage), between the original ASM1 and the reduced 'Model B1', over a period of 3 days.

In addition, it should be kept in mind that the biodegradable fraction $S_S$ and $X_S$ are of the highest significance in describing biological reactions. $S_S$ is assumed directly available for the microorganisms while $X_S$ has to be enzymatically broken into $S_S$ (the hydrolysis mechanism) before the organisms can use it for metabolism. However, the hydrolysis process is still not very well understood (Jeppsson, 1996). A possible solution to the state observer bias problems could be the use of the ASM3 (Henze *et al.*, 2000) as a process model rather than the ASM1, since ASM3 does not include the *death-regeneration* concept. However, this work is beyond the scope this thesis, as it will require a benchmark plant based on the ASM3 model, for comparison purposes.

## Case (5.2c): Toxic input detection

From the previous case study (5.2b), it can be concluded that accurate estimation of slowly biodegradable substrate cannot be achieved using the proposed methodology without available off-line analysis (at least every hour) of $X_S$ concentration. However, toxic inputs from the sewer can sufficiently excite the process to be detected by the state observer. Therefore, in this third case study, it is assumed (similar to the situation on a full-scale system) that neither $S_S$ nor $X_S$ are available from off-line analyses, and the state observer response time is checked. The characteristics of the selected model are described in Table (5.8). Only a single on-line measurement ($S_O$) is assumed available at the influent of the reduced model.

| Selected model | 'Model B1' + 4 state variables ($XS_{S,1}$, $XS_{S,2}$ $XX_{S,1}$, $XX_{S,2}$) |
|---|---|
| Inputs (7) | $S_{O,in}$, $S_{NO,in}$, $S_{NH,in}$, $Q_{in}$, $K_La_{in}$, $\zeta_{SS}$, $\zeta_{SND}$ |
| Disturbances (2) | $S_S$, $X_S$ |
| Measurement (1) | $S_O$ (on-line) |

**Table 5.8** Model description, which is utilised by the state observer.

The implementation of the state observer, including concentrations that are measured on-line as well as state variables that are not available (e.g. $S_S$ and $X_S$), is presented in Figure (5.13). All the remaining assumptions (e.g. on-line measurement characteristic) are also identical to the previous case (5.2a and 5.2b).

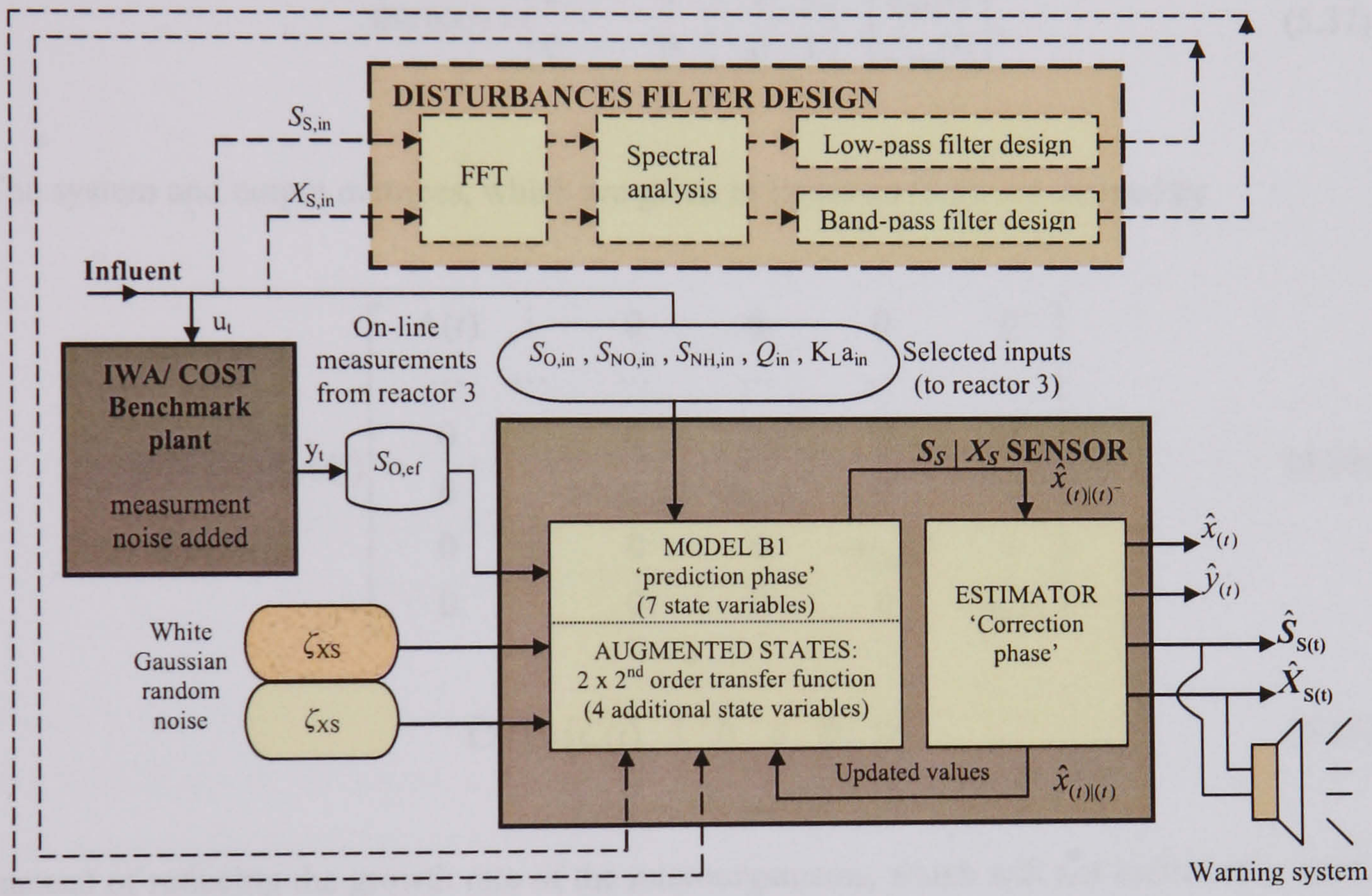


**Figure 5.13** State observer design utilised to estimate $S_S$ and $X_S$ concentrations on-line.

The observer algorithm has a similar structure from the one described by Equations (5.5), with an augmented state vector of the form

$$\tilde{\mathbf{X}}(t) = \begin{bmatrix} S_S(t) & X_S(t) & S_O(t) & S_{NO}(t) \\ & & S_{NH}(t) & XS_{S,1}(t) & XS_{S,2}(t) & XX_{S,1}(t) & XX_{S,2}(t) \end{bmatrix}^T \tag{5.34}$$

With $XS_{S,1}$, $XS_{S,2}$, $XX_{S,1}$, and $XX_{S,2}$ representing the augmented state used to estimate $S_S$ and $X_S$ concentrations, respectively. The estimated output vector is of the form

With $XS_{S,1}$, $XS_{S,2}$, $XX_{S,1}$, and $XX_{S,2}$ representing the augmented state used to estimate $S_S$ and $X_S$ concentrations, respectively. The estimated output vector is of the form

$$\tilde{\mathbf{z}}(t) = \begin{bmatrix} S_{S,ef}(t) & X_{S,ef}(t) & S_{O,ef}(t) & S_{NO,ef}(t) & S_{NH,ef}(t) \end{bmatrix}^T \tag{5.35}$$

The input and disturbances vectors are of the form

$$\mathbf{u}(t) = \begin{bmatrix} S_{O,in}(t) & S_{NO,in}(t) & S_{NH,in}(t) & Q_{in} & K_L a_{in} \end{bmatrix}^T \tag{5.36}$$

$$\tilde{\mathbf{D}}(t)\mathbf{d}(t) = \begin{bmatrix} 0 & \cdots & 0 & | & 1 & 0 \\ 0 & \cdots & 0 & | & 0 & 1 \end{bmatrix}^T \cdot \begin{bmatrix} \zeta_{SS}(t) \\ \zeta_{XS}(t) \end{bmatrix}, \tag{5.37}$$

The system and output matrices, which are given in Equation (5.5), are defined by

$$\tilde{\mathbf{A}}(t) = \begin{bmatrix} \mathbf{A}(t) & \vdots & 0 & 0 & 0 & 0 \\ \cdots & \cdots & \cdots & \cdots & \cdots & \cdots \\ 0 & \vdots & 0 & 1 & 0 & 0 \\ 0 & \vdots & -\omega_{O,SS}{}^2 & \omega_{B,SS} & 0 & 0 \\ 0 & \vdots & 0 & 0 & -\omega_{O,XS}{}^2 & 1 \\ 0 & \vdots & 0 & 0 & 0 & \omega_{B,XS} \end{bmatrix} \tag{5.38}$$

$$\tilde{\mathbf{C}}(t) = \begin{bmatrix} \mathbf{C}(t) & \vdots & 0 & 0 & 0 & 0 \end{bmatrix} \tag{5.39}$$

Instead of reducing the growth rate of the microorganisms, which will not sufficiently excite the plant behaviour, an airflow failure to simulate a toxic event is provoked. The failure occurs after 10.5 days, lasting for half a day, as reflected in Figure (5.14) with the DO concentration. The effect of the airflow failure on $S_{NO}$ and $S_{NH}$ concentrations can also be observed from this graph. Simulation results presenting the detection of abnormally high substrate concentrations are presented in Figure (5.15a) and (5.15b) for $S_S$ and $X_S$ concentrations, respectively. The limit detection level set points, which are marked by dash-dot lines, are set to 0.70 g COD/m$^3$ and 30 g COD/m$^3$ for $S_S$ and $X_S$, respectively. It is seen that the state observer successfully detected: (1) abnormal readily biodegradable substrate after approximately 90 minutes, which corresponds to a level of 3 g COD/m$^3$ in the ASM1 model and (2) abnormal slowly biodegradable substrate concentrations after approximately 60 minutes, which corresponds to a level of 110 g COD/m$^3$ in the ASM1 model.

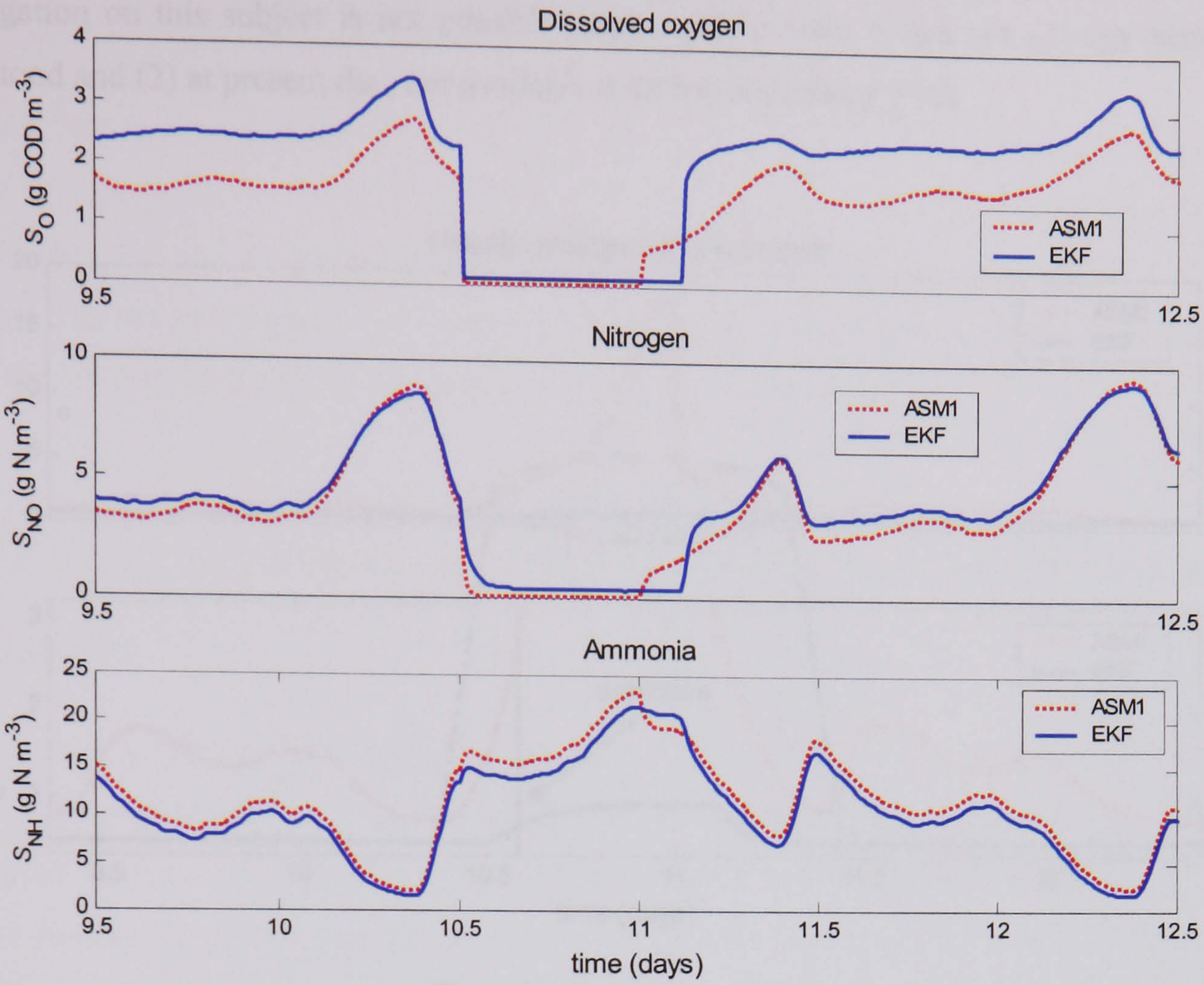


**Figure 5.14** Airflow failure effect on the estimated concentrations resulting from simulation with the original benchmark plant and resulting from simulations with the state observer based-EKF.

It can be concluded that when $S_S$ and $X_S$ concentrations are available from off-line analyses in a WWTP, the state observer converges toward the true state values in about two hours and demonstrates good tracking performances, as presented in case (5.2a). It was also shown that the $S_S$ concentration can be estimated by the state observer when $X_S$ measurements are available and further development can be considered for control application purposes. However, as presented in case (5.2b), it is not possible to use the described technique for estimation of $X_S$ when off-line analysis is not available. It is proposed that this problem is due to the circular structure of the ASM1, i.e. the *death-regeneration* concept. From simulation results presented in case (5.2c), it can be observed that the $S_S|X_S$ state observer detects abnormally high substrate concentrations, for example due to influent substrate shock loads, in 60 and 90 minutes, respectively. However, caution should be considered when implementing the state observer presented in case (5.2c), as it is possible that the observer detect an airflow failure instead of abnormal substrate concentrations. At this stage, a deeper

investigation on this subject is not possible since realistic toxic events are (1) not clearly understood and (2) at present day, not available with the benchmark plant.

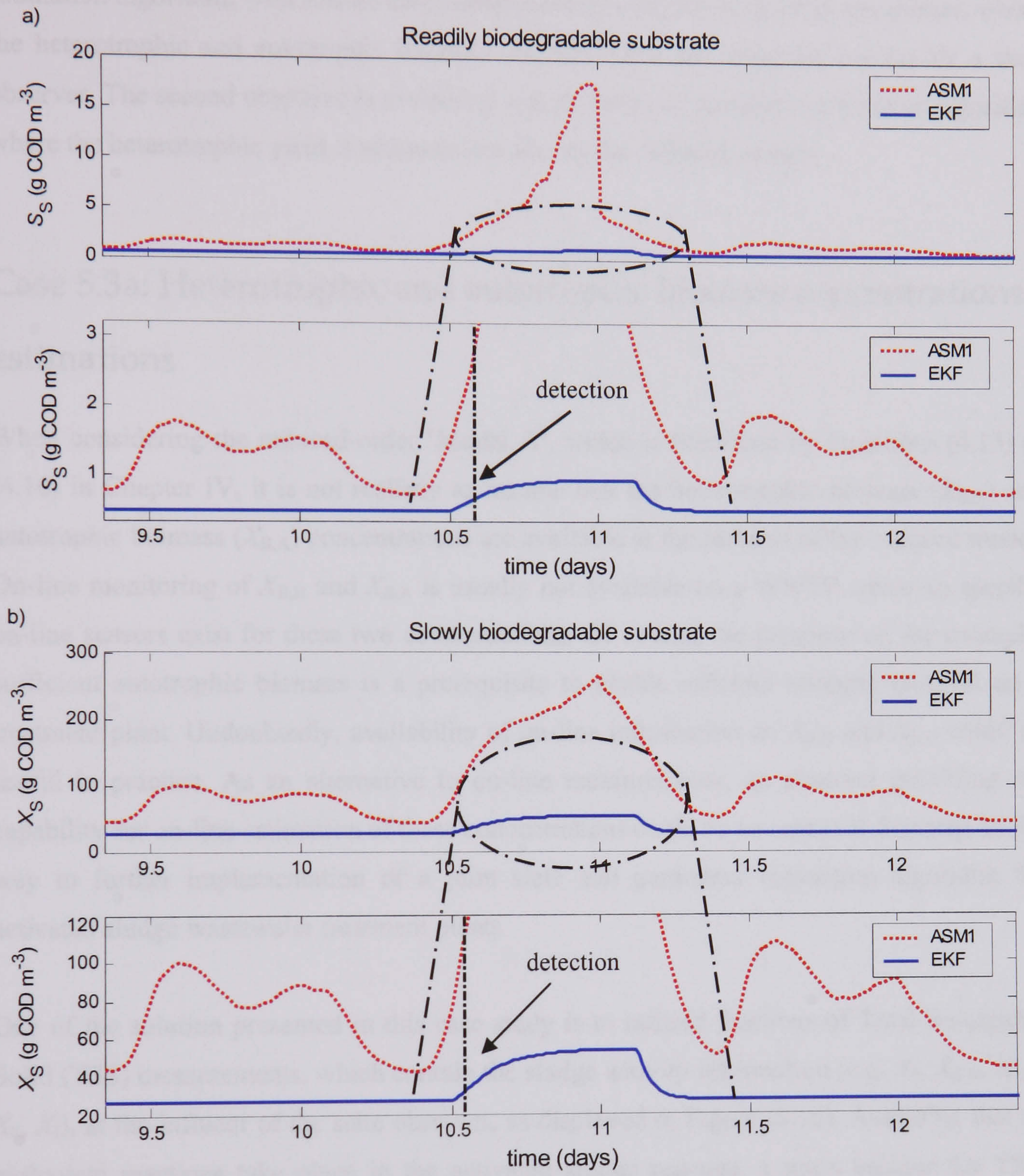


**Figure 5.15** (5.15a) and (5.15b) $S_S$ and $X_S$ concentrations resulting from simulations with the benchmark plant compared with $S_S$ and $X_S$ concentrations resulting from the state observer based-EKF, respectively. The detection arrow indicates the hypothetical alarm activation zones.

## 5.3) ON-LINE MONITORING OF THE SLUDGE ACTIVITY

The final application is presented with two objectives. The first one illustrates a state estimation algorithm, with known and constant kinetic and stoichiometric parameters, where the heterotrophic and autotrophic biomass concentrations are estimated on-line by a state observer. The second objective is to develop a joint state and parameter estimation algorithm where the heterotrophic yield is estimated on-line by the software sensor.

### Case 5.3a: Heterotrophic and autotrophic biomass concentrations estimations

When considering the reduced-order 'Model A', which is described by Equations (4.13) to (4.16) in Chapter IV, it is not realistic to assume that the heterotrophic biomass ($X_{B,H}$) and autotrophic biomass ($X_{B,A}$) concentrations are available at the influent of the reduced model. On-line monitoring of $X_{B,H}$ and $X_{B,A}$ is usually not available on a WWTP, since no specific on-line sensors exist for these two concentrations. Of course, the presence of, for example, sufficient autotrophic biomass is a prerequisite to enable efficient nitrogen removal on a treatment plant. Undoubtedly, availability of on-line information on $X_{B,H}$ and $X_{B,A}$ could be useful in practice. As an alternative to on-line measurements, an observer providing the capability for on-line estimation of these concentrations could be an essential first step on the way to further implementation of a joint state and parameter estimation algorithm for activated sludge wastewater treatment plants

One of the solution presented in this case study is to utilised fractions of Total Suspended Solid (TSS) measurements, which contain the sludge activity information (e.g. $X_S$, $X_{B,H}$, $X_{B,A}$, $X_P$, $X_I$), at the influent of the state observer, as displayed in Figure (5.16). Assuming that no biological reactions take place in the activated sludge reactors, a mass balance for TSS, given by Equation (5.40) to (5.44), over each of the five reactors for the benchmark plant configuration is performed. This mass balance enables a fairly good approximation of the TSS concentration in each activated sludge tank, on the condition that a number of assumptions are fulfilled: 1) An on-line measurement of the TSS concentration in the influent and the return sludge line is available; 2) An on-line measurement of the influent, the return sludge and the internal recirculation flow rate is available.

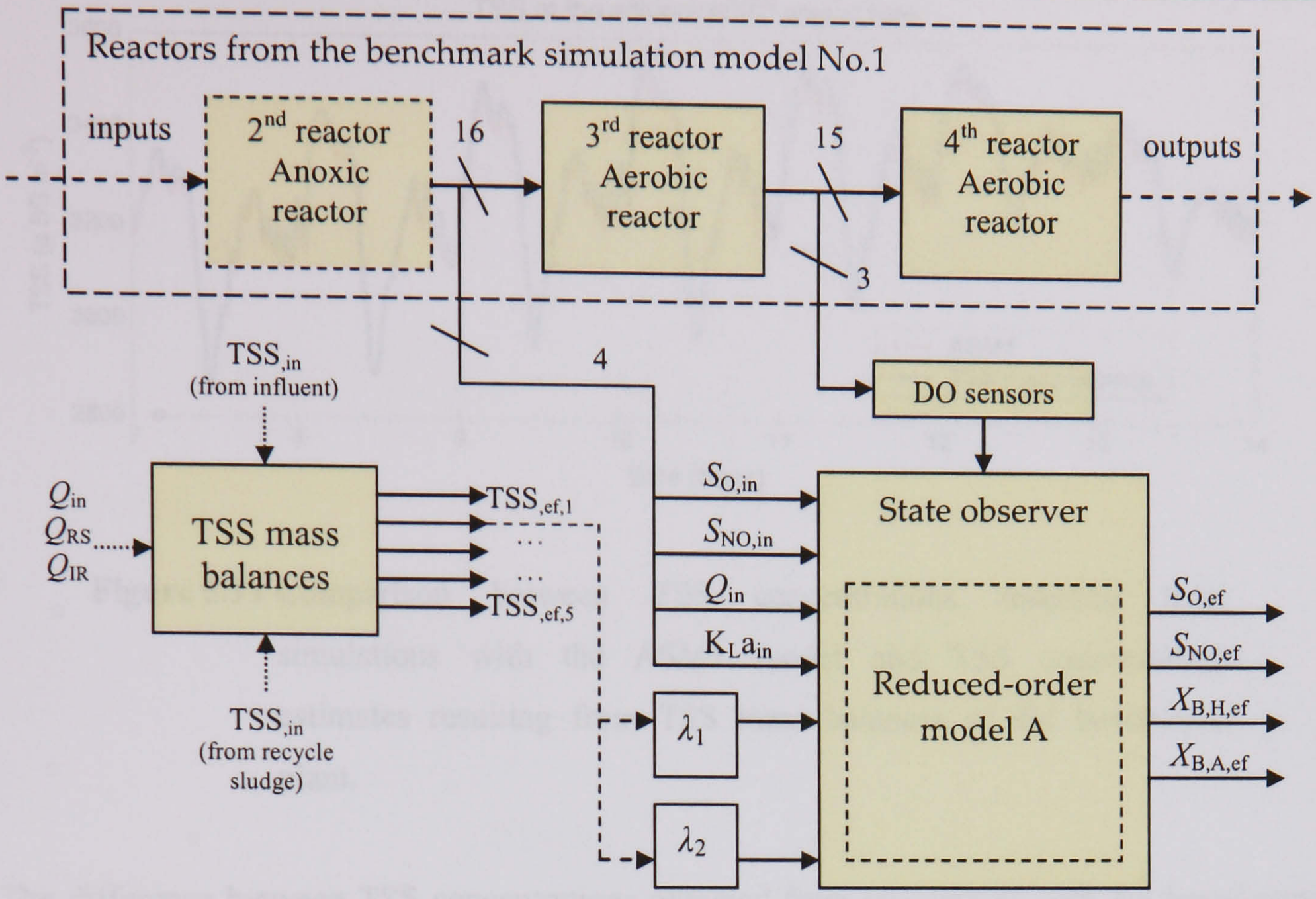


**Figure 5.16** State observer design utilised to estimate $X_{B,H}$ and $X_{B,A}$ concentrations on-line, using fractions of the total suspended solid.

$$\dot{X}_{TSS,1} = \frac{1}{VOL1} \times \left( Q_{in} \times TSS_{in} + Q_{ret} \times TSS_{ret} + Q_{intr} \times X_{TSS,5} - \right.$$
$$\left. (Q_{in} + Q_{ret} + Q_{intr}) \times X_{TSS,1} \right) \quad (5.40)$$

$$\dot{X}_{TSS,2} = \frac{1}{VOL2} \times (Q_{in} + Q_{ret} + Q_{intr}) \times \left( X_{TSS,1} - X_{TSS,2} \right) \quad (5.41)$$

$$\dot{X}_{TSS,3} = \frac{1}{VOL3} \times (Q_{in} + Q_{ret} + Q_{intr}) \times \left( X_{TSS,2} - X_{TSS,3} \right) \quad (5.42)$$

$$\dot{X}_{TSS,4} = \frac{1}{VOL4} \times (Q_{in} + Q_{ret} + Q_{intr}) \times \left( X_{TSS,3} - X_{TSS,4} \right) \quad (5.43)$$

$$\dot{X}_{TSS,5} = \frac{1}{VOL5} \times (Q_{in} + Q_{ret} + Q_{intr}) \times \left( X_{TSS,4} - X_{TSS,5} \right) \quad (5.44)$$

with $Q_{in}$, $Q_{ret}$ and $Q_{intr}$ being the influent, the return sludge and the internal recirculation flow rate, respectively. *VOL* (1 to 5), $TSS_{in}$ and $TSS_{ret}$ represent the volume of the reactors (1 to 5), TSS concentration in the influent and the return sludge line, respectively. The result of applying TSS mass balances to the activated sludge reactors is illustrated in Figure (5.17) at the effluent at the 2nd anoxic tank.

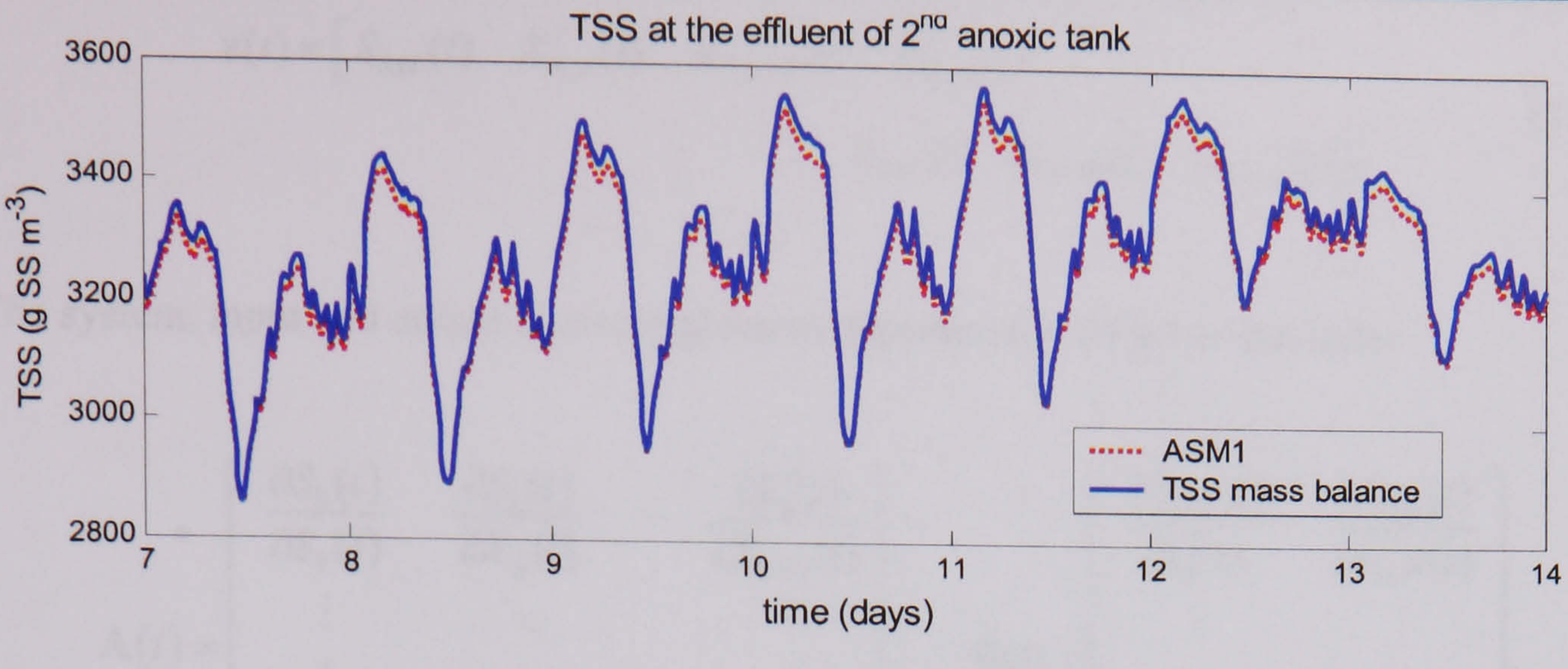


**Figure 5.17** Comparison between TSS concentrations resulting from simulations with the ASM1 model and TSS concentration estimates resulting from TSS mass balances of the benchmark plant.

The difference between TSS concentrations obtained from simulations with the benchmark plant model (ASM1) and the TSS mass balances is about 1%. Applying TSS mass balances results in a slight overestimation of the TSS concentrations since hydrolysis processes lead to a TSS decrease in the ASM1 model. Note that the remaining mass balances are not presented here because the following case study focuses on TSS at the effluent of the 2nd anoxic reactor.

The proposed state observer, which is based on the 'Model A' presented in Chapter IV, Section (4.1), is identical to the linearised one presented in Equation (5.13). However, the state and input and output vectors are of the form

$$\mathbf{X}(t) = \begin{bmatrix} S_S(t) & X_S(t) & X_{B,H}(t) & X_{B,A}(t) \\ & & & S_O(t) \quad S_{NO}(t) \quad S_{NH}(t) \end{bmatrix}^T \tag{5.45}$$

$$\mathbf{u}(t) = \begin{bmatrix} S_{S,in}(t) & X_{S,in}(t) & \lambda_1 TSS_{2,in}(t) & \lambda_2 TSS_{2,in}(t) \\ & & & S_{O,in}(t) \quad S_{NO,in}(t) \quad S_{NH,in}(t) \end{bmatrix}^T \tag{5.46}$$

where $\lambda_1 TSS_{2,in}$ and $\lambda_2 TSS_{2,in}$ correspond to two fractions (with $\lambda_1 \approx 0.78$ and $\lambda_2 \approx 0.04$) of the TSS concentrations, respectively, obtained from the above TSS mass balances results.

$$\mathbf{z}(t) = \left[ S_{\mathrm{S,ef}}(t) \quad X_{\mathrm{S,ef}}(t) \quad X_{\mathrm{B,H,ef}}(t) \quad X_{\mathrm{B,A,ef}}(t) \quad S_{\mathrm{O,ef}}(t) \quad S_{\mathrm{NO,ef}}(t) \quad S_{\mathrm{NH,ef}}(t) \right]^T \tag{5.47}$$

The system, input and output matrices given by Equation (5.13) are of the form:

$$\mathbf{A}(t) = \begin{bmatrix} \frac{\partial S_{\mathrm{S}}(t)}{\partial S_{\mathrm{S}}(t)} & \frac{\partial S_{\mathrm{S}}(t)}{\partial X_{\mathrm{S}}(t)} & \cdots & \frac{\partial S_{\mathrm{S}}(t)}{\partial S_{\mathrm{SNH}}(t)} \\ \vdots & \ddots & & \vdots \\ \vdots & & \ddots & \vdots \\ \frac{\partial S_{\mathrm{SNH}}(t)}{\partial S_{\mathrm{S}}(t)} & \frac{\partial S_{\mathrm{NH}}(t)}{\partial X_{\mathrm{S}}(t)} & \cdots & \frac{\partial S_{\mathrm{SNH}}(t)}{\partial S_{\mathrm{SNH}}(t)} \end{bmatrix}, \quad \mathbf{B}(t) = \begin{bmatrix} \frac{\partial S_{\mathrm{S,in}}(t)}{\partial Q(t)} & \frac{\partial S_{\mathrm{S,in}}(t)}{\partial K_{\mathrm{L}}a(t)} \\ \vdots & \vdots \\ \vdots & \vdots \\ \frac{\partial S_{\mathrm{NH,in}}(t)}{\partial Q(t)} & \frac{\partial S_{\mathrm{NH,in}}(t)}{\partial K_{\mathrm{L}}a(t)} \end{bmatrix}, \tag{5.48}$$

$$\mathbf{C}(t)\mathbf{X}(t) = \begin{bmatrix} \ddots & & 0 \\ & I & \\ 0 & & \ddots \end{bmatrix} . \mathbf{X}(t)$$

The characteristics of the selected model are described in Table (5.9). Two on-line measurements ($S_{\mathrm{O}}$ and TSS) are assumed available at the effluent and influent of the reduced model, respectively.

| Selected model | 'Model A' |
|---|---|
| Inputs (7) | $S_{\mathrm{O,in}}$, $S_{\mathrm{NO,in}}$, $S_{\mathrm{NH,in}}$, $Q_{\mathrm{in}}$, $\mathrm{K_La_{in}}$, $\lambda_1 TSS_{2,\mathrm{in}}$, $\lambda_2 TSS_{2,\mathrm{in}}$ |
| Disturbances (0) | - |
| Measurement (1) | $S_{\mathrm{O}}$ (on-line), TSS (from mass balance equations) |

**Table 5.9** Model description, which is utilised by the state observer.

Simulations results are presented in Figure (5.18) where it can be observed that the state observer failed in converging toward the real state for $S_{\mathrm{O}}$ concentration. However, this result was expected since the reduced 'Model A' is not accurate in describing the dynamic behaviour of the dissolved oxygen (detailed are discuss in Chapter IV). The $S_{\mathrm{NO}}$ concentration is estimated by the state observer with good tracking performances. The absolute error, in terms of the standard deviation, mean and a maximum bias, is displayed in Table (5.10). Note that the standard deviations and means are obtained over a period of 7 days. Comparing these mismatches, for $S_{\mathrm{NO}}$ concentration, with the one presented in Table (4.4) of Chapter IV, an increase of the absolute error in term of standard deviation (+86 %) and mean (+57 %) has occurred.

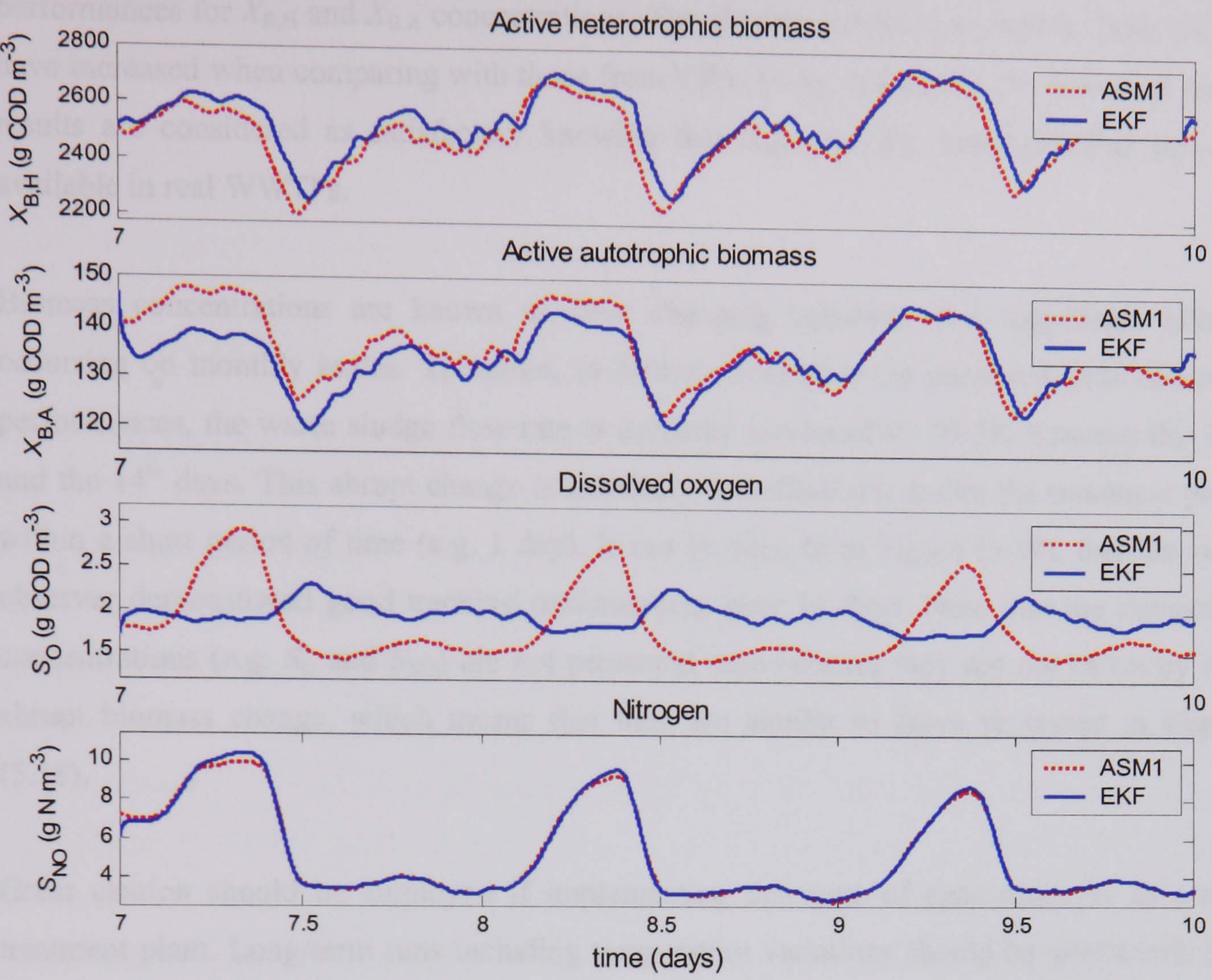


**Figure 5.18** Comparison between the concentrations at the effluent of the third reactor resulting from simulations with the ASM1 model and the state observer based-EKF.

On the other hand, the maximum bias decreased by 20 % when compared with the original reduced 'Model A'. This is explained by the influent biomass concentrations (e.g. $X_{B,H,in}$ and $X_{B,A,in}$), which are replaced by fractions of the TSS concentration from mass balances.

| | $S_O$ | $S_{NO}$ | $X_{B,H}$ | $X_{B,A}$ |
|---|---|---|---|---|
| *Standard Deviation* (%) | - | 27 | 26.2 | 2.1 |
| *Mean* (%) | - | 2.4 | 0.7 | 2.2 |
| *Maximum Bias* (%) | - | 4.7 | 0.2 | 3.6 |

**Table 5.10** Comparison of the absolute errors in term of standard deviation, mean and maximum bias (in percentage), between the ASM1 model and the estimated concentrations from the observer.

As stated previously it is important to estimate $X_{B,H}$ and $X_{B,A}$ concentrations to enable efficient nitrogen removal. Furthermore, The state observer demonstrated good tracking

performances for $X_{B,H}$ and $X_{B,A}$ concentrations. The absolute errors presented in Table (5.10) have increased when comparing with those from Table (4.4), in Chapter IV. However, these results are considered as satisfactory knowing that $X_{B,H}$ and $X_{B,A}$ measurements are not available in real WWTPs.

Biomass concentrations are known as slow changing variables with significant effects occurring on monthly scales. Therefore, to further investigate the proposed state observer performances, the waste sludge flow rate is suddenly increased by 97.5% between the 10$^{th}$ and the 14$^{th}$ days. This abrupt change is necessary to sufficiently excite the treatment plant within a short period of time (e.g. 1 day). It can be seen from Figure (5.19), that the state observer demonstrated good tracking performances over 14 days. Note that the remaining concentrations (e.g. $S_O$ and $S_{NO}$) are not presented here because they are not affect by this abrupt biomass change, which means that they are similar to those presented in Figure (5.18).

Great caution should be employed if implementing this type of state observer in a real treatment plant. Long-term runs including temperature variations should be performed. For instance, the Long-Term BSM1 model (BSM1_LT) proposed by (Gernaey *et al.*, 2006) could be of great interest in monitoring of the sludge activity.

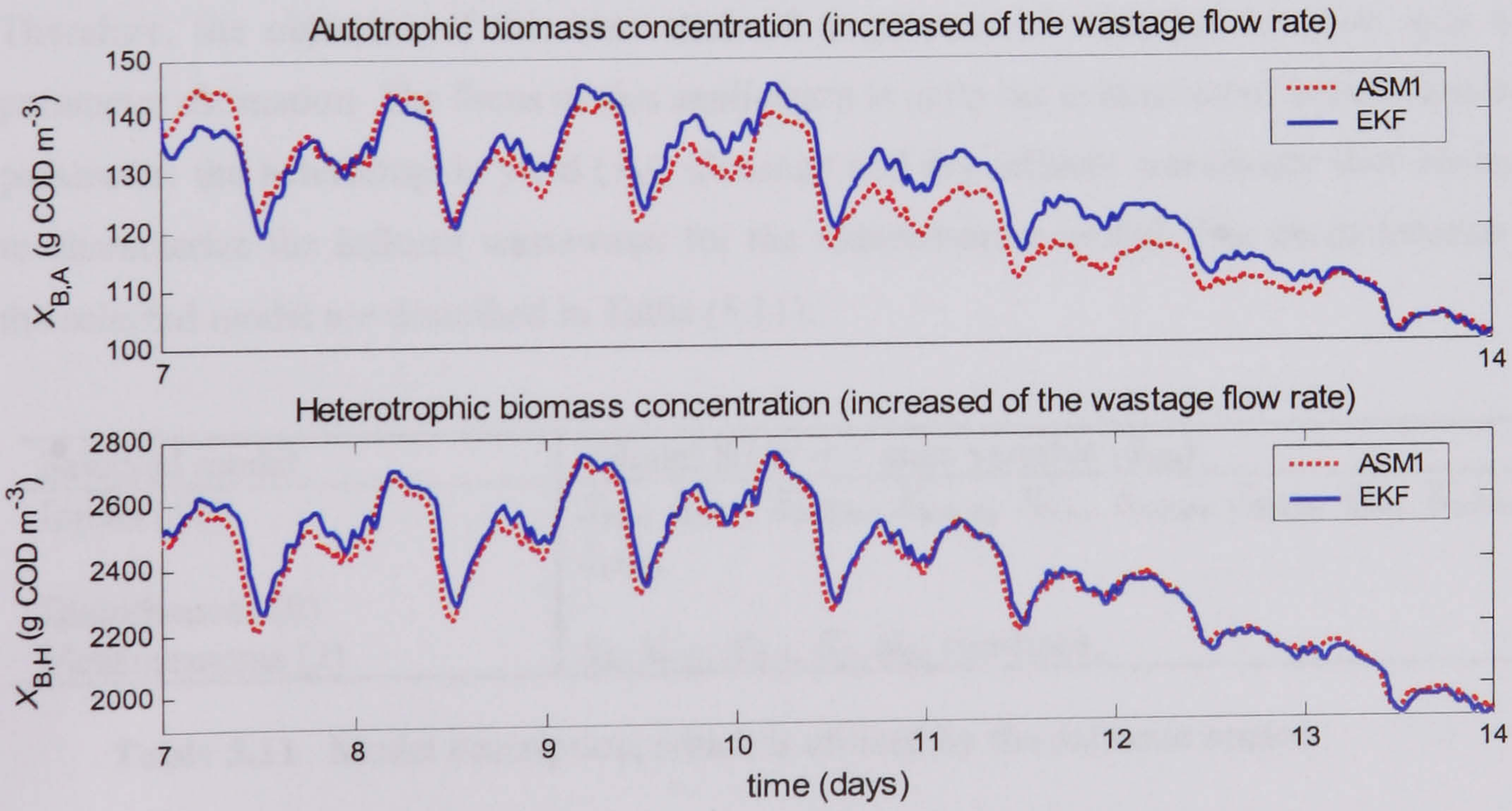


**Figure 5.19** Comparison between $X_{B,A}$ and $X_{B,H}$ concentrations at the effluent of the third reactor resulting from simulations with the ASM1 model and the estimates resulting from the state observer.

In addition, the solid retention time could be decreased (e.g. to 10-13 days) in order to check the software sensor response. However, such investigation is beyond the scope of this work, due to the computational burden that will be generated if running the BSM1_LT for a period of 1 year.

## Case 5.3b: Joint state and parameter estimation

Parameter estimation aims at providing values for the parameters in the model, depending on the quality of the experimental data set available. For instance, the initial benchmark plant has been designed assuming that all kinetic and stoichiometric coefficients are constants, which is not obvious in a real wastewater treatment plant where for example seasonal changes in influent temperature will have a severe influence on the process kinetics. The first type of parameters that can be estimated are those contained in the system matrix of the reduced state space model describing the dynamic behaviour of the plant. However, they are not presented in this work because they represent non-linear combinations of some traditional model parameters. They typically give an idea of how some amalgamated model parameters influence the process dynamic, and are not relevant with the selected ASP. The second type of parameters that can be estimated, which are of interest in this case, are the stoichiometric and/or kinetic parameters described in Appendix B.

Therefore, the objective of this case study is to propose an observer for joint state and parameter estimation. The focus of this application is upon the estimation of a stoichiometric parameter: the heterotrophic yield ($Y_H$). Constant and dry influent wastewater data are used to characterize the influent wastewater for the reduced-order model. The characteristics of the selected model are described in Table (5.11).

| Selected model | 'Model B1.b' + 1 state variable ($\theta_{YH}$) |
|---|---|
| Inputs (10) | $S_{S,in}$, $X_{S,in}$, $X_{B,H,in}$, $X_{B,A,in}$, $S_{O,in}$, $S_{NO,in}$, $S_{NH,in}$, $Q_{in}$, $K_La_{in}$, $\zeta_{YH,in}$ |
| Disturbances (0) | - |
| Measurements (2) | $S_S$, $X_{B,H}$, $X_{B,A}$, $S_O$, $S_{NO}$ (on-line), |

**Table 5.11** Model description, which is utilised by the software sensor.

As some of the ASM1 model parameters are non-identifiable, on-line measurements of $S_S$, $X_{B,H}$, $X_{B,A}$, $S_O$ and $S_{NO}$ are considered to improve the estimation algorithm response. This specific case study remains theoretical and is performed to obtain the profiles parameters on

the BSM1 model. Therefore, on-line measurements are also assumed noise free and sensors delays are not considered.

On-line measurements of $X_{B,H}$ and $X_{B,A}$ can be justified by the results presented in the previous case study (5.3a). In other terms, one can assume that the heterotrophic and autotrophic biomass can be estimated on-line by a state observer using fractions of the TSS concentrations. Furthermore, $S_S$ can also be estimated by the software sensor if the readily biodegradable substrate is assumed available every thirty minutes via respirometer as proposed in the case study (5.2b). Then, the resulting estimated concentrations could be used as measurements in an independent observer in order to accurately estimate some model parameters. However, caution should be considered with such techniques, as propagation of the errors between the state observer and the parameter estimator might occur.

The continuous state space model, augmented with an extra state variable ($\theta_{YH}$) to the initial state vector is of the form

$$\dot{\mathbf{x}}(t) = \mathbf{f}(t)(\mathbf{x}(t), \mathbf{u}(t), \theta_{YH}(t)) + \mathbf{G}(t)(\mathbf{x}(t), \theta_{YH}(t))\mathbf{w}(t) \tag{5.49}$$

$$\mathbf{y}(t) = \mathbf{h}(t)(\mathbf{x}(t), \theta_{YH}(t)) + \mathbf{v}(t), \tag{5.50}$$

with Equation (5.49) corresponding to

$$\dot{\tilde{\mathbf{X}}}(t) = \tilde{\mathbf{f}}(t) + \tilde{\mathbf{G}}(t)\begin{bmatrix} \mathbf{w}(t) \\ \zeta_{YH}(t) \end{bmatrix}, \tag{5.51}$$

which is also equivalent to

$$\begin{bmatrix} \dot{\mathbf{x}}(t) \\ \dot{\theta}_{YH}(t) \end{bmatrix} = \begin{bmatrix} \mathbf{f}(t)(\mathbf{x}(t), \mathbf{u}(t), \theta_{YH}(t)) \\ \theta_{YH}(t) \end{bmatrix} + \begin{bmatrix} \mathbf{G}(t)(\mathbf{x}(t), \theta_{YH}(t)) & 0 \\ 0 & \boldsymbol{I} \end{bmatrix} \begin{bmatrix} \mathbf{w}(t) \\ \zeta_{YH}(t) \end{bmatrix}, \tag{5.52}$$

with $\theta_{YH}(t)$ considered as a random constant vector ($\dot{\theta}_{YH}(t) = \theta_{YH}(t) + \zeta_{YH}(t)$), and $\zeta_{YH}(t)$ a white Gaussian noise sequence with zero mean and uncorrelated with $\mathbf{w}(t)$, similar to Chui and Chen (1991). The linearised augmented software sensor is identical to that introduced by Equation (5.5) with an augmented state vector given by

$$\tilde{\mathbf{X}}(t) = \begin{bmatrix} S_S(t) & X_S(t) & X_{B,H}(t) & X_{B,A}(t) \\ & S_O(t) & S_{NO}(t) & S_{NH}(t) & \theta_{YH}(t) \end{bmatrix}^T, \tag{5.53}$$

with $\theta_{YH}$ introduced as the augmented state variable. The augmented estimated output vector of Equation (5.5) is given by

$$\tilde{\mathbf{z}}(t) = \begin{bmatrix} S_{S,ef}(t) & X_{S,ef}(t) & X_{B,H,ef}(t) & X_{B,A,ef}(t) \\ & S_{O,ef}(t) & S_{NO,ef}(t) & S_{NH,ef}(t) & Y_H(t) \end{bmatrix}^T. \tag{5.54}$$

The linearised augmented state, input and output matrices are of the form

$$\tilde{\mathbf{A}}(t) = \begin{bmatrix} & \vdots & \dfrac{\partial S_s(t)}{\partial Y_H(t)} \\ \mathbf{A}(t) & \vdots & \vdots \\ & \vdots & \dfrac{\partial S_{SNH}(t)}{\partial Y_H(t)} \\ \cdots & \cdots & \cdots \\ 0 & \vdots & 0 \end{bmatrix}, \qquad \tilde{\mathbf{B}}(t) = \begin{bmatrix} \mathbf{B}(t) & \vdots & 0 \\ \cdots & \cdots & \cdots \\ 0 & \vdots & 1 \end{bmatrix},$$

$$\tilde{\mathbf{C}}(t) = \begin{bmatrix} \mathbf{C}(t) & \vdots & 0 \end{bmatrix}^T. \tag{5.55}$$

Further details about the observer algorithm, are presented in Perrier *et al.* (2000), Dochain (2003).

Simulations results are presented in Figure (5.20) where the state variables and the heterotrophic yield ($Y_H$), which is of main interest, are estimated on-line by the software sensor when constant influent wastewater data are considered. It can be observed that the algorithm converge toward the real parameter in less than twelve days with a maximum bias less than 0.1%, when the software sensor is initialised at 0.62 g $X_{B,H}$ COD formed per g substrate COD. The heterotrophic yield estimation from the software sensor using dry influent wastewater data is proposed in Figure (5.21). The observer, which is initialised to 0.70 g $X_{B,H}$ COD formed per g substrate COD, can detect the heterotrophic yield variations with a standard deviation of 0.009 g COD/m$^3$ g $X_{B,H}$ COD formed per g substrate COD.

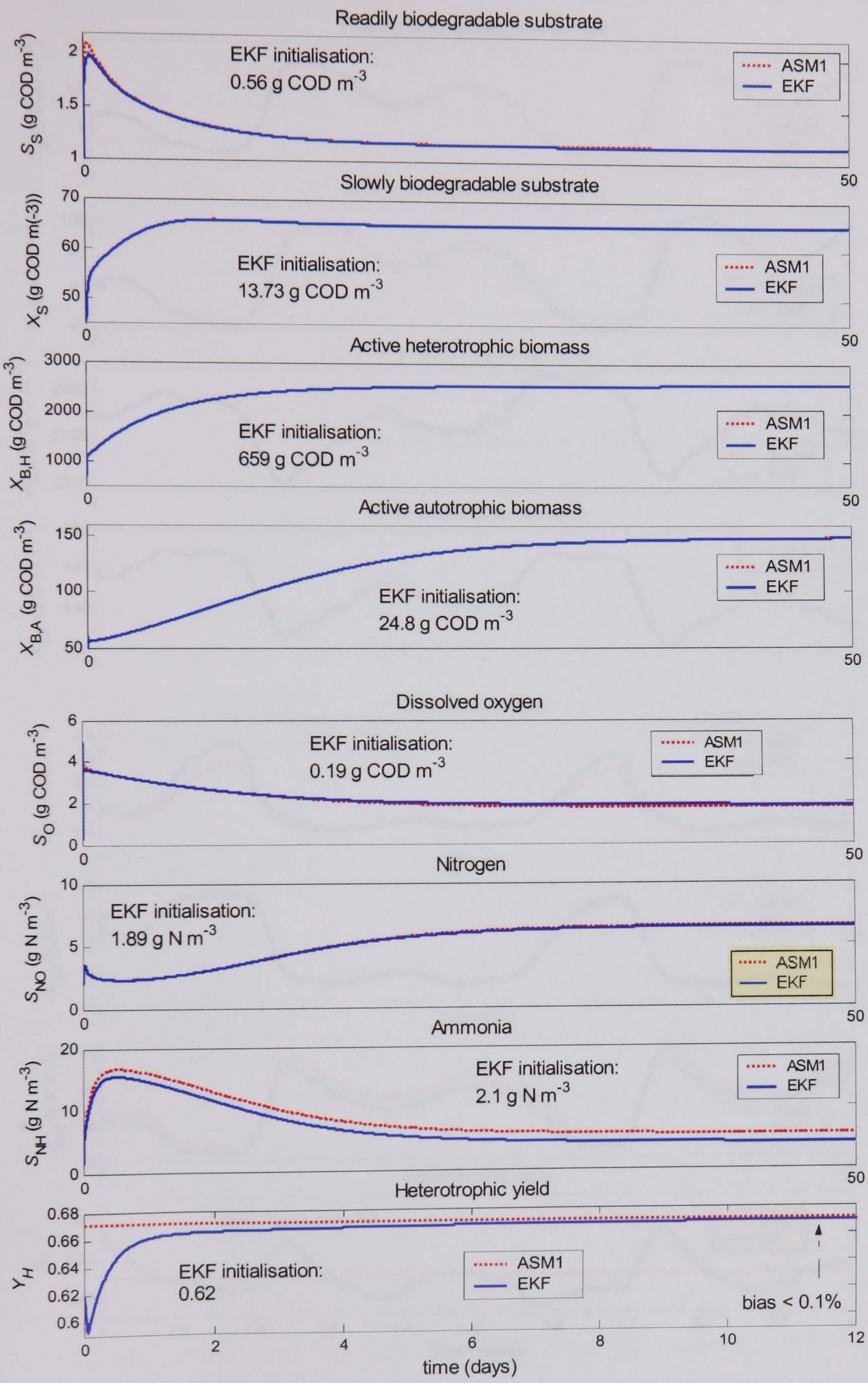


**Figure 5.20** Joint state and parameter estimation comparison between the ASM1 model and the software sensor, with a constant influent.

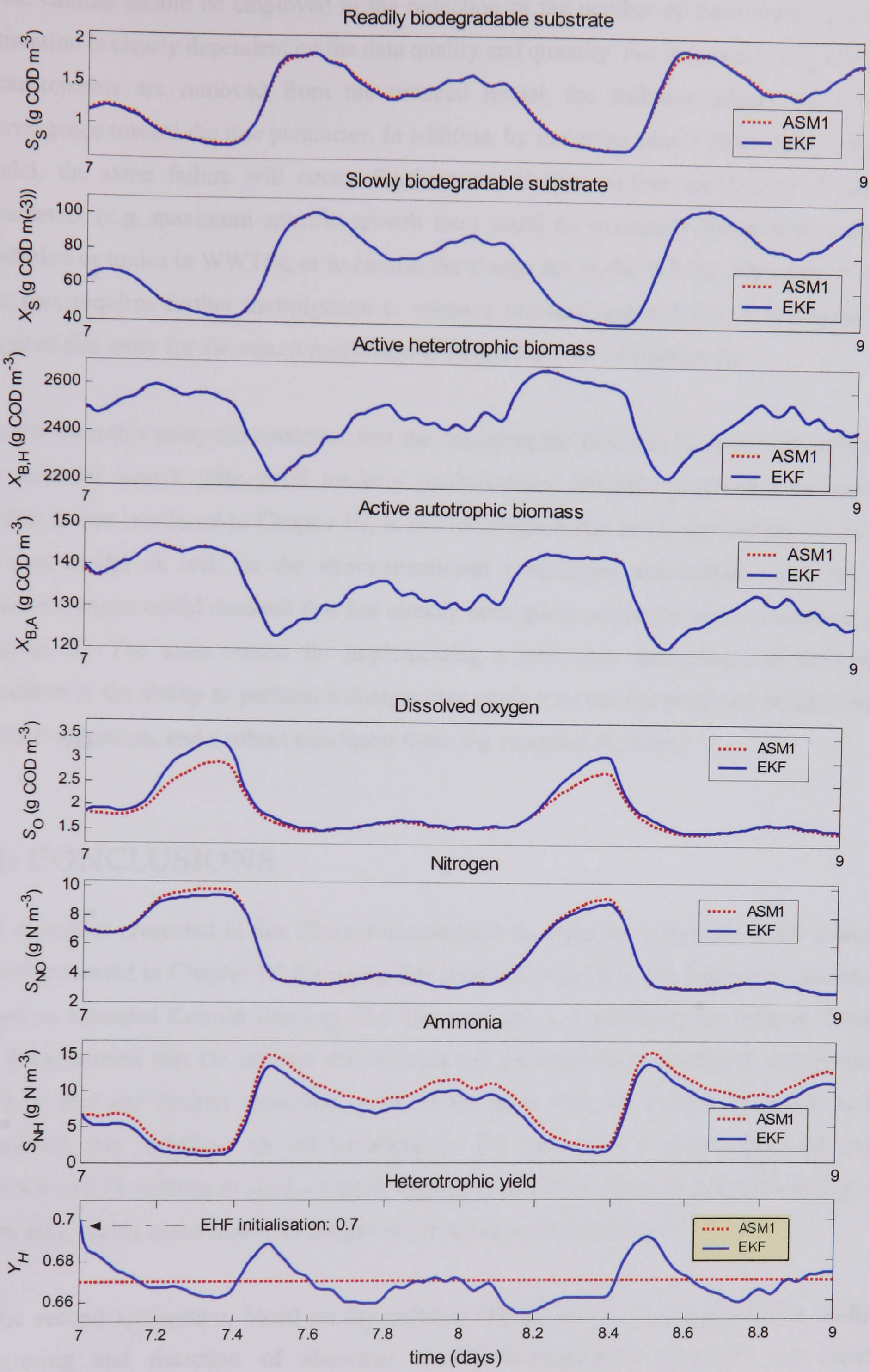


**Figure 5.21** Joint state and parameter estimation comparison between the ASM1 model and the software sensor, with a dry influent.

Great caution should be employed in the reduction of the number of measurements, as the estimation is clearly dependent on the data quality and quantity. For instance, if $X_{B,A}$ and $X_{B,H}$ measurements are removed from the reduced model, the software sensor will fail in convergence toward the true parameter. In addition, by including sensor noise in the reduced model, the same failure will occur. Furthermore, similar on-line monitoring of kinetic parameters (e.g. maximum specific growth rate) could be eventually performed to detect inhibition or toxics in WWTPs, or to control the sludge age in the WWTP. However, even if this area requires further investigation to enhance practical applicability, it is beyond the scope of this work for the reason mentioned in Page 65 and 66 of Chapter III.

Results from this study demonstrated that the heterotrophic yield can be estimated online by the software sensor with good tracking performances. Multiple parametric estimation, similar to that presented in Chapter III, is not investigated due to (1) the complexity of the reduced model as well as the above-mentioned simplifying assumptions, and (2) the extensive unsuccessful research that has already been given within the area, as explained in Chapter III. The main reason for implementing a joint state and parameter estimation algorithm is the ability to perform a comparative study between the proposed results, based on EKF algorithm, and a robust non-linear filter: the extended $H_\infty$ filter.

## 5.4) CONCLUSIONS

The examples presented in this Chapter demonstrate the dynamic behaviour of the reduced model presented in Chapter IV during on-line state and joint state and parameter estimation based on extended Kalman filtering. The first application, considering the reduced 'Model C', demonstrated that the influent disturbances can successfully be modelled with spectral analysis and fast Fourier transform, prior to the state observer design. However, to be consistent, this technique should be adaptive. The successful response from the state observer can be utilised to feed a control algorithm to obtain accurate information (e.g. of ammonia), which could lead to development of robust control strategies.

In the second application, based on the reduced 'Model Ba', a new approach for on-line monitoring and detection of abnormal readily biodegradable substrate and slowly biodegradable substrate concentrations, due to substrate shock load is proposed. The main advantage in designing such algorithm is that toxicity, which depends on substrate concentrations, can now be detected on-line with the proposed observer. However, the

performances of the algorithm should be further investigated in presence of a valid toxic event. Indeed, the proposed solution is based on an airflow failure to simulate such event, as toxicity has not been yet developed with the benchmark plant. Furthermore, toxicity is still not clearly understood.

The first case study of the last application demonstrated that it is possible to estimate on-line the active heterotrophic biomass and the active autotrophic biomass concentrations, with a state observer based on the reduced 'Model A'. Mass balances are initially proposed and enable a relatively accurate approximation of the total suspended solid concentration in each activated sludge tank. Using fractions of these approximations as input to the state observer provided an accurate estimate of $X_{B,H}$ and $X_{B,A}$ concentrations. However, the proposed results are only guaranteed with the selected configuration. In other words, if the ASM2d or ASM3 models, for instance, are selected to describe the dynamic behaviour of the ASP, an accurate estimation of the biomasses is not guarantee, as the selected fractions might differ from one model to another. Furthermore, the observer performances should be investigated on a monthly scale, as the biomass is known as slow changing variable. The last case study illustrated a joint state and parameter estimation where the heterotrophic yield is estimated on-line. The measurement noise is not considered in this application because it generates a loss of information, which leads to a biased estimate of the parameter. Furthermore, five on-line measurements (noise free without delays) are considered to successfully achieve good tracking performances. However, further development should be considered to enhance practical applicability of the proposed results. For instance, process noise should be considered within the original ASM1 model, as proposed in the following Chapter.

The study from this Chapter also demonstrated that the software sensors need to be robust against modelling errors and parameter variations. This has motivated the applications of extended $H_\infty$ filter in the next Chapter.

# Chapter VI

# Robust non-linear filtering based-extended $H_\infty$ filters

In this chapter, three applications based on extended $H_\infty$ filtering are developed and their performances are compared with state observers and software sensors based upon extended Kalman filtering. Initially, the design of a state observer based on the 'Model C' is presented, where disturbances and sensor delays are not considered. The filter gain and convergence properties are compared with the EKF in the presence of significant process noise, before introducing unknown inputs and measurement delays into the system. The second application aims at confirmation of the finding by realising a similar study on the augmented 'Model Bb', including parametric uncertainties. Lastly, the final case study concentrates on investigating the responses of the software sensors when the sewer system and river are connected to the treatment plant. Parts of the material in this chapter are covered in Benazzi *et al.*, (2005a), Benazzi and Katebi (2006), Benazzi *et al.*, (2006).

## 6.1) STATE OBSERVER BASED EXTENDED $H_\infty$ FILTER

The main purpose of the following application is to apply the robust non-linear theory detailed in Chapter III on the 'Model C' described in Chapter IV. In other words, an extended $H_\infty$ filter algorithm is implemented on the 'Model C' and its performances are compared with the standard extended Kalman filter. The state observers and software sensors presented in Chapter V minimise the covariance of the estimation errors, assuming that the

system under consideration is exactly known, as well as the statistical properties of the noise sources. Unfortunately, in real applications, these assumptions are unrealistic as the noise sources statistics are not exactly known. Furthermore, uncertainties in the model are unavoidable, which limits the scope of application of the linear and/or extended Kalman filtering approach and fail to guarantee the robustness of such filters. In the following work, the robustness is defined as the ability of the observer algorithm and/or software sensor to converge toward the real states and parameters of the plant when the model is corrupted by process noise. In other words, a software sensor is robust if it possesses the ability to maintain good tracking performances, measured for example in terms of its tracking accuracy, given that modeling errors exists within the system dynamics.

Therefore, in the following application, a robust estimation technique is proposed. It consist in minimising the worst possible effects of the modelling errors and additive noise on the signal estimation errors by introducing uncertainties in the models. It can deal with nonlinearities through the Extended $H_\infty$ Filter (EHF) feature, from local linearisation occurring at each iteration, as presented in Chapter III.

## Observer based EHF for state estimation

The linearised $H_\infty$ filter algorithm, which is identical to the KF algorithm with the exception of the resolution of the Riccati equation, is given by

$$\begin{aligned}\dot{\mathbf{X}}(t) &= \mathbf{A}(t)\mathbf{X}(t) + \mathbf{B}(t)\mathbf{u}(t) + \mathbf{G}_1\mathbf{w}(t) + \mathbf{K}_h(\mathbf{y}(t) - \mathbf{z}(t)) \\ \mathbf{y}(t) &= \mathbf{C}_1(t)\mathbf{X}(t) + \mathbf{G}_2\mathbf{v}(t) \\ \mathbf{z}(t) &= \mathbf{C}_2(t)\mathbf{X}(t)\end{aligned} \tag{6.1}$$

where the $H_\infty$ gain $\mathbf{K}_h$ is deduced from the properties of the state space model to minimise the worst possible effects of the modelling errors and additive noise on the signal estimation. $\mathbf{z}$ is the estimated output vector, $\mathbf{G}_1\mathbf{w}(t)$ and $\mathbf{G}_2\mathbf{v}(t)$ represent the process and measurement noise with noise sequences of zero means and covariance $\mathbf{Q}$ and $\mathbf{R}$, respectively. Similar to the Kalman filter, which is a linear observer, the extended model must be linearised with respect to augmented states, as described in Chapter III. The state, input and system output vectors are of the form (Nagpal and Khargonekar, 1991; Katebi and Grimble, 1998)

$$\mathbf{X}(t) = \begin{bmatrix} S_S(t) & X_S(t) & S_O(t) & S_{NO}(t) & S_{NH}(t) & S_{ND}(t) & X_{ND}(t) \end{bmatrix}^T \tag{6.2}$$

$$\mathbf{u}(t) = \left[ S_{S,in}(t) \quad X_{S,in}(t) \quad S_{O,in}(t) \quad S_{NO,in}(t) \quad S_{NH,in}(t) \quad S_{ND,in}(t) \quad X_{ND,in}(t) \quad Q_{in} \quad K_L a_{in} \right]^T \tag{6.3}$$

$$\mathbf{z}(t) = \left[ S_{S,ef}(t) \quad X_{S,ef}(t) \quad S_{O,ef}(t) \quad S_{NO,ef}(t) \quad S_{NH,ef}(t) \quad S_{ND,ef}(t) \quad X_{ND,ef}(t) \right]^T \tag{6.4}$$

The system (**A**), input (**B**), system output ($\mathbf{C}_1$) and estimated outputs ($\mathbf{C}_2$) matrices of Equation (6.1), are of the form:

$$\mathbf{A}(t) = \begin{bmatrix} \frac{\partial S_S(t)}{\partial S_S(t)} & \frac{\partial S_S(t)}{\partial X_S(t)} & \cdots & \cdots & \frac{\partial S_S(t)}{\partial X_{ND}(t)} \\ \vdots & & \ddots & & \vdots \\ \frac{\partial X_{ND}(t)}{\partial S_S(t)} & \cdots & & \cdots & \frac{\partial X_{ND}(t)}{\partial X_{ND}(t)} \end{bmatrix}, \quad \mathbf{B}(t) = \begin{bmatrix} \frac{\partial S_S(t)}{\partial Q(t)} & \frac{\partial S_S(t)}{\partial K_L a(t)} \\ \vdots & \vdots \\ \frac{\partial X_{ND}(t)}{\partial Q(t)} & \frac{\partial X_{ND}(t)}{\partial K_L a(t)} \end{bmatrix},$$

$$\mathbf{C}_1(t) = \mathbf{C}_2(t) = \begin{bmatrix} \ddots & & 0 \\ & I & \\ 0 & & \ddots \end{bmatrix} \tag{6.5}$$

The filter minimises the following cost function (Nagpal and Khargonekar, 1991):

$$J = \sup_{\mathbf{w} \in L_2[0,\infty]} \frac{\|\tilde{\mathbf{z}}\|_2^2}{\|\mathbf{w}\|_2^2} < \gamma^2 \tag{6.6}$$

with $\tilde{\mathbf{z}}(t) = \mathbf{z}(t) - \hat{\mathbf{z}}(t)$ and for $\gamma > 0$, where gamma ($\gamma$) is the pre-specified $H_\infty$ performance based on the following assumptions (Doyle *et al.*, 1989)

(i) (**A**,**B**) is stabilisable and ($\mathbf{C}_1$,**A**) is detectable

(ii) (**A**,$\mathbf{G}_1$) is stabilisable and ($\mathbf{C}_2$,**A**) is detectable ,

The filtering problem is stated as the minimisation of the cost function $J$ in Equation (6.6) for a known value of $\gamma > 0$. For the time invariant systems, the optimal value of $\gamma$ is found by selecting a large value of $\gamma$ and solving the algebraic Riccati equation given by (Doyle *et al.*, 1989; Nagpal and Khargonekar, 1991)

$$\mathbf{A}(t)\mathbf{P}(t)+\mathbf{P}(t)\mathbf{A}^{T}(t)-\mathbf{P}(t)(\gamma^{-2}\mathbf{C}_{2}{}^{T}(t)\mathbf{C}_{2}(t)-\mathbf{C}_{1}{}^{T}(t)\mathbf{R}^{-1}(t)\mathbf{C}_{1}(t))\mathbf{P}(t)+\mathbf{G}_{1}(t)\mathbf{Q}\mathbf{G}_{1}^{T}(t)=0\,' \tag{6.7}$$

in order to calculate the $H_\infty$ filter gain ($\mathbf{K}_h$) given by

$$\mathbf{K}_h=\mathbf{P}(t)\mathbf{C}_1^{T}(t)\mathbf{R}^{-1}(t). \tag{6.8}$$

The value of $\gamma$ is reduced in the usual manner until one of the eigenvalues of the reduced model becomes imaginary or negative. However, because the reduced model is time varying, the value of $\gamma$ should be found at each time instant. This will impose a high level of computational load on the filter and make it impractical in real applications. Therefore, an alternative scheme, utilised in this work, is the use of a time decreasing exponential function for $\gamma$ starting from a large value, i.e. (Katebi and Grimble, 1998)

$$\gamma(t)=\gamma_{\max}e^{-\alpha t}+\gamma_{\min} \tag{6.9}$$

The rate of decay of the exponential can be set to 3 to 4 times the plant dominant time constants. The scalar $\gamma_{\min}$ depends on the weighting functions used to design the filter, as illustrated in Figure (6.1). The filter gain is similar to the KF gain when $\gamma$ is large ($H_2$). As $\gamma$ decreases, the filter converges to the optimal $H_\infty$ filter.

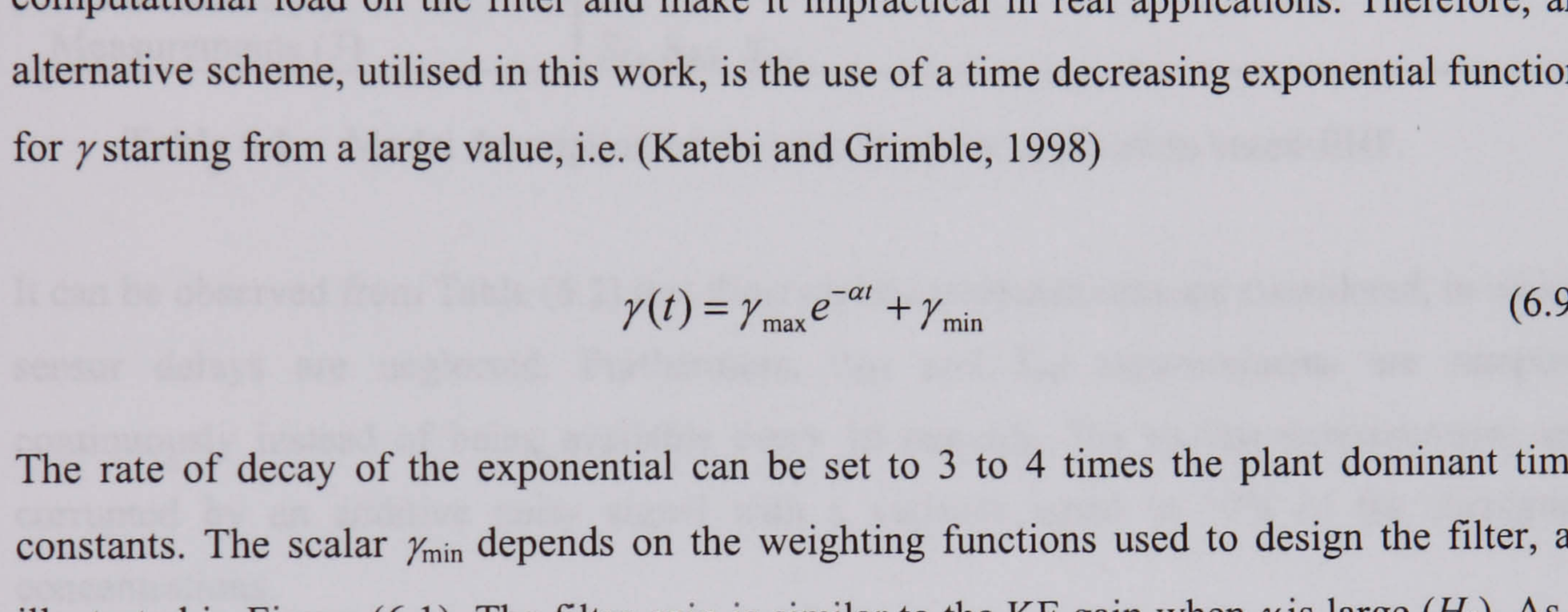


**Figure 6.1** Calculation of gamma ($\gamma$), which is the pre-specified $H_\infty$ performance.

The $\gamma_{min}$ should be usually set to an optimal value to ensure a viable solution to the Riccati equations. This procedure significantly reduces the computational burden and ensures that the filter is stable over the estimation horizon (Katebi and Grimble, 1998).

## State observers application based-EHF

The characteristics of selected model are described in Table (6.1), in terms of inputs and selected measurements. The sensors characteristics are detailed in Table (6.2).

| Selected model | 'Model C' (presented in Chapter IV) |
|---|---|
| Inputs (8) | $S_{S,in}$, $X_{S,in}$, $S_{O,in}$, $S_{NO,in}$, $S_{NH,in}$, $S_{ND,in}$, $Q_{in}$, $K_La_{in}$ |
| Disturbances (0) | - |
| Measurements (3) | $S_O$, $S_{NO}$, $S_{NH}$ |

**Table 6.1** Model description of the state observer application based-EHF.

It can be observed from Table (6.2) that three on-line measurements are considered, in which sensor delays are neglected. Furthermore, $S_{NO}$ and $S_{NH}$ measurements are sampled continuously instead of being available every 10 minutes. The on-line measurements are corrupted by an additive noisy signal with a variance equal to 10% of the corrupted concentrations.

| | Variance (σ) | Delay (min.) | Low-level detec. limit | Sampling time (min.) |
|---|---|---|---|---|
| Oxygen ($S_{O,ef}$) | 0.172 | - | 0.1 | continuous |
| Nitrate and nitrite nitrogen ($S_{NO,ef}$) | 0.654 | - | 0.1 | continuous |
| $NH_4^+ + NH_3$ nitrogen ($S_{NH,ef}$) | 0.555 | - | 0.2 | continuous |

**Table 6.2** On-line ($S_O$, $S_{NO}$ and $S_{NH}$) measurements characteristics, which are included in the simulation parameters.

A schematic overview of the design is presented in Figure (6.2) where it can be observed that the disturbances are not considered. Indeed, for a better comparison of performances, all the inputs of the reduced model are initially assumed to be known. However, an application including disturbances modelling is investigated later in this section. Each of the differential Equations (4.2) to (4.3) and (4.7) to (4.11), describing the dynamic behaviour of the original ASM1 model, are corrupted by uncorrelated white Gaussian noise sequences, with a corresponding covariance matrix (**Q**) given in Equation (6.10).

$$\mathbf{Q} = \begin{bmatrix} 8464 & & & & & & \ddots & \\ & 1.514\times10^{7} & & & & & & \\ & & 29515 & & & 0 & & \\ \ddots & & & 106961 & & & \ddots & \\ & 0 & & & 196993.9 & & & \\ & & & & & 1718.1 & & \\ & & \ddots & & & & 15462.9 & \end{bmatrix} \quad (6.10)$$

Note that only the first aerobic tank is corrupted by process noise, as the software sensor applications are based on this specific reactor. It is possible to corrupt the entire benchmark plant and apply state observers and/or software sensors on each of the reactor but this work is however beyond the scope of this thesis.

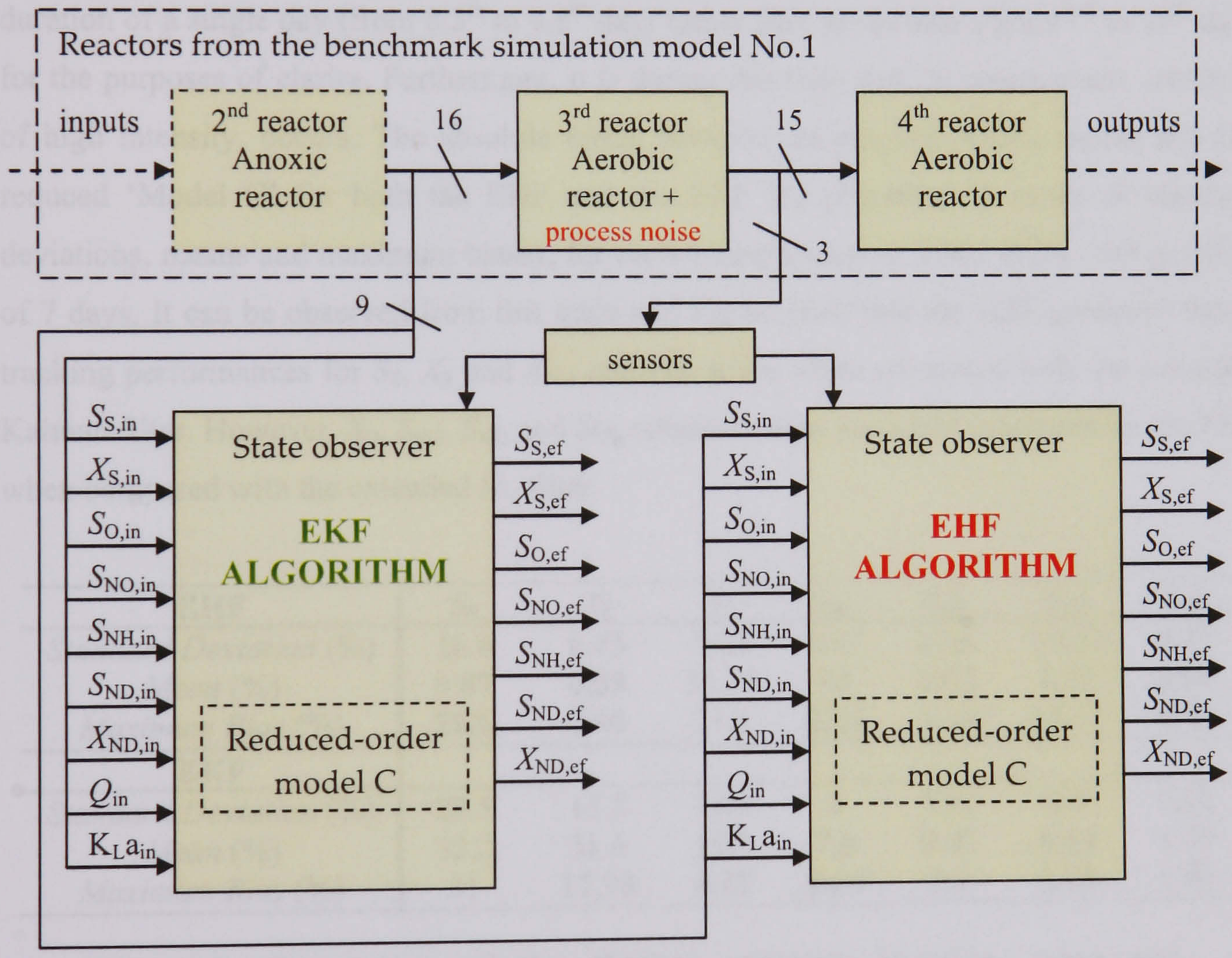


**Figure 6.2** State observer design based extended $H_\infty$ filter and extended Kalman filter. Disturbances are not considered and all inputs are assumed available. Three on-line measurements are considered, which are: $S_O$, $S_{NO}$ and $S_{NH}$.

Simulation results are presented in Figure (6.3), where the storm wastewater data are selected to characterise the influent for the model. Both EHF and EKF minimisation errors between the estimated and the true concentrations are represented in the frequency domain through a power spectral analysis. It can be observed that for each of the estimated variables, the error is significantly improved with the EHF feature when compared with the EKF. In particular, for $X_S$ and $X_{ND}$ concentrations, the error is quasi non-existent between the real and the estimated concentrations with the EHF feature. Therefore, it can be concluded that the sate observer based-extended $H_\infty$ filter is more robust than the extended Kalman filter in terms of minimising the error between the real and the estimated concentrations, in the frequency domain.

Simulation results that are presented in Figure (6.4) illustrate the state observer responses from both the EKF and the EHF, in the time domain. These results concentrate only upon a duration of a single day (from $8.5^{th}$ to $9.5^{th}$ day) rather than seven days (from $7^{th}$ to $14^{th}$ day) for the purposes of clarity. Furthermore, it is during this time that the storm event, which is of high intensity, occurs. The absolute errors between the original ASM1 model and the reduced 'Model C' for both the EHF and the EKF are presented in terms of standard deviations, means and maximum biases, for each concentration in Table (6.3), over a period of 7 days. It can be observed from this table and Figure (6.4) that the EHF produced better tracking performances for $S_S$, $X_S$ and $X_{ND}$ concentrations when compared with the extended Kalman filter. However, $S_O$, $S_{NO}$, $S_{NH}$ and $S_{ND}$ concentrations are better estimated by the EKF when compared with the extended $H_\infty$ filter.

| **EHF** | $S_S$ | $X_S$ | $S_O$ | $S_{NO}$ | $S_{NH}$ | $S_{ND}$ | $X_{ND}$ |
|---|---|---|---|---|---|---|---|
| *Standard Deviation* (%) | **16.6** | **0.15** | **5.21** | 4.35 | **2.06** | 10.52 | **0.13** |
| *Mean* (%) | **9.87** | **0.89** | 33.73 | 20 | 6.54 | 4.49 | **0.53** |
| *Maximum Bias* (%) | **20.6** | **0.80** | 21.1 | 22.8 | 4.98 | 12.37 | **0.25** |
| **EKF** | | | | | | | |
| *Standard Deviation* (%) | 22.5 | 13.5 | 12.4 | **3** | 3.91 | **0.8** | 4.92 |
| *Mean* (%) | 35.2 | 31.6 | **10.1** | **7.8** | **0.47** | **0.14** | 4.09 |
| *Maximum Bias* (%) | 31 | 17.98 | **4.15** | **8.66** | **2.2** | **1.23** | 4.49 |

**Table 6.3** Comparison of the absolute standard deviation, mean and maximum bias, in percentage, between the original ASM1 and the EHF and EKF estimation based on the 'Model C'. The best performances are emphasised.

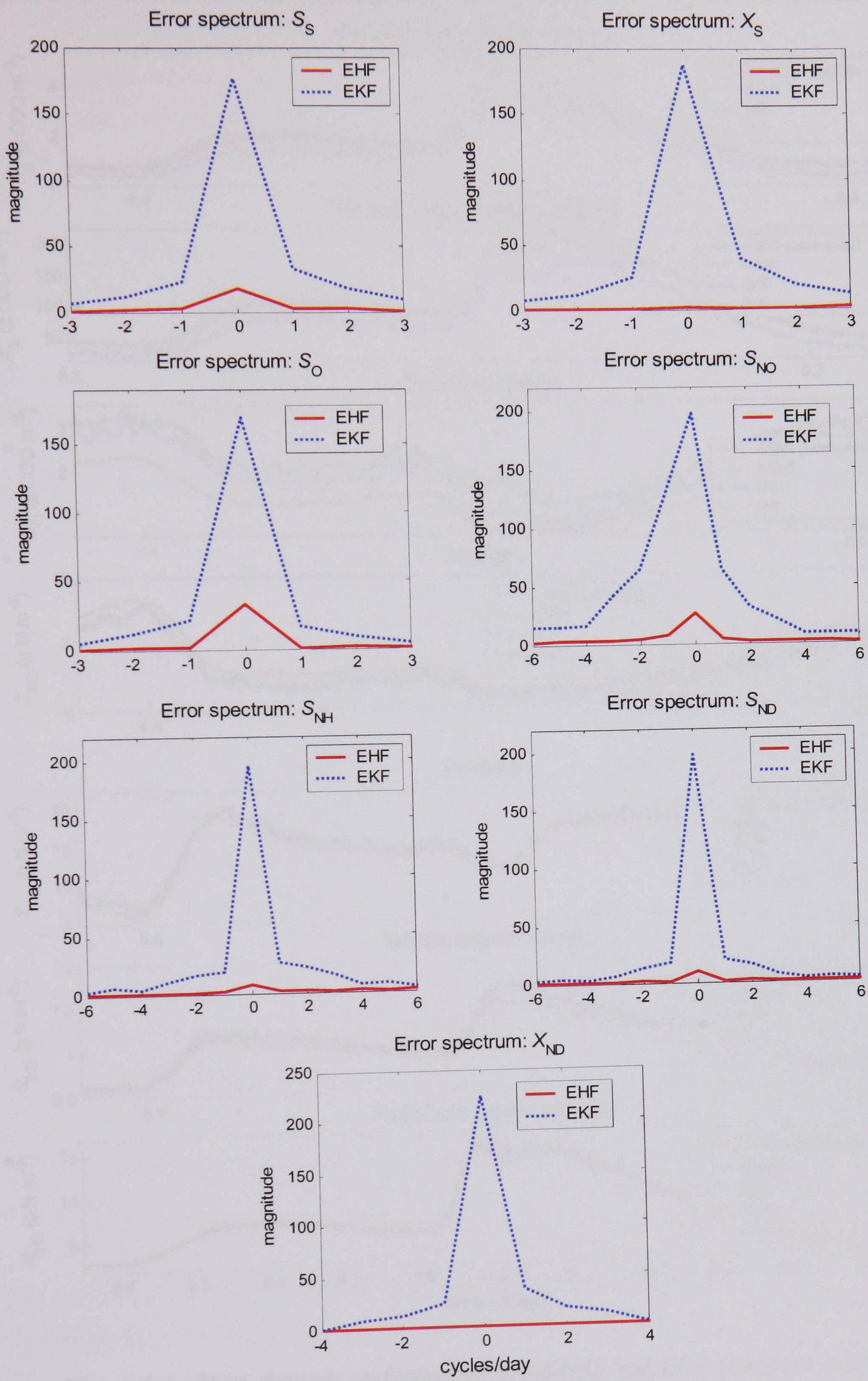


**Figure 6.3** FFT of the relative estimation errors between the estimated concentrations from both the EKF and EHF and the corrupted ASM1 model. Disturbances are not considered and $\gamma = 1.52*10^{-8}$.

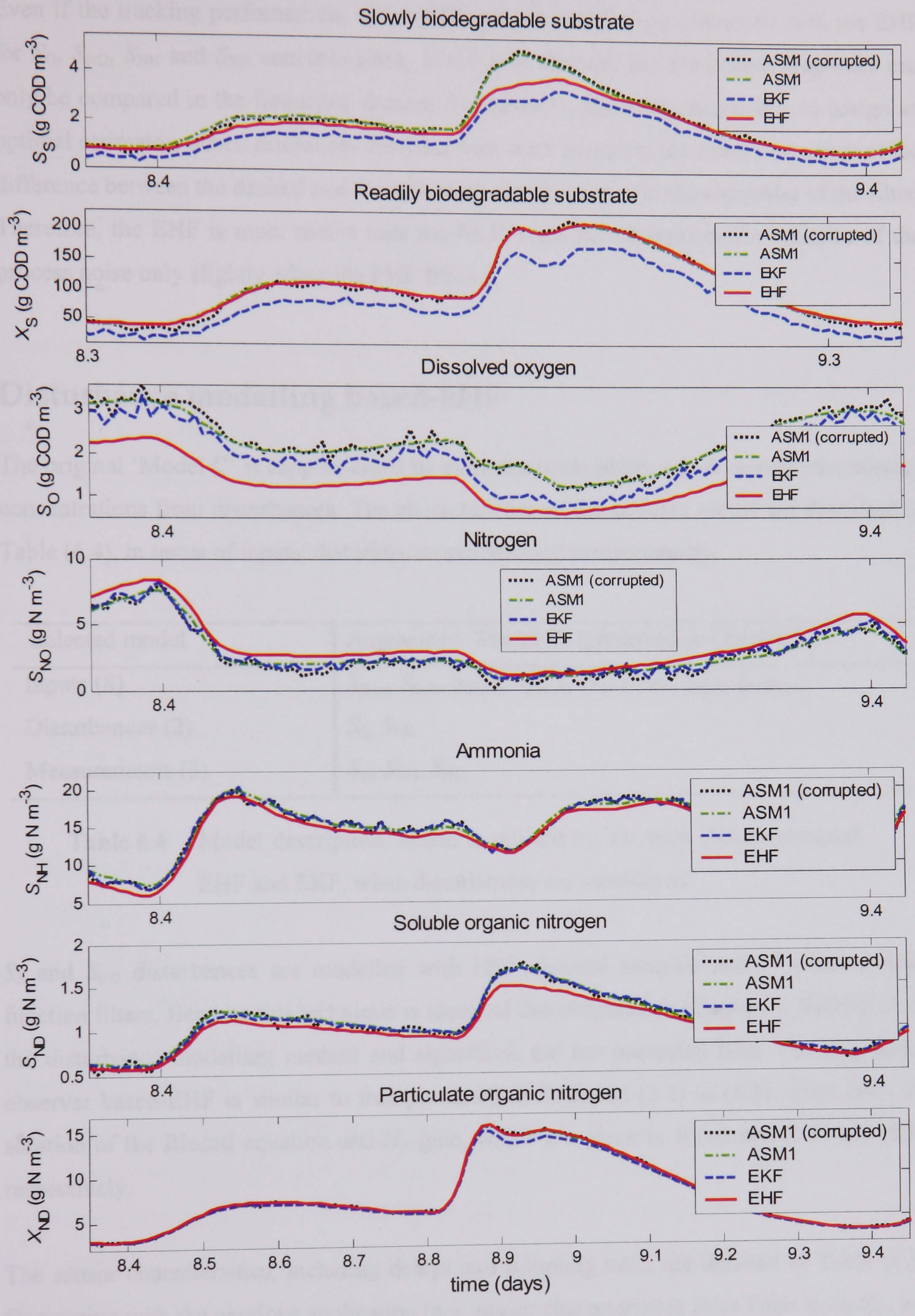


**Figure 6.4** State observer performances based-EHF and EKF compared with the original and corrupted ASM1 models. The initial conditions of the algorithms are assumed to be known. Disturbances are not considered and $\gamma = 1.52*10^{-8}$.

Even if the tracking performances of the EKF are enhanced when compared with the EHF for $S_O$, $S_{NO}$, $S_{NH}$ and $S_{ND}$ concentrations, in the time domain, the robustness properties can only be compared in the frequency domain. Furthermore, the main objective is to design an optimal estimator, which minimises the maximum error spectrum (or worst case error) of the difference between the desired and the estimated signals subject to the constraint of the filter. Therefore, the EHF is more robust than the EKF, since the changes in the variance of the process noise only slightly affect the EHF feature.

## Disturbance modelling based-EHF

The original 'Model C' is supplemented by extra states variables, which recreate the missing concentrations from disturbances. The characteristics of the selected model are described in Table (6.4), in terms of inputs, disturbances and selected measurements.

| Selected model | Augmented 'Model C' (presented in Chapter V) |
|---|---|
| Inputs (8) | $X_{S,in}$, $S_{O,in}$, $S_{NO,in}$, $S_{NH,in}$, $Q_{in}$, $K_La_{in}$, $\zeta_{SS,in}$, $\zeta_{SND,in}$ |
| Disturbances (2) | $S_S$, $S_{ND}$ |
| Measurements (3) | $S_O$, $S_{NO}$, $S_{NH}$ |

**Table 6.4** Model description, which is utilised by the state observers based-EHF and EKF, when disturbances are considered.

$S_S$ and $S_{ND}$ disturbances are modelled with FFT, spectral analysis and 1st order transfer function filters. Because this technique is identical that proposed in Chapter V, Section (2.1), the disturbance modelling method and algorithms are not presented here. The augmented observer based-EHF is similar to that presented in Equation (5.1) to (5.5), apart from the solution of the Riccati equation and $H_\infty$ gain, which are given in Equations (6.7) and (6.8), respectively.

The sensor characteristics, including delays and sampling time, are detailed in Table (6.5). Comparing with the previous application (e.g. sensor characteristics from Table 6.2), $S_{NO}$ and $S_{NH}$ measurements are sampled every ten minutes instead of being available continuously. Furthermore, $X_S$ influent concentration is assumed available from the second reactor every thirty minutes with thirty minutes delays. The on-line measurements are corrupted by an additive noisy signal with a variance equal to 10% of the corrupted concentrations.

| | Variance (σ) | Delay (min.) | Low-level detec. limit | Sampling time (min.) |
|---|---|---|---|---|
| Oxygen ($S_{O,ef}$) | 0.172 | - | 0.1 | continuous |
| Nitrate and nitrite nitrogen ($S_{NO,ef}$) | 0.654 | 10 | 0.1 | 10 |
| $NH_4^+$ +$NH_3$ nitrogen ($S_{NH,ef}$) | 0.555 | 10 | 0.2 | 10 |
| Slowly bio. substrate ($X_{S,in}$) | - | 30 | 0.1 | 30 |

**Table 6.5** On-line ($S_O$, $S_{NO}$ and $S_{NH}$) measurements characteristics included in the simulation parameters when disturbances are considered.

A schematic overview of the design implementation is presented in Figure (6.5) where the disturbances inclusions are clearly illustrated. Similarly to the previous case, each of the differential Equations (4.2) to (4.3) and (4.7) to (4.11), describing the dynamic behaviour of the original ASM1 model, are corrupted by uncorrelated white Gaussian noise sequences, with the covariance matrix given in Equation (6.10). Simulation results are presented in Figure (6.6), where the storm wastewater data are also selected to characterise the influent for the model. Both EHF and EKF minimisation errors between the estimated and the true concentrations are represented in the frequency domain through a power spectral analysis. The error is significantly improved with the EHF feature when compared with the EKF. These results confirm the robustness properties of the EHF even when disturbances are considered within the augmented 'Model C', in the frequency domain.

To further demonstrate the finding presented in Chapter III, Section (3.4), the convergence properties of the extended $H_\infty$ filter are illustrated in the time domain. In other words, the initial conditions of the 'Model C' are not assumed to be exactly known. Results are presented in Figure (6.7) where it can be observed that the EHF converges toward the real state in approximately one hour for all concentrations. Furthermore, when the EKF is initialised similarly to the EHF, the convergence properties toward the real state are achieved in approximately 15 minutes for all concentrations. In this specific application the EKF is 4 times faster than the EHF. The performance of the EHF could be eventually improved by increasing gamma ($\gamma$), but the robustness properties of the extended $H_\infty$ filter would be lost (e.g. leading to an $H_2$ filter). The proposed results confirm that the EKF convergence properties are improved when compared with the EHF.

In simulation results presented in Figure (6.8), it can be observed that the extended $H_\infty$ filter tracking performances are improved when compared with the extended Kalman filter, in the time domain.

The proposed results are illustrated for a single day (from 8.5$^{th}$ to 9.5$^{th}$ day) rather than seven days (from 7$^{th}$ to 14$^{th}$ day) for the purposes of clarity. The absolute errors between the original ASM1 model and the augmented 'Model C' for both the EHF and the EKF are presented in terms of standard deviations, means and maximum biases, for each concentration in Table (6.6) over a period of 7 days. It can be observed that the EHF produced better tracking performances for $S_S$, $X_S$, $S_{NH}$, $S_{ND}$ and $X_{ND}$ concentrations when compared with the EKF.

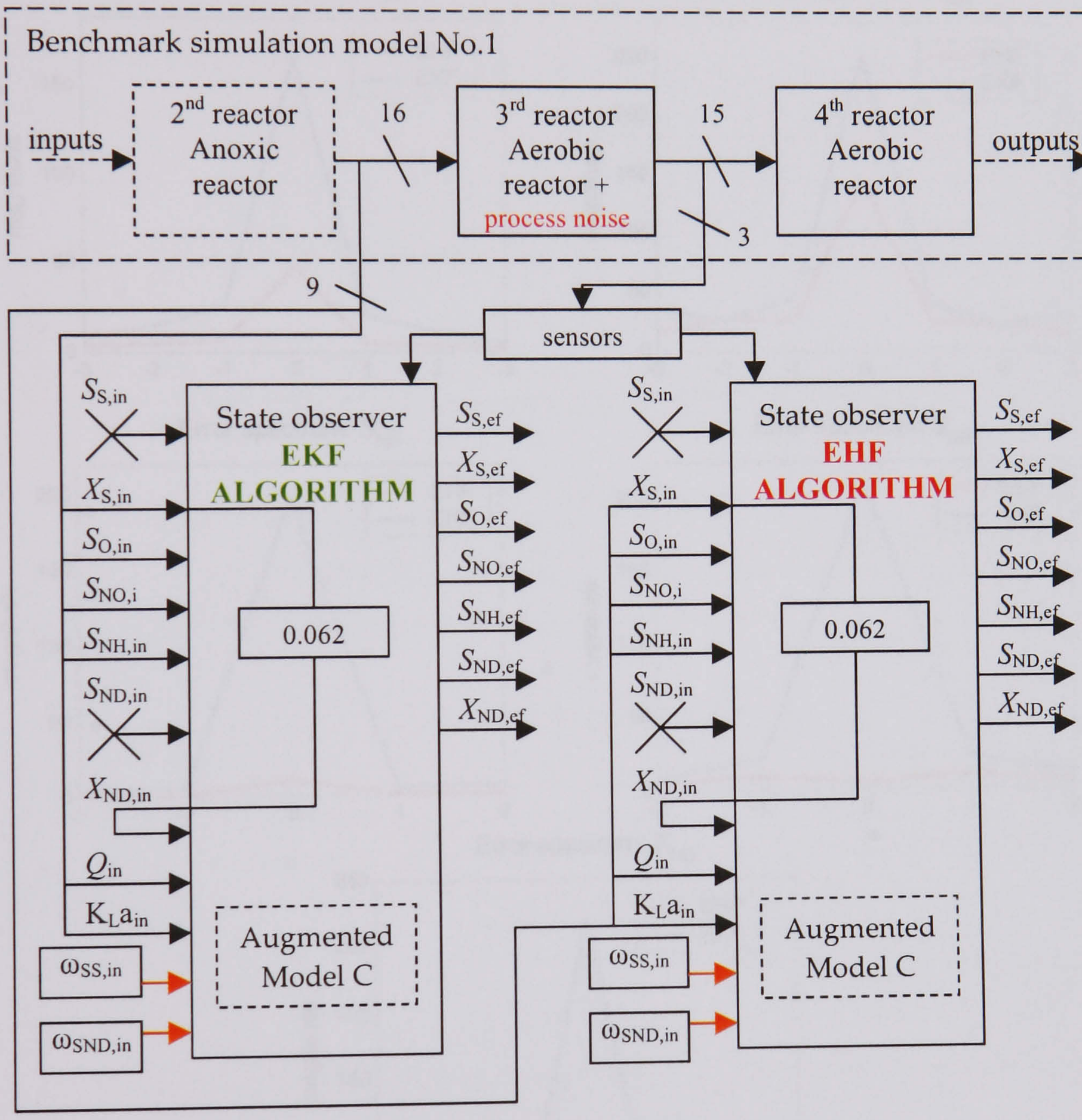


**Figure 6.5** State observer design based extended $H_\infty$ filter and extended Kalman filter. $S_S$ and $S_{ND}$ concentrations are modelled as disturbances with FFT, spectral analysis and 1$^{st}$ order filters. $S_O$, $S_{NO}$ and $S_{NH}$ measurements are considered within the 'sensors' box.

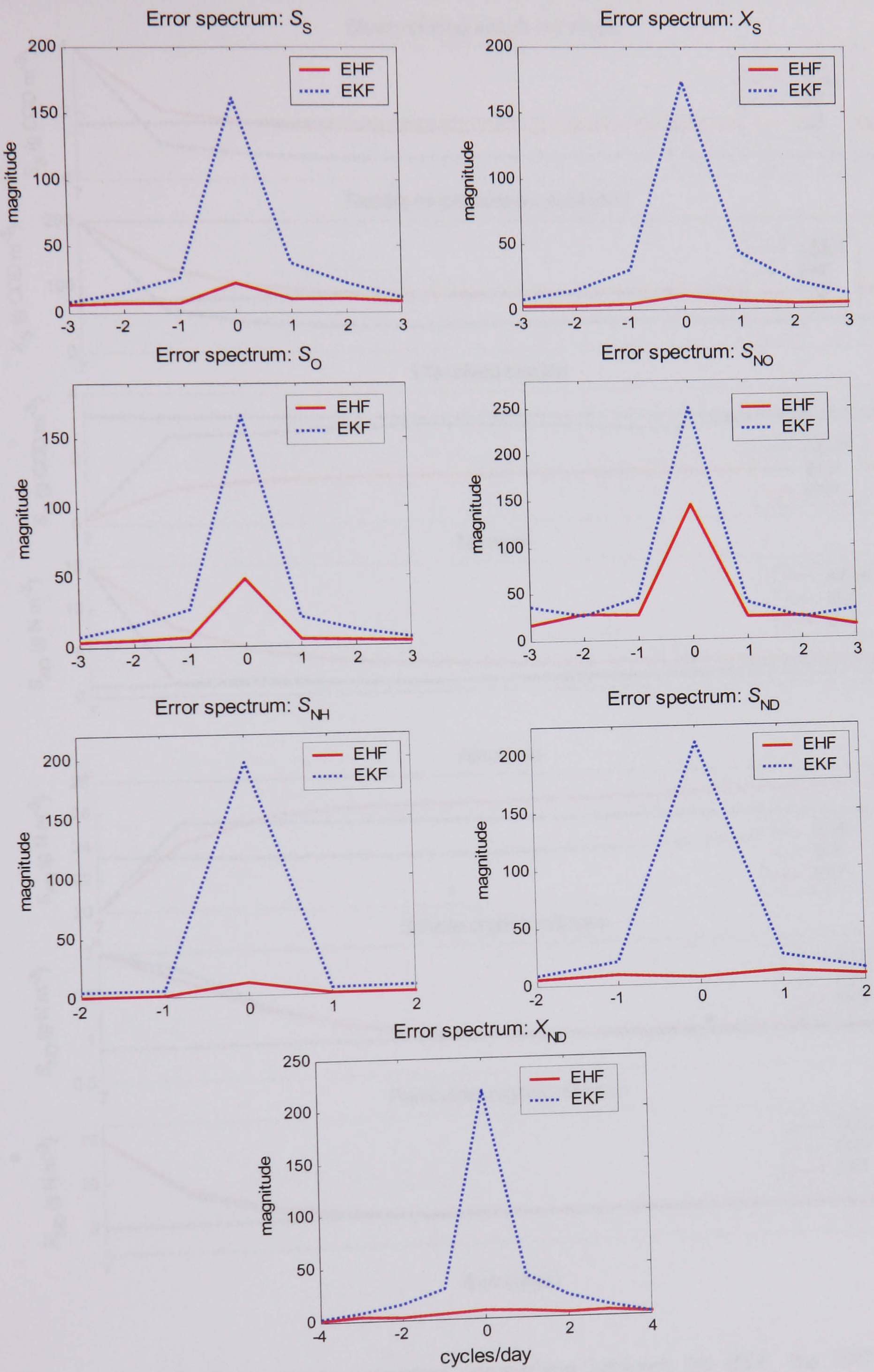


**Figure 6.6** FFT of the relative estimation errors between the estimated concentrations from both the EKF and EHF and the corrupted ASM1 model. Disturbances are not considered and $\gamma = 1.52*10^{-8}$.

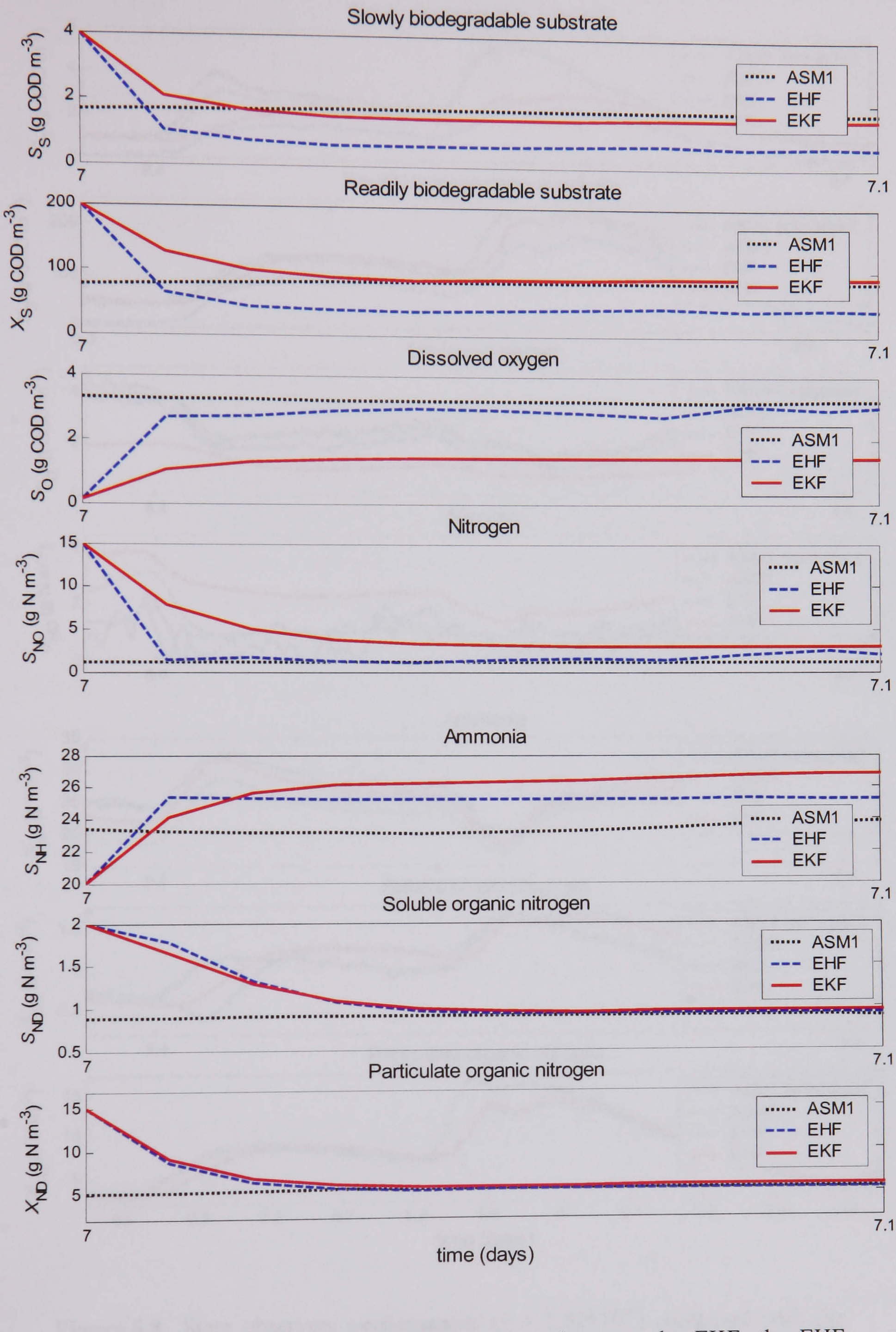


**Figure 6.7** Convergence properties comparison between the EKF, the EHF toward the concentrations of the original ASM1 model. Disturbances are considered within the algorithms based on the augmented 'Model C' presented in Chapter V ($\gamma = 1.52*10^{-8}$).

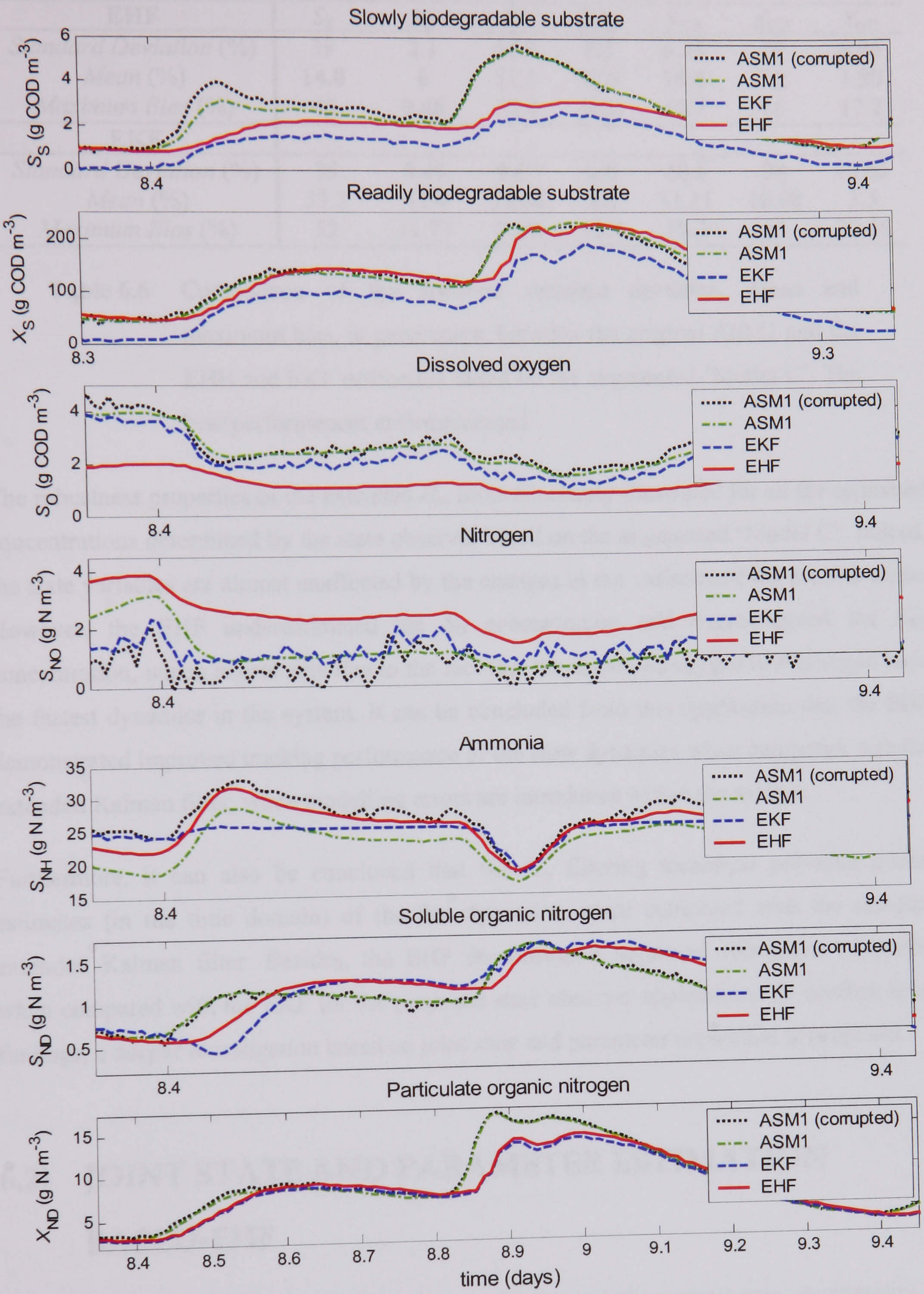


**Figure 6.8** State observers performances ($\gamma = 1.52*10^{-8}$) compared with the original and corrupted ASM1 models, during a storm event. $S_S$ and $S_{ND}$ concentrations are considered as disturbances, as detailed in Chapter V.

| **EHF** | $S_S$ | $X_S$ | $S_O$ | $S_{NO}$ | $S_{NH}$ | $S_{ND}$ | $X_{ND}$ |
|---|---|---|---|---|---|---|---|
| *Standard Deviation* (%) | 39 | 2.1 | 48.8 | 8.8 | **6.35** | **25** | **6.96** |
| *Mean* (%) | **14.8** | **6** | 51.5 | 45.9 | **10.6** | **7.2** | **1.80** |
| *Maximum Bias* (%) | **43** | **0.48** | 50.8 | 46.5 | **10.7** | **16** | **17.2** |
| **EKF** | | | | | | | |
| *Standard Deviation* (%) | **35** | 6.48 | **9.67** | **6.8** | 20.6 | 28 | 10.65 |
| *Mean* (%) | 53.3 | 43.4 | **11.34** | **5.2** | 11.11 | 10.98 | 3.5 |
| *Maximum Bias* (%) | 52 | 11.77 | **3.29** | **15.4** | 18.3 | 63 | 20.46 |

**Table 6.6** Comparison of the absolute standard deviation, mean and maximum bias, in percentage, between the original ASM1 and the EHH and EKF estimation based on the augmented 'Model C'. The best performances are emphasised.

The robustness properties of the extended $H_\infty$ filter are clearly illustrated for all the estimated concentrations determined by the state observer based on the augmented 'Model C'. Indeed, the state variables are almost unaffected by the changes in the variance of the process noise. However, the EHF underestimated the $S_O$ concentration and overestimated the $S_{NO}$ concentration, which is probably due to the fact that the dissolved oxygen and nitrogen have the fastest dynamics in the system. It can be concluded from this application that the EHF demonstrated improved tracking performance of the slow dynamics when compared with the extended Kalman filter, when modelling errors are introduced within the system.

Furthermore, it can also be concluded that the $H_\infty$ filtering technique provided poorer estimates (in the time domain) of the fast dynamics, when compared with the standard extended Kalman filter. Besides, the EHF demonstrated improved robustness properties when compared with the EKF for the proposed state observer application. To confirm these findings, a deeper investigation based on joint state and parameter estimation is proposed.

## 6.2) JOINT STATE AND PARAMETER ESTIMATION BASED-EHF

It is not sufficient to develop state observers without including parametric uncertainties in the model. Indeed, to verify the robustness of software sensor, it is important to also perform parameter estimation. Therefore, the main objective of this application is to perform joint state and parameter estimation, where the heterotrophic yield is estimated online and the results are compared with the standard extended Kalman filter.

$Y_H$ is modelled as an integrator that is driven by white noise and augmented to the initial reduced-order 'Model Bb' where constant and dry influent wastewater data are used to characterize the influent wastewater for the reduced model. The characteristics of the selected model are described in Table (6.7).

| Selected model | Augmented 'Model Bb' (presented in Chapter V) |
|---|---|
| Inputs (10) | $S_{S,in}$, $X_{S,in}$, $X_{B,H,in}$, $X_{B,A,in}$, $S_{O,in}$, $S_{NO,in}$, $S_{NH,in}$, $Q_{in}$, $K_La_{in}$, $\zeta_{YH,in}$ |
| Disturbances (0) | - |
| Measurements (2) | $S_S$, $X_{B,H}$, $X_{B,A}$, $S_O$, $S_{NO}$ (on-line), |

**Table 6.7** Model description, which is utilised by the software sensor.

As some of the ASM1 model parameters are non-identifiable, on-line measurements of $S_S$, $X_{B,H}$, $X_{B,A}$, $S_O$ and $S_{NO}$ are considered to improve the estimation algorithm response. Similar to the application presented in Chapter V, this specific case study remains theoretical and is performed to compare the profiles parameters on the BSM1 model between the EHF and EKF. A schematic overview of the design implementation is presented in Figure (6.9). On-line measurements are also assumed noise free and sensors delays are not considered. The extended $H_\infty$ filter algorithm is not presented here, as it is similar to the one given by Equations (5.49) to (5.55), introduced in Chapter V. The computation of the augmented $H_\infty$ gain and Riccati equations, which differ from the standard EKF ones, are of the form of Equations (6.7) and (6.8), respectively.

Simulation results are presented in Figure (6.10) where the constant wastewater data file is selected to characterise the influent for the model. Both EHF and EKF minimisation errors between the estimated and the true concentrations are represented in the frequency domain through a spectral analysis. For each of the estimated concentrations, it is obvious that the error is significantly improved and quasi non-existent with the EHF feature when compared with the EKF. However, the FFT of the minimisation error between the estimated and the true parameter $Y_H$ is similar, but still improved with the EHF, when compared to the EKF one. This is explained by the fact that gamma, the pre-specified $H_\infty$ performance, is not set to its optimum value. In other words, if $\gamma$ is set to $6.25*10^{-8}$ (e.g. the optimum value) for which the eigenvalues of the reduced model becomes imaginary, the augmented software sensor fails to converge toward the true parameter. Therefore, $\gamma$ is set to $1*10^{-3}$ to guarantee the algorithm convergence.

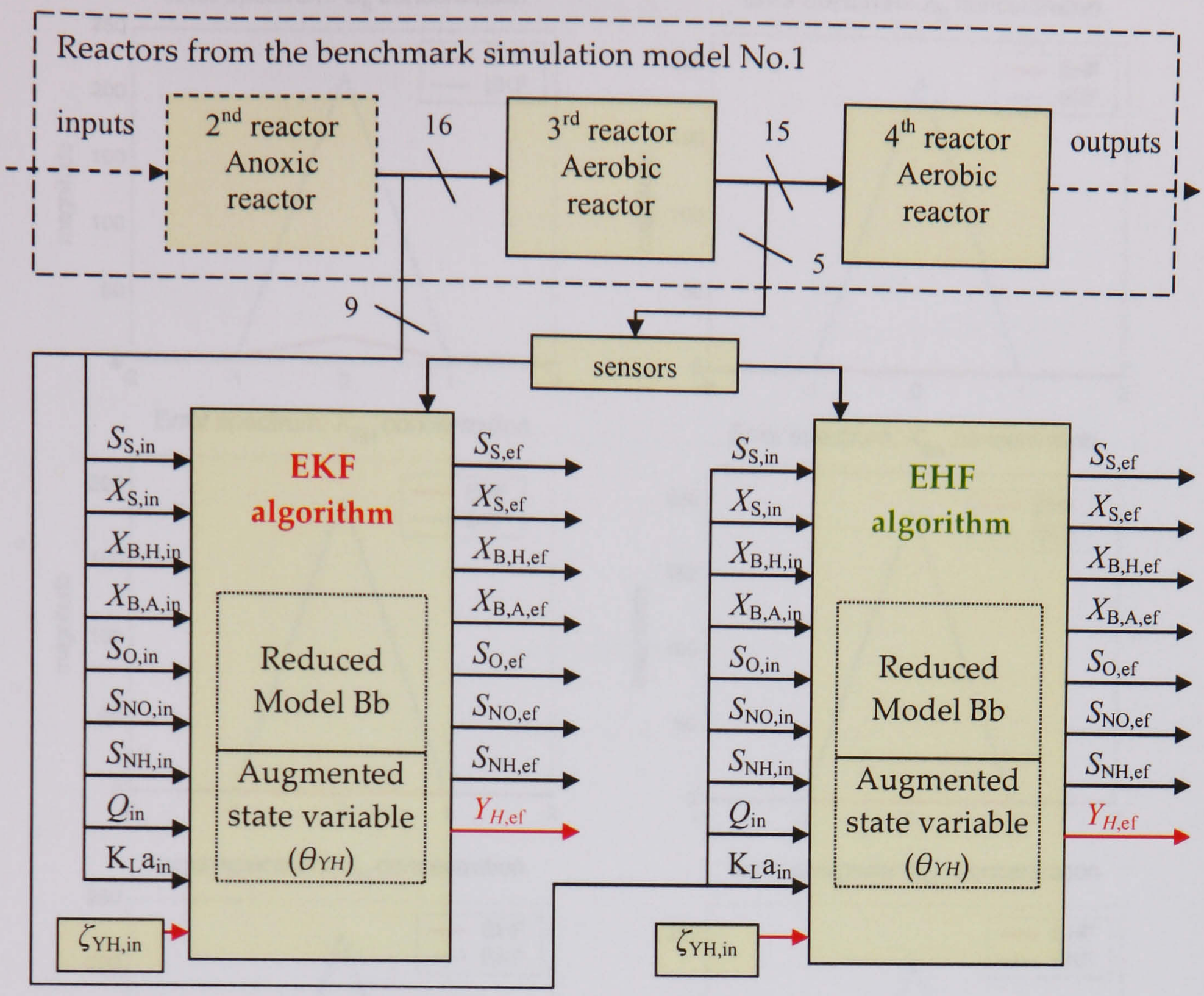


**Figure 6.9** State observer design based extended $H_\infty$ filter and extended Kalman filter. $Y_H$ is modelled as an integrator that is driven by white noise and augmented to the original 'Model Bb' presented in Chapter IV.

Simulation results that are presented in Figure (6.11) illustrate the software sensor responses for both the EKF and the EHF, in the time domain. Results concentrate on the software sensors convergence properties toward the real states, when the initial estimates are assumed unknown. It can be observed that the extended $H_\infty$ filter converges toward the real states and parameter as fast as the software sensor based EKF. The fastest convergence speed, which is about 1 hour and 10 minutes, is obtained for $X_{B,H}$ concentration while the slowest, which is about 5 days, is obtained for the heterotrophic yield. The simulation results also illustrated that both the EHF and EKF failed to converge toward $S_{NH}$ concentration, which is explained by the simplifying assumptions made to produce the 'Model Bb'. For further details on this reduced model, the reader can refer to Chapter IV, Section (4.1).

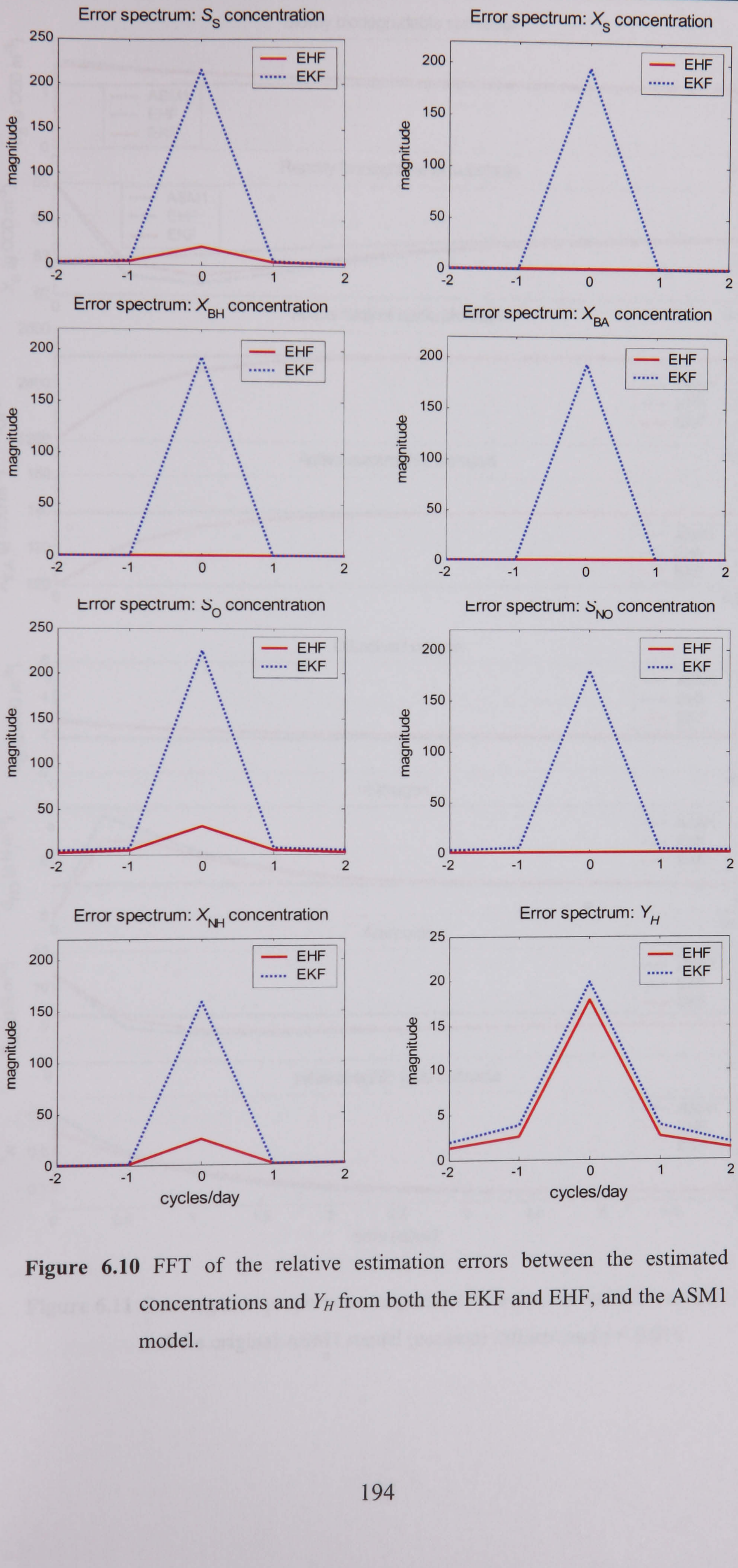


**Figure 6.10** FFT of the relative estimation errors between the estimated concentrations and $Y_H$ from both the EKF and EHF, and the ASM1 model.

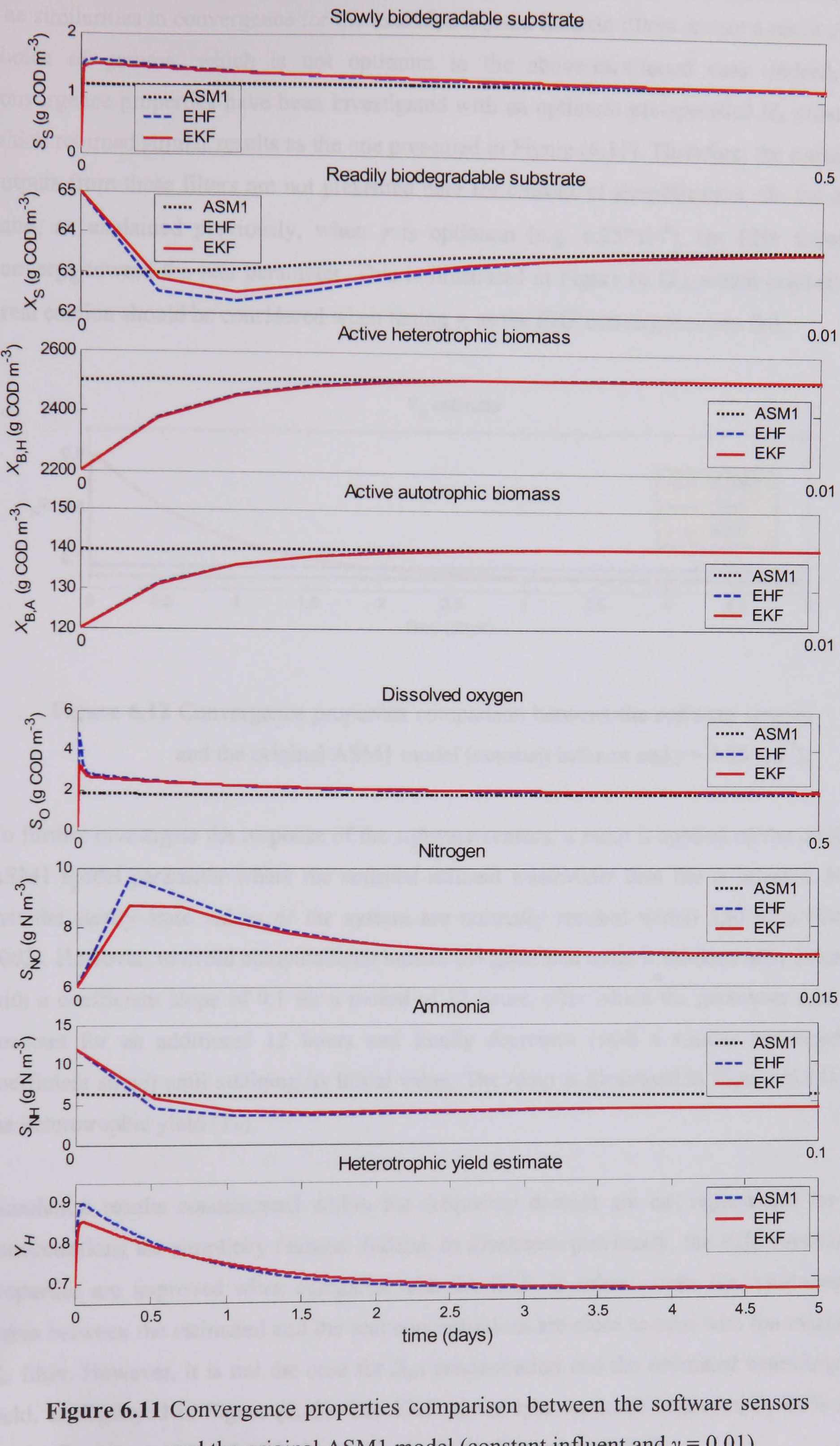


**Figure 6.11** Convergence properties comparison between the software sensors and the original ASM1 model (constant influent and $\gamma = 0.01$).

The similarities in convergence for the extended $H_\infty$ and Kalman filters are not a result of the choice of gamma, which is not optimum in the above-mentioned case. Indeed, the convergence properties have been investigated with an optimum pre-specified $H_\infty$ criterion, which returned similar results as the one presented in Figure (6.11). Therefore, the estimated outputs from these filters are not presented here for reasons of simplification. On the other hand, as explained previously, when $\gamma$ is optimum (e.g. $6.25*10^{-8}$), the EHF failed to converge toward the real parameter. This is illustrated in Figure (6.12), which implies that great caution should be considered when tuning $\gamma$, as the EHF convergence can fail.

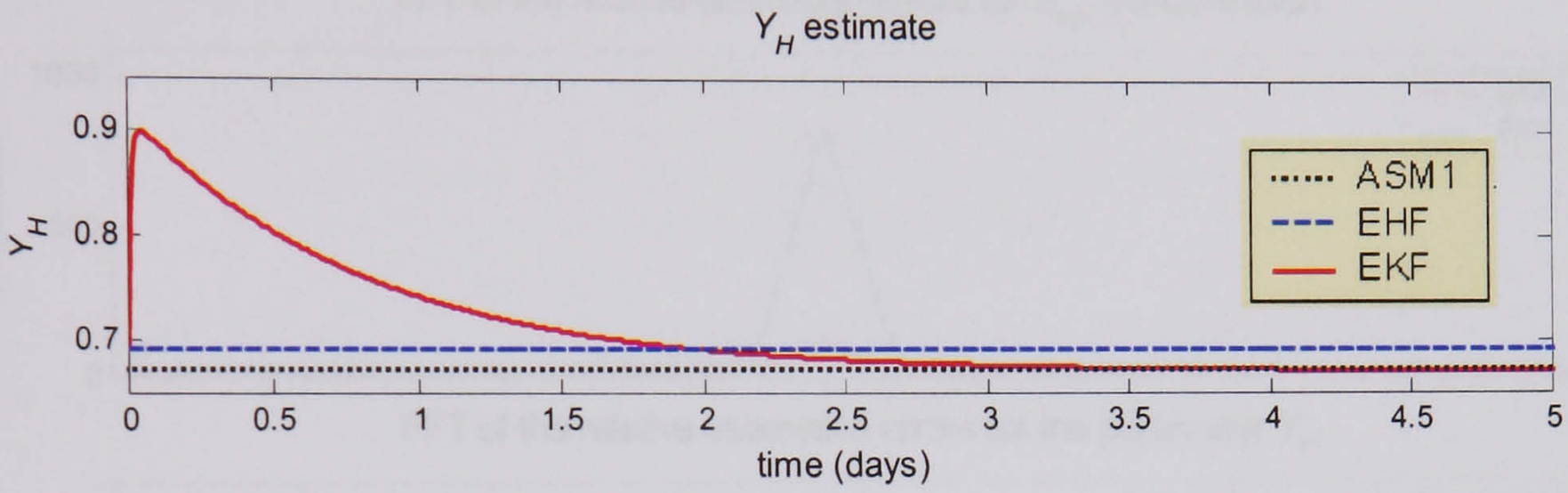


**Figure 6.12** Convergence properties comparison between the software sensors and the original ASM1 model (constant influent and $\gamma = 6.25*10^{-8}$).

To further investigate the response of the software sensors, a ramp is applied on the original ASM1 model parameter where the constant influent wastewater data file is selected. Note that the steady state values of the system are normally reached within 150 days (Copp, 2002). However, to avoid computational burden the generated ramp is initiated after 30 days, with a coefficient slope of 0.1 for a period of 12 hours, after which the parameter remains constant for an additional 12 hours and finally decreases (with a similar but negative coefficient slope) until attaining its initial value. The ramp is illustrated in Figure (6.14) for the heterotrophic yield ($Y_H$).

Simulation results concentrated within the frequency domain are not represented for all concentrations for simplicity reasons. Indeed, as illustrated previously, the EHF robustness properties are improved when compared with the EKF. In other words, the minimisation errors between the estimated and the real concentrations are close to zero with the extended $H_\infty$ filter. However, it is not the case for $S_{NH}$ concentration and the estimated heterotrophic yield, as displayed in Figure (6.13). The EHF power spectrums are improved by 86% and 5% for $S_{HN}$ concentration and $Y_H$, respectively, in the frequency domain.

The software sensors responses in the time domain are presented in Figure (6.14) where it can be observed that both the EHF and EHF provided good tracking performances for $X_S$, $X_{B,H}$, $X_{B,A}$, and $S_{NO}$ concentrations. Furthermore, the algorithms also produced good tracking performances for $S_{NH}$ concentration, even though a bias between the real and the estimated variables occurred. This bias is generated by the simplifying assumptions selected to produce the augmented 'Model Bb'. It can also be observed from Figure (6.14) that $S_S$, $S_O$ concentrations and the heterotrophic yield are poorly estimated by the extended $H_\infty$ filter, when compared to the extended Kalman filter.

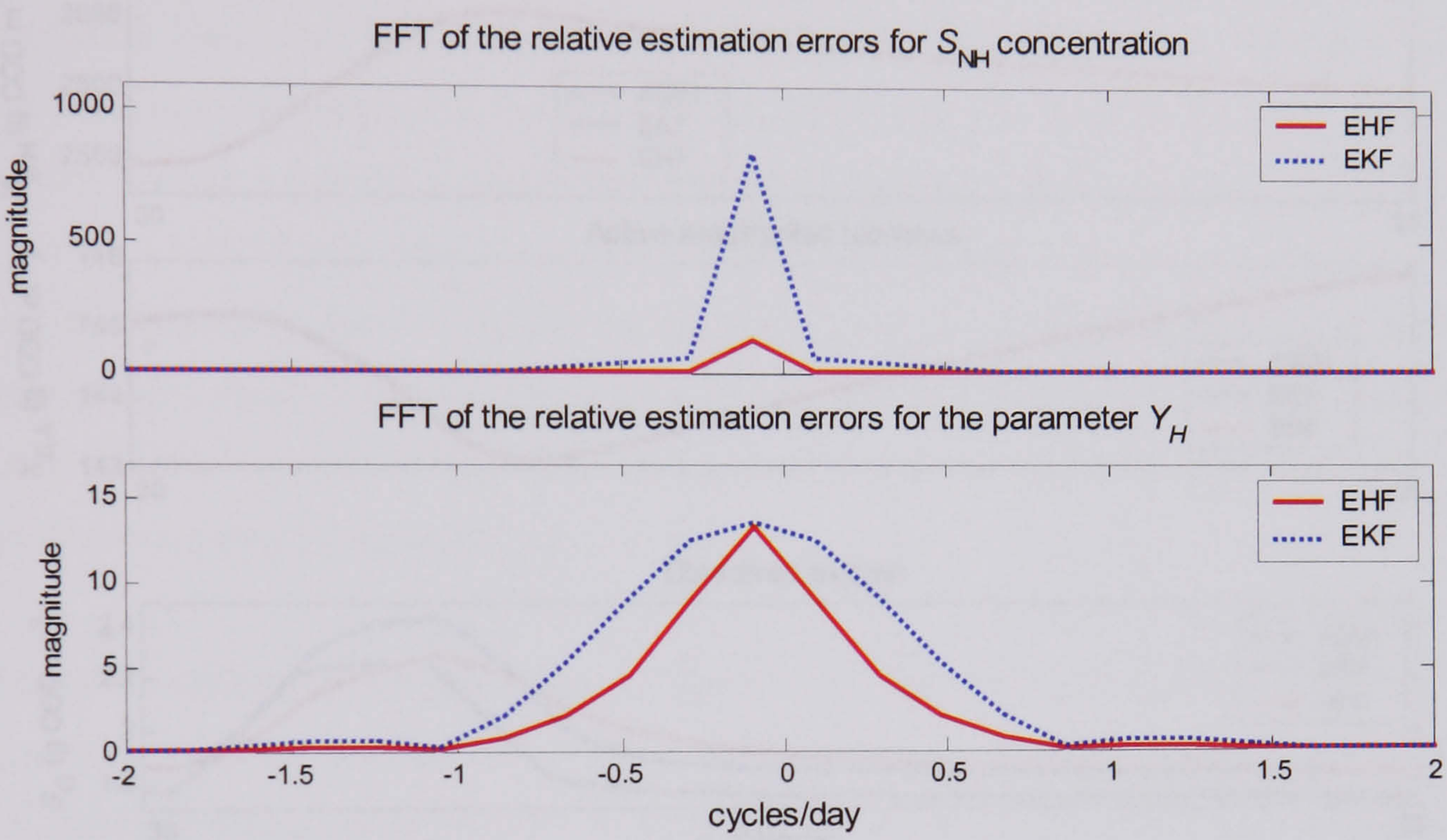


**Figure 6.13** FFT of the relative estimation errors between the estimated concentrations from both the EKF and EHF, based on the augmented 'Model Bb'.

It appears for $S_S$ concentrations and the heterotrophic yield that the software sensors converged toward the true variables with a maximum bias of 8.4% and 6.5% for the EHF and 3.8%, and 0.91% for the EKF, respectively. In addition, the abrupt changes of the dissolved oxygen are tracked with a maximum bias of 7% for the extended Kalman filter and less than 1% for the extended $H_\infty$ filter. This improved tracking performance in the case of the EHF is explained by the fact that the system had not reached its steady state values. In other words, if the ramp is generated after 130 days, which guarantee that the system has reach its steady states conditions, the tracking performances of the DO concentration should be better for the EKF when compared with the EHF.

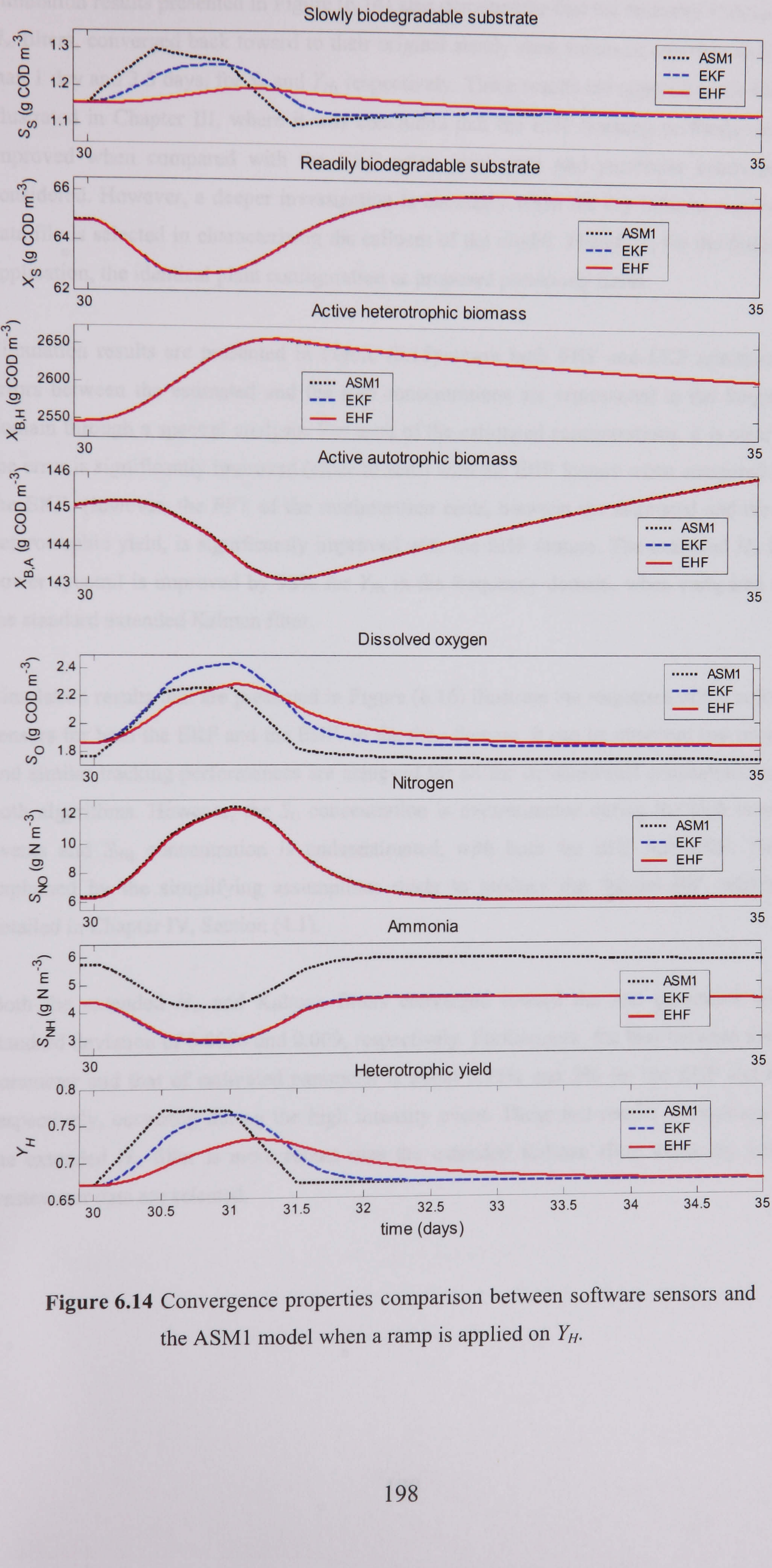


**Figure 6.14** Convergence properties comparison between software sensors and the ASM1 model when a ramp is applied on $Y_H$.

Simulation results presented in Figure (6.14) also demonstrate that the extended Kalman and $H_\infty$ filters, converged back toward to their original steady state values in approximately less than 1 day and 3.5 days, for $S_S$ and $Y_H$, respectively. These results are opposed to the finding illustrated in Chapter III, where it was concluded that the EHF tracking performances are improved when compared with the EKF when joint state and parameter estimation is considered. However, a deeper investigation is necessary when the dry influent wastewater data file is selected in characterising the influent of the model. Therefore, for the following application, the identical plant configuration as proposed previously holds.

Simulation results are presented in Figure (6.15) where both EHF and EKF minimisation errors between the estimated and the true concentrations are represented in the frequency domain through a spectral analysis. For each of the estimated concentrations, it is clear that the error is significantly improved (close to zero) with the EHF feature when compared with the EKF. However, the FFT of the minimisation error, between the estimated and the real heterotrophic yield, is significantly improved with the EHF feature. The extended $H_\infty$ filter power spectral is improved by 92% for $Y_H$, in the frequency domain, when compared with the standard extended Kalman filter.

Simulation results that are presented in Figure (6.16) illustrate the responses of the software sensors for both the EKF and the EHF, in the time domain. It can be observed that accurate and similar tracking performances are achieved for all the demonstrated concentrations, for both algorithms. However, the $S_O$ concentration is overestimated during the high intensity events and $S_{NH}$ concentration is underestimated, with both the EHF and EKF. This is explained by the simplifying assumptions made to produce the 'Model Bb', which are detailed in Chapter IV, Section (4.1).

Both the extended $H_\infty$ and Kalman filters converged toward the real parameter with a standard deviation of 0.0056 and 0.009, respectively. Furthermore, the bias between the true parameter and that of estimated parameter is about 0.75% and 3% for the EHF and EKF, respectively, occurring during the high intensity event. These last results demonstrate that the extended $H_\infty$ filter is more robust than the extended Kalman filter when dry influent wastewater data are selected.

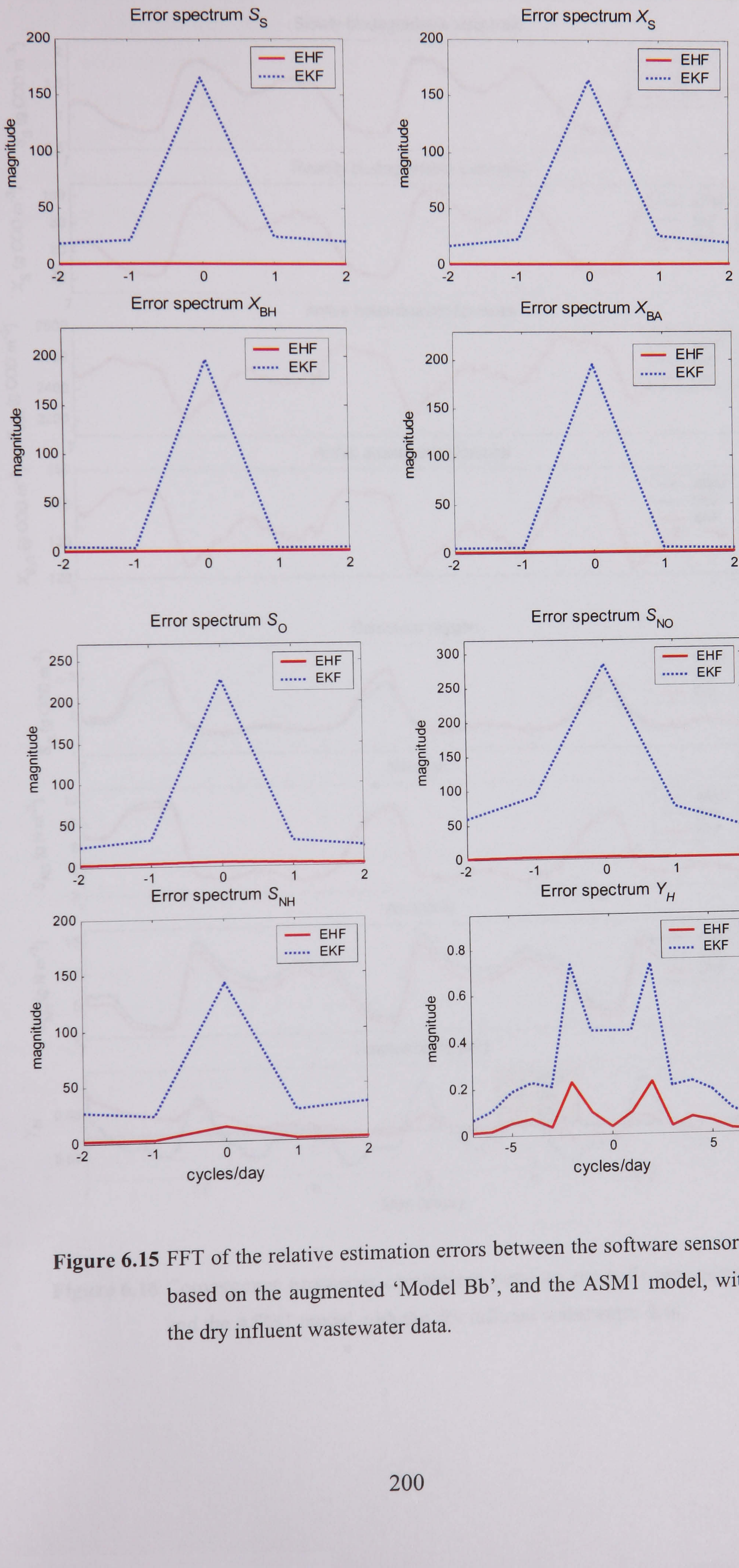


**Figure 6.15** FFT of the relative estimation errors between the software sensors, based on the augmented 'Model Bb', and the ASM1 model, with the dry influent wastewater data.

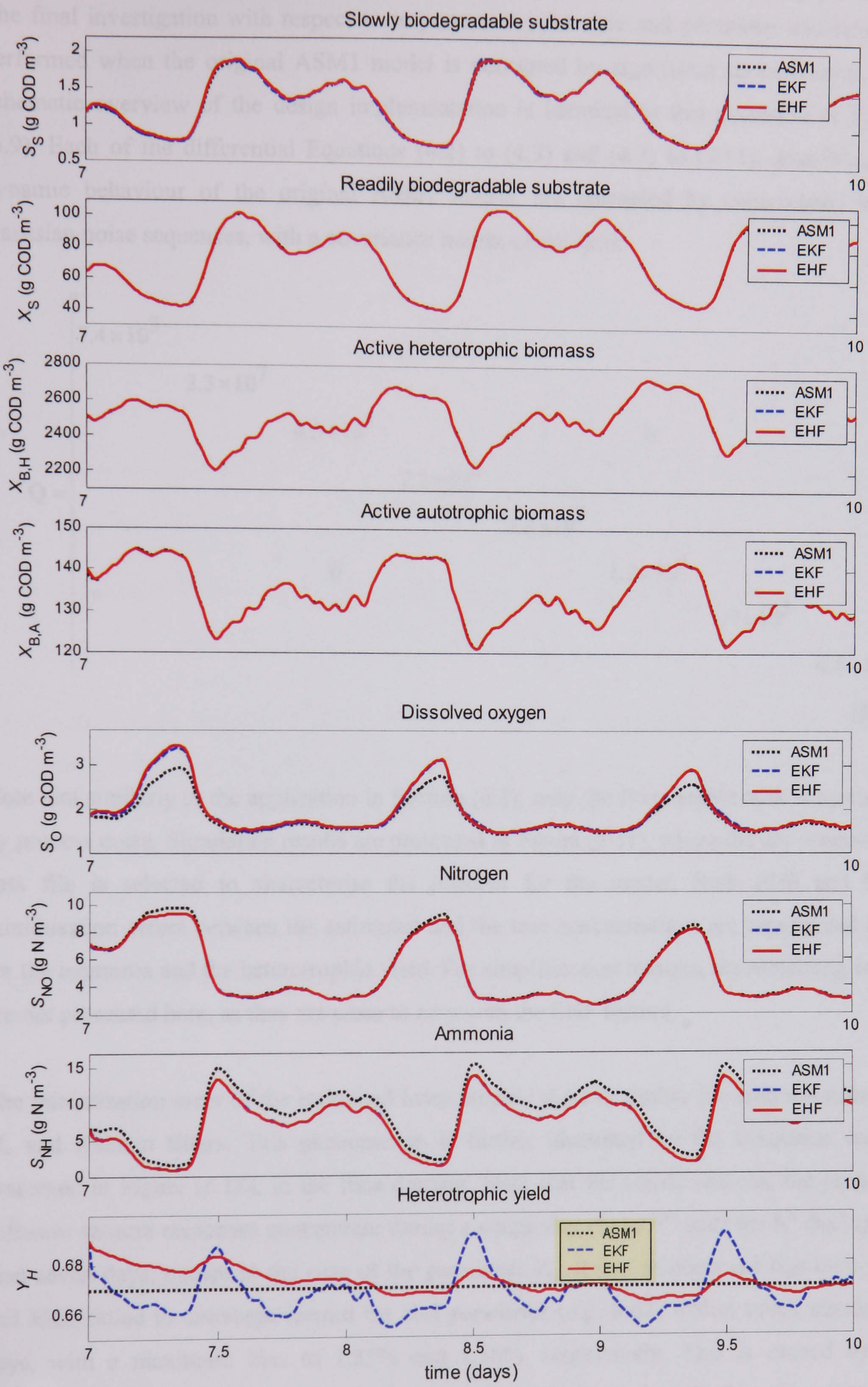


**Figure 6.16** Convergence properties comparison between the software sensors and the ASM1 model with the dry influent wastewater data.

The final investigation with respect to responses to joint state and parameter estimation is performed when the original ASM1 model is corrupted by significant process noise. The schematic overview of the design implementation is identical to that presented in Figure (6.9). Each of the differential Equations (4.2) to (4.3) and (4.7) to (4.11), describing the dynamic behaviour of the original ASM1 model, are corrupted by uncorrelated white Gaussian noise sequences, with a covariance matrix of the form

$$\mathbf{Q} = \begin{bmatrix} 7.4\times10^{3} & & & & & & & & \ddots \\ & 2.3\times10^{7} & & & & & & & \\ & & 6.5\times10^{8} & & & & 0 & & \\ & & & 2.2\times10^{6} & & & & & \\ \ddots & & & & 3.6\times10^{3} & & & & \ddots \\ & & 0 & & & 1.2\times10^{5} & & & \\ & & & & & & 1.7\times10^{5} & & \\ & & & & \ddots & & & & 4.6\times10^{7} \end{bmatrix} \tag{6.11}$$

Note that similarly to the application in Section (6.1), only the first aerobic tank is corrupted by process noise. Simulation results are presented in Figure (6.17), where the dry wastewater data file is selected to characterise the influent for the model. Both EHF and EKF minimisation errors between the estimated and the true concentrations are represented only for the ammonia and the heterotrophic yield. For simplification reasons, the remaining errors are not presented here, as they are close to zero with the EHF feature.

The minimisation error of the estimated heterotrophic yield is similar for both the extended $H_\infty$ and Kalman filters. This phenomenon is further illustrated by the simulation results presented in Figure (6.18), in the time domain. Note that for clarity reasons, the proposed software sensors responses concentrate during a single day (from $7^{th}$ until the $8^{th}$ day) rather than seven days, except in the case of the parameter $Y_H$. It can be observed that both EHF and EKF failed to converge toward the real parameter (e.g. 0.67) within seven simulation days, with a maximum bias of 1.35% and 1.36%, respectively. This is caused by the modelling errors introduced within the ASM1 model, which are described by the covariance matrix given by Equation (6.11).

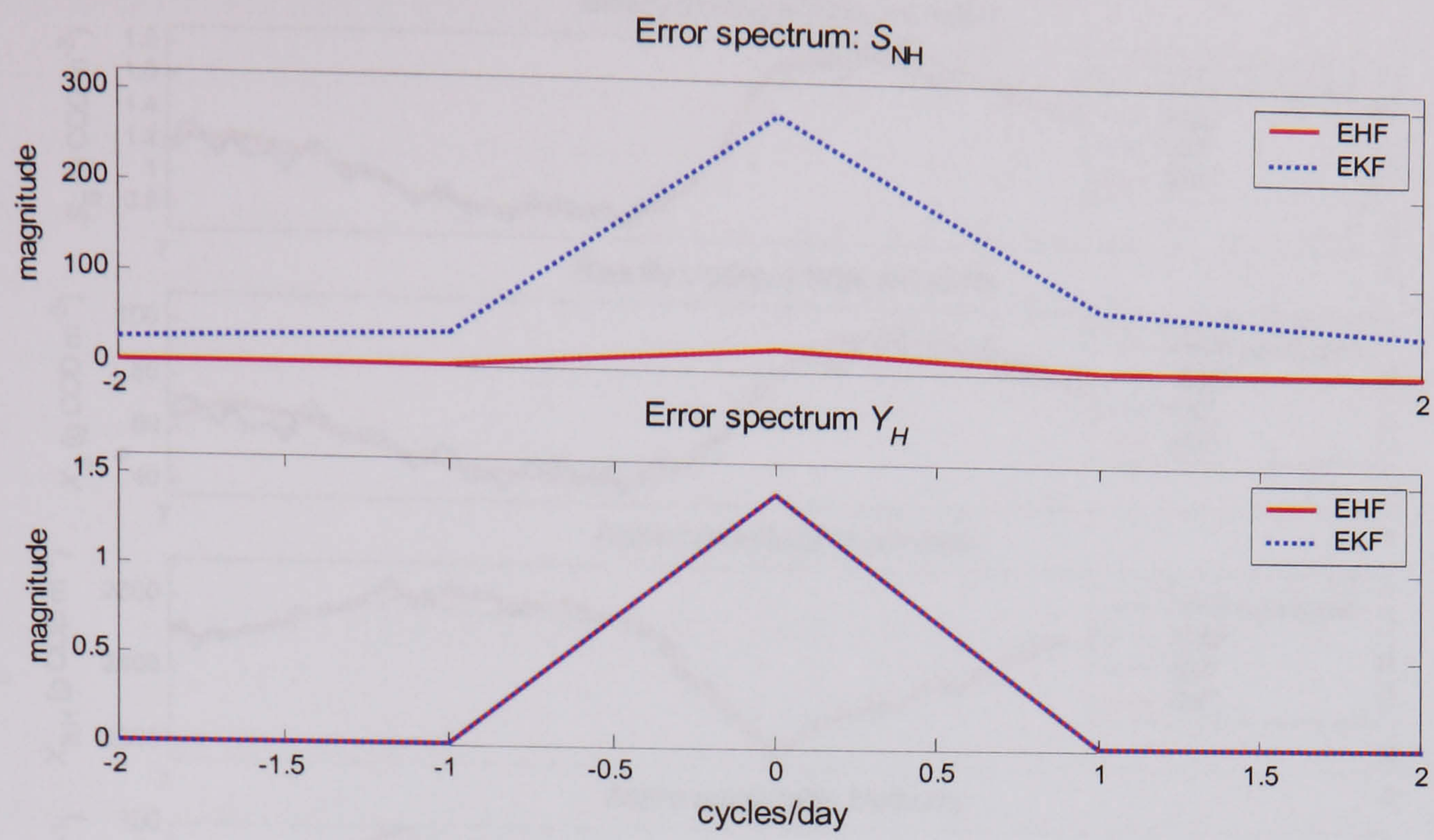


**Figure 6.17** FFT of the relative estimation errors between the software sensors, and the corrupted ASM1 model.

The absolute errors between the original ASM1 model and the reduced 'Model Bb' for both the EHF and the EKF are presented in terms of standard deviations, means and maximum biases, for each concentration in Table (6.8), over a period of 7 days. It can be observed that the EHF performances are generally improved when compared with the EKF, apart from the $S_{NH}$ concentration, which is due to robustness properties of the EHF. It can also be concluded from this last case that both the augmented software sensors based-EHF and EKF failed to converge toward the real parameter when the model is corrupted by process noise.

| **EHF** | $S_S$ | $X_S$ | $X_{B,H}$ | $X_{B,A}$ | $S_O$ | $S_{NO}$ | $S_{NH}$ |
|---|---|---|---|---|---|---|---|
| *Standard Deviation* (%) | **>0.1** | 0.42 | **15.2** | **21.9** | **6.22** | **5.4** | 5 |
| *Mean* (%) | **0.16** | 1.4 | **2.7** | 0.88 | 3.07 | **0.18** | 15.02 |
| *Maximum Bias* (%) | **0.63** | **0.47** | **4.6** | **2.95** | 6.92 | **7.2** | 12 |
| **EKF** | | | | | | | |
| *Standard Deviation* (%) | 0.4 | **>0.1** | 16 | 22.3 | 7.12 | 6.1 | **4** |
| *Mean* (%) | 1.14 | **0.2** | 2.8 | **0.81** | **0.5** | 0.48 | **3.87** |
| *Maximum Bias* (%) | 0.78 | 2.2 | 5.4 | 3.34 | **2.97** | 8.8 | **2.7** |

**Table 6.8** Comparison of the absolute standard deviation, mean and maximum bias, in percentage, between the original ASM1 and the EHH and EKF estimation based on the reduced 'Model Bb'. The best performances are emphasised.

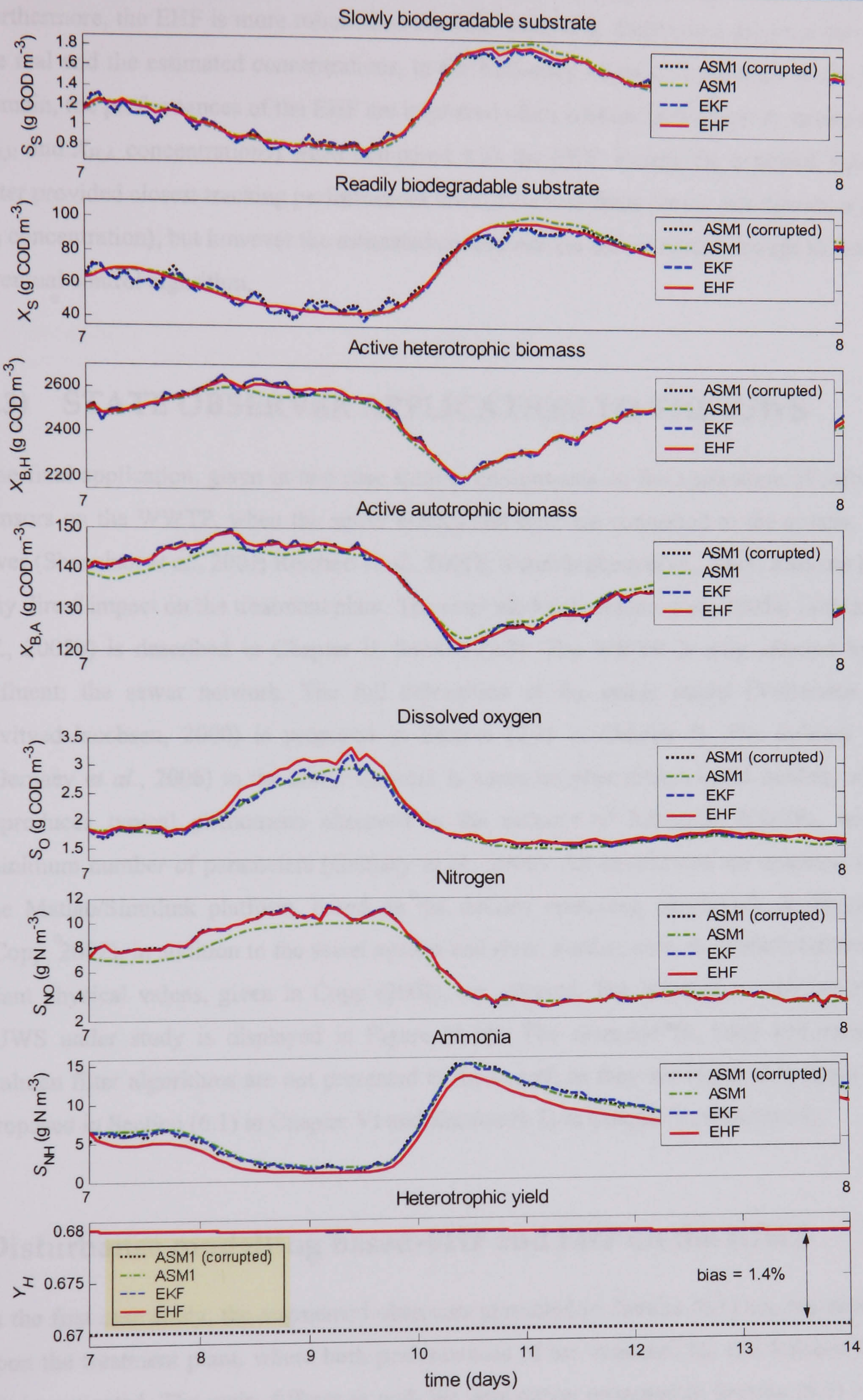


**Figure 6.18** Convergence properties comparison between the software sensors and the corrupted ASM1 model.

Furthermore, the EHF is more robust than the EKF in term of minimising the error between the real and the estimated concentrations, in the frequency domain. In addition, in the time domain, the performances of the EHF are improved when estimating the slow dynamics (e.g. $X_{B,H}$ and $X_{H,A}$ concentrations) when compared with the EKF. Finally the extended Kalman filter provided closest tracking performances toward the real states for the fast dynamics (e.g. $S_O$ concentration), but however the estimated concentrations are not robust enough to feed an eventual control algorithm.

## 6.3) STATE OBSERVER APPLICATION TO THE IUWS

The final application, given in two case studies, concentrates on the application of software sensors on the WWTP, when the sewer system and river are connected to the system. The river (Shanahan *et al.*, 2001; Reichert *et al.*, 2001b; Vanrolleghem *et al.*, 2001) does not have any direct impact on the treatment plant. The river model (Linblom *et al.*, 2005a; Linblom *et al.*, 2005b) is described in Chapter II, Section (2.3). The WWTP is only affected by its influent: the sewer network. The full description of the sewer model (Vollertsen and Hvitved-Jacobsen, 2000) is proposed in Section (2.3) in Chapter II. The influent data (Gernaey *et al.*, 2006) to the sewer network is based on phenomenological models, which reproduces typical phenomena observed in the influent of full-scale WWTPs, with a minimum number of parameters (Gernaey *et al.*, 2006). All simulations are executed using the Matlab/Simulink platform, based on the defined open-loop benchmark configuration (Copp, 2002), in addition to the sewer system and river. Furthermore, the default benchmark plant physical values, given in Copp (2002), are selected. The schematic overview of the IUWS under study is displayed in Figure (2.10). The extended $H_\infty$ filter and extended Kalman filter algorithms are not presented in the sequel, as they are identical to those ones proposed in Section (6.1) in Chapter VI and Section (5.1) in Chapter V, respectively.

### Disturbance modelling based-EHF and EHF on the IUWS

In the first case study, the augmented observers presented in Section (6.1) are implemented upon the treatment plant, where both performances of the extended $H_\infty$ and Kalman filters are investigated. The main difference with the application proposed in Section (6.1) is that the sewer model and river are connected to the treatment plant. The inclusion of the former aims at investigation of the effect of diurnal variations of the influent from the sewer

network rather than the available influent files provided with the original benchmark configuration. In other words, the software sensors tracking and convergence performances are investigated from a more realistic viewpoint, as the sewer system is integrated into the full scale-system. A general schematic overview of the software sensors implementation within the urban wastewater system is presented in Figure (6.19). It can be observed that both state observers are still implemented in parallel to the 1st aerobic reactor (e.g. 3rd tank).

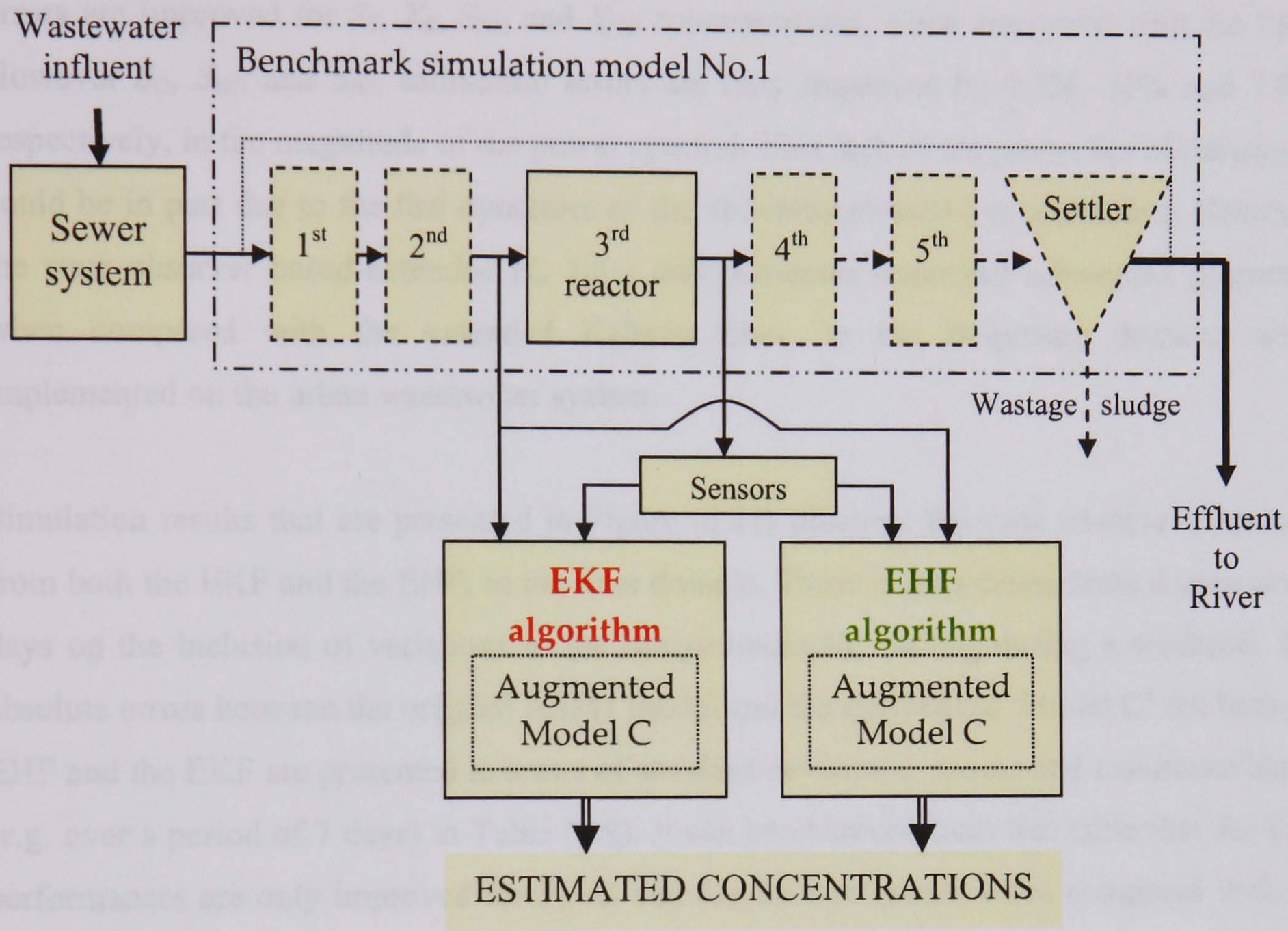


**Figure 6.19** Schematic representation of the software sensor implementation on the urban wastewater system composed of the sewer network, wastewater treatment plant and river. Three on-line measurements are considered, which are: $S_O$, $S_{NO}$ and $S_{NH}$.

The selected sensors ($S_O$, $S_{NO}$ and $S_{NH}$ measurements) are assumed noise free and sensor delays are not included within the design. The steady state simulation procedure involves the simulation of the system under study (for 130 days) using an influent of constant flow and composition. This is performed to ensure a consistent starting point and get rid of the influence of starting conditions on the generated dynamics outputs. The starting point for evaluating the dynamic response of the plant to the influent disturbances file is that of the

last (saved) state variables. The dynamic influent weather file is different from that one initially utilised with the benchmark plant (Chapter IV, V, and VI).

Simulation results are presented in Figure (6.20), where both EHF and EKF minimisation errors between the estimated and the true concentrations are represented in the frequency domain. Note that the optimum gamma is tuned to a level of $1.52*10^{-8}$ and the initial conditions of the system are assumed to be known. It can be observed that EHF minimisation errors are improved for $S_S$, $X_S$, $S_{NH}$ and $X_{ND}$ concentrations, when compared with the EKF. However $S_O$, $S_{NO}$ and $S_{ND}$ estimation errors are only improved by 0.3%, 11% and 7.9%, respectively, in the magnitude of the power spectral. This lack of the properties of robustness could be in part due to the fast dynamics of the above-mentioned concentrations. However, the state observer based-extended $H_\infty$ filter still possesses improved robustness properties when compared with the extended Kalman filter, in the frequency domain, when implemented on the urban wastewater system.

Simulation results that are presented in Figure (6.21) illustrate the state observer responses from both the EKF and the EHF, in the time domain. These results concentrate during seven days on the inclusion of variations in the design hydraulic loading during a weekend. The absolute errors between the original ASM1 model and the augmented 'Model C' for both the EHF and the EKF are presented in terms of standard deviations, means and maximum biases (e.g. over a period of 7 days) in Table (6.9). It can be observed from this table that the EHF performances are only improved for $S_S$, $X_S$ and $S_{ND}$ concentrations when compared with the EKF.

| **EHF** | $S_S$ | $X_S$ | $S_O$ | $S_{NO}$ | $S_{NH}$ | $S_{ND}$ | $X_{ND}$ |
|---|---|---|---|---|---|---|---|
| *Standard Deviation* (%) | **65.1** | **4.1** | 3 | 6.1 | 2.3 | **16.8** | 41.4 |
| *Mean* (%) | **47.6** | **1** | 20.5 | 14.3 | 2.6 | **6.4** | 28.8 |
| *Maximum Bias* (%) | **75.3** | **1.5** | 46.6 | 62.8 | 2.6 | **23.8** | 36.9 |
| **EKF** | | | | | | | |
| *Standard Deviation* (%) | 66.2 | 9 | **2** | **2** | **0.7** | 19.1 | **40.5** |
| *Mean* (%) | 57.9 | 16.8 | **6.4** | **13.7** | **1.5** | 5.1 | **27.6** |
| *Maximum Bias* (%) | 76.8 | 8.1 | **15.3** | 27.4 | **0.3** | 24.5 | **36.5** |

**Table 6.9** Comparison of the absolute standard deviation, mean and maximum bias, in percentage, between the original ASM1 and the EHH and EKF estimation based on the augmented 'Model C', within the urban wastewater system. The best performances are emphasised.

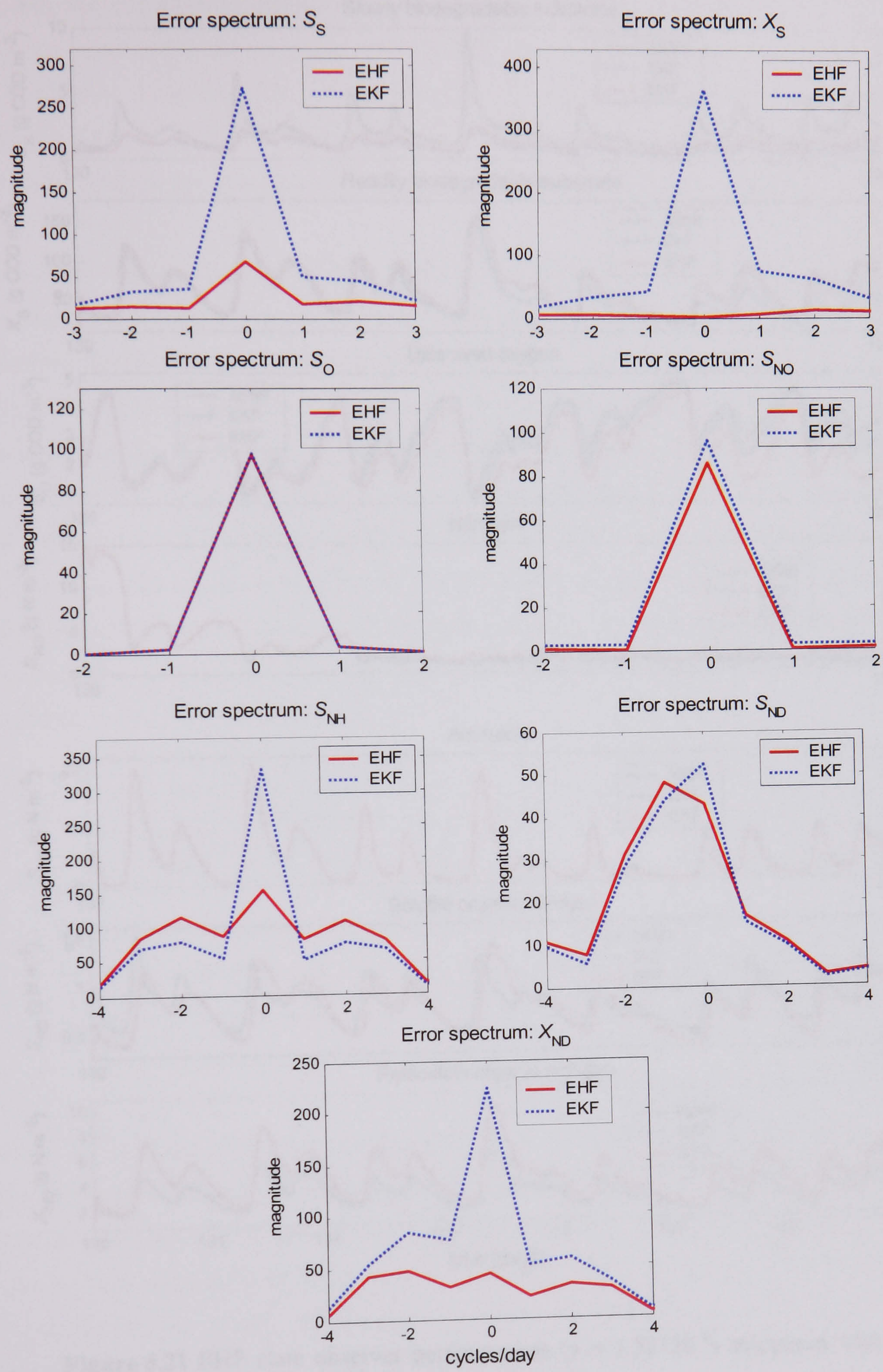


**Figure 6.20** FFT of the relative estimation errors between the estimated concentrations from both the EKF and EHF and the ASM1 model within the urban wastewater system.

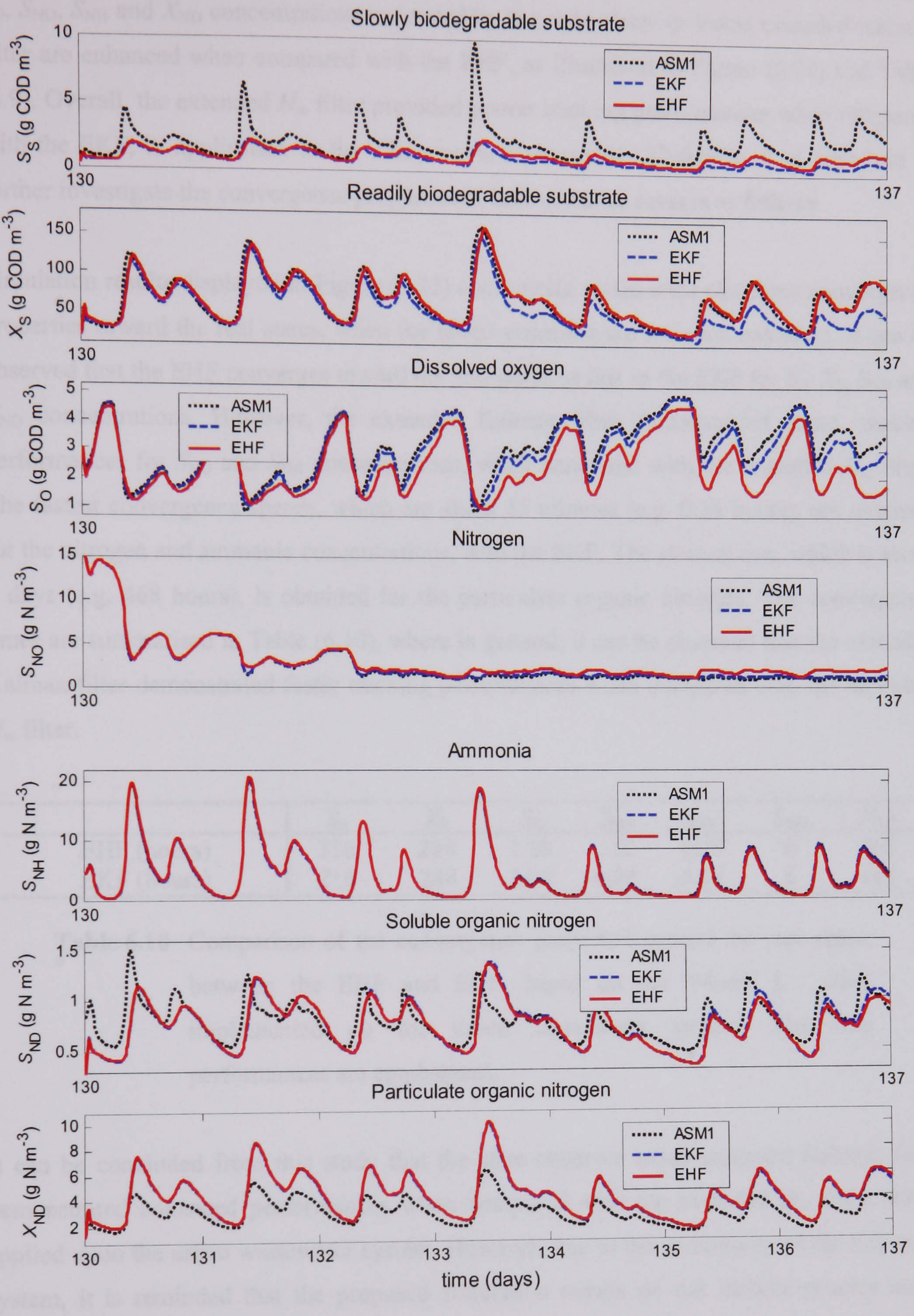


**Figure 6.21** EHF state observer performances ($\gamma$ = 1.52*10$^{-8}$) compared with the standard EKF and the ASM1 model noise free when the influent of the plant is generated by the sewer system. Results are based on the augmented 'Model C'.

$S_O$, $S_{NO}$, $S_{NH}$ and $X_{ND}$ concentrations estimated by the state observer based extended Kalman filter are enhanced when compared with the EHF, as illustrated in Figure (6.21) and Table (6.9). Overall, the extended $H_\infty$ filter provided poorer tracking performances when compared with the EKF, in application to the urban wastewater system. Therefore, it is important to further investigate the convergence properties of both software sensors as follows.

Simulation results displayed in Figure (6.22) concentrate on the state observers convergence properties toward the real states, when the initial estimates are assumed unknown. It can be observed that the EHF converges toward the real states as fast as the EKF for $S_S$, $X_S$, $S_{ND}$ and $X_{ND}$ concentrations. However, the extended Kalman filter demonstrated faster tracking performances for $S_{NO}$ and $S_{NH}$ concentrations, when compared with the extended $H_\infty$ filter. The fastest convergence speeds, which are about 15 minutes (e.g. 0.24 hours), are obtained for the nitrogen and ammonia concentrations, with the EKF. The slowest one, which is about 8 days (e.g. 468 hours), is obtained for the particulate organic nitrogen. The convergence times are summarised in Table (6.10), where in general, it can be observed that the extended Kalman filter demonstrated faster tracking performances when compared with the extended $H_\infty$ filter.

| | $S_S$ | $X_S$ | $S_O$ | $S_{NO}$ | $S_{NH}$ | $S_{ND}$ | $X_{ND}$ |
|---|---|---|---|---|---|---|---|
| EHF (hours) | 216 | 288 | 1.08 | 1.2 | 16.8 | 6 | 468 |
| EKF (hours) | 216 | 288 | 1.08 | **0.24** | **0.24** | 6 | 468 |

**Table 6.10** Comparison of the convergence properties toward the real states, between the EHF and EKF, based on the 'Model C', when implemented on the urban wastewater system. The best performances are emphasised.

It can be concluded from this study that the state observer based extended Kalman filter demonstrated enhanced performances when compared with the extended $H_\infty$ filter, when applied upon the urban wastewater system. However, due to the complexity of the full-scale system, it is reminded that the proposed simulation results do not include process noise corruption of the system. Furthermore, a deeper investigation, where joint state and parameter estimation are performed on-line on the integrated system, is proposed.

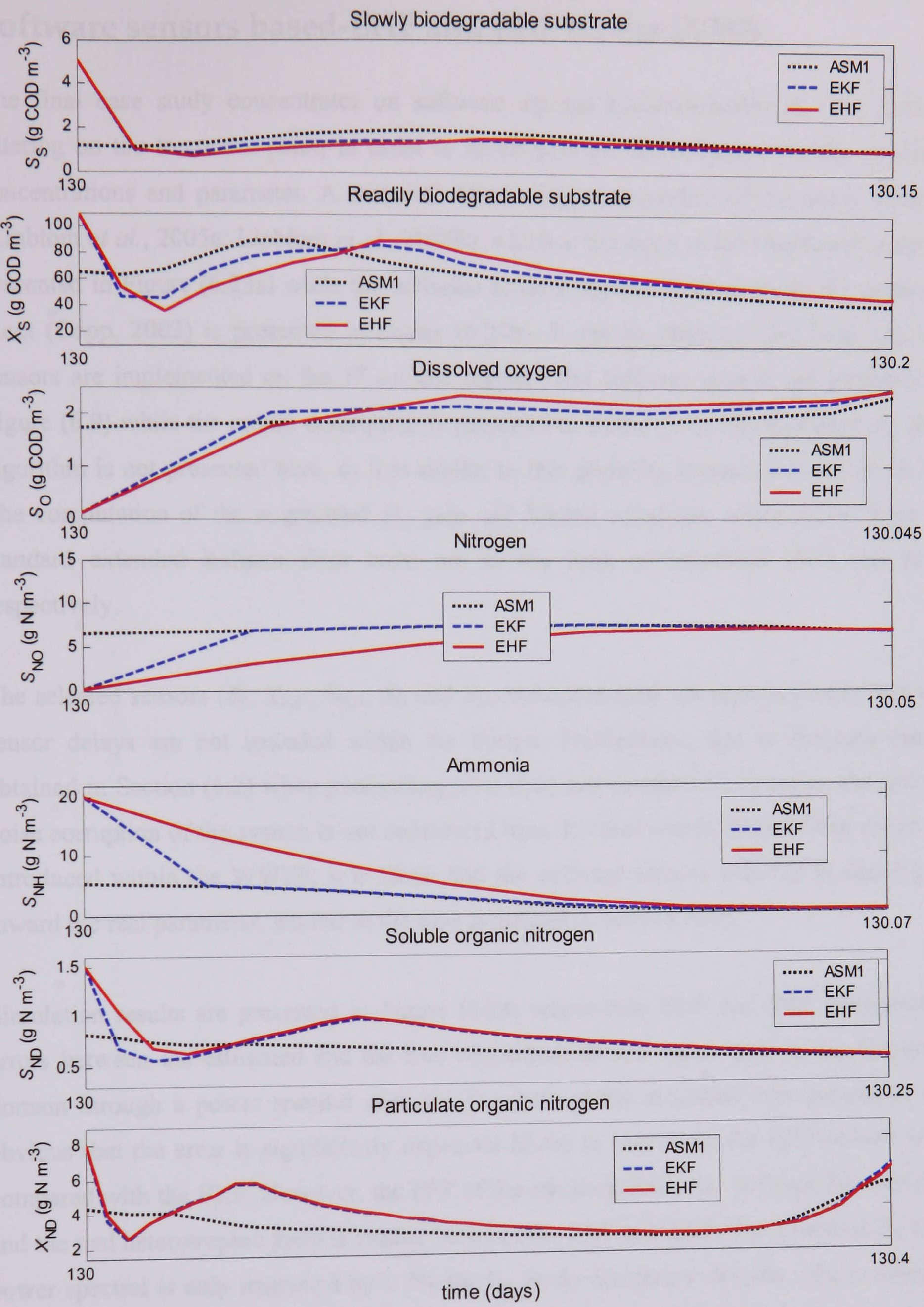


**Figure 6.22** Convergence properties comparison between the EKF, the EHF and the original ASM1 model when the urban wastewater system, is considered.

## Software sensors based-EHF and EHF on the IUWS

The final case study concentrates on software sensors based-extended $H_\infty$ and Kalman filtering on the treatment plant, in order to investigate the sewer impact on the estimated concentrations and parameter. A Simulink block diagram overview of the sewer network (Linblom *et al.*, 2005a; Linblom *et al.*, 2005b), which is the input of the benchmark plant, is presented in Figure (6.23a) while the software sensors implementation within the treatment plant (Copp, 2002) is presented in Figure (6.23b). It can be observed that both software sensors are implemented on the 1st aerobic reactor. The software sensors are presented in Figure (6.9) while the model description is proposed in Table (6.7). The extended $H_\infty$ filter algorithm is not presented here, as it is similar to that given by Equations (5.26) to (5.36). The computation of the augmented $H_\infty$ gain and Riccati equations, which differ from the standard extended Kalman filter ones, are of the form of Equations (6.7) and (6.8), respectively.

The selected sensors ($S_S$, $X_{B,H}$, $X_{H,A}$, $S_O$ and $S_{NO}$ measurements) are assumed noise free and sensor delays are not included within the design. Furthermore, due to the bias results obtained in Section (6.2) when performing joint state and parameter estimation, the process noise corruption of the system is not considered here. In other words, if modelling errors are introduced within the WWTP, it is likely that the software sensors will fail in converging toward the real parameter, similar to the case presented in Section (6.2).

Simulation results are presented in Figure (6.24) where both EHF and EKF minimisation errors between the estimated and the true concentrations are represented in the frequency domain through a power spectral analysis. For each of the estimated concentrations, it is obvious that the error is significantly improved (close to zero) with the EHF feature when compared with the EKF. However, the FFT of the minimisation error between the estimated and the real heterotrophic yield is similar between the EHF and EKF. The extended $H_\infty$ filter power spectral is only improved by 1.7% for $Y_H$, in the frequency domain, when compared with the standard extended Kalman filter. It is reminded that the EHF power spectral is enhanced by 92% for $Y_H$, when compared with the EKF in the similar application presented in Section (6.2). Therefore, when the extended $H_\infty$ filter is implemented into the urban wastewater, its performance decreases by 98%, with the proposed configuration, when compared with the EKF application presented in Section (6.2).

**SEWER SYSTEM including the primary clarifier (Linblom *et al.*, 2005a; Linblom *et al.*, 2005b)**

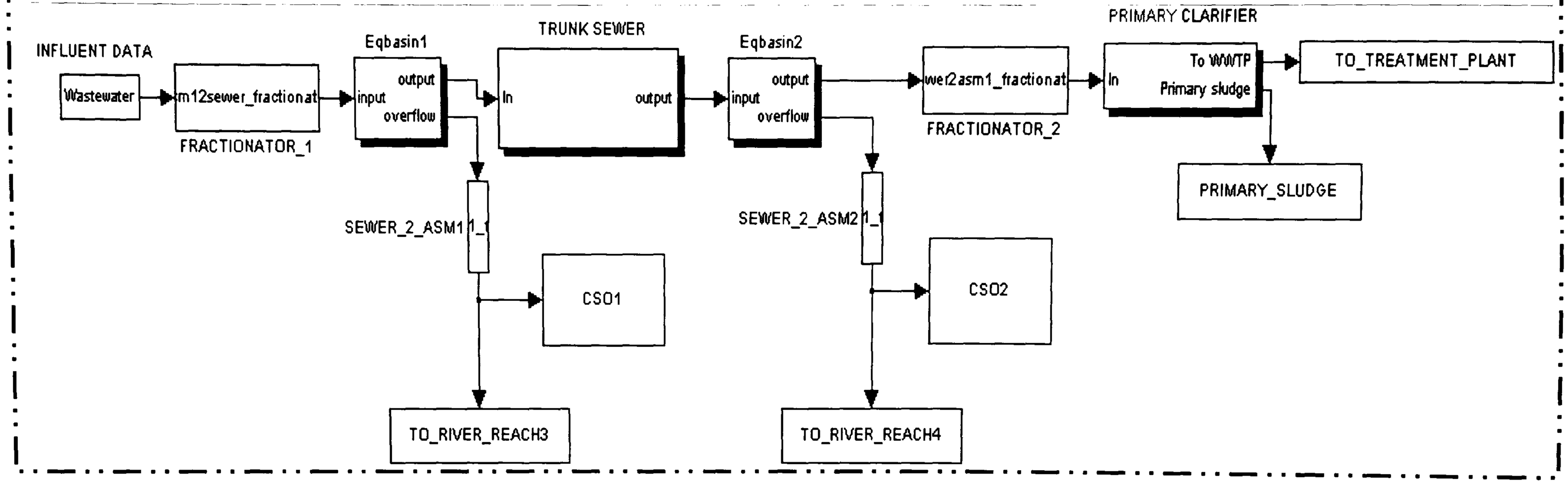


**Figure 6.23a** Simulink block diagram representation of the sewer system (Linblom *et al.*, 2005a; Linblom *et al.*, 2005b). The influent data (Gernaey *et al.*, 2006) to the sewer network are based on phenomenological models. The full-scale model description is presented in Chapter II.

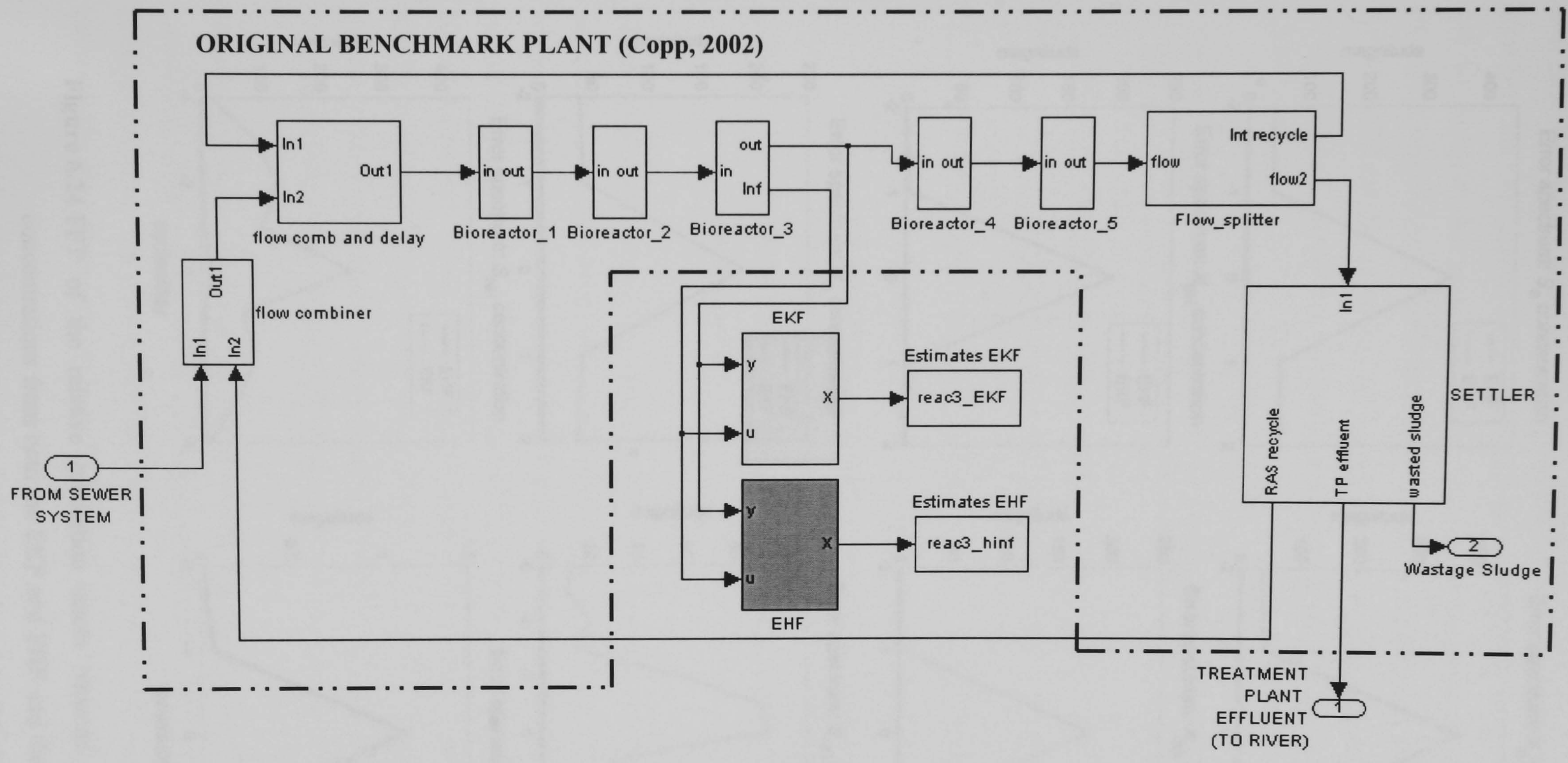


**Figure 6.23b** Simulink block diagram representation of the software sensors based EKF and EHF on the benchmark plant (Copp, 2002), within the urban wastewater system composed of the sewer system (Figure 6.23a) as input and the river (Linblom *et al.*, 2005a; Linblom *et al.*, 2005b) as output, which is not represented here for simplification reasons. A detailed description of the integrated system is available in Chapter II and the full description of the benchmark plant is proposed by Copp (2002).

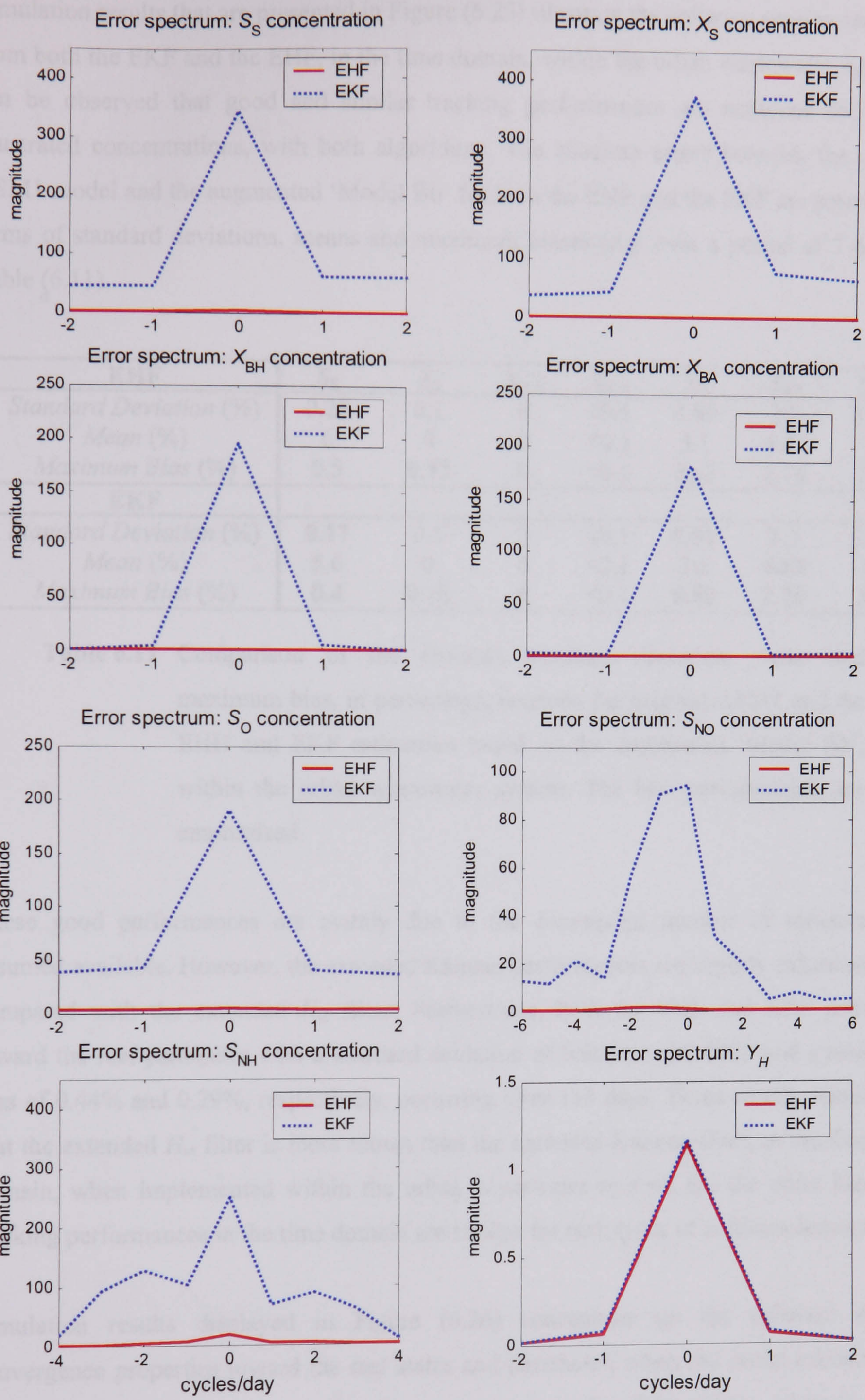


**Figure 6.24** FFT of the relative estimation errors between the estimated concentrations from both the EKF and EHF and the ASM1 model within the urban wastewater system, based on 'Model Bb'.

Simulation results that are presented in Figure (6.25) illustrate the software sensors responses from both the EKF and the EHF, in the time domain, within the urban wastewater system. It can be observed that good and similar tracking performances are achieved for all the illustrated concentrations, with both algorithms. The absolute errors between the original ASM1 model and the augmented 'Model Bb' for both the EHF and the EKF are presented in terms of standard deviations, means and maximum biases (e.g. over a period of 7 days) in Table (6.11).

| **EHF** | $S_S$ | $X_S$ | $X_{B,H}$ | $X_{B,A}$ | $S_O$ | $S_{NO}$ | $S_{NH}$ |
|---|---|---|---|---|---|---|---|
| *Standard Deviation* (%) | 0.25 | 0.1 | 0 | <0.1 | 6.99 | 2.2 | 5.20 |
| *Mean* (%) | 6 | 0 | 0 | <0.1 | 3.1 | 4.47 | 13 |
| *Maximum Bias* (%) | 0.5 | **0.12** | 0 | <0.1 | 0.62 | 2.76 | 5.4 |
| **EKF** | | | | | | | |
| *Standard Deviation* (%) | **0.17** | 0.1 | 0 | <0.1 | **6.91** | 2.2 | **5.17** |
| *Mean* (%) | **5.6** | 0 | 0 | <0.1 | 3.1 | **4.43** | 13 |
| *Maximum Bias* (%) | **0.4** | 0.18 | 0 | <0.1 | **0.60** | 2.76 | 5.4 |

**Table 6.11** Comparison of the absolute standard deviation, mean and maximum bias, in percentage, between the original ASM1 and the EHH and EKF estimation based on the augmented 'Model Bb', within the urban wastewater system. The best performances are emphasised.

These good performances are mainly due to the consequent number of measurements assumed available. However, the extended Kalman performances are slightly enhanced when compared with the extended $H_\infty$ filter. Furthermore, both the EHF and EKF converged toward the real parameter with a standard deviation of 0.0028 and 0.0033 and a maximum bias of 0.44% and 0.29%, respectively, occurring after 133 days. These results demonstrate that the extended $H_\infty$ filter is more robust than the extended Kalman filter, in the frequency domain, when implemented within the urban wastewater system. On the other hand, the tracking performances in the time domain are similar for both types of software sensors.

Simulation results displayed in Figure (6.26) concentrate on the software sensors convergence properties toward the real states and parameter, when the initial estimates are assumed unknown. The convergence times are summarised in Table (6.12), where it can be observed that the software sensors both demonstrated similar convergence performances.

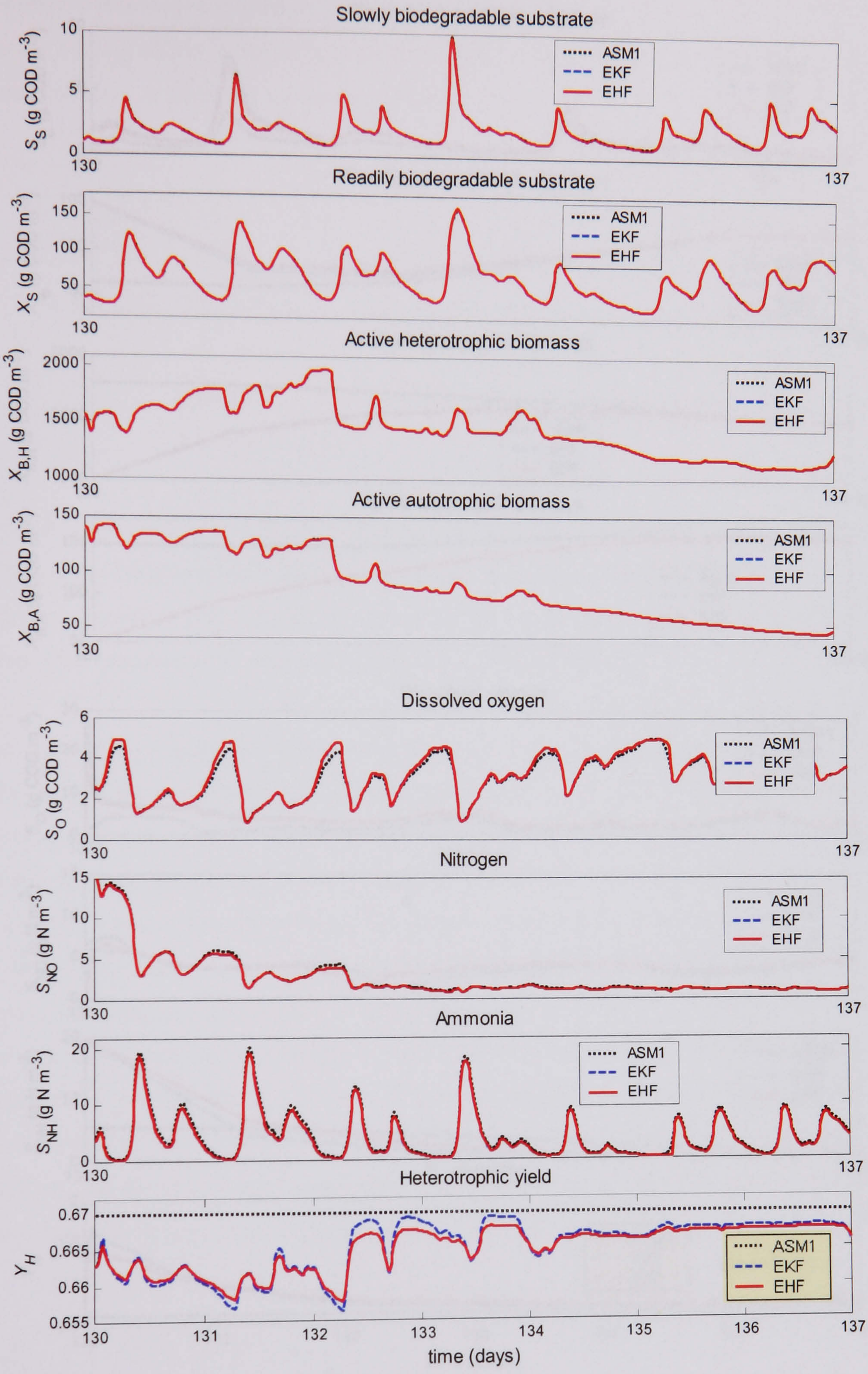


**Figure 6.25** Tracking performances comparison between the software sensors ($\gamma = 0.01$) and the ASM1 model when the influent of the plant is generated by the sewer system.

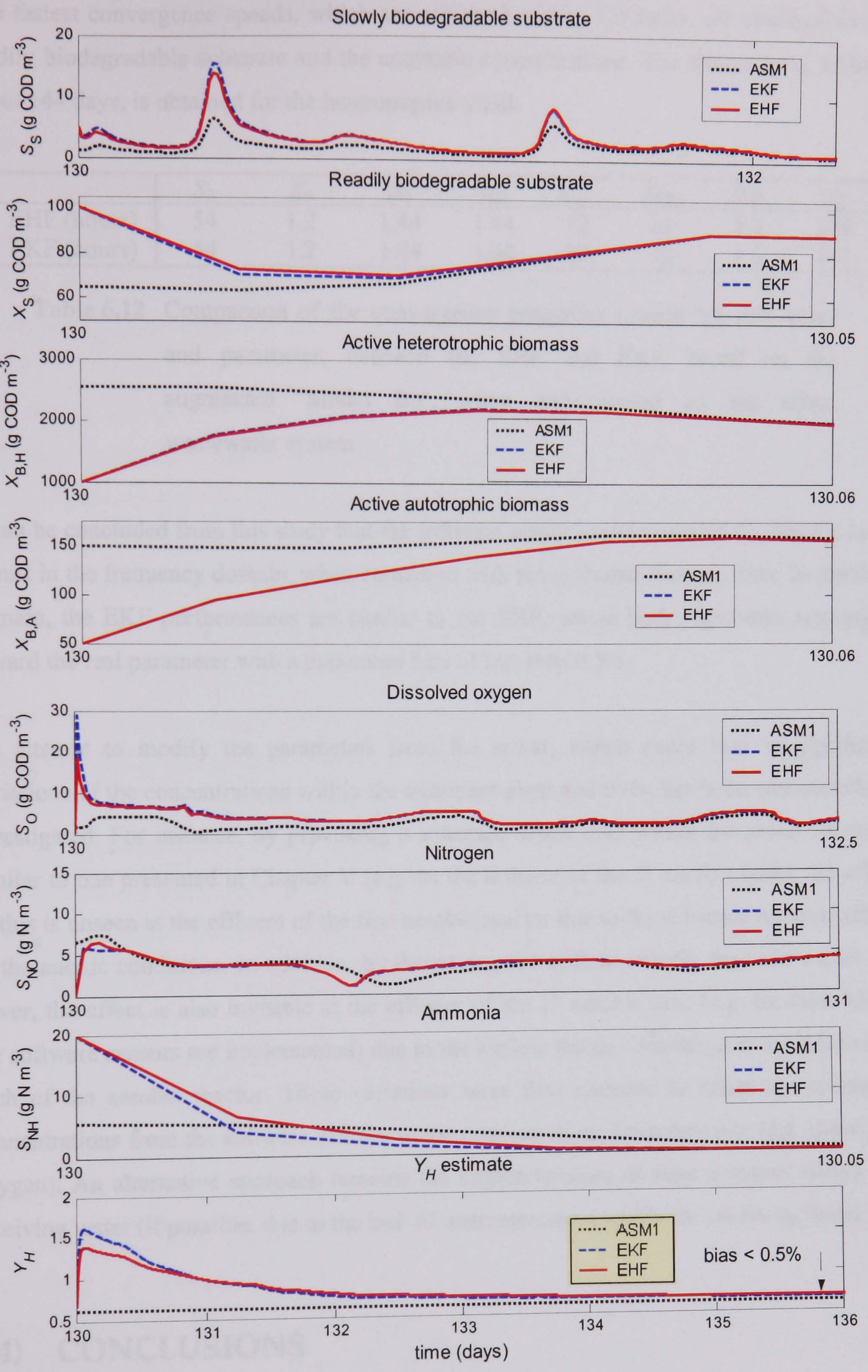


**Figure 6.26** Convergence performances comparison between the software sensors ($\gamma = 0.01$) and the ASM1 model when the influent of the plant is generated by the sewer system.

The fastest convergence speeds, which are achieved within 1.2 hours, are obtained for the readily biodegradable substrate and the ammonia concentrations. The slowest one, which is about 144 days, is obtained for the heterotrophic yield.

| | $S_S$ | $X_S$ | $S_O$ | $S_{NO}$ | $S_{NH}$ | $S_{ND}$ | $X_{ND}$ | $Y_H$ |
|---|---|---|---|---|---|---|---|---|
| EHF (hours) | 54 | 1.2 | 1.44 | 1.44 | 12 | 24 | 1.2 | 144 |
| EKF (hours) | 54 | 1.2 | 1.44 | 1.44 | 12 | 24 | 1.2 | 144 |

**Table 6.12** Comparison of the convergence properties toward the real states and parameter, between the EHF and EKF, based on the augmented 'Model Bb', when implemented on the urban wastewater system.

It can be concluded from this study that the software sensor based extended $H_\infty$ filter is more robust in the frequency domain, when compared with the extended Kalman filter. In the time domain, the EKF performances are similar to the EHF, where both algorithms converged toward the real parameter with a maximum bias of less than 0.5%.

An attempt to modify the parameters from the sewer, which could lead to significant variations of the concentrations within the treatment plant and river, has been unsuccessfully investigated. For instance, by provoking a substrate shock load within the sewer network, similar to one presented in Chapter V (e.g. on the influent of the 1st aerobic tank), the effect of this is unseen at the effluent of the first aerobic reactor due to the substrate removal effect of the anoxic conditions. In addition, by decreasing the airflow transfer function within the sewer, the effect is also invisible at the effluent of the 1st aerobic tank (e.g. location where the software sensors are implemented) due to the airflow inputs considered at the influent of each of the aerobic reactor. These variations were first intended to relate the estimated concentrations from the software sensors to the concentrations from the river (e.g. dissolved oxygen). An alternative approach remains the implementation of state observer within the receiving water (if possible, due to the lack of instrumentation within the receiving body).

## 6.4) CONCLUSIONS

The software sensor application presented in this chapter demonstrated the dynamic behaviour of the reduced 'Model C' and 'Model Bb', presented in Chapter IV, based on extended $H_\infty$ and Kalman filtering techniques. The first application, based on the augmented

'Model C', demonstrated the EHF robustness performances when minimising the error criterion between the estimated concentrations and the real ones from the benchmark plant. Furthermore, it was also illustrated that the extended $H_\infty$ filter enhanced the tracking performances of the disturbances when compared with the EKF. In addition, the faster convergence performances from the extended Kalman filter, when compared with the EHF, were demonstrated through simulation studies. These results implied that the extended $H_\infty$ filtering enhance the tracking performance when modelling errors are introduced within the benchmark plant model.

The second application, based on the augmented 'Model Bb', illustrated the robustness performances of the EHF, through FFT of the minimisation errors, when performing joint state and parameter estimation. When designing the parameter estimator based-EHF, the pre-specified $H_\infty$ performance, gamma, cannot be set to its optimal value, since this results in the failure of the algorithm to converge toward the real parameter. However the EHF demonstrated enhanced tracking performances of the parameter (e.g. when properly tuned by trial and error) when compared to the extended Kalman filter. In addition, when parametric uncertainties are included within the model, both software sensors converge toward the real parameter with approximately similar performances. Even though the EKF estimation was improved overall, the selection of an extended $H_\infty$ filtering technique is recommended for such an approach, as the stability properties of the extended Kalman filter, which is (at this current date) an open problem, are not guaranteed. Furthermore, due to its robustness properties, an EHF feature could probably improve the overall performances of an eventual control algorithm if the estimated concentrations are utilised to feed this last.

The final case study illustrated the extended $H_\infty$ filter performances when implemented on the urban wastewater system. Interesting results were proposed where the robustness performances of the EHF and the enhanced convergence properties of the EKF were demonstrated trough simulation studies, when a state observer was considered. Furthermore, when performing joint state and parameter estimation, both algorithms converged toward the real states and parameter with similar performances. The convergence toward the heterotrophic yield was achieved within six days when the urban wastewater system was selected and within a single day when the design was performed on the benchmark plant only. This finding clearly emphasised the importance of considering an integrated approach rather than an independent unit (e.g. the WWTP).

# Part III

# Conclusions and Future Work

# Chapter VII

# Conclusions and future work

The aim of the work presented in this thesis is the design of software sensors for urban wastewater system with a special emphasis on the wastewater treatment plant. This has been motivated by the clear lack of instrumentation and automation systems within the wastewater industry, and also by the recently adopted water framework directive, which sets a fundamental objective of 'good' overall river quality. Therefore, the main objectives of this thesis are summarised as follows:

1. The development of software sensors for monitoring purposes in order to overcome the lack of instrumentation.

2. The inclusion of disturbances and process noise sources statistics to enhance practical applicability of the algorithms.

3. The investigation of the proposed solutions within a full scale urban wastewater system.

The work presented in this thesis has successfully achieved all the objectives by proposing:

1. The development of three reduced order models based on the activated sludge model No.1.

2. The investigation of the linear and non-linear observability properties of each of the reduced models based on the Kalman rank test and the Lie derivatives, respectively.

3. The development of software sensors including disturbances in the design, which are modelled by spectral analyses and augmented models.

4. The development and investigation of a non-linear robust technique, which is based on extended $H_\infty$ filtering.

5. The investigation of the software sensors responses within an integrated urban wastewater system.

The proposed results indicate that there is a potential in the use of non-linear filtering algorithms for monitoring of wastewater systems. However, it has also revealed that the development of an appropriate observable mathematical model and the selection of sufficient physical sensors are a prerequisite to enhance satisfactory tracking and convergence performances of the algorithms.

The main achievements are towards the development of locally observable reduced-order model based on the well established ASM1 model. In addition, a new state observer is proposed to detect abnormally high substrate concentrations within the wastewater treatment plant. The proposed results still require a deeper investigation (e.g. validation with real data) but are the first step in the detection of toxicity, which is directly related to substrate concentrations levels. Furthermore, a solution to provide on-line monitoring of the heterotrophic and autotrophic biomass concentrations, which is currently not available in real WWTP, is proposed. Moreover, the implementation of extended $H_\infty$ filter algorithms is also a major achievement due to the inclusion of unknown noise source statistic within the models describing the dynamic behaviour of the treatment plant. The following sections summarise and comment the findings, and provide future lines of work.

## 7.1 SUMMARY OF RESULTS

**Development of three reduced-order models based on the original ASM1 for monitoring purposes of the substrate, biomass and ammonia concentrations.** The 'Model A' is reduced to four state variables and is accurate for monitoring purposes of the heterotrophic and autotrophic biomass concentrations within the IWA/COST benchmark

simulation No.1. However, the dissolved oxygen concentration provided significant mismatches when compared with the original model. This is not crucial as the DO sensor is the most widespread measurements in WWTP. The 'Model B' is initially reduced to five state variables ('Model Ba') to include the dynamic behaviour of the readily and slowly biodegradable substrates concentrations. The proposed model is accurate with respect to the purpose it is designed for, which consist of the estimation of the substrate activities within the WWTP. The 'Model Bb', which is similar to the Ba, includes two extra state variables (e.g. the heterotrophic and autrophic biomass concentrations) and is mainly developed for joint state and parameter estimation investigations. The seventh order 'Model C', which is also accurate in describing the dynamics of the selected concentrations, is intensively used when designing augmented observers for modelling the disturbances and estimating the ammonia concentration.

**Investigation of the linear piece-wise and non-linear local observability properties, based on the Kalman rank test and the Lie derivatives theories, respectively, of each of the proposed reduced-order models ('A', 'Ba', 'Bb', C).** The studies demonstrated that the 'Model A' is linearly piece-wise observable assuming a single measurement: the dissolved oxygen. When performing the non-linear observability analysis, similar results are obtained at the selected operating conditions. The 'Model Ba' is observable with two measurements ($S_O$ and $S_{NO}$) when performing the piece-wise approach and a single ($S_O$) with the non-linear method. However, great caution should be considered regarding the results based on the Lie derivatives. To be consistent, this theory should be investigated (if possible) for the whole domain of definition, similarly to the linear piece-wise approach, to guarantee the local observability of the proposed reduced model. In addition these studies also revealed that for models greater than a fifth order, computational burden occur when applying the non-linear theory based on the Lie derivative. Therefore, the observability analyses of the 'Model Bb' and 'Model C' are based on the piece-wise approach. Results illustrated that both models are linearly observable with three measurements. The 'Model B2' requires the assumption of the DO, the heterotrophic and autotrophic biomass measurements while for the 'Model C', the dissolved oxygen, nitrogen and ammonia sensors are necessary in achieving the observability conditions. It is not consistent to assume measurements of the biomass concentrations since these types of sensors are not available. However, a new approach is proposed in this thesis to overcome this major problem.

**Modelling the disturbances through spectral analysis, FFT, 1st order and 2nd order transfer functions and augmented systems driven by white Gaussian noise sequences.** The major drawback of the original ASM1 model for monitoring purposes is related to the significant amount of disturbances that are considered. Therefore, results from this thesis illustrated the possibility of inclusion of some of these disturbances when designing of state observers. The method consists of analysing the theoretical data available with the benchmark plant, in the frequency domain with FFT and spectral analysis, and design 1st and/or 2nd order transfer functions that can cover the spectral energy of the disturbances. Once constructed, the initial software sensors are augmented with additional sate variables, which are excited by white Gaussian random sequences. These techniques demonstrated that the readily biodegradable substrate and particulate organic nitrogen can be successfully estimated when measurements of the readily biodegradable substrate is assumed available from respirometer, at least every 30 minutes. However, if such technique is to be implemented for practical application, the spectral analysis and transfer function coefficients computations should be adaptive (performed at each sampling time) in order to be consistent.

**Development of three new state observers based extended Kalman filtering to monitor abnormal substrate concentrations, biomass activities and the particulate organic nitrogen within the benchmark simulation model No.1.** Firstly, a new state observer is presented in this thesis, which has the ability to detect abnormally high substrate concentrations within the first aerobic reactor of the benchmark plant. Since currently it is possible to obtain substrate measurement only through laboratory analysis, this observer is a major step in the monitoring of toxicity events contained in the wastewater. The design consists in considering the readily and slowly biodegradable substrate concentrations as disturbances. Therefore, an augmented state observer based on disturbance modelling is proposed, in which the dissolved oxygen measurements are assumed available. Due to the successful algorithms responses, real-time control strategies with on-line monitoring of abnormal substrate concentrations can be implemented. The warning detection system could also be further enhanced to send signals to a mobile phone to alert the operator on duty, and allow for a rapid response by modifying the plant's operational strategy. Furthermore, the detection limit is important because it could assist operators for instance to: modify the dissolved oxygen set point, to decrease the wastage sludge flow rate, or to increase the sludge recirculation flow rate to improve the overall performance of the plant when such toxic events or substrate overloads occur. Naturally, the next step in the developments described in this thesis is to try applying the state observer to full-scale systems. However, a

deeper investigation is necessary to validate the proposed algorithm since the substrate shock load is provoked by an air flow rate shut down. Consequently, it is not obvious whether or not the proposed state observer detects the substrate increased or the air flow failure. Therefore, the modelling of toxicity events is currently under research and if successful, it might provide an answer to this open problem. Secondly, a state observer with the capability to monitor the heterotrophic and autotrophic biomass concentrations is proposed. This is also a motivating approach since it is not possible to measure the biomass activity in the real WWTP. This approach, with is based on fractions of the total suspended solid measurements at the influent of the 1st aerobic reactor of the benchmark plant, demonstrated successful tracking performances. The next step to valid this work consists in investigating the state observer response with the Benchmark Simulation Model No.1 Long-Term (BSM1_LT), which included 360 days of data and temperature variations since the biomass is known as a slow changing variable (e.g. monthly scale). Thirdly, a new state observer is proposed to monitor the particulate organic nitrogen, which is also not available in WWTP at current time. The design, which is based on a fraction of the slowly biodegradable substrate concentration, also presented successful tracking performances. Such an approach leaded motivating results since it could provide further information on the particulate nitrogen concentration dynamic behaviour, which could lead to a more robust control strategy of the nitrogen, correlated and dependent on $S_{ND}$ concentration. However, this algorithm requires a validation step (e.g. with real data) if it is considered for practical applications.

**Development of software sensors based on a robust non-linear filtering technique: the extended $H_\infty$ filter.** This work is motivated by the fact that: (1) the software sensors need to be robust against modelling errors and parameter variations, and (2), the extended Kalman filter presents drawbacks in term of poor tracking performances in the presence of unknown noise source statistics. Various algorithms are proposed in this thesis to demonstrate the robustness capabilities of the extended $H_\infty$ filter in the frequency domain, when compared with the standard extended Kalman filter. Furthermore the successful performances of the EHF in the time domain and in the presence of disturbances are also demonstrated through simulation studies. Results also illustrated the slow convergence properties of the EHF toward the real states and parameter when it is not properly initialised. The poor convergence and tracking performances of both software sensors is also established when the original benchmark plant is corrupted by significant process noise. This work also presented insightful results in term of the convergence failure of the EHF when the pre-specified $H_\infty$ performance is set to its optimal value. A trade off between the extended $H_\infty$ filtering and

extended Kalman filtering in terms of robustness performances and fast convergence properties exist. The selection of an appropriate filtering technique is clearly dependent upon the main objectives of the application. The extended $H_\infty$ filter is probably more appropriate for parametric estimation cases, since the convergences properties of the EKF are not guaranteed. On the other hand, the extended Kalman filter is most likely to be a suitable solution when designing state observers, in comparison with the EHF.

**Development of a General procedure for model reduction and software sensor implementation.** A general procedure for model reduction and for the design of observable software sensors is proposed in this thesis. It is based on a six steps procedure, which provides methods for model reduction, observability analyses, modelling disturbances and finally, joint state and parameter estimation algorithm implementation. This procedure is exemplified through the thesis by all the proposed applications.

**Development of state observers and software sensors simulated on an integrated urban wastewater system.** The initial application based on the 'Model C', demonstrated the poor performances of both the EHF and EKF when the sewer system is connected to the wastewater treatment plant. The enhanced robustness properties in the frequency domain of the extended $H_\infty$ filter when compared with the extended Kalman filter were demonstrated through simulation studies. Furthermore the EKF demonstrated improved tracking performances in the time domain when compared with the EHF. The final application, based on the augmented 'Model B1.b', illustrated the good tracking performances of both software sensors when the initial conditions of the system are assumed to be known. On the contrary, both algorithms converged toward bias values when not carefully initialised. This finding clearly emphasises the importance of considering an integrated model rather than an independent unit such as the wastewater treatment plant, as the convergence and tracking performances of an estimator are drastically affected by the selection of the model.

## 7.2 TOPICS FOR FUTURE RESEARCH

In the course of the work presented in this thesis, several types of problems and question that deserve future attention have been encountered. In relation to the results that have been presented, a number of important issues and extensions can be defined. Some of them are summarised below

An interesting approach would be to perform a similar study but using the activated sludge model No.3 to further investigate the toxicity application findings. Of course, this would include the development of new reduced observable models with similar capabilities as those proposed within this thesis. In addition, the design should be investigated within an integrated urban wastewater system.

Concerning the observability of the proposed reduced model, similar analyses could be performed with the rain and storm weather influent wastewater data available with the benchmark plant to confirm the proposed results on non-linear observability. In addition, the local and global observability of the reduced-order ASM1 models, augmented with additional state variables (e.g. for parameter estimation and FFT used for disturbances modelling) could be performed.

With regards to the proposed software sensors, a similar design as that proposed in Chapter V to VI could be performed, but on the closed loop benchmark plant configuration. However, the proposed reduced models should be slightly modified to include the fact that the dissolved oxygen is assumed constant in the closed loop benchmark plant configuration.

An attempt to design software sensors within the river and sewer system to develop a decentralised non-linear filtering technique could probably be valuable. Last but not least, the proposed software sensors should be validated with real data.

# Bibliography


Ademoroti, C.W.A. (1986). Model to predict BOD from COD values. *Effluent & Water Treatment*, **26**, 80-84.

Alcock, S.J. (2004). New developments in sensor technology for water quality surveillance and early warning. *Wat. Sci. & Tech.*, **50**(11), pp 1–6.

Alex, J., Jumar, U. and Schütze, M. (2003a). On-line measurements data of wastewater systems via WAP mobile phones. *Wat. Sci. & Tech.*, **47**(2), pp 205-211.

Alex, J., Rieger, L., Winkler, S. and Siegrist H. (2003b). Progress in sensor technology – progress in process control? Part II: results from a simulation benchmark study. *Wat. Sci & Tech.*, **47**(2), pp 113-120.

An, L., Niu, H. and Zeng, H. (1998). A new biosensor for rapid oxygen demand measurement. *Water Environ. Res.*, **70**, 1070–1074.

Andrews, J.F. (1992). *Dynamic and control of the activated sludge process*. Water quality management library, volume 6, edited by J.F. Andrews, Technomic publishing company, Lancaster, PA, USA.

Anguelova, M. (2004). *Nonlinear Observability and Identifiability: General Theory and a Case Study of Kinetic Model for S. cerevisiae,* (Thesis). School of Mathematical Sciences, Chalmers University of technology and Göteborg University, Göteborg.

Ayesa, E., Florez, J., García-Heras, J.L. and Larrea, L. (1991). State and coefficients estimation for the activated sludge process using a modified Kalman filter algorithm. *Wat. Sci. Tech.*, **24**(6), 235-247.

Barraud, S., Gibert, J., Winiarski, T. and Bertrand-Krajewski J.L. (2002). Implementation of a monitoring system to measure impact of stormwater runoff infiltration. *Wat. Sci. & Tech.*, **45**(3), pp 203–210.

Bastin, G. and Dochain, D. (1990). *On-line Estimation and Adaptive Control of Bioreactors*. Elsevier Science publisher, ISBN 0-444-88430-0. Amsterdam, The Netherlands.

Beck, M. B. (1986). Identification, estimation and control of biological waste-water treatment processes. *IEE Proc.*, 133, 254-264.

Benazzi, F., Katebi, R. and Wilkie, J. (2003). Application of Extended Kalman Filter to Activated Sludge Process. *2nd WWT&SYSENG Workshop, EU Research Training Network, HPRN-CT-2001-00200*, September 17-20 2003, Copenhagen, Denmark.

Benazzi, F. and Katebi, R. (2004). Software Sensor Based-Extended Kalman Filter Applied to Activated sludge Process. *3rd WWT&SYSENG Workshop, EU Research Training Network, HPRN-CT-2001-00200*, September 5-11 2004, Pavia, Italy.

Benazzi, F. and Katebi, R. (2005). Nonlinear Observability of Activated Sludge Process Models. *In Proc. 16th IFAC World Congress*, July 4 – 8 2005, Prague, Czech Republic.

Benazzi, F, Linblom, E. and Katebi, R. (2005a). Software sensor application to WWT processes and future perspectives when applied to integrated urban wastewater systems. *In Proc. 4th World Wide Workshop for Young Environmental scientists*, 10-13 May 2005, Paris, France.

Benazzi, F., Gernaey, K.V., Jeppsson, U. and Katebi, R. (2005b). On-line Estimation and Detection of Abnormal Substrate Concentrations in WWTPs using a Software Sensor: A Benchmark Study. *In Proc. 2nd IWA Conference on Instrumentation, Control and Automation (9th ICA series)*, 29 May - 2 June 2005, Busan, Korea.

Benazzi, F., Gernaey, K.V. and Katebi, R. (2005c). Joint state and parameter estimation based extended Kalman filter of activated sludge processes. 4th *WWT&SYSENG Workshop, EU Research Training Network, HPRN-CT-2001-00200*, August 20-25 2005, Crete, Greece.

Benazzi, F., Jeppsson, U. and Katebi, R. (2005d). On an Application of Extended Kalman Filtering to Activated Sludge Processes: A benchmark study. *In Proc. 10th International Conference on Urban drainage*, August 21 – 26 2005, Copenhagen, Denmark.

Benazzi, F., Gernaey, K.V. and Katebi, R. (2005e). Joint state and parameter estimation based extended Kalman filter of activated sludge processes: A benchmark study. *In Proc. 17th European Symposium and Exhibition*, October 20-22 2005, Marseille, France.

Benazzi, F. and Katebi, R. (2006). Extended Kalman filter versus extended $H_\infty$ filter - An application to activated sludge processes. *In Proc. 6th UKACC Control Conf*, 30 August - 1 September 2006, Glasgow, UK.

Benazzi, F., Steyer J.P. and Katebi, R. (2006). On an application of extended $H_\infty$ filtering to activated sludge processes: a benchmark study. *In Proc. 4eme colloque STIC et Environement*, April 5-7 2006, Narbonne, France.

Bergh, S-G. (1996). *Diagnosis problems in wastewater settling.* Licentiate of Technology Thesis, IEA, Lund Institute of Technology, Lund, Sweden, ISBN 91-88934-01-2.

Bertrand-Krajewski, J.L. (2004). TSS concentration in sewers estimated from turbidity measurements by means of linear regression accounting for uncertainties in both variables. *Wat. Sci. & Tech.*, **50**(11), pp 81–88.

Bode, H.W. and Shannon, C.E. (1950). A simplified derivation of linear least square smoothing and prediction theory. *Proc. IRE.*, **38**, 417-425.

Bogaerts, Ph. and Vande Wouwer, A (2004). Parameter identification for state estimation-application to bioprocess software sensors. *Che. Eng. Sci.*, **59**, pp. 2465-2474.

Bohlin, T. (1991). *Interactive System Identification: Prospects and Pitfalls*, Springer-Verlag, Berlin, Germany.

Bourgeois, W., Burgess, J.E. and Stuetz, R.M. (2001). On-line monitoring of wastewater quality: a review. *J. Chem. Technol. Biotechnol.*, **76**, 337-348.

Bretting, A.E. (1941). Lærebog i hydraulic. Polyteknisk forening, Copenhagen, Denmark. In Danish.

Brookman, S.K.E. (1997). Estimation of biochemical oxygen demand in slurry and effluent using ultra-violet spectrophotometry. *Wat. Res.*, **31**, 372-374.

Brombach, H., Weiss, G. and Fuchs, S. (2005). A new database on urban runoff pollution: comparison of separate and combined sewer systems. *Wat. Sci. & Tech.*, **51**(2), pp 119–128.

Brown, R.G. and Hwang, P.Y.C (1997). *Introduction to Random Signals and Applied Kalman Filtering*. 3rd edition, John Willey & Sons, New York, USA, ISBN 0-471-12839-2.

Butterworth, F.M., Gunatilaka, A. and Diehl, P. (2002). The Rhine/Danube monitoring paradigm: broader applications in sensor technologies. *In: Fleishmann et al. (Eds): Preprints of the International IWA Conference on Automation in Water Quality Monitoring* – AutoMoNet 2002, May 21-22, 2002.

Caminal, G., Lafuente, F.J., Lopez-Santin, J., Poch, M. and Sola, C. (1987). Application of the extended Kalman filter to identification of enzymatic deactivation. *Biotechnol. and Bioeng.*, **24**, 366-369.

Chéruy A. (1996). Software sensors in bioprocess engineering. *J. Biotechnol.*, **52**, 193-199.

Chocat, B., Krebs, P., Marsalek, J., Rauch, W. and Schilling, W. (2001). Urban drainage redefined: from stormwater removal to integrated management. *Wat. Sci. Tech.*, **43**(5), 61–68.

Chui, C. K., and Chen, G. (1991). Kalman filtering with real-time applications. Springer-Verlag, Berlin, Germany.

Copp, J.B. and Spanjers, H. (1999) Applicability of a simulation benchmark to respirometry-based control strategies. *In: Proceedings 9th European Congress on Biotechnology*, Brussels, Belgium July 11-15.

Copp, J.B. (Ed.) (2002). *The COST Simulation Benchmark. Description and Simulator Manual*. ISBN 92-894-1658-0. Office for official publications of the European communities, Luxembourg.

Council of the European Communities (2000). Directive 2000/60/EC of the European parliament and of the council of 23 October 2000 establishing a framework for Community action in the field of water policy. *Official journal*, L327, 1.

Darlington, S. (1958). Linear least-squares smoothing and prediction, with applications. *Bell Sys. Tech. J.*, **37**, 1221-1294.

Delattre, C., Dochain, D. and Winkin, J. (2002). Observability Analysis of a Nonlinear Tubular Bioreactor. *Proc. Int. Symp. Math. Theory of Networks and Systems (MTNS 2002), University of Notre-Dame*, Indiana, USA.

Demuynck, C., Vanrolleghem, P.A., Mingneau, C., Liessens, J. and Verstraete, W. (1994). NDBEPR process optimization in SBRs: Reduction of external carbon source and oxygen supply. *Wat. Sci. Tech.*, **30**(4), 169–179.

Dobbs, R.A., Wise, R.H. and Dean, R.B. (1972). The use of ultra-violet absorbance for monitoring the total organic carbon of water and wastewater. *Wat. Res.*, **6**, 1173–1180.

Dochain, D. (2003). State and parameter estimation in chemical and biochemical processes: a tutorial. *J. Process Control*, **13**, 801-818.

Dochain, D., and Vanrolleghem, P.A. (2001). *Dynamical modeling and Estimation in Wastewater Treatment Processes*. International Water Association, London, UK, ISBN 1 900222 50 7.

Dominguez, E. and Alcock, S.J. (2002). Sensing technologies for contaminated sites and groundwater. *Biosensors and Bioelectronics*, **17**(6–7), 625–633.

Doyle, J. C., Glover, K. and khargonekar, P. P. (1989). State-space solutions to standard $H_2$ and $H_\infty$ control problems. *IEEE Trans. On Automatic Control*, **34**(8), 831-847.

Elsayed, A. (1988). Design of $H_\infty$ filters. Ph.D. dissertation, EEE, University of Strathclyde, Glasgow, UK.

Farza, M., Hammouri, H., Othman, S. and Busawon, K. (1997). Nonlinear observers for parameter estimation in bioprocesses. *Chem. Eng. Sci.*, **52**, 4251-4267.

Francis, B.A. and Zames, G. (1984). On optimal sensitivity theory for SISO feedback systems. *IEEE Trans. Automat. Contr.*, **29**, 9-16.

Francis, B.A., Helton, J.W. and Zames, G. (1984). $H^\infty$-optimal feedback controllers for linear multivariables systems. *IEEE Trans. Automat. Contr.*, **29**, 888-900.

Franklin, G.F., Powel, J.D. and Emami-Naeini, A. (2002). *Feedback Control of Dynamic System*. 4th Edition., Prentice Hall, pp. 849. Upper Saddle River, New Jersey.

Gauthier, J.-P., Kupka, I. (1994). Observability and observers for nonlinear systems. *SIAM J. Cont. and Opt.*, **32**(4), pp. 975–994.

Gernaey, K.V., Rosen, C. and Jeppsson, U. (2006). WWTP Dynamic Disturbance Modelling – an Essential Module for Long-Term Benchmarking Development. *Wat. Sci. and Tech.* (in press).

Gernaey, K.V., Rosen, C. and Jeppsson, U. (2005). Phenomenological modeling of wastewater treatment plant influent disturbance scenarios. In: *Proc. 10th Int. Conf. Urban Drainage*, Copenhagen, Denmark, 21-26 August 2005.

Gobet, J., Rychen, Ph., Cardot, F., and Santoli, E. (2003). Microelectrode array sensor for water quality monitoring. *Wat. Sci. & Tech.*, **47**(2), 127-134.

Gopal, M. (1993). *Modern Control System Theory*. 2nd Edition, John Wiley & Sons, New York, ISBN: 0-470-22157-7.

Grau, P., Sutton, P.M., Henze, M., Elmaleh, S., Grady, Jr., C.P.L., Gujer, W., Koller, J. (1982), "Recommended Notation for Use in the Description of Biological Wastewater Treatment Processes". *Wat. Res.*, **16**, 1501-1505.

Grimble, M.J. (1985). $H_\infty$ and LQG robust design methods for uncertain linear systems. *IFAC Workshop on Model Error Concepts and Compensation*, Boston USA.

Grimble, M.J. (1986). Optimal $H_\infty$ robustness and the relationship to LQG design problems. *Int. J. Control*, **43**, 351-372.

Gudjonsson, G., Vollertsen, J. and Hvitved-Jacobsen, T. (2002). Dissolved oxygen in gravity sewers – measurement and simulation. *Wat. Sci. & Tech.*, **45**(3), pp 35–44.

Gunatilika, A. and Dreher, J. (2003). Use of real-time data in environmental monitoring: current practices. *Wat. Sci. & Tech.*, **47**(2), 53-61.

Hansen, M.M. and Carstensen, J. (1997). Continuous quality control of measurements in a real time controlled sewer system in the municipality of Copenhagen. *Wat. Sci. & tech.*, **36**(8-9), pp 349-353.

Harremoës, P. (2002). Integrated urban drainage, status and perspectives. *Wat. Sci. & Tech.*, **45**(3), pp 1–10.

Harremoës, P., Capodaglio, A.G., Hellström, B.G., Henze, M., Jensen, K.N., Lynggaard-Jensen, A., Otterpohl, R. and Soeberg, H. (1993). Wastewater treatment plants under transient loading – performance, modeling and control. *Wat. Sci. & Tech.*, **27**(12), 71-115.

Harremoës, P. and Rauch, W. (1999). Optimal design and real time control of the integrated urban runoff system. *Hydrobiologica*, **410**, 177-184.

Healey, M.J. (1989). Improvements in the activated sludge process in the U.K. and U.S. *J. Water Pollut. Control Fed.*, **61**, 447–451.

Helton, J.W. (1976). Operator theory and broadband matching. *In Proc. 11th Allerton Conf. on Comm. Contr. and Computing.*

Henze, M., Harremoës, P., La Cour Jansen, J. and Arvin, E. (1995). *Wastewater treatment: Biological and chemical processes*. Springer-Verlag, Heidelberg, Berlin, Germany.

Henze, M. (1997). Wastewater Treatment – Biological and chemical processes. 2nd ed., Srringler-Verlag. Berlin, Germany. Pp55-111.

Henze, M., Gujer, W., van Loosdrecht, M. and Mino, T. (2000). *Activated Sludge Models ASM1, ASM2, ASM2d and ASM3*. Scientific and Technical Report No 9, IWA Publishing, London, UK. ISBN-1 900222-24-8.

Herman, R. and Krener, A.J. (1977). Nonlinear controllability and observability. *IEEE Trans. Aut. Cont.*. **22**(5), pp. 728-740.

Holmberg, U., Olsson, G. and Andersson, B. (1989). Simultaneous DO control and respiration estimation. *Wat. Sci. Tech.*, **21**(10-11), 1185–1195.

Hvitved-Jacobsen, J., Vollertsen, J., and Nielsen, P.H. (1998). A process and model concept for microbial wastewater transformations in gravity sewers. *Wat. Sci. Tech.*, **37**(1), 233-241.

Ingildsen, P. (2002). *Realising full-scale control in wastewater treatment systems using in situ nutrient sensors*. PhD thesis, Department of Industrial Electrical Engineering and Automation, Lund University, Lund, Sweden, ISBN 91-88934-00-4.

Isidori, A. (1985). *Nonlinear Control Systems*. 2nd Edition, pp 5-14, Springer-Verlag Edition, Germany.

Janata, J., Josowicz, M., Vanysek, P. and DeVaney, D. M. (1998). Chemical sensors. *Analytical Chemistry*, **70**, 179-208.

Jeppsson, U. (1996). *Modelling Aspects of Wastewater Treatment Processes.* Ph.D. dissertation, IEA, Lund Institute of Technology, Lund, Sweden, ISBN 91-88934-00-4.

Jeppsson, U., Alex, J., Pons, M.-N., Spanjer, H. and Vanrolleghem, P.A. (2002). Status and future trends of ICA in wastewater treatment – A European perspective. *Wat. Sci. & Tech.*, **45**(4-5), 485-494.

Jeppsson, U. and Pons, M.-N. (2004). Editorial: The COST benchmark simulation model – current state and future perspective. *Control Engineering Practice*, **12**, 299-304.

Johnson, M., Mogens, H., Vilanova, R., Capodaglio, A., Olsson, G., Buttler, D., Papageorgiou, M. (2001). WWT & SYSENG: Getting Systems Engineering into Regional Wastewater Treatment Strategies. *Research Training Network Proposal, HPRN-CT-2001-00200*, 2nd May 2001, UK.

Kabouris, J.C. and Georgakakos, A.P. (1995). Parameter and state estimation of the activated sludge process-II. Applications. *Wat. Res.*, **30**(12), 2867-2882.

Kailath, T. (1974). A view of three decades of linear filtering theory. IEEE Trans. Inform. Theory, **20**(2), 146-181.

Kalman, R.E. (1960). A new approach to linear filtering and prediction problems. *J. Basic Eng.*, **85**, pp. 34-35.

Kalman, R. E., Ho, Y. C., and Narendra K.S. (1962). Controllability of linear dynamical system. *Contrib. Dif. Eq.*, **1**, 189-213.

Katebi, M. R. and Grimble, M. J. (1998). Extended H-infinity filtering for dynamic ship positioning. *Proc. IFAC Conf. ACAS*P, Glasgow, UK.

Kolmogorov, A.N. (1939). Sur l'interpolation et l'extrapolation des suites stationnaires (in French). *Com. Rend. Acad. Sci.*, **208**, 2043-5.

Kolmogorov, A.N. (1941). Stationary sequences in Hilbert space (in Russian). *Bull. Moscow State Univ.*, **2**(6), 1-40.

Korenaga, T., Takahashi, T., Moriwake, T. and Sanuki, S. (1990). Water quality monitoring system using a flow-through sensing device. In: *Instrumentation, Control and Automation of Water and Wastewater Treatment and Transport Systems (Advances in Water Pollution Control 10)*. Ed. Briggs R., Pergamon Press, London. 625–631.

Langergraber, G. Fleischmann, N. and Hofstädter, F. (2003a). A Multivariate Calibration Procedure for UV/VIS Spectrometric Quantification of Organic Matter and Nitrate in Wastewater. *Wat. Sci. & Tech.*, **47**(2), 63-71.

Langergraber, G., Wuchty, M., Fleischmann, and Lechner, M. (2003b). Rapid automated detection of nitrification kinetics using respirometry. *Wat. Sci. & Tech.*, **47**(2), 149-155.

Legendre, A.M. (1810). Méthode des moindres quarrés, pour trouver le milieu le plus probable entre les résultats de différentes observations (in French). *Mem. Inst. France*, 149-154.

Lijklema, L., Tyson, J.M. and Lesouef, A. (1993). Interactions between sewers, treatment plants and receiving waters in urban areas: a summary of the interurba '92 workshop conclusions. *Wat. Sci. Tech.*, **27**(12), 1–29.

Lindblom, E., Gernaey, K.V., Henze, M. & Mikkelsen, P.S. (2005a). Integrated modelling of two xenobiotic organic compounds. In: Eriksson, E., Genc-Fuhrman, H., Vollertsen, J., Ledin, A., Hvitved-Jacobsen, T. & Mikkelsen, P. S. (eds.). *10th Int. Conf. Urban Drainage*, 21-26 August, Copenhagen, Denmark.

Lindblom, E., Raduly, B. & Mikkelsen, P.S. (Eds.) (2005b). *System process modelling report*. Environment & Resources DTU, Technical University of Denmark, 116 pp. EU research training network (contract HPRN-CT-2001-00200).

Ljung, L. (1979). Asymptotic behavior of the extended Kalman filter as parameter estimator for linear systems. *IEEE Trans. Aut. Cont.*, **24**, 34-50.

Ljung, L. (1999). *System identification: Theory for the user.* 2nd Edition, Prentice-Hall, Inc., Englewood Cliffs, New Jersey, USA:

Lynggaard-Jensen, A., Eisum, N. H., Rasmussen, I., Jacobsen, H. S. and Stenstrom, T. (1996). Description and test of a new generation of nutrient sensors. *Wat. Sci. & Tech.*, **33**(1), 25-35.

Marini, G. W. and Weilguni, H. (2003). Hydrological information system based on on-line monitoring – from strategy to implementation in the Brantas River Basin, East Java, Indonesia. *Wat. Sci. & Tech.*, **47**(2), 189-196.

Marikani, M., Papageorgiou, M. and Olsson, G. (2003). Technology review report, *EU Research Training Network (WWT&SYSENG), HPRN-CT-2001-00200*. Internal report.

Meirlaen, J., (2002). Immission based real-time control of the integrated urban wastewater system. Ph.D. Thesis. Faculty of Agricultural and Applied Biological Sciences, Ghent University, Belgium.

Meirlaen, J., Huyghebaert, B., Sforzi, F., Benedetti, L. and Vanrolleghem, P.A. (2001). Fast, simultaneous simulation of the integrated urban wastewater system using mechanistic surrogate models. *Wat. Sci. & Tech.*, **43**(7), 301-309.

Meirlaen, J. and Vanrolleghem, P.A. (2002). Model reduction through boundary relocation to facilitate real-time control optimization in the integrated urban wastewater system. *Wat. Sci. & Tech.*, **45**(4-5), 373-381.

Meredith, W.D. (1990). Recent innovations in instrumentation for sewage treatment plant monitoring and control. *Instrumentation, Control and Automation of Water and Wastewater Treatment and Transport Systems (Advances in Water Pollution Control 10)*. Ed. Briggs R., Pergamon Press, London. 699–703.

Metcalf and Eddy (2003). *Wastewater Engineering Treatment and Reuse.* 4th edition, McGraw-Hill editor. New York, USA, ISBN 0-07-112250-8.

Miloshova, M. Baltes, D. and Bychkov, E. (2003). New chalcogenide glass chemical sensors for $S^{2-}$ and dissolved H2S monitoring. *Wat. Sci. & Tech.*, **47**(2), 135-140.

Mizaikoff, B. (2003). Infrared optical sensors for water quality monitoring. *Wat. Sci. & Tech.*, **47**(2), 35-42.

Murthy, D.N.P., Page, N.W., Rodin, E.Y. (1990), *Mathematical Modelling*, Pergamon Press, New York, New York, USA.

Nagpal, K.M. and Khargonekar, P.P. (1991). Filtering and Smoothing in an $H_\infty$ Setting. *IEEE trans. on Automatic and Control.* **36**(2), 152-166.

Nielsen, M., Revsbech, N. P., Larsen, L. H. and Lynggaard-Jensen, A. (2000). On-line determination of nitrite in wastewater treatment by use of a biosensor. *Wat. Sci. & Tech.*, **45**(4-5), 69-76.

Nijmeijer, H. and Van der Schaft, A.J. (1990). *Nonlinear Dynamical Control Systems.* Springer, Berlin.

Olsson, G. (1976). State of the art in sewage treatment plant control. *A.-I- Ch- E- Symp. Ser.*, **72**,52-76.

Olsson, G. (1994). Advancing ICA technology by eliminating the constraints, plenary presentation, *Wat. Sci.Tech.*, **28**, 1-7.

Perrier, M., Feyo, de Azevedo, S., Ferreira, E.C. and Dochain, D. (2000). Tuning of observer-based estimators: theory and application to the on-line estimation of kinetic parameters. *Control Eng. Practice*, **8**, 377-388.

Petersen, E.E. (1965), *Chemical Reaction Analysis,* Prentice Hall, Inc., Englewood Cliffs, New Jersey, USA.

Piatyszek, E., Joannis, C. and Aumond, M. (2002). Using typical daily flow patterns and dry-weather scenarios for screening flow rate measurements in sewers. *Wat. Sci & Tech.*, **45**(7), pp 75–82.

Preissmann, A. (1961). Propagation des intumescences dans les canaux et rivières. *Proc., 1st Congress Association Francaise de Calcul*, Grenoble, AFC, Paris, 433–442 (in French).

Qian, Z. and Tan, T.C. (1998). Response characteristics for a dead-cell BOD sensor. *Wat. Res.*, **32**, 801–807.

Reichert, P., Borchardt, D., Henze, M., Rauch, W., Shanahan, P., Somlyódy, L. and Vanrolleghem, P.A. (2001a). River Water Quality Model No. 1. *Scientific and Technical Report No 12.*, IWA Publishing, London, UK.

Rauch, W. and Harremoës, P. (1997). Acute pollution of recipients in urban areas. *Wat. Sci. Tech.*, **36**(8-9), 179–184.

Rauch, W., Aalderink, H., Krebs, P., Schilling, W. and Vanrolleghem, P. A. (1998). Requirements for integrated wastewater models - driven by receiving water objectives. *Wat. Sci.Tech.*, **38**(11), 97–104.

Reichert, P., Borchardt, D., Henze, M., Rauch, W., Shanahan, P., Somlyódy, L. and Vanrolleghem, P.A. (2001b). River Water Quality Model No. 1. (RWQM1): II. Biochemical process equations. *Wat. Sci. & Tech.*, **43**(5), 11-30.

Rieger, L., Alex, J., Winkler, S., Boehler, M., Thomann, M. and Siegrist, H. (2003). Progress in sensor technology – progress in process control? Part I: Sensor property investigation and classification. *Wat. Sci. & Tech.*, **47**(2), 103-112.

Rosen, C. (2001). A chemometric approach to process monitoring and control with applications to wastewater treatment operation. *Ph.D. Thesis*, Lund University, Lund, Sweden, ISBN 91-88934-20-9.

Rosen, C., Rottorp, L. and Jeppsson, U. (2003). Multivariate on-line monitoring: Challenges and solutions for modern wastewater treatment operation. *Wat. Sci. & Tech.*, **47**(2), 117-179.

Russell, N.L., Marshallsay, D.R., MacCraith, B. and Devisscher, M. (2003). Non-contact measurement of wastewater polluting load-the Loadmon project. *Wat. Sci. & Tech.*, **47**(2), 79-86.

Schilling, W. (Ed) (1989). Real time control of urban drainage systems. The state-of-the-art. *IAWPRC Task Group on Real Time-Time Control Urban Drainage Systems*, London, UK.

Schilling, W., Bauwens, W., Borchardt, D., Krebs, P., Rauch, W. and Vanrolleghem, P.A. (1997). Receiving water objectives - Scientific arguments versus urban wastewater management practice. In: Proceedings XXVII IAHR Congress "Water for a Changing Community", vol. 1, pp. 510–515. San Francisco, USA. August 10-15, 1997.

Schütze, M., Campisano, A., Colas, H., Vanrolleghem, P.A. and Schilling W. (2003). Real-time control of urban water systems. *Proc. Int. Conf. on Pumps, Electromechanical Devices and Systems Applied to Urban Water Management*, Valencia, Spain, 22-25 April.

Schütze, M., Campisano, A., Colas, H., Schilling, W. and Vanrolleghem, P.A. (2004). Real time control of urban wastewater systems – where do we stand today?. *J. Hydro.*, **299**, 335-348.

Shanahan, P., Henze, M., Koncsos, L., Rauch, W., Reichert, P., Somlyódy, L., and Vanrolleghem, P.A. (1998). River Water Quality Modelling: II. Problems of the art. *Wat. Sci. & Tech.*, **38**(11), 245-252.

Shanahan, P., Brochardt, D., Henze, M., Rauch, W., Reichert, P., Somlyódy, L., and Vanrolleghem, P.A. (2001). River Water Quality Model no. 1 (RWQM1): I. Modeling approach. *Wat. Sci. & Tech.*, **43**(5), 1-9.

Shinbrot, M. (1958). Optimazation of time-varying linear systems with nonstationary inputs. *Trans. ASME*, **80**, 457-462.

Sin, G. Malisse, K. and Vanrolleghem, P.A. (2003). An Integrated Sensor for the Monitoring of Aerobic and Anoxic Activated Sludge Activities in Biological Nitrogen Removal Plants. *Wat. Sci. & Tech.*, **47**(2), 141-148.

Smith, P.G. and Scott, J.S. (2002). *Dictionary of Water and Wastewater management.* Butterworth-Heinemann publisher, Co-published by IWA, Oxford, UK, ISBN 0 7506 4638 1.

Sontag, E. (1979). On the observability of Polynomial Systems. *SIAM J. Cont. and Opt.* **17**, 139-152.

Spanjers, H., Vanrolleghem, P.A., Olsson, G. and Dold, P.L. (1998a). *Respirometry in Control of the Activated Sludge Process: Principles*. IAWQ Scientific and Technical Report No. 7, London, UK.

Spanjers, H., Vanrolleghem, P.A., Nguyen, K., Vanhooren, H., and Patry, G.G. (1998b). Towards a simulation-benchmark for evaluating respirometry-based control strategies. *Wat. Sci. Tech.*, **37**(12), 219-226.

Stephanopoulos, G. and San, K.Y. (1984). Studies on on-line bioreactor identification. *Biotechnol. and Bioeng.*, **26**, 1176-1188.

Stumwöhrer, K., Matsché, N. and Winkler, S. (2003). Influence of the wastewater composition on the applicability of UV-absorption measurements at combined sewer overflows. *Wat. Sci. & Tech.*, **47**(2), 73-78.

Tebbutt, T.H.Y. (2002), *Principles of Water Quality Control.* Butterworth-Heinemann publisher, Fifth edition, Jordan Hill, Oxford, UK. ISBN 0 7506 3658 0.

Tewari, A. (2002). *Modern Control Design With MATLAB and SIMULINK.* John Willey & Sons Ltd, England, UK.

Tsobanakis, P., Lee, S.H., Phillips, J.A., and Georgakis, C. (1992). Issues in the optimization, estimation and control of fed-batch bioreactors using tendency models. *In: N.M. Karim, G. Stephanopoulos, Proc. 5th Int. Conf. Comp. App.*, pp. 71-76. Oxford: Pergamon Press.

Vanrolleghem, P. A. (1994). Building blocks for wastewater treatment process control: A review. In: Advanced Course on Environmental Biotechnology. Delft, The Netherlands, May 25 – June 3 1994. pp. 27.

Vanrolleghem, P.A., Borchardt, D., Henze, M., Rauch, W., Reichert, P., Shanahan, P. and Somlyódy, L. (2001). River Water Quality Model No. 1. (RWQM1): III. Biochemical submodel selection. *Wat. Sci. & Tech.*, **43**(5), 31-40.

Vanrolleghem, P.A. and Lee, D.S. (2003). On-line Monitoring Equipment for Wastewater Treatment Processes: State of the Art. *Wat. Sci. & Tech.*, **47**(2), 1-34.

Vollertsen, J. and Hvitved-Jacobsen, T. (2000). Sewer quality modelling – a dry weather approach. *Urban Wat.*, **2**, 295-303.

Watts, J.B., Evans, K. and Molloy, A. (1990). A wastewater/water process monitoring system allowing operational control – Developed by an operational manager. *Instrumentation, Control and Automation of Water and Wastewater Treatment and Transport Systems (Advances in Water Pollution Control 10)*. Ed. Briggs, R., Pergamon Press, London, 143–154.

WEF (1997). *The Clean Water Act (CWA), updated for 1997. 25th Anniversary Edition.* Water Environment Federation, Alexandria, VA, USA.

Weijers, S. (2000). Modelling, Identification and Control of Activated Sludge Plants for Nitrogen Removal. PhD thesis, Technische Universiteit Eindhoven, Veldhoven, The Netherlands, ISBN 90-386-0997-3.

Welch, G., and Bishop, G. (2002). *An Introduction to the Kalman Filter*. Technical report TR 95-041, Department of Computer Science, University of North Carolina at Chapel Hill, Los Angeles, CA.

Wiener, N. (1949). *Extrapolation, interpolation and smoothing of stationary time series, with engineering applications*. New York: Willey, ISBN 0262730057.

Wilderer, P.A., Bungartz, H.J., Lemmer, H., Wagner, M., Keller, J. and Wuertz, S. (2002). Modern scientific methods and their potential in waste water science and technology. *Wat. Res.*, **36**, 370-393.

Wilson, G.T. (1972). The factorization of matricial spectral densities. *SIAM J. Appl. Math.*, **23**, 420-426.

Wilson, F. (1997). Total Organic Carbon as a predictor of biological wastewater treatment efficiency and kinetic reaction rate. *Wat. Sci. & Tech.*, **35**, 119-126.

Zacharof, A., Butler, D., Mikkelsen, P.S. and A. Capodaglio, (2003). System review and definition report. *Research Training Network, HPRN-CT-2001-00200, WWT&SYSENG,* March 2003, UK.

Zadeh, L.A. and Ragazzini, J.R. (1950). An extension of Wiener's theory of prediction. *J. Appl. Phys.*, **21**, 645-655.

Zames, G. (1981). Feedback and optimal sensitivity: Model approximate inverses. *IEEE Trans. Automat. Contr.*, **26**, 301-320.

Zames, G. and Francis, B.A. (1983). Feedback minimax sensitivity, and optimal robustness. *IEEE Trans. Automat. Contr.*, **28**, 585-601.

# Appendix A

## List of Abbreviations

| | |
|---|---|
| **ASM1/2/2d/3** | Activated Sludge Model no.1/2/2d/3 |
| **ASP** | Activated Sludge Process |
| **ASS** | Activated Sludge System |
| **BC** | Before Christ |
| **BNR** | Biological Nutrient Removal |
| **BOD** | Biological Oxygen Demand |
| **BSM1** | Benchmark Simulation Model No.1 |
| **COD** | Chemical Oxygen Demand |
| **COST** | European Co-Operation in the field of Scientific and Technical Research |
| **CSO** | Combined Sewer Overflows |
| **DO** | Dissolved Oxygen |
| **DW** | Dry Weather |
| **EC** | European Commission |
| **EFF** | Effluent |
| **EHF** | Extended $H_\infty$ Filter |
| **EKF** | Extended Kalman Filter |
| **EMSS** | European Modelling and Simulation Symposium |
| **EU** | European Union |
| **FFT** | Fast Fourier Transform |
| **HRT** | Hydraulic Retention Time |
| **ICA** | Instrumentation Control and Automation |

## Appendix A: List of Abbreviations

| | |
|---|---|
| **ICUD** | International Conference on Urban Drainage |
| **IFAC** | International Federation of Automatic Control |
| **IR** | Infra Red |
| **IUWS** | Integrated Urban Wastewater System |
| **IWA** | International Water Association |
| **IWAQ** | International Association on Water Quality (formerly IAWPRC) |
| **KF** | Kalman Filter |
| **MIMO** | Multiple-Input Multiple-Output |
| **MMSE** | Minimum Mean Square Error |
| **PAO** | Phosphorous Accumulating Organism |
| **PES** | Primary Excess Sludge |
| **PID** | Proportional Integral Derivative |
| **RI** | Rain Influent |
| **PRBS** | PseudoRandom Binary Sequence |
| **QUAL2E** | Enhanced Stream Water Quality Model |
| **RWQM1** | River Water Quality Model No.1 |
| **RAS** | Return Activated Sludge |
| **RTC** | Real Time Control |
| **SES** | Secondary Excess Sludge |
| **SI** | Storm Influent |
| **SISO** | Single-Input Single-Output |
| **STIC** | Sciences et Techniques de l'Information et de la Communication |
| **TSS** | Total Suspended Solid |
| **TOC** | Total Organic Carbon |
| **UKACC** | United Kingdom Automatic Control Council |
| **UV** | Ultra Violet |
| **VIS** | Visible |
| **WAP** | Wireless Application Protocol |
| **WFD** | Water Framework Directive |
| **WWT** | Wastewater Treatment |
| **WWTP** | Wastewater Treatment Plant |
| **WWW-YES** | World Wide Workshop for Young Environmental Scientists |

# Appendix B

# List of State Variables and Parameters

**Table B1. State variables considered in the trunk sewer model**

| State variable description | Symbol | Units |
|---|---|---|
| Soluble inert organic matter | $S_I$ | mg COD $L^{-1}$ |
| Readily biodegradable substrate | $S_S$ | mg COD $L^{-1}$ |
| Particulate inert organic material | $X_I$ | mg COD $L^{-1}$ |
| Hydrolysable substrate, fast biodegradable | $X_{S1}$ | mg COD $L^{-1}$ |
| Hydrolysable substrate, slowly biodegradable | $X_{S2}$ | mg COD $L^{-1}$ |
| Heterotrophic active biomass in the water phase | $X_{BW}$ | mg COD $Ll^{-1}$ |
| Heterotrophic active biomass in the biofilm phase | $X_{BF}$ | mg COD $L^{-1}$ |
| Oxygen | $S_O$ | mg COD $L^{-1}$ |
| Nitrate + nitrite nitrogen | $S_{NO}$ | mg N $L^{-1}$ |
| $NH_4$-$NH_3$ nitrogen | $S_{NH}$ | mg N $L^{-1}$ |
| Soluble biodegradable organic nitrogen | $S_{ND}$ | mg N $L^{-1}$ |
| Particulate biodegradable nitrogen | $X_{ND}$ | mg N $L^{-1}$ |
| Alkalinity | $S_{ALK}$ | mol $L^{-1}$ |
| Soluble xenobiotic compound | $S_{XOC}$ | mg XOC $L^{-1}$ |

**Table B2. The State variables of the ASM1 model (Copp, 2002).**

| State variable Description | Symbol | Units |
|---|---|---|
| Soluble inert organic matter | $S_I$ | g COD $m^{-3}$ |
| Readily biodegradable substrate | $S_S$ | g COD $m^{-3}$ |
| Particulate inert organic matter | $X_I$ | g COD $m^{-3}$ |
| Slowly biodegradable substrate | $X_S$ | g COD $m^{-3}$ |
| Activated heterotrophic biomass | $X_{B,H}$ | g COD $m^{-3}$ |
| Activated autotrophic biomass | $X_{B,A}$ | g COD $m^{-3}$ |
| Particulate products arising from biomass decay | $X_P$ | g COD $m^{-3}$ |
| Oxygen | $S_O$ | g COD $m^{-3}$ |
| Nitrate and nitrite nitrogen | $S_{NO}$ | g N $m^{-3}$ |
| $NH4^+$ + NH3 nitrogen | $S_{NH}$ | g N $m^{-3}$ |
| Soluble biodegradable organic nitrogen | $S_{ND}$ | g N $m^{-3}$ |
| Particulate biodegradable organic nitrogen | $X_{ND}$ | g N $m^{-3}$ |
| Alkalinity | $S_{ALK}$ | mol $L^{-1}$ |

**Table B2.1. Kinetic parameters used for the ASM1 (Copp, 2002).**

| Parameter description | Sym. | Value | Units |
|---|---|---|---|
| Maximum heterotrophic growth rate | $\mu_{mH}$ | 4.0 | $day^{-1}$ |
| Half-saturation (hetero. growth) | $K_S$ | 10.0 | g COD $m^{-3}$ |
| Half-saturation (hetero. oxygen) | $K_{OH}$ | 0.2 | g $O_2$ $m^{-3}$ |
| Half-saturation (nitrate) | $K_{NO}$ | 0.5 | g $NO_3$-N $m^{-3}$ |
| Heterotrophic decay rate | $b_H$ | 0.3 | $day^{-1}$ |
| Anoxic growth rate correction factor | $\eta_g$ | 0.8 | dimensionless |
| Anoxic hydrolysis rate correction factor | $\eta_h$ | 0.8 | dimensionless |
| Maximum specific hydrolysis rate | $K_h$ | 3.0 | g $X_S$ (g $X_{B,H}$ COD day) $^{-1}$ |
| Half saturation (hydrolysis) | $K_X$ | 0.1 | g $X_S$ (g $X_{B,H}$ COD) $^{-1}$ |
| Maximum autotrophic growth rate | $\mu_{mA}$ | 0.5 | $day^{-1}$ |
| Half-saturation (auto. growth) | $K_{NH}$ | 1.0 | g $NH_3$-N $m^{-3}$ |
| Autotrophic decay rate | $b_A$ | 0.05 | $day^{-1}$ |
| Half-saturation (auto. oxygen) | $K_{OA}$ | 0.4 | g $O_2$ $m^{-3}$ |
| Ammonification rate | $k_a$ | 0.05 | $m^3$ (g COD day) $^{-1}$ |

**Table B2.2. Stoichiometric parameters used for the ASM1 (Copp, 2002)**

| Parameter description | Sym. | Value | Units |
|---|---|---|---|
| Autotrophic yield | $Y_A$ | 0.24 | g $X_{B,A}$ COD formed (g N utilised) $^{-1}$ |
| Heterotrophic yield | $Y_H$ | 0.67 | g $X_{B,H}$ COD formed (g COD utilised)$^{-1}$ |
| Fraction of biomass to part. products | $f_p$ | 0.08 | dimensionless |
| Fraction nitrogen in biomass | $i_{XB}$ | 0.08 | g N (g COD) $^{-1}$ in biomass |
| Fraction nitrogen in particulate products | $i_{XP}$ | 0.06 | g N (g COD) $^{-1}$ in $X_P$ |

**Table B3. State variables in the river model.**

| State variable description | Symbol | Units |
|---|---|---|
| Readily biodegradable substrate | $S_S$ | mg COD $L^{-1}$ |
| Soluble inert organic matter | $S_I$ | mg COD $L^{-1}$ |
| Ammonium | $S_{NH4}$ | mg N $L^{-1}$ |
| Nitrite | $S_{NO2}$ | mg $L^{-1}$ |
| Nitrate | $S_{NO3}$ | mg $L^{-1}$ |
| Part of inorganic dissolved phosphorus | $S_{HPO4}$ | mg P $L^{-1}$ |
| Oxygen | $S_O$ | mg COD $L^{-1}$ |
| Organisms oxidising ammonia to nitrite | $X_{N1}$ | mg COD $L^{-1}$ |
| Heterotrophic organisms | $X_{N2}$ | mg COD $L^{-1}$ |
| Organisms oxidising nitrite to nitrate | $X_S$ | mg COD $L^{-1}$ |
| Particulate inert organic material | $X_I$ | mg COD $L^{-1}$ |
| Particulate products arising from biomass decay | $X_P$ | g COD $m^{-3}$ |
| Soluble xenobiotic compound | $S_{XOC}$ | mg XOC $L^{-1}$ |
| Sorbed xenobiotic compound | $X_{XOC}$ | mg XOC $L^{-1}$ |
| Specific active XOC degraders | $X_{BZ}$ | mg $L^{-1}$ |
| Volume of river stretch *I* | $V_{RIV,I}$ | $m^3$ |

# Appendix C

# The Extended Kalman Filter

The extended Kalman filters (EKF), which is derived from the linear Kalman filters, is computed for the case where the system dynamics vary with operating and control points . This type of non-linear systems are usually described by non-linear equations, with a non-linear state space model of the form

$$\begin{cases} \mathbf{x}(k+1) = \mathbf{f}\left(\mathbf{x}(k), \mathbf{u}(k)\right) + \mathbf{G}(k)\mathbf{w}(k) \\ \mathbf{y}(k) = \mathbf{h}\left(\mathbf{x}(k)\right) + \mathbf{v}(k) \end{cases} \tag{C.1}$$

where $\mathbf{x} \in \mathcal{R}^n$, $\mathbf{w} \in \mathcal{R}^m$, $\mathbf{D} \in \mathcal{R}^{n \times m}$, $\mathbf{v}$ and $\mathbf{y} \in \mathcal{R}^r$, and $\mathbf{f}$ and $\mathbf{h}$ are general non-linear functions, of appropriate dimension. $\mathbf{G}(k)\mathbf{w}(k)$ and $\mathbf{v}(k)$ represent the process and measurement noise with noise sequences of zero means and covariance $\mathbf{Q}$ and $\mathbf{R}$, respectively, which are of the form

$$\mathbf{E}\{\mathbf{w}\mathbf{w}'\} = \mathbf{Q}, \qquad \mathbf{E}\{\mathbf{v}\mathbf{v}'\} = \mathbf{R} \tag{C.2}$$

The method to compute the EKF algorithm is to use a linearisation of the process dynamics in order to minimize the effect of process and measurement noise. Such linearisation technique is performed on-line, around the current state estimates. As was described in Chapter III, Section (3.3), the calculations are often divided in a *prediction* and a *correction* phase. The predictor phase includes the following calculations (Jeppsson, 1996):

$$\hat{\mathbf{x}}(k+1|k)=\mathbf{f}\left(\hat{\mathbf{x}}(k|k),\mathbf{u}(k)\right) \tag{C.3}$$

$$\mathbf{P}(k+1|k)=\mathbf{F}(k)\mathbf{P}(k|k)\mathbf{F}^{T}(k)+\mathbf{Q} \tag{C.4}$$

and the corrector phase calculations include

$$\hat{\mathbf{x}}(k+1|k+1)=\hat{\mathbf{x}}(k+1|k)+\mathbf{K}(k+1)\left[\mathbf{y}(k+1)-\mathbf{h}\left(\hat{\mathbf{x}}(k+1|k)\right)\right] \tag{C.5}$$

$$\mathbf{P}(k+1|k+1)=\mathbf{P}(k+1|k)-\mathbf{K}(k+1)\mathbf{H}(k+1)\mathbf{P}(k+1|k) \tag{C.6}$$

$$\mathbf{K}(k+1)=\mathbf{P}(k+1|k)\mathbf{H}^{T}(k+1)\left[\mathbf{H}(k+1)\mathbf{P}(k+1|k)\mathbf{H}^{T}(k+1)+\mathbf{R}\right]^{-1} \tag{C.7}$$

where $\boldsymbol{F}(k)$ and $\boldsymbol{H}(k)$, which corresponds to the Jacobian matrices of $\boldsymbol{f}(\cdot)$ and $\boldsymbol{h}(\cdot)$, respectively are defined as

$$\mathbf{F}(k)=\left.\frac{\partial\mathbf{f}\left(\mathbf{x}(k),\mathbf{u}(k)\right)}{\partial\mathbf{x}(k)}\right|_{\mathrm{x}(k)=\hat{\mathrm{x}}(k)} \tag{C.8}$$

$$\mathbf{H}(k)=\left.\frac{\partial\mathbf{h}\left(\mathbf{x}(k)\right)}{\partial\mathbf{x}(k)}\right|_{\mathrm{x}(k)=\hat{\mathrm{x}}(k)} \tag{C.9}$$

This approach was used in the study presented in Chapters III and V. The methods presented in this appendix not only hold for state estimation but also for simultaneously state and parameter estimation. The equations given are still valid although the estimated states becomes a generalized state vector which includes both the unknown state variables and the uncertain model parameters, as presented in Chapter III.

# Appendix D

# ASM1 Matrix Representation

The model considered state of the art for modelling biological nitrogen removal processes is the ASM1 model of the International Water Association (IWA, Henze *et al.*, 2000). This model, which describes carbon removal and nitrification-denitrification processes, was first introduced in 1987 (Henze *et al.*, 2000) as a result of the work by the 'Task Group on Mathematical Modelling for Design and Operation of Biological Wastewater Treatment Systems' formed by the International Association on Water Quality (IAWQ) in 1983. The major goal of this group was to review existing models and reach a consensus regarding the simplest model having the capability of realistic predictions of the performance of single-sludge systems carrying out carbon oxidation, nitrification and denitrification (Jeppsson, 1996). The ASM1 model is highly mechanistic where the major components of relevance and the most important biological processes are considered. It is usually presented in the matrix format suggested by Peterson (1965) using the notation recommended by Grau *et al.* (1982). This matrix representation allows rapid and easy recognition of the fate of each component. Indeed, by moving down a column for a specific component, the full differential equation with all the biological processes can be directly formulated and by moving across the matrix, the continuity of the model can be checked by calculating the sum of the stoichiometric coefficients.

**Table D.1** (Next two pages) Matrix representation of the process kinetics and stoichiometry for carbon oxidation, nitrification and denitrification, according to the IAWQ ASM1 model (Henze *et al.*, 2000).

| Component → | $i$ | 1 | 2 | 3 | 4 | 5 | 6 | 7 | 8 | 9 |
|---|---|---|---|---|---|---|---|---|---|---|
| $j$ | Process ↓ | $S_I$ | $S_S$ | $X_I$ | $X_S$ | $X_{B,H}$ | $X_{B,A}$ | $X_P$ | $S_O$ | $S_{NO}$ |
| 1 | Aerobic growth of heterotrophs | | $-\frac{1}{Y_H}$ | | | 1 | | | $-\frac{1-Y_H}{Y_H}$ | |
| 2 | Anoxic growth of heterotrophs | | $-\frac{1}{Y_H}$ | | | 1 | | | | $-\frac{1-Y_H}{2.86Y_H}$ |
| 3 | Aerobic growth of autotrophs | | | | | | 1 | | $-\frac{4.57}{Y_A}+1$ | $\frac{1}{Y_A}$ |
| 4 | 'Decay' of heterotrophs | | | | $1-f_P$ | −1 | | $f_P$ | | |
| 5 | 'Decay' of autotrophs | | | | $1-f_P$ | | −1 | $f_P$ | | |
| 6 | Ammonification of soluble organic nitrogen | | | | | | | | | |
| 7 | 'Hydrolysis' of entrapped organics | | 1 | | −1 | | | | | |
| 8 | 'Hydrolysis' of entrapped organic nitrogen | | | | | | | | | |
| Observed Conversion Rates [ML$^{-3}$T$^{-1}$] | | $r_i = \sum_j \nu_{ij}\rho_j$ | | | | | | | | |
| Stoichiometric Parameters:<br>Heterotrophic yield: $Y_H$<br>Autotrophic yield: $Y_A$<br>Fraction of biomass yielding particulate products: $f_P$<br>Mass N/Mass COD in biomass: $i_{XB}$<br>Mass N/Mass COD in products from biomass: $i_{XP}$ | | Soluble inert organic matter [ML$^{-3}$ COD] | Readily biodegradable substrate [ML$^{-3}$ COD] | Particulate inert organic matter [ML$^{-3}$ COD] | Slowly biodegradable substrate [ML$^{-3}$ COD] | Active heterotrophic biomass [ML$^{-3}$ COD] | Active autotrophic biomass [ML$^{-3}$ COD] | Particulate products arising from biomass decay [ML$^{-3}$ COD] | Oxygen (negative COD) [ML$^{-3}$ COD] | Nitrate and nitrite nitrogen [ML$^{-3}$ N] |

| 10<br>$S_{NH}$ | 11<br>$S_{ND}$ | 12<br>$X_{ND}$ | 13<br>$S_{ALK}$ | Process Rate, $\rho_j$ [$ML^{-3}T^{-1}$] |
|---|---|---|---|---|
| $-i_{XB}$ | | | $-\frac{i_{XB}}{14}$ | $\mu_H\left(\frac{S_S}{K_S+S_S}\right)\left(\frac{S_O}{K_{O,H}+S_O}\right)X_{B,H}$ |
| $-i_{XB}$ | | | $\frac{1-Y_H}{14\cdot 2.86Y_H}-\frac{i_{XB}}{14}$ | $\mu_H\left(\frac{S_S}{K_S+S_S}\right)\left(\frac{K_{O,H}}{K_{O,H}+S_O}\right)\left(\frac{S_{NO}}{K_{NO}+S_{NO}}\right)\eta_g X_{B,H}$ |
| $-i_{XB}-\frac{1}{Y_A}$ | | | $-\frac{i_{XB}}{14}-\frac{1}{7Y_A}$ | $\hat{\mu}_A\left(\frac{S_{NH}}{K_{NH}+S_{NH}}\right)\left(\frac{S_O}{K_{O,A}+S_O}\right)X_{B,A}$ |
| | | $i_{XB}-f_P i_{XP}$ | | $b_H X_{B,H}$ |
| | | $i_{XB}-f_P i_{XP}$ | | $b_A X_{B,A}$ |
| 1 | −1 | | $\frac{1}{14}$ | $k_a S_{ND} X_{B,H}$ |
| | | | | $k_h\frac{X_S/X_{B,H}}{K_X+(X_S/X_{B,H})}\left[\left(\frac{S_O}{K_{O,H}+S_O}\right)+\eta_h\left(\frac{K_{O,H}}{K_{O,H}+S_O}\right)\left(\frac{S_{NO}}{K_{NO}+S_{NO}}\right)\right]X_{B,H}$ |
| | 1 | −1 | | $\rho_7(X_{ND}/X_S)$ |
| $r_i=\sum_j \nu_{ij}\rho_j$ | | | | |

$S_{NH}$ = $NH_4+NH_3$ nitrogen [$ML^{-3}$]

$S_{ND}$ = Soluble biodegradable organic nitrogen [$ML^{-3}$]

$X_{ND}$ = Particulate biodegradable organic nitrogen [$ML^{-3}$]

$S_{ALK}$ = Alkalinity — Molar units

Kinetic Parameters:

Heterotrophic growth and decay: $\hat{\mu}_H$, $K_S$, $K_{O,H}$, $K_{NO}$, $b_H$

Autotrophic growth and decay: $\hat{\mu}_A$, $K_{NH}$, $K_{O,A}$, $b_A$

Correction factor for anoxic growth of heterotrophs: $\eta_g$

Ammonification: $k_a$

Hydrolysis: $k_h$, $K_X$

Correction factor for anoxic hydrolysis: $\eta_h$